microorganisms

Special Issue Reprint

Microbial Biotechnologies and Microorganism Interactions for Sustainable Agriculture

Edited by
Dario Rafael Olicón-Hernández and Guerra-Sánchez Guadalupe

mdpi.com/journal/microorganisms

MDPI

Microbial Biotechnologies and Microorganism Interactions for Sustainable Agriculture

Microbial Biotechnologies and Microorganism Interactions for Sustainable Agriculture

Guest Editors

Dario Rafael Olicón-Hernández
Guerra-Sánchez Guadalupe

MDPI

Basel • Beijing • Wuhan • Barcelona • Belgrade • Novi Sad • Cluj • Manchester

Guest Editors

Dario Rafael Olicón-Hernández
Departamento de Micriobiología
Instituto Politécnico Nacional
Mexico City
Mexico

Guerra-Sánchez Guadalupe
Departamento de Microbiología
Instituto Politécnico Nacional
Mexico City
Mexico

Editorial Office
MDPI AG
Grosspeteranlage 5
4052 Basel, Switzerland

This is a reprint of the Special Issue, published open access by the journal *Microorganisms* (ISSN 2076-2607), freely accessible at: https://www.mdpi.com/journal/microorganisms/special_issues/G4NT290LC3.

For citation purposes, cite each article independently as indicated on the article page online and as indicated below:

Lastname, A.A.; Lastname, B.B. Article Title. *Journal Name* **Year**, *Volume Number*, Page Range.

ISBN 978-3-7258-8125-3 (Hbk)
ISBN 978-3-7258-8126-0 (PDF)
https://doi.org/10.3390/books978-3-7258-8126-0

Cover image courtesy of Thabata Montserrat Hernández-Cruz

Contents

About the Editors

Dario Rafael Olicón Hernández

Dario Rafael Olicón Hernández is a full-time professor and researcher at the Instituto Politécnico Nacional (IPN), where he teaches in the Biochemical Engineering and Bacteriology and Parasitology programs. He holds a PhD in Chemical Biological Sciences from the IPN and has completed postdoctoral research in Germany, Spain, and Mexico. With nearly 15 years of teaching/research experience, he has trained professionals in multiple fields such as Biochemical Engineering, Chemical Engineering, and Medical Science. His research focuses on agricultural biotechnology, fungal biotechnology, biopolymers, bioremediation, and post-harvest food conservation. He has published more than 30 scientific papers and is a member of Mexico's National System of Researchers (SNI) with Level 1 recognition since 2017.

Guerra-Sánchez Guadalupe

Guerra-Sánchez Guadalupe is a chemist with a Ph.D. in Basic Biomedical Research from UNAM. She is a researcher and full-time professor at the National School of Biological Sciences at IPN, teaching undergraduate and master's level courses. She has completed postdoctoral stays in the United States. With 35 years of experience, her research focuses on the biochemistry and physiology of fungi and yeasts, microorganism metabolism, and the interaction between microorganisms for biological control applications. She has published over 50 articles in JCR/SCI-indexed journals and has supervised 26 undergraduate theses, 15 master's theses, and 7 doctoral theses. She is a member of the Mexican Society of Biochemistry and the College of Graduate Professors at ENCB, IPN, and is part of the National System of Researchers (SNI) with Level II recognition.

Preface

This Reprint presents a collection of scientific contributions dedicated to microbial biotechnology and microorganism interactions as fundamental pillars for sustainable agriculture. Its scope encompasses both applied and fundamental research, including the development of biofertilizers, biocontrol strategies, microbial consortia, and the study of ecological interactions that influence plant productivity and soil health. The aim of this Reprint is to provide an integrated perspective on how microbial systems can be harnessed to improve agricultural sustainability while reducing dependence on chemical inputs.

The motivation for assembling this Reprint arises from the increasing need to address global challenges such as soil degradation, environmental pollution, and food security through innovative and biologically based approaches. Microorganisms offer versatile and efficient solutions, yet their complex interactions and full biotechnological potential remain insufficiently explored. By bringing together diverse studies, this Reprint seeks to bridge knowledge gaps and promote the translation of microbial research into practical agricultural applications.

This Reprint is intended for researchers, professionals, and graduate students working in microbial biotechnology, agricultural sciences, environmental microbiology, and related fields. It also aims to support interdisciplinary collaboration by providing insights that connect molecular, ecological, and technological perspectives.

Dario Rafael Olicón-Hernández and Guerra-Sánchez Guadalupe
Guest Editors

microorganisms

MDPI

Article

Fertilization Induced Soil Microbial Shifts Show Minor Effects on *Sapindus mukorossi* Yield

Juntao Liu [1,2,3,4,†], Zhexiu Yu [1,†], Yingyun Gong [1], Jie Chen [5], Ling Zhou [1], Weihua Zhang [4,*] and Liming Jia [1,2,3,*]

[1] Key Laboratory of Silviculture and Conservation of the Ministry of Education, College of Forestry, Beijing Forestry University, Beijing 100083, China; ljt1120@bjfu.edu.cn (J.L.); yzhexiu@bjfu.edu.cn (Z.Y.); oxalis623@163.com (Y.G.); zhouling89757@bjfu.edu.cn (L.Z.)
[2] National Energy R&D Center for Non-Food Biomass, Beijing Forestry University, Beijing 100083, China
[3] National Innovation Alliance of Sapindus Industry, Beijing Forestry University, Beijing 100083, China
[4] Guangdong Provincial Key Laboratory of Silviculture, Protection and Utilization, Guangdong Academy of Forestry, Guangzhou 510520, China
[5] Research Institute of Tropical Forestry, Chinese Academy of Forestry, Guangzhou 510520, China; chenjiecaf@hotmail.com
* Correspondence: zwh523@sinogaf.cn (W.Z.); jlm@bjfu.edu.cn (L.J.); Tel.: +86-13501103773 (L.J.)
† These authors have contributed equally to this work.

Abstract: Fertilization can improve soil nutrition and increase the yield of *Sapindus mukorossi*, but the response of soil microbial communities to fertilization treatments and their correlation with soil nutrition and *Sapindus mukorossi* yield are unclear. In order to investigate the characteristics of soil physicochemical qualities and the bacterial community, we carried out a field experiment comparing various quantities of nitrogen (N), phosphorus (P), and potassium (K) fertilizers to the unfertilized control treatments and the yield of *Sapindus mukorossi* in raw material forests in response to different applications of fertilizers and to try to clarify the interrelation among the three. Results showed that (1) there are significant differences in the effects of different fertilization treatments on the soil properties of *Sapindus mukorossi* raw material forests. The increase in the application rates of nitrogen or phosphorus fertilizers significantly reduced the soil pH value. (2) Compared with control, the α-diversity of bacterial communities was significantly lower in $N_3P_2K_2$ and $N_1P_1K_2$ treatments. Among the dominant groups of soil bacteria at the phylum level, the relative abundance of *Chloroflexi* showed an increase and then a decrease trend with the increase in N application. The relative abundance of *Firmicutes*, *Bacteroidota*, and *Fusobacteriota* was positively correlated with the application of P and K fertilizers, while the relative abundance of *Acidobacteriota* and *Verrucomicrobiota* decreased with the increase in P and K fertilizers. (3) The $N_2P_2K_2$ treatment produced the highest *sapindus* yield (1464.58 kg/ha), which increased by 258.67% above the control. (4) Redundancy analysis (RDA) showed that the primary determinants of bacterial community structure were soil pH, total K, and effective P concentration. (5) Structural equation modeling (SEM) showed that soil nutrient content was the main direct factor driving the yield of *Sapindus mukorossi*, whereas the bacterial community attributes (e.g., diversity and structure) had minor effects on the yield. In summary, the rational use of formulated fertilization can change the bacterial community structure, improve the bacterial diversity, and increase the soil nutrient content, with the latter exerting a significant effect on the improvement of the yield of *Sapindus mukorossi*.

Keywords: bacterial community; diversity; fertilization; *Sapindus mukorossi*; soil fertility; structural distribution

1. Introduction

A type of energy forest belonging to the genus *Sapindus* in the family Sapin-daceae, *Sapindus mukorossi* is primarily found in tropical and subtropical areas [1–3]. Due to the growing demand for energy worldwide in recent years, bioenergy species have gained a lot of interest as a new and promising energy source [4,5]. Many industries use *Sapindus mukorossi*, including biomedicine, bioenergy. and cosmetics. In traditional Chinese medicine, the entire plant of *Sapindus*—fruit, root, bark, and leaves—is utilized. It is a woody oilseed tree species that has been marketed for usage in recent years. Its soap pods contain roughly 22% crude protein, and the kernels of the soap berries contain roughly 40% fatty acids. The planting area is 20,000 ha in Fujian Province alone, which is one of its primary production locations [4]. However, the production and quality of bio-energy species are significantly influenced by the nutritional conditions of the soil. Massive nutrients like nitrogen (N), phosphate (P), and potassium (K) are essential for plant growth and are crucial for crop productivity and the synthesis of oil products. In order to achieve high yields and high quality of economic tree species, it is effective to apply N, P, and K fertilizers rationally [6,7]. However, farmers usually over-apply N, P, and K fertilizers in order to rapidly increase the yield of *Sapindus mukorossi* fruits [8,9]. Unexpected fertilization can result in major environmental issues, including groundwater source pollution as well as issues like sloughing, acidification, and deterioration of soil quality, all of which lower crop yields [10,11]. Exploring scientific fertilization techniques is essential to enhance the sustainable development of the *Sapindus mukorossi* industrial forest.

Fertilization has a direct impact on the physicochemical characteristics of soil [12] and it has been demonstrated that balanced NPK fertilization significantly influences the physicochemical characteristics of crops. increases the amount of organic matter and quick-acting nutrients in the soil, encourages root growth and inter-root soil microbial growth, and ultimately influences yield. [2,7,12,13]. Proper fertilization management can maximize crop yield [7]. However, overuse of fertilizer will result in soil acidification and severe soil nutrient imbalance, which will then create leaf nutrient imbalance and ultimately impact production and economic efficiency [11,14]. Continuous fertilization can increase soil organic carbon content, total nitrogen content, and soil productivity [15,16]. Therefore, fertilization not only affects soil properties but also influences microbial diversity in soil.

Soil microorganisms have a strong connection with soil physicochemical properties and are drivers of processes such as organic matter decomposition, nutrient cycling, and humus formation [17]. Since soil microorganisms are highly sensitive to environmental changes [18,19], a significant amount of research has been conducted on the impacts of nutrient addition or deficiency on soil microbial communities [20,21]. It was demonstrated that N application was able to significantly alter the bacterial community, soil properties, and yield of sugarcane (*Saccharum officinarum*). In particular, bacterial species richness and evenness were higher in the moderately fertilized treatment than in the control without fertilization [22,23]. Ma et al. [23] found that nitrogen fertilization increased the number of nitrifying bacteria but did not affect the number of other flora. Phosphorus fertilizer application decreased the number of nitrate-reducing bacteria and archaeal ammonia-oxidizing bacteria and increased the number of nitrifying bacteria and nitrous oxide-reducing bacteria. Tang et al. [24] showed that N and P additions altered the abundance and community structure of nitrification and denitrification genes in a subtropical Chinese fir plantation forest, and that the combined application of nitrogen and phosphorus drove changes in the ammonia-oxidizing archaeal community. Li et al. [7] reported a significant decrease in soil bacterial diversity after N addition, while potassium fertilizer had relatively little effect on soil bacteria. Conversely, N deficiency will limit the increase in soil microbial biomass and reduce community diversity [25]. It has been demonstrated that combined application of

N, P, and K elevated *Panax ginseng* (*Panax ginseng C. A. Mey.*) yield and saponin content by increasing the relative abundance of potentially beneficial fungi and decreasing the relative abundance of potentially pathogenic fungi [6]. Therefore, NPK fertilizer addition can drive changes in soil bacterial community structure, abundance, and function by altering soil physicochemical properties. Overall changes in soil physicochemical properties and microbial community structure and diversity were observed after fertilizer application, but how these changes relate to fruit yield of plants still needs to be further investigated.

Presently, the area of plantation of *Sapindus mukorossi* in China is vast, and the economic benefits are considerable [3,26]. Fertilization is the main measure to regulate the yield and quality of *Sapindus mukorossi;* due to that, the soil fertility can be improved and soil productivity can be restored by raising the deficient nutrients. However, the effects of combined NPK fertilizer applications on soil properties and microorganisms in *Sapindus mukorossi* plantations have not been reported. The relationships between soil physicochemical properties, soil microbial attributes, and *Sapindus mukorossi* yield under different fertilization strategies are still unclear. To address these questions, we conducted a field experiment in a typical production area of *Sapindus mukorossi* in China, with the objective of exploring the following inquiries: (1) how N, P, and K fertilization would separately or combined affect the soil properties, bacterial community composition and diversity, and *Sapindus mukorossi* yield, and (2) whether fertilization could indirectly affect microbial community characteristics by altering soil properties, thereby increasing plant fruit yield.

2. Materials and Methods

2.1. Experimental Site

The research site was situated in Jianning County, Fujian Province, specifically at coordinates 116°47′20″ E and 26°40′3″ N. It experiences an average annual temperature of 17.0 °C, an average annual rainfall amounting to 1792 mm, and a high relative humidity of 84%. The soil type at the test site was sandy clay loam. The nutrient status of the soil in this experimental area was 7.75 g·kg^{-1} of soil organic carbon, 1.40 g·kg^{-1} of total nitrogen, 0.36 g·kg^{-1} of total phosphorus, 27.95 g·kg^{-1} of total potassium, 48.16 mg·kg^{-1} of fast-acting potassium, 1.32 mg·kg^{-1} of effective phosphorus, and 36.01 mg·kg^{-1} of alkaline dissolved nitrogen [8,9]. The raw material forest comprises the "Yuanhua" asexual line of Sapindales trees, featuring an average tree height of 2.38 m, an average ground diameter of 6.97 cm, and an average crown width of 2.4 m × 2.2 m (Figure 1).

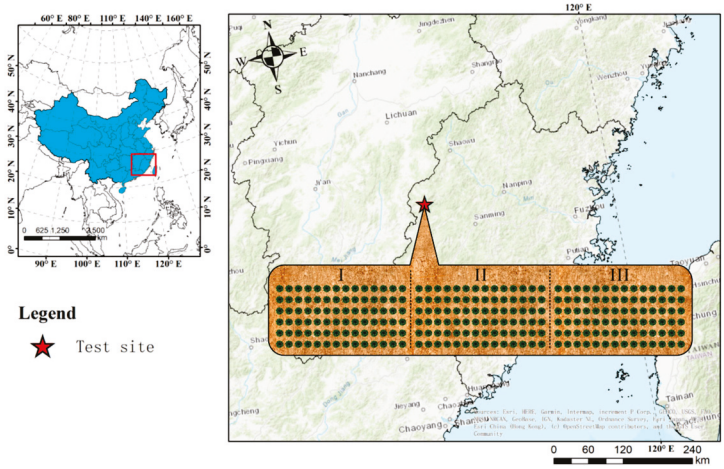

Figure 1. Location of the experimental site and experimental design of different NPK treatments.

2.2. Experimental Design

The six-year-old asexual *Sapindus mukorossi* raw material forest, known as "Yuanhua", served as the test material, featuring a row spacing of 4 m × 4 m. Three hectares made up the entire experimental sample area. A "3414" randomized block design was adopted for the formulation of the fertilizer trial, i.e., three elements (N, P, K), four fertilization levels (0 level: 0 kg/hm^2 of N, P, and K; 1 level: 300 kg/hm^2 of N, 250 kg/hm^2 of P, and 200 kg/hm^2 of K; 2 level: 600 kg/hm^2 of N, 500 kg/hm^2 of P, and 400 kg/hm^2 of K; and 3 level: 900 kg/hm^2 of N, 750 kg/hm^2 of P, and 600 kg/hm^2 of K), 14 treatments, three replications, and a total of 42 treatment plots. Fertilizer application rates and levels are based on the results of our team's previous research and the preliminary experiments we conducted, combined with the soil background data of our experimental area to derive the fertilizer application rates for this experiment. The fertilizer application rates are outlined in Table 1, with isolation rows established between the various treatment plots. Fertilizers were applied on 10 April 2021 (flowering fertilizer, 30% of the total), 20 July 2021 (fruit-strengthening fertilizer, 30% of the total), and 1 November 2021 (post-harvest fertilizer, 40% of the total) [8,9], using the furrow method of fertilizer application and mulching the soil immediately after mixing and applying the fertilizers according to the amount of fertilizer, and the remaining maintenance and management measures were identical to those of the control group. The test fertilizers were potassium sulfate (containing K_2O 60.0%) as the sole source of K, calcium sulfate (containing P_2O_5 12.0%) as the sole source of P, and urea (containing N 46.0%) as the sole source of N.

Table 1. Factor-level combinations in each treatment.

Processing Number	Fertilization Level (kg·hm^{-2})		
	N	P	K
$N_0P_0K_0$	0	0	0
$N_0P_2K_2$	0	500	400
$N_1P_2K_2$	300	500	400
$N_2P_0K_2$	600	0	400
$N_2P_1K_2$	600	250	400
$N_2P_2K_2$	600	500	400
$N_2P_3K_2$	600	750	400
$N_2P_2K_0$	600	500	0
$N_2P_2K_1$	600	500	200
$N_2P_2K_3$	600	500	600
$N_3P_2K_2$	900	500	400
$N_1P_1K_2$	300	250	400
$N_1P_2K_1$	300	500	200
$N_2P_1K_1$	600	250	200

Soil sampling: In 2021, during the expansion stage of *Sapindus mukorossi*, each plot adopted the "five-point sampling method" (sampling points were evenly distributed at regular intervals (equidistant) within the area), digging 0–20 cm soil profile at each sampling point for sampling, and mixing uniformly on a plot-by-plot basis. The mixed soil samples were split into two sections. One section, after being air-dried, finely ground, and sieved to 2 mm, was transported back to the laboratory for the assessment of soil chemical properties. In order to determine the soil microorganisms, the remaining soil samples were separated from contaminants and root residues, placed in sterile bags, and then promptly transported to the laboratory under low-temperature conditions to be kept in the freezer at −80 °C.

2.3. Soil Physical and Chemical Properties and Yield Determination

Using a 2300 Kjeltec analyzer (FOSS, Sweden), the Kjeldahl nitrogen determination method was used to measure the total nitrogen of the soil, while the potassium dichromate oxidation-external heating method was applied to determine the organic carbon of the soil [27]. Alkaline dissolution diffusion was used to determine the amount of available nitrogen (AN); the molybdenum-antimony antimicrobial colorimetric method was used to determine the amount of total and available phosphorus in the soil; atomic absorption was used to determine the amount of potassium in the soil; flame photometry was used to determine the amount of quick potassium; and a pH meter was used to measure the pH of the soil in a mixture of soil and water (1:2.5).Yield measurement: Yield measurements for *Sapindus mukorossi* were conducted on 5 November 2021, at the point of fruit maturity during harvest. All fruits were ripe at the time of harvesting the plants. To determine the fruit yield for each plot, all ripe fruits were collected from each entire tree, weighed using an electronic scale post-harvest, and subsequently, the yields per tree were summed for each respective plot.

2.4. DNA Extraction, PCR Amplification and Sequencing

Total DNA was isolated from 0.5 g of soil samples using the Soil Rapid DNA SPIN Kit (Q-BIO gene, Irvine, CA, USA), and DNA quality and concentration were assessed by agarose gel electrophoresis and Invitrogen (Carlsbad, CA, USA). The bacterial 16S rRNA V3–V4 region was amplified using primers 338F (50-ACTCCTACGGGGAG GCAGCA-30) and 806 (50-GGACTACHVGGGGTWTCTAAT-30) [2,28]. PCR amplification was performed in a total reaction volume of 10 μL containing DNA template (5–50 ng), Vn F (10 μM) 0.3 μL, Vn R (10 μM) 0.3 μL, KOD FX Neo Buffer 5 μL, dNTP (2 mM) 2 μL, KOD FX-Neo 0.2 μL, ddH2O to 10 μL. PCR amplification conditions were: initial denaturation at 95 °C for 5 min, followed by denaturation at 95 °C for 30 s, annealing at 55 °C for 20 s and extension at 72 °C for 30 s for a total of 30 cycles, and finally extension at 72 °C for 10 min. PCR amplicons were purified with Agencourt AMPure XP Beads (Beckman Coulter, Indianapolis, IN, USA). Finally, these PCR products were sent to Biomark Technologies (Beijing, China) for sequencing.

2.5. Sequence Splicing and Annotation

The raw sequences underwent quality filtering and merging processes, facilitated by Fastp (v.0.19.6) and FLASH (v.1.2.11), respectively. Subsequently, operational taxonomic unit (OTU) clustering and chimera removal were executed using Upraise software (v.11), adhering to a 97% similarity threshold. Taxonomic assignment of 16S rRNA sequence reads was determined using the bacterial SILVA reference database (Release 138) and the Unite reference database (Release 8.0), respectively. For both databases, the RDP classifier (version 2.11) was employed to annotate the OTU representative sequences taxonomically, with a confidence threshold of 0.7 set to ensure the accuracy of the taxonomic annotation results. The sample sequence was normalized based on the minimum sequence count to generate standardized data, which were then used to calculate the Shannon index and Chao index, following the methodology outlined by Liu et al. [27], and compositions of the soil microbial community were analyzed at the phylum level.

Simpson's diversity and Shannon's diversity index were calculated. It is defined as: D and H'

$$D = 1 - \sum_{i=1}^{S} P_i^2 \tag{1}$$

$$H' = -\sum_{i=1}^{S} p_i \ln P_i \tag{2}$$

Equations (1) and (2): P_i denotes the relative abundance of species inside the ith soil.

2.6. Data Processing and Analysis

One-way analysis of variance (ANOVA) and multiple range tests for least significant difference were performed to assess the effects of different NPK fertilization on soil properties, indices of soil bacterial community diversity (OTU richness, Simpson, and Shannon indices), soil microbial community composition, and the relative abundance of genes associated with different functional classes. The differences in bacterial community distribution were analyzed by PCoA using the BMK Cloud (www.biocloud.net 25 November 2022) platform. Redundancy analysis (RDA) and mapping of bacterial community-soil property relationships were performed using Canoco 5 software. Heat maps of correlation between bacterial dominant phyla and soil environmental factors were plotted using R 4.2.0, and partial least squares path modeling (PLS-PM) was used to investigate the possible causal relationships between nitrogen, phosphorus, and potassium fertilizer application, soil properties, soil community diversity, community structure, and saprotrophic yield. We used 999 bootstraps to calculate the coefficient of determination (R^2) and the path coefficient. The variance explained by the model is represented by the R^2 value. The goodness of fit indicates the best overall predictive performance. Path coefficients provide information on the direction and magnitude of the relationship between variables. Indirect effects can be determined by multiplying the path coefficients between two variables [29].

3. Results

3.1. Effect of Fertilization on Soil Properties

The impact of various fertilization treatments on the soil characteristics of *Sapindus mukorossi* varied significantly, as Table 2 illustrates. The $N_2P_2K_2$ treatments resulted in a considerable increase in soil total nitrogen, total potassium, organic carbon, available nitrogen, available phosphorus, and quick-acting potassium contents when compared to the control (Table 2). Soil pH was considerably lowered by increasing N or P treatment at different levels of nitrogen and phosphorus addition, respectively. After fertilization, the soil's nutrient contents all showed an upward trend when compared to the control. The $N_2P_2K_2$ and $N_3P_2K_2$ treatments had comparatively higher total and available nitrogen contents, which were 1.4 times higher than those of the control. The $N_1P_2K_1$ treatment had the greatest total phosphorus concentration, 2.5 times that of the control. The $N_2P_3K_2$ and $N_2P_2K_2$ treatments had comparatively high available phosphorus contents, which were 5.1 and 3.8 times the control, respectively. The $N_2P_2K_3$ treatment had comparatively high total and quick potassium concentrations, which were 1.3 and 1.4 times greater than the control, respectively. The $N_1P_1K_2$ treatment had the highest organic carbon content, 1.5 times that of the control. Each of these fertilization treatments differed from the control in a significant way ($p < 0.05$).

Table 2. Changes in soil properties under different fertilization treatments.

	pH	TN (g·kg^{-1})	TP (g·kg^{-1})	TK (g·kg^{-1})	SOC (g·kg^{-1})	AN (mg·kg^{-1})	AP (mg·kg^{-1})	AK (mg·kg^{-1})
$N_0P_0K_0$	5.02 ± 0.04 a	1.28 ± 0.08 i	0.42 ± 0.01 i	22.95 ± 0.69 h	11.08 ± 0.75 h	90.21 ± 6.51 f	1.13 ± 0.07 h	81.79 ± 2.90 g
$N_0P_2K_2$	5.09 ± 0.02 a	1.33 ± 0.06 hi	0.46 ± 0.03 i	26.58 ± 0.57 de	12.76 ± 0.53 fg	93.49 ± 0.99 f	2.47 ± 0.14 g	93.57 ± 1.25 cdef
$N_1P_2K_2$	4.82 ± 0.07 c	1.51 ± 0.05 def	0.52 ± 0.05 hi	26.27 ± 0.32 e	13.74 ± 0.81 def	105.59 ± 3.82 cd	2.97 ± 0.08 g	104.36 ± 1.54 abc
$N_2P_0K_2$	5.04 ± 0.02 a	1.53 ± 0.02 de	0.49 ± 0.06 hi	24.92 ± 0.45 fg	13.52 ± 0.68 defg	97.36 ± 4.17 ef	2.80 ± 0.45 g	92.68 ± 4.55 defg
$N_2P_1K_2$	4.84 ± 0.07 c	1.64 ± 0.03 bc	0.61 ± 0.05 g	27.72 ± 0.66 cd	14.21 ± 0.67 d	113.92 ± 5.86 bc	4.32 ± 0.58 cde	86.17 ± 9.31 fg
$N_2P_2K_2$	4.82 ± 0.03 cd	1.79 ± 0.04 a	0.87 ± 0.04 bcd	28.26 ± 0.93 bc	15.41 ± 0.68 bc	126.66 ± 5.42 a	5.29 ± 0.22 ab	107.46 ± 6.89 ab
$N_2P_3K_2$	4.67 ± 0.05 f	1.49 ± 0.06 def	0.96 ± 0.02 b	25.79 ± 0.43 ef	14.05 ± 0.78 de	95.77 ± 5.23 f	5.73 ± 0.26 a	88.81 ± 3.15 efg
$N_2P_2K_0$	4.91 ± 0.03 b	1.44 ± 0.06 efg	0.63 ± 0.03 fg	24.76 ± 0.81 fg	12.99 ± 0.37 efg	109.63 ± 6.12 cd	4.46 ± 0.29 cd	96.26 ± 4.52 cdef
$N_2P_2K_1$	4.81 ± 0.04 cd	1.60 ± 0.01 cd	0.56 ± 0.06 gh	24.12 ± 0.91 gh	15.68 ± 0.47 b	106.3 ± 1.39 cd	4.78 ± 0.15 bc	90.53 ± 7.27 efg

Table 2. *Cont.*

	pH	TN (g·kg^{-1})	TP (g·kg^{-1})	TK (g·kg^{-1})	SOC (g·kg^{-1})	AN (mg·kg^{-1})	AP (mg·kg^{-1})	AK (mg·kg^{-1})
$N_2P_2K_3$	4.71 ± 0.00 ef	1.67 ± 0.09 bc	0.72 ± 0.05 ef	28.97 ± 0.76 ab	14.38 ± 0.34 cd	115.11 ± 3.88 b	3.84 ± 0.39 ef	114.26 ± 10.78 a
$N_3P_2K_2$	4.56 ± 0.04 h	1.74 ± 0.03 ab	0.80 ± 0.02 de	27.65 ± 0.77 cd	13.85 ± 0.67 de	123.92 ± 2.97 a	4.85 ± 0.29 bc	87.99 ± 4.36 efg
$N_1P_1K_2$	4.78 ± 0.04 cde	1.47 ± 0.06 ef	0.92 ± 0.06 bc	29.78 ± 0.38 a	16.90 ± 0.29 a	103.93 ± 2.64 de	3.96 ± 0.29 def	98.40 ± 6.33 bcde
$N_1P_2K_1$	4.80 ± 0.03 cd	1.42 ± 0.09 fgh	1.05 ± 0.09 a	24.86 ± 0.67 fg	14.46 ± 0.28 cd	111.74 ± 6.49 bcd	3.57 ± 0.16 f	94.70 ± 6.86 cdef
$N_2P_1K_1$	4.74 ± 0.02 def	1.36 ± 0.03 ghi	0.84 ± 0.02 cd	23.27 ± 0.49 h	12.65 ± 0.41 g	112.85 ± 4.27 bc	2.77 ± 0.26 g	101.91 ± 3.44 bcd

Note: SOC: organic carbon; TN: total nitrogen; TP: total phosphorus; TK: total potassium; AN: alkaline nitrogen; AP: active phosphorus; AK: acute potassium; pH: soil acidity and alkalinity. Different letters in the same indicator indicate significant differences between treatments ($p < 0.05$).

3.2. Impact of Fertilization on Soil Bacterial Community Structure and Diversity

Soil bacterial community structure produced changes under different fertilization treatments. Based on the composition of the top 10 species of bacterial community distribution in the samples analyzed at the phylum level (Figure 2a), the dominant phyla in the different treatments, except for unclassified bacteria, were Proteobacteria, Acidobacteriota, Firmicutes, Bacteroidota, Actinobacteriota, Green Benders (Chloroflexi), Verrucomicrobiota, Planctomycetota and Fusobacteriota, with a combined relative abundance of 91.89–97.09%. Among them, the relative abundance of Proteobacteria was the highest in the $N_1P_1K_2$ treatment and significantly different from all other treatments ($p < 0.05$); Bacteroidota was relatively high in the $N_2P_3K_2$ and $N_1P_1K_2$ treatments and significantly different from all other treatments except $N_2P_1K_1$ ($p < 0.05$). At different levels of nitrogen addition, the highest relative abundance of Acidobacteriota and Verrucomicrobiota microbiota was found in the $N_1P_2K_2$ treatment, the highest relative abundance of Chloroflexi was found in the $N_2P_2K_2$ treatment, and the lowest relative abundance of green Chloroflexi was found in the $N_3P_2K_2$ treatment, with a significant difference between the two treatments as the nitrogen fertiliser application increased ($p < 0.05$).

Principal component analysis based on different fertilization treatments at the OTU level showed (Figure 2b) that the total variance explained by the first two axes (PC_1 and PC_2) of the bacterial community under different fertilization treatments was 18.72% and 12.65%, respectively, with a cumulative contribution of 31.37% (Figure 2b). In the first principal component, the bacterial community of $N_1P_1K_2$ and $N_1P_2K_1$ treatments differed the most, and in the second principal component, the bacterial community of $N_1P_2K_2$ and $N_3P_2K_2$ treatments differed the most.

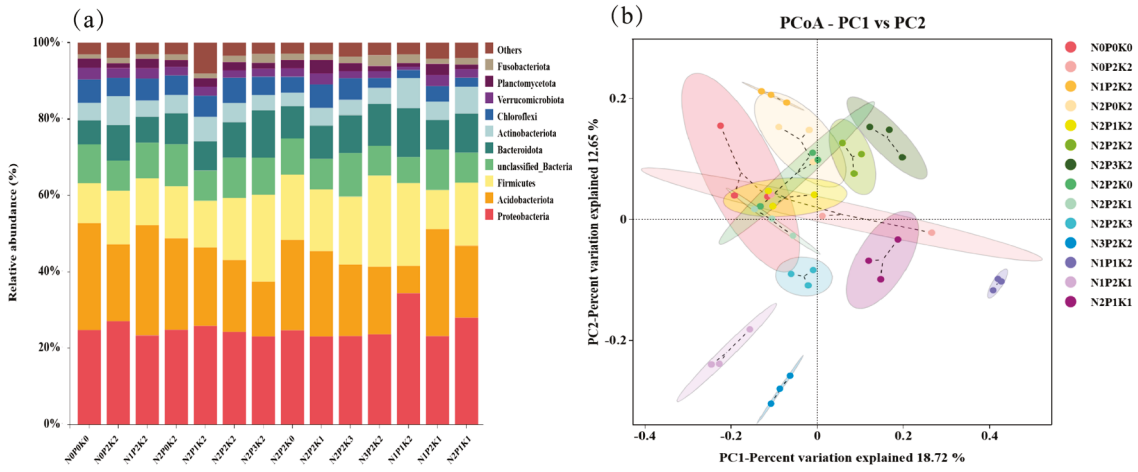

Figure 2. Relative abundance of horizontal species of soil bacteria under different fertilization treatments. (**a**) Relative abundance of portal bacterial level species. (**b**) Bacterial OTU horizontal principal component analysis.

Various fertilization methods exerted specific influences on bacterial α-diversity (Table 3). Bacterial community diversity demonstrated a pattern of initial increase followed by a decline in response to increasing levels of nitrogen, phosphorus, and potassium fertilization; the richness index and Shannon index of $N_3P_2K_2$ and $N_1P_1K_2$ were at a lower level and differed significantly from the other treatments ($p < 0.05$), and the Shannon index of $N_1P_2K_2$, $N_2P_0K_2$, and $N_2P_2K_2$ treatments was notably elevated compared to all other treatments.

Table 3. Soil bacterial community diversity under different fertilization treatments.

Fertilizer Treatment	OTU Richness	Simpson	Shannon
$N_0P_0K_0$	617.38 ± 18.54 abc	0.9954 ± 0.0004 a	8.5353 ± 0.0666 ab
$N_0P_2K_2$	591.33 ± 47.04 bcd	0.995 ± 0.0012 a	8.4455 ± 0.2553 ab
$N_1P_2K_2$	674.67 ± 25.66 a	0.9955 ± 0.0004 a	8.6310 ± 0.0846 a
$N_2P_0K_2$	664.38 ± 6.58 ab	0.9954 ± 0.0003 a	8.6146 ± 0.0321 a
$N_2P_1K_2$	610.33 ± 14.64 abc	0.9949 ± 0.0007 ab	8.4685 ± 0.0948 ab
$N_2P_2K_2$	682.00 ± 21.79 a	0.9951 ± 0.0005 a	8.6451 ± 0.0716 a
$N_2P_3K_2$	615.67 ± 22.19 abc	0.9932 ± 0.0011 b	8.3062 ± 0.1299 c
$N_2P_2K_0$	630.67 ± 21.83 abc	0.9945 ± 0.0011 ab	8.4917 ± 0.0870 ab
$N_2P_2K_1$	571.45 ± 37.08 cd	0.9948 ± 0.0010 ab	8.4505 ± 0.1507 ab
$N_2P_2K_3$	619.04 ± 45.10 abc	0.9946 ± 0.0006 ab	8.4946 ± 0.1153 ab
$N_3P_2K_2$	456.33 ± 110.35 e	0.9910 ± 0.0010 c	7.9449 ± 0.2511 d
$N_1P_1K_2$	463.33 ± 12.70 e	0.9889 ± 0.0017 d	7.6773 ± 0.0709 e
$N_1P_2K_1$	536.00 ± 26.15 d	0.9948 ± 0.0004 ab	8.4118 ± 0.0359 ab
$N_2P_1K_1$	610.33 ± 14.64 abc	0.9942 ± 0.0006 ab	8.4310 ± 0.0190 ab

Note: Different letters in the same index signify statistically significant differences at $p < 0.05$.

3.3. Analysis of Sapindus mukorossi Yield

Effects of various fertilization treatments with nitrogen, phosphorus, and potassium on *Sapindus mukorossi* yield and financial gains (Figure 3). The yield can be significantly increased by fertilization, which also enhances the financial gains. While the yield of nutrient deficiency treatment was significantly higher than that of total nutrient treatment and significantly lower than that of fertilization treatment, $N_2P_2K_2$ was the highest yield compared to both fertilization and nutrient deficiency treatments. The yield of low, medium, and high nitrogen fertilizer treatments improved by 51%, 85%, and 61%, respectively, at different levels of nitrogen addition, while the economic revenue increased by 7275, 12,150, and 8700 yuan/hm^2. At different levels of alkaline addition, compared with no phosphate fertilizer, the low, medium, and high phosphate fertilizer treatments increased the yield by 67%, 85%, and 45% and increased the economic income by 9376, 12,150, and 6362 yuan/hm^2. At different levels of phosphate addition, the low, medium, and high phosphate fertilizer treatments raised the yield by 67%, 85%, and 45% and the economic revenue by 9376, 12,150, and 6362 yuan/hm^2, respectively, in comparison to no phosphate fertilizer. When low, medium, and high potassium fertilizers were applied at different levels of alkaline addition, the yield and economic income increased by 45%, 85%, and 20%, respectively, and by 7275, 12,150, and 3263 yuan/hm^2, in comparison to no potassium fertilizer. Balanced application of nitrogen, phosphorus, and potassium fertilizer significantly impacts yield formation.

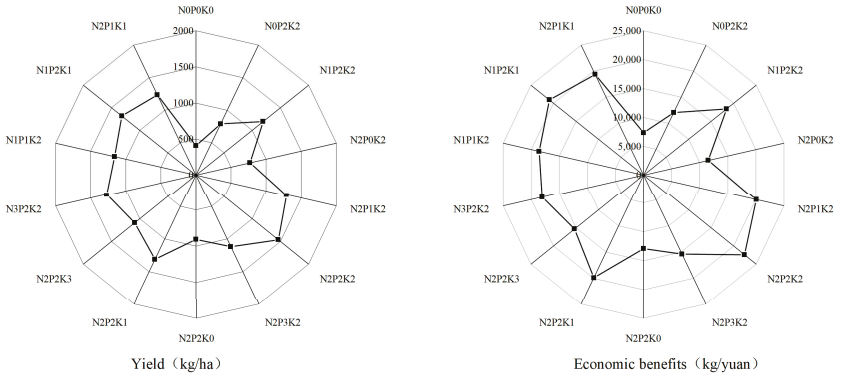

Figure 3. Yield and economic benefit of *Sapindus mukorossi* under different fertilization treatments.

3.4. Relationships Between Bacterial Communities, Sapindus mukorossi Yield and Soil Properties

There were correlations between bacterial community α-diversity (species richness, Simpson and Shannon indices), yield, and soil environmental factors (Table 4). Soil pH and total phosphorus content were significant factors ($p < 0.05$) affecting bacterial community α-diversity, where soil pH was positively correlated with species richness, Simpson, and Shannon indices, while total phosphorus was negatively correlated with all three. Except for total potassium and quick-acting potassium content, all other soil property indicators were significantly correlated ($p < 0.05$) with fruit yield of *Sapindus mukorossi*, where pH was negatively correlated with yield and the rest of the nutrient contents were positively correlated with yield.

Table 4. Relationship between bacterial community diversity, fruit yield, and soil environmental factors.

	pH	TN	TP	TK	SOC	AN	AP	AK
OTU richness	0.336 *	0.110	−0.345 *	−0.097	−0.211	−0.047	−0.109	0.288
Simpson	0.542 **	−0.062	−0.532 **	−0.248	−0.200	−0.172	−0.349 *	0.126
Shannon	0.484 **	0.044	−0.445 **	−0.149	−0.185	−0.036	−0.275	0.331 *
Yield	−0.699 **	0.645 **	0.634 **	0.405	0.699 **	0.773 **	0.707 **	0.378

Note: * indicates significant correlation at the 0.05 level; ** indicates significant correlation at the 0.01 level.

The relationship between bacterial community and soil physicochemical properties at the portal level was studied and analyzed by RDA, and the first axis explained 36.07% of the bacterial community, the second axis explained 7.54% of the bacterial community, and the two axes together explained 43.61% of the bacterial community (Figure 4a). On the first axis, the factors with significant correlation with bacterial community structure were pH, total potassium, organic carbon, total phosphorus and available phosphorus. The correlation between each soil factor and bacterial community structure on the second axis was not significant. The relative abundance of *Acidobacteriota*, *Verrucomicrobiota*, *Actinobacteriota*, *Planctomycetota* and *Chloroflexi* in the bacterial community were all positively correlated with soil pH. The relative abundance of *Firmicutes*, *Fusobacteriota* and *Bacteroidota* decreased with increasing pH, but exhibited a positive correlation with other soil environmental factors. As shown in Figure 4b, the soil environmental factors of pH, total potassium, and available phosphorus content all had a significant effect on the dominant phylum of soil microbial bacteria ($p < 0.05$).

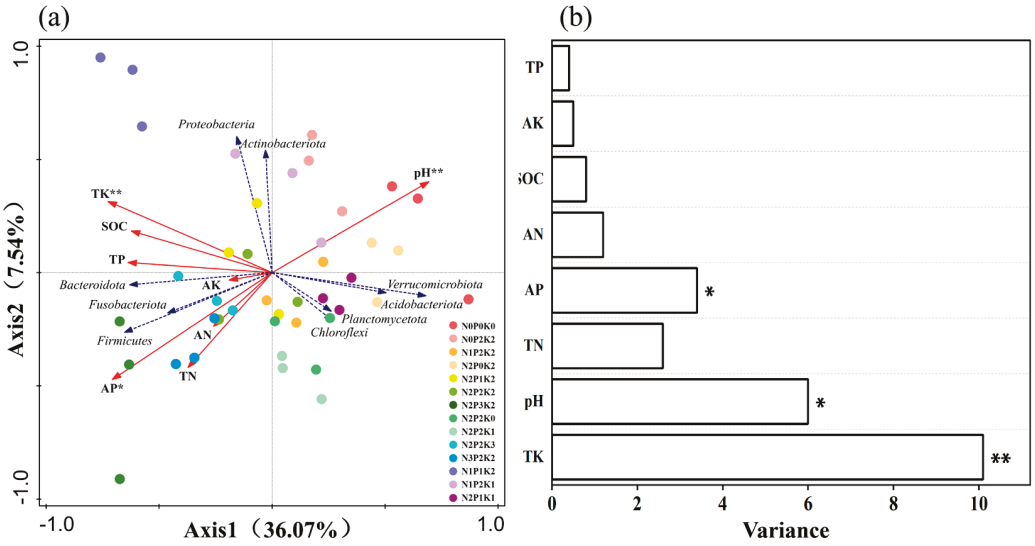

Figure 4. Biplot of the RDA analysis of soil bacterial communities under different fertilization treatments. (**a**) RDA analysis of bacterial communities. (**b**) Soil environmental factor parameter variables. Note: * is significant at the 0.05 level and ** is significant at the 0.01 level.

By correlating the relative abundance of the dominant phyla with soil environmental factors (Figure 5), it could be learned that *Fusobacteriota* and *Firmicutes* were all significantly negatively correlated with soil pH ($p < 0.05$), whereas there was a significant positive correlation ($p < 0.05$) with the contents of total phosphorus and available phosphorus ($p < 0.05$). Among them, *Firmicutes* and *Bacteroidota* were also significantly ($p < 0.05$) positively correlated with organic carbon content. Both *Acidobacteriota* and *Verrucomicrobiota* were significantly ($p < 0.05$) negatively correlated with total phosphorus, total potassium, available phosphorus, and organic carbon content. In addition, both *Acidobacteriota* and *Chloroflexi* showed a statistically significant positive correlation with soil pH ($p < 0.05$).

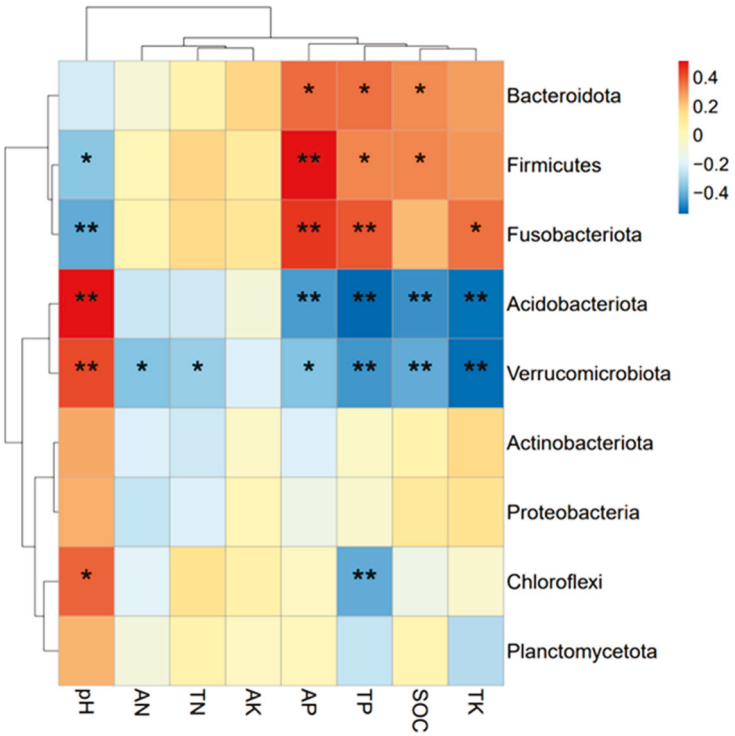

Figure 5. Correlation analysis between dominant bacteria and soil environmental factors. Note: * is significant at the 0.05 level and ** is significant at the 0.01 level.

3.5. Partial Least Squares Path Model (PLS-PM) Analysis

The relationship between NPK fertilization on *Sapindus mukorossi* yield, soil properties, soil community diversity, and community structure was analyzed based on PLS-PM (Figure 6a). In this model predicting *Sapindus mukorossi* yield, the variance attributed to soil properties was 0.67, soil bacterial diversity was 0.21, bacterial community structure was 0.57, and the goodness-of-fit index was 0.54 (Figure 6a). Fertilization had a direct positive effect on soil properties (0.82), as well as on soil bacterial community diversity (0.30) and community structure (0.002). Meanwhile, soil properties had a direct significant effect (0.93) on yield, while community diversity (0.14) and community structure (−0.05) contributed less to the variation in *Sapindus mukorossi* yield. In addition, the indirect effect of nitrogen, phosphorus, and potassium fertilization on *Sapindus mukorossi* yield was 0.71, while the direct effect by soil properties was 0.93 (Figure 6b). Overall, soil nutrient content was the direct driver of *Sapindus mukorossi* yield, while bacterial community diversity and structure did not significantly affect yield.

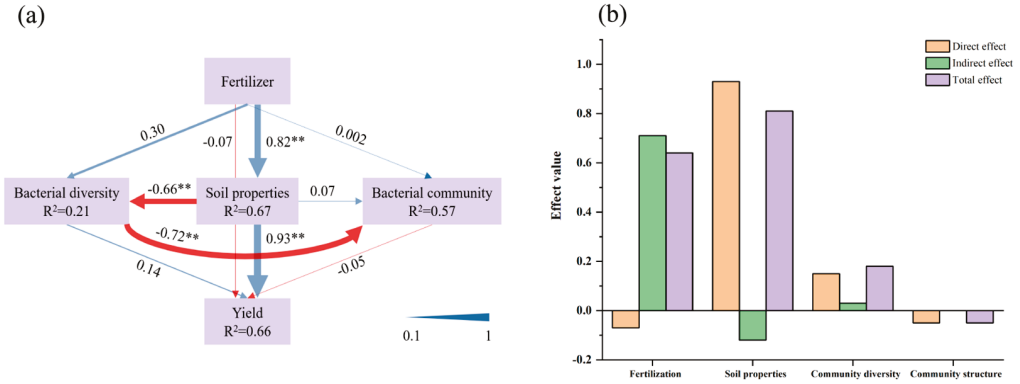

Figure 6. (**a**) Direct and indirect effects of fertilizer, soil properties, and bacterial attributes on the *Sapindus mukorossi* yield. (**b**) Overall effects of fertilization, *Sapindus mukorossi* soil properties, community diversity, and structure on yield. Note: Soil properties refer to total nitrogen, available nitrogen, total phosphorus, available phosphorus, total potassium, quick-acting potassium, organic carbon content, and pH; bacterial diversity is OTU richness, Shannon index, and Simpson index; and community structure is the first two axes of principal components (PC_1 and PC_2). The numbers on the arrows are standardized path coefficients, with blue arrows indicating positive effects and red arrows indicating negative effects. Path coefficients and coefficients of determination (R^2) were derived after 999 bootstrapping attempts. R^2 values indicate the variance explained by the model. The model was evaluated using the goodness-of-fit statistic, which is a measure of overall predictive performance. Significance is indicated by different path coefficients, ** $p < 0.01$.

4. Discussion

4.1. Effect of Fertilization on Soil Properties

The study revealed that augmenting nitrogen application on the basis of P_2K_2 and phosphorus application on the basis of N_2K_2 notably decreased soil pH, likely due to the urea treatment exacerbating soil acidification [30]. During the oxidation process of NH^{4+}, H^+ is released back into the soil, exchanging cations that are absorbed by plants, thereby accelerating soil acidification [30–32]. $N_2P_2K_2$ fertilization treatment is more efficient in increasing soil nutrient content, especially the content of soil available nutrients, which is at a lower level when the nitrogen application is too low or too high. A certain degree of N addition has a positive effect on soil fertilization and can accelerate the decomposition of soil organic matter [33–35]. Some studies have shown that the application of N, P, and K in pairs or individually can promote plant root growth and increase the input of inter-root organic matter, which in turn increases the organic carbon content [36,37]. However, excessive fertilizer application resulted in a decrease in the overall amount of organic carbon,

which could be because excessive fertilizer application can speed up the biodegradation of organic carbon sources by altering the quantity and activity of soil microorganisms [35]. In this study, it was found that the soil total and available nitrogen contents showed an increase and then a decrease trend with the increase in nitrogen application, which was inconsistent with the results of Qiao et al. [36] and could be explained by the theory of "stoichiometric decomposition" proposed by Hessen et al. [38]. The stoichiometric imbalance after adding nitrogen has been proven to accelerate the decomposition of soil organic carbon to maintain soil carbon/nitrogen ratios, with decomposition rates and microbial activity being highest when carbon and nitrogen inputs corresponded to microbial stoichiometric carbon to nitrogen ratios [39,40]. In a previous study conducted in energy forests, N additions accompanied by meeting the needs of microbial growth and stimulating the mineralization of native soil organic matter as well as the release of reactive N during nitrification, denitrification, and leaching [31]. This highlights the importance of rational application of nitrogen fertilizers.

4.2. Effect of Fertilizer Application on Soil Bacterial Communities

Soil microorganisms play an important role in both energy flow and nutrient cycling processes in the soil, and the richer the soil microbial species, the greater the plant resistance to diseases [41,42]. Meanwhile, soil microorganisms can reflect soil fertility and its quality status, and changes in their diversity and activity can also indicate soil health [43]. However, in this study, it was found that the application of nitrogen fertilizer at low versus moderate levels was beneficial in increasing the bacterial community diversity, while excessive nitrogen additions instead decreased the bacterial community diversity. Consistent with the results of most previous studies, N addition could significantly affect bacterial community diversity, but excessive nitrogen fertilization reduced the number of species in the soil microbial community, which may be due to the fact that the high nitrogen environment is more favorable for some nitrogen-loving microorganisms, but their microbial metabolisms still showed a general decreasing trend [44,45]. The reduction in species diversity resulting from nitrogen enrichment poses a risk to ecosystem stability and can disrupt interactions between above- and below-ground ecosystems. Furthermore, phosphorus addition not only boosts microbial biomass but also modifies the makeup of soil microbial communities [46]. We further found that nitrogen addition and phosphorus addition led to significant changes in the diversity of bacterial communities in the soil, while there was no significant difference in the effect of potassium fertilization on bacterial community diversity (Table 3). Our results were consistent with those of previous authors [14,21], with nitrogen deficiency having the greatest effect on bacterial community structure and composition, phosphorus deficiency having the greatest effect on network construction and bacterial activity, and potassium deficiency having the least effect. In our experiment, bacterial community diversity showed an increasing and then decreasing trend with increasing N, P, and K fertilization (Table 3), suggesting that lower nutrient inputs may lead to higher plant abundance, which may result in a homogenizing effect on the soil bacterial community, and vice versa. Some studies have found that the application of N, P, and K fertilizers had no or a positive effect on bacterial communities [45,47,48]. The inconsistent results of these studies may be due to different durations and doses of applied N [42,49].

In addition, the reduction in bacterial diversity may also be related to host plant characteristics, as the organs of *Sapindus mukorossi* have a certain saponin content [50,51]. which has strong bacteriostatic activity, and it has been noted that it significantly inhibits the growth of *Staphylococcus aureus* [51], *Bacillus subtilis* [50], *Bacillus cereus* [52], *Escherichia coli* [50,53], and other microbial taxa. Our previous study found that fertilization significantly increased the saponin content of *Sapindus mukorossi*, further confirming that saponin may be a potential

factor affecting bacterial activity [53]. In addition, in the process of *Sapindus mukorossi* cultivation, weeds and pests are easy to grow, and inevitably a certain amount of pesticides needs to be sprayed, which may indirectly affect the root secretion or directly inhibit the reproduction of certain microorganisms in the soil [54,55].

Fertilization, herbicides, and external environmental changes are the main factors that hinder natural selection in cash crops [54]. Fertilization significantly affected soil microbial community composition [56]. In this study, the first dominant phylum was *Ascomycetes*, which is mainly involved in soil nutrient regulation and has a major impact on soil nutrient cycling, although *Ascomycetes* varied with different levels of fertilization and crop selection [54]. Our finding aligns with previous studies that fertilization increases the relative abundance of *Ascomycetes* [44,45]. The relative abundance of *Acidobacteriota*, a typical nutrient-poor taxon, was highest in the $N_1P_2K_2$ treatment [57]. The organic carbon pool in the soil can be increased by fertilizer application to give the soil a higher nutrient affinity, and high soil fertility can drive the shift from nutrient-poor to eutrophic taxa in the bacterial community, resulting in superior soil conditions, which consequently increased community diversity and intensified competition [58]. From the perspective of fertilization, the increase in nitrogen application can change the soil nitrogen content and thereafter affect the distribution of the soil bacterial community or indirectly affect the structure of the soil bacterial community by changing the pH value of the soil, the content of organic carbon, and the soil carbon and nitrogen ratio, etc. [49,58,59].

4.3. Soil Bacterial Communities in Relation to Environmental Factors

To date, there is sufficient evidence that soil physicochemical factors such as SOC, TP, TN, AP, AN, and AK are enhanced by bacterial diversity, while other fertilizers can ameliorate soil acidification to some extent [60]. According to the results of RDA analysis, soil environmental factors play a major role in microbial community structure, and this result has been confirmed by a large number of studies [18,61]. We found that soil pH, available phosphorus, and total potassium were the main environmental factors affecting the distribution of bacterial microbial communities, accounting for 80% of the variation in the composition of community structure (Figure 4b). It is generally accepted that soil pH is often considered the main factor regulating soil bacterial communities, and bacteria are very sensitive to soil pH, with lower pH soils being accompanied by aluminum toxicity and nutrient leaching, which negatively affects bacterial growth [62]. Microbial communities typically thrive more vigorously in neutral or slightly alkaline environments [62], whereas they tend to grow poorly in conditions of low pH [63]. This may be due to the fact that a strongly acidic environment inhibits enzyme activity and whole cell metabolism [62,64]. This is in agreement with our results that the number of *Acidobacteriota* and *Chloroflexi* were significantly and positively correlated with pH. In addition, changes in soil pH were also produced during fertilization, suggesting that different fertilization treatments can alter soil bacterial habitat conditions, thus causing changes in soil microbial community structure. For example, fertilizer application caused a decrease in alkaline cations and an increase in acidic cations. This is consistent with the observations of Chen et al. [65].

Available phosphorus in soil has a significant effect on bacterial communities. Phosphorus is essential for the synthesis of RNA, DNA, and ATP, and the source of nutrients plays a crucial role in bacterial growth [19]. Soil microorganisms are key regulators of soil phosphorus mobilization and transformation, and they enhance soil phosphorus effectiveness through inorganic phosphorus solubilization and organic phosphorus mineralization through the regulation of phosphorus cycling genes and phosphatase expression [18]. Fertilizer management can provide a suitable environment for soil microbial growth by stimulating microbial activity [66,67]. We found that the numbers of *Fusobacteriota*, *Firmi-*

cutes, and *Bacteroidota* were significantly and positively correlated with total and available phosphorus after fertilization. This indicates that different fertilization treatments cause changes in microbial nutrient sources, which in turn affects the distribution of bacterial communities. This is further evidenced by the fact that balanced application of NPK improves soil fertility while promoting soil ecosystem stability and health. Therefore, fertilizer application and soil microbial activity are frequently studied in these studies, but there is still a need to assess the optimal application rate of NPK fertilizers.

4.4. Fertilizer Application Affects the Sapindus mukorossi Yield by Influencing Soil Properties Rather Bacteria

Soil microbial diversity is positively correlated with biotic and abiotic stress resistance and nutrient cycling rates, as well as increasing plant productivity through selective effects or complementarity, but soil properties and plant production do not always increase with increased microbial community diversity and structure [68]. After fertilization, fertilizers may be absorbed and utilized by plants or remain in the soil, leading to changes in protists [69], bacteria [70], and fungal communities [59]. Therefore, the increase in plant yield after fertilization may be related to the physical, chemical, and biological properties of the soil. According to PLS-PM analysis in this study, NPK fertilization had a direct effect on *Sapindus mukorossi* yield with a direct path coefficient of −0.07, which could be attributed to the fact that fertilization provided essential nutrients for *Sapindus mukorossi* growth. However, the path coefficient of the indirect effect of fertilizer application on *Sapindus mukorossi* yield (0.74) was significantly higher than the direct effect (Figure 6b), mainly due to nutrient variation in soil properties (0.93) (Figure 6a), suggesting a preliminary role of soil nutrient content in driving the yield. More importantly, nitrogen, phosphorus, and pH in the soil were the most important key factors affecting the yield (Table 4). This is similar to the results of Lv et al. [16], where phosphorus level in the soil was the limiting factor for crop yield. Soil nutrient levels, especially total nutrient levels, are the main cause of variation in crop yield, while bacteria indirectly affect yield through enzyme activities and nutrient levels [71]. In this study, high nitrogen, phosphorus, and potassium treatments resulted in lower pH and caused soil acidification, hindering bacterial diversity. This is due to the fact that fertilizer application provides the N, P, and K sources needed for soil microbial growth; therefore, the change in soil pH caused by nitrogen, phosphorus, and potassium application is the main reason for the diversity of microbial communities. Furthermore, excessive fertilizer application can cause significant soil erosion, disrupting the balance of soil nutrient structure. This imbalance, in turn, hinders the growth and development of plant roots, diminishes their capacity to absorb nutrients and water, and ultimately results in decreased crop yields [21]. Fertilization also had a direct effect on soil bacterial diversity with a path coefficient of 0.30, and soil properties had a significant direct effect on soil microbial diversity with a path coefficient of −0.66, suggesting that a shift in the diversity of microbial communities was driven by the soil environmental factors under the different fertilization treatments.

Interestingly, according to the PLS-PM results, soil microbial diversity and community structure had little direct effect on *Sapindus mukorossi* yield, with direct path coefficients of 0.15 and −0.05, respectively (Figure 6a), which is in agreement with the results of Ma et al. [39]. This further confirmed the fact that crop growth was mainly influenced by soil fertility. Therefore, soil nutrients become a key environmental factor influencing microbial community succession and yield enhancement [59,68,72], and a balanced fertilization pattern provides a relatively balanced nutrient environment. Our results suggest that the $N_2P_2K_2$ treatment maximizes *Sapindus mukorossi* yield and maintains soil health and bacterial microbial diversity.

5. Conclusions

In this study, we investigated the response of soil nutrients and bacterial communities to balanced fertilization with nitrogen, phosphorus, and potassium and their correlations with the yield of *Sapindus mukorossi* in raw material forests of *Sapindus mukorossi*. Different fertilization treatments had significant effects on soil acidity (pH) and nutrient content. The addition of nitrogen or phosphorus led to an increase in the degree of soil acidification, which would lead to the accelerated decomposition of organic carbon in the soil. Fertilization with combinations of nitrogen (N), phosphorus (P), and potassium (K) can significantly change soil bacterial community structure and improve microbial diversity in *Sapindus mukorossi* forests by changing soil properties, but the changes in bacterial community structure and diversity did not significantly affect *Sapindus mukorossi* yield. The primary determinants influencing *Sapindus mukorossi* output under fertilization treatments were variations in soil nutrients, particularly N and P concentrations. However, we believe that more research is necessary to examine how the fertilization treatments affect the functions of the microbial community and how this can affect future *Sapindus mukorossi* yield. In order to increase soil productivity and lower environmental pollution, scientific fertilizer application strategies should be established, given that soil parameters have a substantial impact on the structure of bacterial communities. Meanwhile the research holds broader implications for sustainable agriculture and soil health management.

Author Contributions: J.L. and L.J. conceived the research and designed the experiments; J.L. and L.J. wrote the manuscript; J.L. and Y.G. analyzed the data; L.Z. and W.Z. performed the experiments; J.L., L.J., Z.Y. and J.C. modified the language and revised the manuscript. All authors have read and agreed to the published version of the manuscript.

Funding: This work was supported by the National Natural Science Foundation of China (No. 32071793) and the Special Foundation for National Science and Technology Basic Research Program of China (No. 2019FY100803).

Institutional Review Board Statement: Not applicable.

Informed Consent Statement: Not applicable.

Data Availability Statement: The original contributions presented in the study are included in the article material, further inquiries can be directed to the corresponding authors.

Acknowledgments: We sincerely thank Shui Jing Luo for his tending of the plants. We are also grateful to Shi Xiong Wu and Yi Yong Chen for their guidance in the experiment. We gratefully acknowledge the assistance of Xiaoli Yan and Yuanyuan Xu in this study.

Conflicts of Interest: The research was conducted in the absence of any commercial or financial relationships that could be construed as a potential conflict of interest.

References

1. Xu, Y.; Gao, Y.; Chen, Z.; Zhao, G.; Liu, J.; Wang, X.; Gao, S.; Zhang, D.; Jia, L. Metabolomics analysis of the soapberry (*Sapindus mukorossi* Gaertn.) pericarp during fruit development and ripening based on UHPLC-HRMS. *Sci. Rep.* **2021**, *11*, 11657. [CrossRef] [PubMed]
2. Liu, J.; Xu, Y.; Sun, C.; Wang, X.; Zheng, Y.; Shi, S.; Chen, Z.; He, Q.; Weng, X.; Jia, L. Distinct ecological habits and habitat responses to future climate change in three east and southeast Asian Sapindus species. *Forest Ecol. Manag.* **2022**, *507*, 119982. [CrossRef]
3. Gao, Y.; Gao, S.; Jia, L.; Dai, T.; Wei, X.; Duan, J.; Liu, S.; Weng, X. Canopy characteristics and light distribution in *Sapindus mukorossi* Gaertn. are influenced by crown architecture manipulation in the hilly terrain of Southeast China. *Sci. Hortic.* **2018**, *240*, 11–22. [CrossRef]
4. Xu, Y.; Liu, J.; Ji, X.; Zhao, G.; Zhao, T.; Wang, X.; Wang, L.; Gao, S.; Hao, Y.; Gao, Y.; et al. Integrative analysis of microRNAs and mRNAs reveals the regulatory networks of triterpenoid saponin metabolism in Soapberry (*Sapindus mukorossi* Gaertn.). *Front. Plant Sci.* **2023**, *13*, 1037784. [CrossRef] [PubMed]

5. Wang, X.; Zhang, R.; Yun, Q.; Xu, Y.; Zhao, G.; Liu, J.; Shi, S.; Chen, Z.; Jia, L. Comprehensive analysis of complete mitochondrial genome of *Sapindus mukorossi* Gaertn.: An important industrial oil tree species in China. *Ind. Crop Prod.* **2021**, *174*, 114210. [CrossRef]
6. Sun, J.; Luo, H.; Yu, Q.; Kou, B.; Jiang, Y.; Weng, L.; Xiao, C. Optimal NPK Fertilizer Combination Increases *Panax ginseng* Yield and Quality and Affects Diversity and Structure of Rhizosphere Fungal Communities. *Front. Microbiol.* **2022**, *13*, 919434. [CrossRef]
7. Li, Z.; Zhang, R.; Xia, S.; Wang, L.; Liu, C.; Zhang, R.; Fan, Z.; Chen, F.; Liu, Y. Interactions between N, P and K fertilizers affect the environment and the yield and quality of satsumas. *Glob. Ecol. Conserv.* **2019**, *19*, e00663. [CrossRef]
8. Liu, J.; Wang, D.; Yan, X.; Jia, L.; Chen, N.; Liu, J.; Zhao, P.; Zhou, L.; Cao, Q. Effect of nitrogen, phosphorus and potassium fertilization management on soil properties and leaf traits and yield of *Sapindus mukorossi*. *Front. Plant Sci.* **2024**, *15*, 1300683. [CrossRef]
9. Liu, J.T.; Zhou, L.; Wang, D.N.; Gong, Y.Y.; Yan, X.L.; Cao, Q.L.; Wu, S.X.; Weng, J.H.; Zhang, G.Q.; Jia, L.M. The Effect of Balanced N, P and K Fertilization on Fine Root Traits and Soil Properties in *Sapindus mukorossi*. *Forests* **2024**, *15*, 94. [CrossRef]
10. Luo, X.; Fu, X.; Yang, Y.; Cai, P.; Peng, S.; Chen, W.; Huang, Q. Microbial communities play important roles in modulating paddy soil fertility. *Sci. Rep.* **2016**, *6*, 20326. [CrossRef]
11. Xue, C.; Zhang, T.; Yao, S.; Guo, Y. Effects of Households' Fertilization Knowledge and Technologies on Over-Fertilization: A Case Study of Grape Growers in Shaanxi, China. *Land* **2020**, *9*, 321. [CrossRef]
12. Zhang, M.; Sun, D.; Niu, Z.; Yan, J.; Zhou, X.; Kang, X. Effects of combined organic/inorganic fertilizer application on growth, photosynthetic characteristics, yield and fruit quality of *Actinidia chinesis* cv 'Hongyang'. *Glob. Ecol. Conserv.* **2020**, *22*, e00997. [CrossRef]
13. Shi, L.; Zheng, W.; Lei, T.; Liu, X.; Hui, M. The Effect of Different Soil Amendments on Soil Properties and on the Morphological and Physiological Characteristics of Chinese Cabbage. *J. Soil Sci. Plant Nutr.* **2021**, *21*, 1500–1510. [CrossRef]
14. Ma, L.; Zhao, B.; Guo, Z.; Wang, D.; Li, D.; Xu, J.; Li, Z.; Zhang, J. Divergent responses of bacterial activity, structure, and co-occurrence patterns to long-term unbalanced fertilization without nitrogen, phosphorus, or potassium in a cultivated vertisol. *Environ. Sci. Pollut. Res.* **2019**, *26*, 12741–12754. [CrossRef]
15. Ren, N.; Wang, Y.; Ye, Y.; Zhao, Y.; Huang, Y.; Fu, W.; Chu, X. Effects of Continuous Nitrogen Fertilizer Application on the Diversity and Composition of Rhizosphere Soil Bacteria. *Front. Microbiol.* **2020**, *11*, 1948. [CrossRef] [PubMed]
16. Lv, M.; Li, Z.; Che, Y.; Han, F.X.; Liu, M. Soil organic C, nutrients, microbial biomass, and grain yield of rice (*Oryza sativa* L.) after 18 years of fertilizer application to an infertile paddy soil. *Biol. Fert. Soils* **2011**, *47*, 777–783. [CrossRef]
17. Banerjee, S.; Schlaeppi, K.; van der Heijden, M.G.A. Keystone taxa as drivers of microbiome structure and functioning. *Nat. Rev. Microbiol.* **2018**, *16*, 567–576. [CrossRef]
18. Yan, T.; Xue, J.; Zhou, Z.; Wu, Y. Biochar-based fertilizer amendments improve the soil microbial community structure in a karst mountainous area. *Sci. Total Environ.* **2021**, *794*, 148757. [CrossRef]
19. Tian, J.; He, N.; Kong, W.; Deng, Y.; Feng, K.; Green, S.M.; Wang, X.; Zhou, J.; Kuzyakov, Y.; Yu, G. Deforestation decreases spatial turnover and alters the network interactions in soil bacterial communities. *Soil Biol. Biochem.* **2018**, *123*, 80–86. [CrossRef]
20. Kamaa, M.; Mburu, H.; Blanchart, E.; Chibole, L.; Chotte, J.; Kibunja, C.; Lesueur, D. Effects of organic and inorganic fertilization on soil bacterial and fungal microbial diversity in the Kabete long-term trial, Kenya. *Biol. Fert. Soils* **2011**, *47*, 315–321. [CrossRef]
21. Eo, J.; Park, K. Long-term effects of imbalanced fertilization on the composition and diversity of soil bacterial community. *Agric. Ecosyst. Environ.* **2016**, *231*, 176–182. [CrossRef]
22. Tamilselvi, S.M.; Chinnadurai, C.; Ilamurugu, K.; Arulmozhiselvan, K.; Balachandar, D. Effect of long-term nutrient managements on biological and biochemical properties of semi-arid tropical Alfisol during maize crop development stages. *Ecol. Indic.* **2015**, *48*, 76–87. [CrossRef]
23. Ma, W.; Jiang, S.; Assemien, F.; Qin, M.; Ma, B.; Xie, Z.; Liu, Y.; Feng, H.; Du, G.; Ma, X.; et al. Response of microbial functional groups involved in soil N cycle to N, P and NP fertilization in Tibetan alpine meadows. *Soil Biol. Biochem.* **2016**, *101*, 195–206. [CrossRef]
24. Tang, Y.; Zhang, X.; Li, D.; Wang, H.; Chen, F.; Fu, X.; Fang, X.; Sun, X.; Yu, G. Impacts of nitrogen and phosphorus additions on the abundance and community structure of ammonia oxidizers and denitrifying bacteria in Chinese fir plantations. *Soil Biol. Biochem.* **2016**, *103*, 284–293. [CrossRef]
25. Liu, C.; Gong, X.; Dang, K.; Li, J.; Yang, P.; Gao, X.; Deng, X.; Feng, B. Linkages between nutrient ratio and the microbial community in rhizosphere soil following fertilizer management. *Environ. Res.* **2020**, *184*, 109261. [CrossRef] [PubMed]
26. Liu, H.; Li, S.; Qiang, R.; Lu, E.; Li, C.; Zhang, J.; Gao, Q. Response of Soil Microbial Community Structure to Phosphate Fertilizer Reduction and Combinations of Microbial Fertilizer. *Front. Environ. Sci.* **2022**, *10*, 899727. [CrossRef]
27. Liu, K.; Chen, B.; Zhang, B.; Wang, R.; Wang, C. Understory vegetation diversity, soil properties and microbial community response to different thinning intensities in *Cryptomeria japonica* var. *sinensis* plantations. *Front. Microbiol.* **2023**, *14*, 1117384. [CrossRef] [PubMed]

28. Ihtisham, M.; Fahad, S.; Luo, T.; Larkin, R.M.; Yin, S.; Chen, L. Optimization of Nitrogen, Phosphorus, and Potassium Fertilization Rates for Overseeded Perennial Ryegrass Turf on Dormant Bermudagrass in a Transitional Climate. *Front. Plant Sci.* **2018**, *9*, 487. [CrossRef] [PubMed]
29. Ma, Q.; Kuzyakov, Y.; Pan, W.; Tang, S.; Chadwick, D.R.; Wen, Y.; Hill, P.W.; Macdonald, A.; Ge, T.; Si, L.; et al. Substrate control of sulphur utilisation and microbial stoichiometry in soil: Results of ^{13}C, ^{15}N, ^{14}C, and ^{35}S quad labelling. *ISME J.* **2021**, *15*, 3148–3158. [CrossRef]
30. Tian, D.; Niu, S. A global analysis of soil acidification caused by nitrogen addition. *Environ. Res. Lett.* **2015**, *10*, 024019. [CrossRef]
31. Tang, S.; Ma, Q.; Luo, J.; Xie, Y.; Hashmi, M.L.U.R.; Pan, W.; Zheng, N.; Liu, M.; Wu, L. The inhibition effect of tea polyphenols on soil nitrification is greater than denitrification in tea garden soil. *Sci. Total Environ.* **2021**, *778*, 146328. [CrossRef] [PubMed]
32. Li, Y.; Tremblay, J.; Bainard, L.D.; Cade-Menun, B.; Hamel, C. Long-term effects of nitrogen and phosphorus fertilization on soil microbial community structure and function under continuous wheat production. *Environ. Microbiol.* **2020**, *22*, 1066–1088. [CrossRef]
33. Yang, X.; Ni, K.; Shi, Y.; Yi, X.; Zhang, Q.; Fang, L.; Ma, L.; Ruan, J. Effects of long-term nitrogen application on soil acidification and solution chemistry of a tea plantation in China. *Agric. Ecosyst. Environ.* **2018**, *252*, 74–82. [CrossRef]
34. Kumar, U.; Shahid, M.; Tripathi, R.; Mohanty, S.; Kumar, A.; Bhattacharyya, P.; Lal, B.; Gautam, P.; Raja, R.; Panda, B.B.; et al. Variation of functional diversity of soil microbial community in sub-humid tropical rice-rice cropping system under long-term organic and inorganic fertilization. *Ecol. Indic.* **2017**, *73*, 536–543. [CrossRef]
35. Chen, C.; Hall, S.J.; Coward, E.; Thompson, A. Iron-mediated organic matter decomposition in humid soils can counteract protection. *Nat. Commun.* **2020**, *11*, 2255. [CrossRef] [PubMed]
36. Qiao, C.; Xu, B.; Han, Y.; Wang, J.; Wang, X.; Liu, L.; Liu, W.; Wan, S.; Tan, H.; Liu, Y.; et al. Synthetic nitrogen fertilizers alter the soil chemistry, production and quality of tea. A meta-analysis. *Agron. Sustain. Dev.* **2018**, *38*, 10. [CrossRef]
37. Feng, J.; Tang, M.; Zhu, B. Soil priming effect and its responses to nutrient addition along a tropical forest elevation gradient. *Glob. Change Biol.* **2021**, *27*, 2793–2806. [CrossRef]
38. Hessen, D.O.; Agren, G.I.; Anderson, T.R.; Elser, J.J.; De Ruiter, P.C. Carbon, sequestration in ecosystems: The role of stoichiometry. *Ecology* **2004**, *85*, 1179–1192. [CrossRef]
39. Ma, L.; Yang, X.; Shi, Y.; Yi, X.; Ji, L.; Cheng, Y.; Ni, K.; Ruan, J. Response of tea yield, quality and soil bacterial characteristics to long-term nitrogen fertilization in an eleven-year field experiment. *Appl. Soil Ecol.* **2021**, *166*, 103976. [CrossRef]
40. Chen, R.; Senbayram, M.; Blagodatsky, S.; Myachina, O.; Dittert, K.; Lin, X.; Blagodatskaya, E.; Kuzyakov, Y. Soil C and N availability determine the priming effect: Microbial N mining and stoichiometric decomposition theories. *Glob. Change Biol.* **2014**, *20*, 2356–2367. [CrossRef]
41. Li, Z.; Zeng, Z.; Song, Z.; Wang, F.; Tian, D.; Mi, W.; Huang, X.; Wang, J.; Song, L.; Yang, Z.; et al. Vital roles of soil microbes in driving terrestrial nitrogen immobilization. *Glob. Change Biol.* **2021**, *27*, 1848–1858. [CrossRef] [PubMed]
42. Hartmann, M.; Frey, B.; Mayer, J.; Maeder, P.; Widmer, F. Distinct soil microbial diversity under long-term organic and conventional farming. *ISME J.* **2015**, *9*, 1177–1194. [CrossRef]
43. Geisseler, D.; Scow, K.M. Long-term effects of mineral fertilizers on soil microorganisms—A review. *Soil Biol. Biochem.* **2014**, *75*, 54–63. [CrossRef]
44. Wang, C.; Liu, D.; Bai, E. Decreasing soil microbial diversity is associated with decreasing microbial biomass under nitrogen addition. *Soil Biol. Biochem.* **2018**, *120*, 126–133. [CrossRef]
45. Ramirez, K.S.; Lauber, C.L.; Knight, R.; Bradford, M.A.; Fierer, N. Consistent effects of nitrogen fertilization on soil bacterial communities in contrasting systems. *Ecology* **2010**, *91*, 3463–3470. [CrossRef] [PubMed]
46. Cheng, H.; Yuan, M.; Duan, Q.; Sun, R.; Shen, Y.; Yu, Q.; Li, S. Influence of phosphorus fertilization patterns on the bacterial community in upland farmland. *Ind. Crop Prod.* **2020**, *155*, 112761. [CrossRef]
47. Yuan, H.; Ge, T.; Zhou, P.; Liu, S.; Roberts, P.; Zhu, H.; Zou, Z.; Tong, C.; Wu, J. Soil microbial biomass and bacterial and fungal community structures responses to long-term fertilization in paddy soils. *J. Soils Sediment.* **2013**, *13*, 877–886. [CrossRef]
48. Wang, J.; Xue, C.; Song, Y.; Wang, L.; Huang, Q.; Shen, Q. Wheat and Rice Growth Stages and Fertilization Regimes Alter Soil Bacterial Community Structure, But Not Diversity. *Front. Microbiol.* **2016**, *7*, 1207. [CrossRef]
49. Zhang, J.; Ai, Z.; Liang, C.; Wang, G.; Xue, S. Response of soil microbial communities and nitrogen thresholds of *Bothriochloa ischaemum* to short-term nitrogen addition on the Loess Plateau. *Geoderma* **2017**, *308*, 112–119. [CrossRef]
50. Wei, M.; Yu, H.; Guo, Y.; Cheng, Y.; Xie, Y.; Yao, W. Antibacterial activity of Sapindus saponins against microorganisms related to food hygiene and the synergistic action mode of Sapindoside A and B against Micrococcus luteus in vitro. *Food Control* **2021**, *130*, 108337. [CrossRef]
51. Huang, X.; Liu, W.; Dong, F.; Xu, Y.; Tian, S.; Chen, T. *Sapindus mukorossi* saponins inhibit gray mold on strawberry fruit by impairing membrane integrity and organellar homeostasis of Botrytis cinerea. *Postharvest Biol. Tec.* **2024**, *207*, 112594. [CrossRef]

52. Elouafy, Y.; El Yadini, A.; Mortada, S.; Hnini, M.; Harhar, H.; Khalid, A.; Abdalla, A.N.; Bouyahya, A.; Goh, K.W.; Ming, L.C.; et al. Antioxidant, antimicrobial, and a-glucosidase inhibitory activities of saponin extracts from walnut (*Juglans regia* L.) leaves. *Asian Pac. J. Trop. Biomed.* **2023**, *13*, 60–69. [CrossRef]
53. Xia, P.; Guo, H.; Zhao, H.; Jiao, J.; Deyholos, M.K.; Yan, X.; Liu, Y.; Liang, Z. Optimal fertilizer application for *Panax notoginseng* and effect of soil water on root rot disease and saponin contents. *J. Ginseng Res.* **2016**, *40*, 38–46. [CrossRef]
54. Spain, A.M.; Krumholz, L.R.; Elshahed, M.S. Abundance, composition, diversity and novelty of soil *Proteobacteria*. *ISME J.* **2009**, *3*, 992–1000. [CrossRef] [PubMed]
55. Fierer, N.; Bradford, M.A.; Jackson, R.B. Toward an ecological classification of soil bacteria. *Ecology* **2007**, *88*, 1354–1364. [CrossRef] [PubMed]
56. Zhou, J.; Guan, D.; Zhou, B.; Zhao, B.; Ma, M.; Qin, J.; Jiang, X.; Chen, S.; Cao, F.; Shen, D.; et al. Influence of 34-years of fertilization on bacterial communities in an intensively cultivated black soil in northeast China. *Soil Biol. Biochem.* **2015**, *90*, 42–51. [CrossRef]
57. Mhete, M.; Eze, P.N.; Rahube, T.O.; Akinyemi, F.O. Soil properties influence bacterial abundance and diversity under different land-use regimes in semi-arid environments. *Sci. Afr.* **2020**, *7*, e00246. [CrossRef]
58. Zeng, J.; Liu, X.; Song, L.; Lin, X.; Zhang, H.; Shen, C.; Chu, H. Nitrogen fertilization directly affects soil bacterial diversity and indirectly affects bacterial community composition. *Soil Biol. Biochem.* **2016**, *92*, 41–49. [CrossRef]
59. Zhou, J.; Jiang, X.; Zhou, B.; Zhao, B.; Ma, M.; Guan, D.; Li, J.; Chen, S.; Cao, F.; Shen, D.; et al. Thirty four years of nitrogen fertilization decreases fungal diversity and alters fungal community composition in black soil in northeast China. *Soil Biol. Biochem.* **2016**, *95*, 135–143. [CrossRef]
60. Wang, Q.; Wang, C.; Yu, W.; Turak, A.; Chen, D.; Huang, Y.; Ao, J.; Jiang, Y.; Huang, Z. Effects of Nitrogen and Phosphorus Inputs on Soil Bacterial Abundance, Diversity, and Community Composition in Chinese Fir Plantations. *Front. Microbiol.* **2018**, *9*, 1543. [CrossRef]
61. Xu, L.; Yi, M.; Yi, H.; Guo, E.; Zhang, A. Manure and mineral fertilization change enzyme activity and bacterial community in millet rhizosphere soils. *World J. Microb. Biot.* **2018**, *34*, 8. [CrossRef] [PubMed]
62. Rousk, J.; Brookes, P.C.; Baath, E. Contrasting Soil pH Effects on Fungal and Bacterial Growth Suggest Functional Redundancy in Carbon Mineralization. *Appl. Environ. Microb.* **2009**, *75*, 1589–1596. [CrossRef]
63. Ji, L.; Wu, Z.; You, Z.; Yi, X.; Ni, K.; Guo, S.; Ruan, J. Effects of organic substitution for synthetic N fertilizer on soil bacterial diversity and community composition: A 10-year field trial in a tea plantation. *Agric. Ecosyst. Environ.* **2018**, *268*, 124–132. [CrossRef]
64. Beales, N. Adaptation of microorganisms to cold temperatures, weak acid preservatives, low pH, and osmotic stress: A review. *Compr. Rev. Food Sci. Saf.* **2004**, *3*, 1–20. [CrossRef]
65. Chen, L.; Zhang, J.; Zhao, B.; Zhou, G.; Ruan, L. Bacterial community structure in maize stubble-amended soils with different moisture levels estimated by bar-coded pyrosequencing. *Appl. Soil Ecol.* **2015**, *86*, 62–70. [CrossRef]
66. Bian, X.; Xiao, S.; Zhao, Y.; Xu, Y.; Yang, H.; Zhang, L. Comparative analysis of rhizosphere soil physiochemical characteristics and microbial communities between rusty and healthy ginseng root. *Sci. Rep.* **2020**, *10*, 15756. [CrossRef]
67. Yuste, J.C.; Baldocchi, D.D.; Gershenson, A.; Goldstein, A.; Misson, L.; Wong, S. Microbial soil respiration and its dependency on carbon inputs, soil temperature and moisture. *Glob. Change Biol.* **2007**, *13*, 2018–2035. [CrossRef]
68. Tang, S.; Pan, W.; Tang, R.; Ma, Q.; Zhou, J.; Zheng, N.; Wang, J.; Sun, T.; Wu, L. Effects of balanced and unbalanced fertilisation on tea quality, yield, and soil bacterial community. *Appl. Soil Ecol.* **2022**, *175*, 104442. [CrossRef]
69. Zhao, Z.; He, J.; Geisen, S.; Han, L.; Wang, J.; Shen, J.; Wei, W.; Fang, Y.; Li, P.; Zhang, L. Protist communities are more sensitive to nitrogen fertilization than other microorganisms in diverse agricultural soils. *Microbiome* **2019**, *7*, 33. [CrossRef] [PubMed]
70. Sun, R.; Dsouza, M.; Gilbert, J.A.; Guo, X.; Wang, D.; Guo, Z.; Ni, Y.; Chu, H. Fungal community composition in soils subjected to long-term chemical fertilization is most influenced by the type of organic matter. *Environ. Microbiol.* **2016**, *18*, 5137–5150. [CrossRef]
71. Liu, J.; Shu, A.; Song, W.; Shi, W.; Li, M.; Zhang, W.; Li, Z.; Liu, G.; Yuan, F.; Zhang, S.; et al. Long-term organic fertilizer substitution increases rice yield by improving soil properties and regulating soil bacteria. *Geoderma* **2021**, *404*, 115287. [CrossRef]
72. Tang, S.; Zhou, J.; Pan, W.; Sun, T.; Liu, M.; Tang, R.; Li, Z.; Ma, Q.; Wu, L. Effects of combined application of nitrogen, phosphorus, and potassium fertilizers on tea (*Camellia sinensis*) growth and fungal community. *Appl. Soil Ecol.* **2023**, *181*, 104661. [CrossRef]

microorganisms

MDPI

Article

Unlocking Nature's Microbial Defenders: Genetic Mechanisms and Potential Against *Monilinia* spp. Pathogens

Augustina Kolytaitė, Ingrida Mažeikienė *, Monika Kurgonaitė, Saulė Raklevičiūtė, Gabija Paškevičiūtė and Birutė Frercks

Institute of Horticulture, Lithuanian Research Centre for Agriculture and Forestry, Kaunas Str. 30, 54333 Babtai, Lithuania; augustina.kolytaite@lammc.lt (A.K.); monika.kurgonaite@lammc.lt (M.K.); saule.rakleviciute@stud.lsmu.lt (S.R.); birute.frercks@lammc.lt (B.F.)
* Correspondence: ingrida.mazeikiene@lammc.lt

Abstract: *Monilinia* spp., which causes brown rot, is one of the most damaging pathogens in stone fruits. Researchers are exploring epiphytic and endophytic microorganisms with the potential to suppress pathogens, control pathogenic microorganisms, and/or promote plant growth. In this study, microorganisms with antagonistic activity against three *Monilinia* species were isolated from plum orchard soil and plum fruits. Antagonism tests in vitro showed strong antagonistic properties of six strains of bacteria and two yeast-like fungi against *M. fructigena*, *M. fructicola*, and *M. laxa*, with growth inhibition from 45.5 to 84.6%. The antagonists were identified and characterized at the genetic level using whole genome sequencing (WGS). Genes involved in antibiotic resistance, virulence, secondary metabolite synthesis, and plant growth promotion were identified and characterized through genome mapping, gene prediction, and annotation. None of the microorganisms studied were predicted to be pathogenic to humans. The results of this study indicate that the bacteria *Bacillus pumilus*, *B. velezensis*, two strains of *Lysinibacillus agricola*, *Pseudomonas chlororaphis* isolated from stone fruit orchard soil, and the yeast-like fungus *Aureobasidium pullulans*, isolated from plums, are promising candidates for the biological control of *Monilinia* spp.

Keywords: microbial antagonists; European plum; brown rot; biological control; whole-genome sequencing

1. Introduction

The diversity of plant microbiomes can directly or indirectly provide nutrients, help relieve stress, and resist disease [1–3]. Microorganisms can regulate plant growth through nitrogen fixation [4], phosphate-solubilization [5], plant hormones secretion [4,6], or siderophore synthesis [7]. Microorganisms are already used for biological control in agriculture. The soil and plant surface are characterized by an endless number of microorganisms with advantageous activities that support plant health [8–10]. The bacteria *Pseudomonas*, *Bacillus*, *Burkholderia*, *Streptomyces*, *Serratia*, and *Stephanobacteria*, as well as fungi from the *Trichoderma* genus, are recognized as suitable for biological control, and their synthesized antimicrobial properties and bioactive compounds have been widely studied [11–13]. Secondary metabolites, low-molecular-weight antibiotics, and high-molecular-weight antimicrobial proteins or cell wall enzymes—hydrolases—can act as antimicrobial agents [14–17].

Monilinia spp. can cause brown rot, blossom blight, twig cankers, and fruit rot diseases, and are among the world's most important dangers to stone fruit [18]. The identification of new biological control agents (BCAs) that effectively inhibit disease development is a major

challenge for organic horticultural management [19]. Various biocontrol products based on bacterial or yeast antagonists (*Candida oleophila*, *Aureobasidium pullulans*, *Pantoea agglomerans*) have advanced through the development or commercialization stages, and several are successful [20]. In agricultural research, finding novel native biologically active compounds is relevant [21], but processes take too long when classical microbiology methods are used. Whole genome sequencing (WGS) is a technique that provides deep insights into the biosynthetic potential of selected microbial species. WGS analysis of microorganisms allows us to categorize genes associated with antagonistic and plant growth-promoting properties, understand their molecular and functional mechanisms, and thus reduce resources and time in developing biological products [20–25].

The aim of this study was to identify microorganisms isolated from soil and plum fruits and describe their properties at the genetic potential level and their antagonistic abilities to inhibit *Monilinia* spp. pathogens. In summary, we provide essential insights into the eight microbial isolates and their antagonistic and plant growth-promoting (PGP) mechanisms, which will benefit future applications aiming at enhancing the biocontrol of *Monilinia* spp. spread in stone orchards.

2. Materials and Methods

2.1. Isolation of Microorganisms

Microorganisms were isolated from the surrounding soil and fruits of *Prunus domestica* trees, maintained at the collection site of genetic resources for stone fruit orchards (Lithuanian Research Centre for Agriculture and Forestry, Institute of Horticulture, map for 55.0562814 23.8088851) in 2023. The procedure for isolation is as follows. Six genotypes with different resistances to *Monilinia* spp. were chosen: highly resistant No. 293 (free pollination of Cacanska najbolja), resistant No. 202 (Amitar × Jure), No. 219 (free pollination of Cacanska najbolja), No. 242 (Cacanska najbolja × Jure), susceptible No. 212 (Amitar × Jure), and No. 250 (Harmonija × Jure). Isolate names are assigned by tree number. The soil was collected at three places, with the distance from the trunk being 50 cm and the depth being 20 cm, and processed immediately for microbe isolation. The same trees were chosen for the collection of fruits. Five fruits of plums of approximately the same size and with no visual defects were selected at a similar height (around 150 cm) and sun exposure. The fruits were picked wearing sterile gloves, placed into clean plastic bags, and processed to further steps for microbe isolation. The soil and fruits (flesh with skin) were weighed (5 g for each sample). Additionally, fruit samples were homogenized. After adding 10 mL of NaCl 0.9%, the samples were shaken for 30 min at 200 rpm at room temperature. A total of 20 μL of suspension was spread on Petri dishes with lysogeny broth (LB) with agar media in five replicates and incubated for 7 days at 22 °C. Emerging colonies from these plates were further re-streaked until pure colonies were attained. The microbial stock cultures, containing LB and 30% glycerol, were kept at −80 °C until further analysis.

M. fructigena MFS01 was isolated, identified, and described by Kolytaite et al. [26]. The cultures of *M. fructicola* CBS 101512 (USA) and *M. laxa* CBS 489.50 (The Netherlands, Baarn) were obtained from Westerdijk Fungal Biodiversity Institute (The Netherlands, Utrecht) (https://wi.knaw.nl/Collection (accessed on 17 June 2024)).

The collection of isolates was stored in deep-freezing conditions according to the description of the rules of the Garden Plant Genetics and Biotechnology Laboratory in the Cryopreservation laboratory of LAMMC in liquid nitrogen.

2.2. Evaluation of Morphological Characteristics of Microorganism Isolates

Visual characteristics of all eight plum microbial isolates were evaluated to assess how groups of cells appear in pure cultures on LB agar plates at 22 °C. After 48 h of incubation,

the colony shape, elevation, margin, color, smoothness, opacity, consistency, and overall appearance were assessed.

A rub or string test was performed as an alternative to the Gram stain as a confirmatory test [27] for bacterial isolates. A 3% potassium hydroxide solution was used. A small bacterial scrape was placed on a glass slide and, subsequently, one to two drops of the potassium hydroxide (KOH) solution was carefully pipetted on top of the specimen. The resulting suspension was mixed using a sterile plastic loop. Gram-negative bacteria cell walls undergo lysis with 3% KOH, whereas the cell walls of gram-positive bacteria remain intact. Upon lysis of the cell walls of gram-negative bacteria, the release of intracellular DNA occurs, resulting in a viscous (stringy) mixture. The formation of a string in KOH within 60 s is interpreted as a positive test result and indicates that an isolate is a gram-negative organism [27].

2.3. In Vitro Inhibition Assay for Monilinia spp.

The inhibition of pathogens *M. fructigena*, *M. fructicola*, and *M. laxa* was assessed using 88 isolated microbial strains. The mycelium plug from the actively growing zone of a 1-week-old fungus (5 mm in diameter) was placed in the middle of the Petri dish containing potato dextrose agar (PDA). Fresh bacterial or yeast-like fungal isolates were streaked in a square pattern around the mycelium plug. Five replicates were created for every microbial isolate. As a control, a plate containing only the fungus disc was used. The dual culture plates were incubated at 22 °C until the mycelium in the control plates reached the edge. Three sites on each plate were used to measure radial growth inhibition, and were determined as follows:

$$\%I = \frac{(C - T)}{C} \cdot 100$$

where I is the percent of the inhibition of growth, C is the average radius of the fungus on the control plates (5 replicates), and T is the average radius of the fungus on the plates with the isolated microbes (5 replicates).

Antagonistic microorganisms were selected according to the percentage of growth inhibition > 30%. The test was performed using Fisher's LSD test, followed by Duncan's multiple range test to test differences between different antagonists.

2.4. Evaluation of Genetic Profiles of Potential Antagonists

Only bacteria showing more than 30% inhibition of *Monilinia* spp. were selected for taxonomic identification. Genomic DNA was extracted from an overnight LB liquid cell suspension of isolated microbial antagonists using DNeasy PowerSoil Pro Kit according to the manufacturer's instructions (Qiagen, Hilden, Germany). DNA quality and concentration were evaluated using NanoPhotometer™ sUV/Vis Spectrophotometer (Implen GmBH, Munich, Germany). Microbial whole genome sequencing was performed at Novogene (Cambridge, UK) using the NovaSeq X Plus Series (PE150) sequencing platform (1 G raw data per sample). Sequences were assembled, and contigs were obtained using Unicycler software (v0.5.1) [28]. BUSCO analysis was used to assess the completeness of the genome assembly [29]. Species were identified using BLAST and the National Center for Biotechnology Information (NCBI) database [30].

The complete genome sequences (cleaned data) of the isolates have been submitted to GenBank under the accession numbers: SAMN44109744, SAMN44109745, SAMN44109747, SAMN44109746, SAMN44109750, SAMN44109751, SAMN44109752, SAMN44109754. Plant growth-promoting genes were predicted using the Kyoto Encyclopedia of Genes and Genomes (KEGG) database [31]. The web-based tool, Antibiotics and Secondary Metabolites Analysis SHell (antiSMASH 7.0) software was used to predict the biosynthesis gene

clusters of secondary metabolites in selected isolates [32]. The Comprehensive Antibiotic Resistance Database (CARD) was used to collect information on the putative antimicrobial resistance genes [33]. A web server PathogenFinder [34] and the virulence factor database (VFDB, [35]) were used to predict bacterial pathogenicity. To evaluate the relationships between predicted gene clusters involved in the synthesis of secondary metabolites in antagonists to *Monilinia* spp., a Sankey diagram was generated using SRplot software on web https://sankeymatic.com/ (accessed on 27 January 2025) [36].

3. Results

3.1. Morphology of Antagonistic Microorganisms

In total, 88 monocultures were isolated and tested against *Monilinia* spp. in vitro. Eight tested microorganisms were selected as strong antagonists against *M. fructicola*, *M. fructigena*, and *M. laxa*, which were used further in our research. Six bacterial isolates were obtained from the soil of the plum orchard. Two microbial strains were isolated from plum fruits and appeared to be yeast-like fungi.

The bacterial isolates with strong antifungal properties were separated into four distinct morphotypes, as shown in Table 1. The isolates could be divided based on several traits: color, form, margin, opacity, appearance, elevation, consistency, and smoothness. Two creamy circular isolates, 202R2 and 293R14, were grouped into the A morphotype. Orange circular isolate R212R1 and white circular isolate 219R3 were placed separately into two different morphotypes, B and C, respectively. Two creamy irregular isolates, R242R3 and 250R3, were grouped into the D morphotype. Most colonies were circular, but R242R3 and 250R3 were irregular. The margin of isolates was entire or undulate. Both isolates 202R2 and 293R14 were opaque. The R212R1 and 219R3 colonies were opaque as well. Both R242R3 and 250R3 isolates were translucent. Morphotypes B and D had a glistening appearance, while morphotypes A and C did not. The investigated isolates were characterized by flat or convex elevation and had butyrous or mucoid consistency. Isolates R212R, R242R3, and 250R3 were smooth, but 202R2, 293R14, and 219R3 had a coarse surface. All isolates were gram-positive, except isolate R212R1, which appeared to be gram-negative.

Table 1. Morphological characteristics of isolated antagonistic bacteria.

Morphotype	**A**		**B**	**C**	**D**		**E**	
Isolate	202R2	293R14	R212R1	219R3	R242R3	250R3	(1)R293V2	R293V5
Source	soil	soil	soil	soil	soil	soil	fruits	fruits
Color	creamy		orange	white	creamy		creamy	
Form	circular		circular	circular	irregular		circular	
Margin	entire			undulate	undulate		entire	
Opacity	opaque				translucent		opaque	
Appearance	non-glistening		glistening	non-glistening	glistening		glistening	
Elevation	flat			convex	flat		flat	
Consistency	butyrous			mucoid	butyrous		butyrous	
Smoothness	coarse		smooth	coarse	smooth		smooth	
Gram	+	+	−	+	+	+	n.a.	

Two yeast-like fungi isolates (1)R293V2 and R293V5, were separated into distinct morphotype E. They both were creamy, circular, opaque, flat, butyrous, and smooth. The margin was entire, and the appearance was glistening.

3.2. Antagonistic Activity of Microorganisms Against Monilinia spp. In Vitro

The *Monilinia* spp. growth inhibition level varied from 45.5% to 84.6% for eight antagonists (Figures 1 and 2). The highest inhibition percentage rates—81.3% and 84.6% against *M. fructigena* and *M. fructicola*, respectively—were obtained with bacteria 219R3. The highest inhibition rate of 81.5% against *M. laxa* was reached using bacteria 250R3. Both isolates (1)R293V2 and R293V5 with a morphological similarity to yeast-like fungi showed similar antagonism levels for each pathogen. Strong antifungal activity against *M. fructigena* was observed using 202R2 (70.3%) and 293R14 (76.3%) bacteria. The strongest effect on the *M. fructicola*—74.1% and 84.6%—was observed using R212R1 and 219R3 bacteria, respectively. The strongest antagonistic activity against *M. laxa*—79.3% and 81.6%—was reached with R242R3 and 250R3 bacteria, respectively.

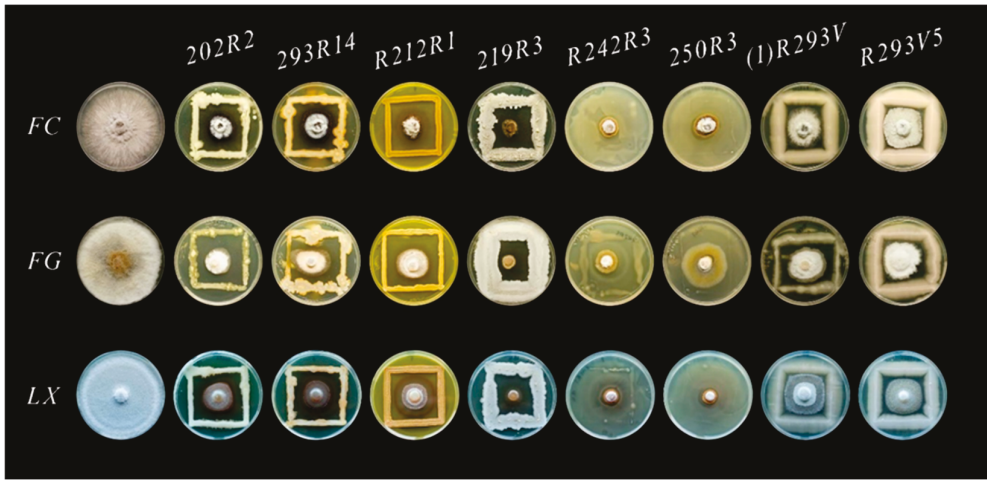

Figure 1. Dual culture antagonism assay of *M. fructicola* (**FC**), *M. fructigena* (**FG**), and *M. laxa* (**LX**) and microbial isolates on PDA, as compared with the control plates (shown on the left).

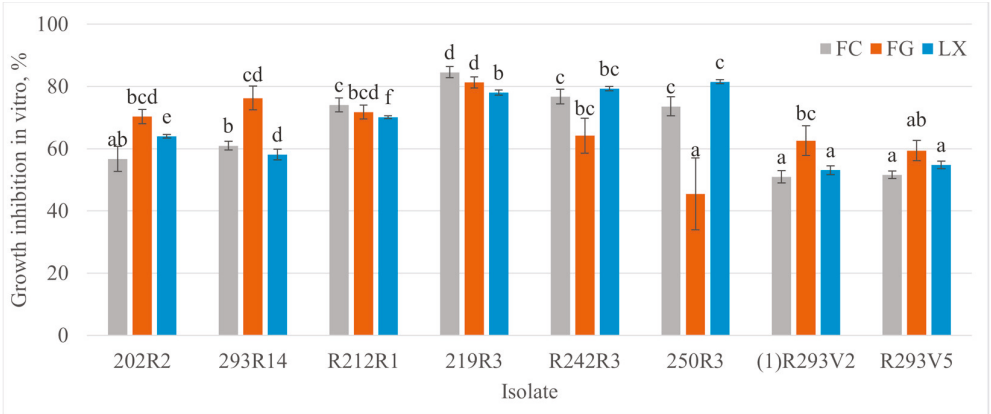

Figure 2. Inhibition of the growth of *M. fructicola* (**FC**), *M. fructigena* (**FG**), and *M. laxa* (**LX**) in vitro on PDA medium as percentages ± SE. The test was performed using Fisher's LSD and Duncan's multiple range test. The different letters (a, b, c, d, e and f) above the columns represent significance within the group of antagonists against the same fungal pathogen. Columns, representing average growth inhibition, with the same letters (ab, bcd, bc and cd) are not significantly different ($p > 0.05$). Only columns marked with the same color are comparable for significant differences. LSD 0.05 = 6.77 (for FC); LSD 0.05 = 15,226 (for FG); LSD 0.05 = 2811 (for LX).

3.3. Genetic Characteristics of the Isolated Microbial Strains

All morphotypes were identified as bacteria, and the other two isolates proved to be yeast-like fungi upon WGS analysis (Table 2). The morphotype A (202R2 and 293R14) had an identity with the *Bacillus pumilus* reference genome of 95.65% and 95.64%, respectively. The morphotype C (219R3) had 98.87% identity with the *B. velezensis* reference genome. The morphotype D (R242R3, 250R3) was identified as *Lysinibacillus agricola* with identities of 90.65% and 90.71% to the reference genome. Gram-negative morphotype B (R212R1), forming orange colonies, showed the identity of 95.11% with the *Pseudomonas chlororaphis* subsp. *chlororaphis*. Two yeast-like fungi strains, (1)R293V2 and R293V5, were identified as *Aureobasidium pullulans* fungi, with 97% identity to the reference genome.

Table 2. The general genome features of isolated microbial antagonists.

Characteristics of Microorganisms—Antagonists of *Monilinia* spp.							
B. pumilus	*B. pumilus*	*B. velezensis*	*P. chlororaphis* subsp. *chlororaphis*	*L. agricola*	*L. agricola*	*A. pullulans*	*A. pullulans*
Accession number in NCBI database and isolate strain in current research							
SAMN 44109744	SAMN 44109745	SAMN 44109747	SAMN 44109746	SAMN 44109750	SAMN 44109751	SAMN 44109752	SAMN 44109754
202R2	293R14	219R3	R212R1	R242R3	250R3	(1)R293V2	R293V5
Mapping statistics with the reference genome (accession number in NCBI and identity with the reference genome (%)							
NC_009848		NC_009725	NZ_CP144767	NZ_CP067341	NZ_CP067341	GCF_000721785	
95.65	95.64	98.87	95.11	90.65	90.71	97.06	97.00
Statistics of sequencing data and annotation Genome size (bp)							
3,733,453	3,721,408	3,976,132	6,995,087	4,901,210	4,923,664	30,364,197	28,396,646
GC content (%)							
41.55	41.52	46.36	62.69	36.74	36.66	50.26	50.33
Gene length (bp)							
3,312,802	3,313,672	3,520,942	6,125,621	3,922,538	3,964,603	21,770,735	20,714,412
Genes % in genome							
88.73	89.04	88.55	87.57	80.03	80.52	71.70	72.95
Total number of genes							
3764	3753	3835	6233	4776	4764	8337	5784
Transfer RNA/Ribosomal RNA (5S, 16S, 23S)/Transfer-messenger RNA							
70/4/1	70/6/1	83/5/1	61/4/1	80/8/1	75/5/1	158/59/N	156/59—N
Noncoding RNA							
16	14	20	62	180	156	78	76
Repeat region/CRISPR							
3/3	1/1	N/N	N/N	3/2	N/N	N/N	N/N
Genes assigned according to NR							
3425	3654	3489	5672	4346	4335	6886	6256
Genes assigned according to GO							
3321	3415	3356	4387	4091	4210	4856	3066
Genes assigned according to KEGG							
3078	3002	3321	4128	4005	3845	3798	3088

B. pumilus strains 202R2, 293R14, and *B. velezensis* 219R3 genome sizes ranged from ~3.7 to ~3.9 Mb (Table 1). The *P. chlororaphis* isolate had a genome size of ~6.9 Mb, and *L. agricola* isolates' genome sizes were ~4.9 and ~4.9 Mb, respectively. Eucaryotes *A. pullulans* (isolates (1)R293V2 and R293V5) genome sizes were ~30,364 and 28,396 Mb, respectively. The overall GC content, protein-coding genes' number, and other genome components (RNAs, repeat regions, and CRISPR) are shown in Table 2. Only *B. pumilus* 202R2, *B. pumilus* 293R14, and *L. agricola* R242R3 were predicted to have 3, 1, and 2 CRISPRs, respectively. The number of coding sequences (CDS) assigned in the NR, Gene Ontology (GO), and KEGG databases of the isolates are shown in Table 2. The CDS differences between isolates of the same species were determined.

3.4. Genetic Background for Synthesizing Secondary Metabolites

The types of secondary metabolites of each isolate are presented in a Sankey diagram (Figure 3). All analyzed microorganisms were characterized by the synthesis of nonribosomal peptides (NRPSs) and betalactone. NPRS-like enzymes were mostly abundant in fungi *A. pullulans*. They were also detected in bacteria *P. chlororaphis* and *B. velezensis*. A large part (in total 18) of the secondary metabolite types were specific only to bacteria, and one type, the fungal-ribosomally synthesized and post-translationally modified peptides (RiPP)-like gene cluster, was inherent only for fungi. The characteristics of secondary metabolites and comparative analysis with NCBI of the gene clusters are shown in Tables S1–S8. *B. velezensis* 219R3 was predicted to have the highest number of gene clusters responsible for secondary metabolites' synthesis among selected bacterial isolates. Fungal isolates were identified with an even higher number of gene clusters, but their diversity was greater in bacteria. *A. pullulans* R293V5 was determined to have 26, and *A. pullulans* (1)R293V2 to have 24. *B. velezensis* 219R3 was identified with 21 gene clusters involved in synthesizing secondary metabolites, while *P. chlororaphis* R212R1 had 18, *B. pumilus* 202R2 had 14, and *B. pumilus* 293R14 had 11. *L. agricola* R242R3 and 250R3 were predicted to have five gene clusters involved in synthesizing secondary metabolites, but only this species was characterized by non-ribosomal peptides (NRP)-metallophore synthesis. Both *B. pumilus* isolates and *P. chlororaphis* R212R1 had NI-siderophore clusters, an important factor that helps the plant in nitrogen metabolism.

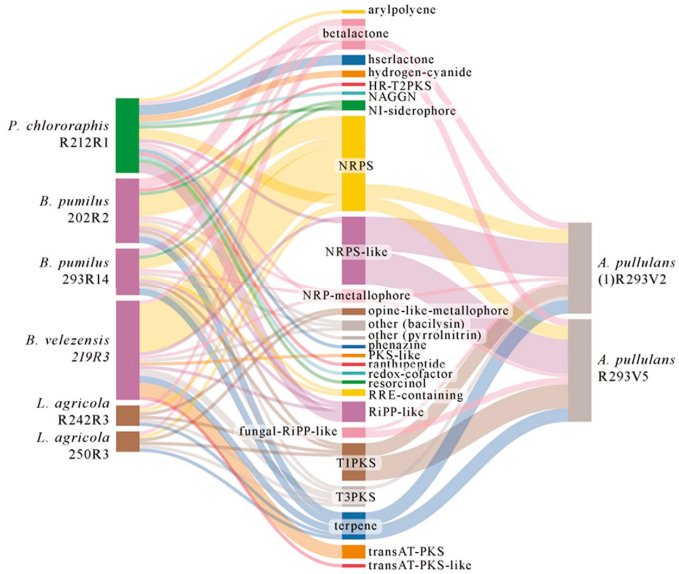

Figure 3. Sankey's diagram of predicted gene clusters involved in the synthesis of secondary metabolites in the isolated antagonists to *Monilinia* spp., where the different colors represent different gene clusters.

There were few unique gene clusters specific for isolate *B. pumilus* 202R2 encoded HR-T2PKS; *B. velezensis* 219R3—PKS-like, transAT-PKS and transAT-PKS-like; *P. chlororaphis* R212R1—arylpolyene, hserlactone, hydrogen-cyanide, NAGGN, phenazine, ranthipeptide, redox-cofactor, and resorcinol. After comparison with known secondary metabolite gene clusters, it was predicted that all *Bacillus* spp. isolates might be able to produce bacillibactin and bacilysin. Additionally, *B. pumilus* 293R14 was predicted to synthesize lichenysin and *B. velezensis* 219R3 to synthesize macrolactin H, bacillaene, fengycin, and difficidin. *P. chlororaphis* R212R1 was predicted to synthesize pyrrolnitrin, hydrogen cyanide, and pyocyanine. Both *A. pullulans* isolates were predicted to produce choline and UNII-YC2Q1O94PT. Additionally, it was estimated that *A. pullulans* R293V5 should synthesize chaetoglobosin.

3.5. Genes Linked with Plant Growth Promotion (PGP) and Antagonism

Genes related to PGP activity and antagonism in the isolated microbial genomes were screened (Table 3). Phosphate transporters encoded genes involved in phosphate metabolism and tryptophan biosynthesis genes (*trp*) related to IAA synthesis were found in all isolates. Nitrogen metabolism genes were identified for all eight isolates, including *gudB* and *rocG*, which catalyze the reduction of L-glutamate to ammonia; *nasD* and *nasE*—the reduction of nitrite to ammonia; *gltD*—glutamate synthase (NADPH) small chain. The nitrogen-fixation-related genes *nifS* and *nifU* were annotated in *Bacillus* spp. genomes. Additionally, *salA* and *sufU* were identified in *B. velezensis* 219R3. Only *nifU* was found in both *L. agricola* isolates. Siderophore production genes were not found in *P. chlororaphis*, however, in other species they were identified. Hydrolase genes were annotated only for *Bacillus* spp. and fungi *A. pullulans* genomes. Chitinase activity was predicted only for isolates *B. velezensis* 219R3 and *A. pullulans* R293V5. All eight isolated microorganisms were identified as having biofilm synthesis genes as well as some key genes for the synthesis of volatile substances. Homologs of the *ilv* gene for 2,3-butanediol synthesis, or genes *metH* and *ispE* for methanethiol and isoprene synthesis involved in the biocontrol mechanism of antagonistic isolates, were characteristic of all antagonistic microorganisms in this study.

Table 3. Predicted genes related to PGP activity and antagonism in the isolated microbial genomes.

PGP Activities Description	*B. pumilus*		*B. velezensis*	*P. chlororaphis*	*L. agricola*		*A. pullulans*	
	202R2	**293R14**	**219R3**	**R212R1**	**R242R3**	**R250R3**	**(1)R293V2**	**R293V5**
Phosphate metabolism	*pstA*, *pstC*, *pstS*	*pstA*, *pstB*, *pstC*, *pstS*, *iolU*, *mmsA*	*pstA*, *pstB*, *pstC*, *pstS*, *gdh*, *hxlB*, *glpX*, *pfk*, *hxlA*, *kdgK*, *rbsK*	*pstA*, *pstB*, *pstS*, *iolG*, *iolE*, *iolD*, *mmsA*, *iolC*	*pstA*, *pstB*, *pstC*, *pstS*, *mmsA*	*pstA*, *pstB*, *pstC*, *pstS*, *mmsA*	*pstB*, *iolG*, *pstA*, *pstC*, *pstS*, *iolU*	*pstB*, *iolG*, *pstA*, *pstC*, *iolU*
Nitrogen fixation	*nifS*, *nifU*	*nifS*, *nifU*	*nifS*, *salA*, *sufU*	-	*nifU*	*nifU*	-	-
Nitrogen metabolism	*gltB*, *ltD*, *glnA*	*gltB*, *ltD*, *glnA*	*nasE*, *nasD*, *gudB*, *rocG*, *narG*, *narH*, *narI*, *glnA*, *cah*, *gltB*	*cynS*, *cynT*, *arcC*, *gltB*, *gltD*, *glnA*, *nirB*, *nirD*, *norB*	*cynT*	*cynT*, *glnA*	*ncd2*, *nirB*, *mbtB*, *cah*, *cynT*, *nirD*, *glnA*, *gltB*, *gltD*	*ncd2*, *nirB*, *mbtB*, *cah*, *cynT*, *glnA*, *gltB*
Siderophore	*menF*, *entE*, *ntA*	*fhuC*, *enF*	*menF*	-	*fhuC*, *menF*	*fhuC*, *menF*	*fhuC*, *fhuG*, *fhuB*, *fhuD*	*fhuC*, *fhuG*, *huB*, *fhuD*
IAA production	*trpA*, *rpB*, *trpC*, *rpD*, *trpE*	*trpA*, *rpB*, *trpC*, *rpD*, *trpE*	*trpA*, *trpB*, *trpC*, *trpD*, *trpE*, *trpF*	*trpA*, *trpB*, *trpC*, *trpD*, *trpE*, *trpF*	*trpA*, *trpB*, *trpE*	*trpA*, *trpB*, *trpE*	*trpA*, *trpB*, *trpD*, *trpE*	*trpA*, *trpE*
Hydrolase	*eglS*	*gmuD*, *ganB*	*eglS*	-	-	-	*trpE*, *eglS*, *pqsH*, *pelF*	*eglS*, *pqsH*, *pelF*
Chitinase activity	-	-	*ydhD*	-	-	-	-	*sleL*, *ydhD*
Biofilm	*trpE*, *flgM*, *fliA*, *csrA*	*trpE*, *flgM*, *fliA*, *csrA*	*tasA*, *bslA*, *bslB*, *trpE*, *flgM*, *csrA*	*crp*, *cpdA*, *trpG*, *trpE*, *flgM*	*trpE*, *fliA*	*trpE*, *fliA*, *csrA*	*tasA*, *bslA*, *bslB*	*tasA*, *bslA*, *bslB*

Table 3. *Cont.*

PGP Activities Description	*B. pumilus*		*B. velezensis*	*P. chlororaphis*	*L. agricola*		*A. pullulans*	
	202R2	293R14	219R3	R212R1	R242R3	R250R3	(1)R293V2	R293V5
2,3-butanediol	*ilvE*, *ilvA*, *ilvD*, *ilvC*, *ilvB*	*ilvE*, *ilvA*, *ilvD*, *ilvC*, *ilvB*	*ilvE*, *ilvA*, *ilvD*, *ilvC*, *ilvB*	*ilvE*, *ilvA*, *ilvD*, *ilvC*, *ilvB*	*ilvA*, *ilvD*, *ilvC*, *ilvB*	*ilvA*, *ilvD*, *ilvC*, *ilvB*	*ilvY*, *ilvA*, *ilvD*, *ilvC*, *ilvH*	*ilvK*, *ilvE*, *ilvY*, *ilvD*, *ilvC*, *ilvH*, *ilvB*

3.6. Pathogenicity and Virulence Annotation of Isolated Bacteria

The bacteria pathogenicity was analyzed using PathogenFinder. Both *B. pumilus* isolates matched 16 non-pathogenic families, whereas *B. velezensis* matched 101, *P. chlororaphis* matched 84, *L. agricola* R242R3 matched 26, and *L. agricola* 250R3 matched 28. All *Bacillus* and *Lysinibacillus* spp. isolates did not have any pathogenic families, while *P. chlororaphis* had two of them. All six bacterial isolates were predicted as non-pathogenic microorganisms.

The genome sequences of isolated bacterial isolates were analyzed in the virulence factor database (VFDB), and 30–32 virulence factor genes were identified for *B. pumilus* isolates, 39 for *B. velezensis*, 211 for *P. chlororaphis*, and 29 and 32 for *L. agricola* R242R3 and 250R3 isolates, respectively (Tables 4 and S9–S11). These genes were mainly involved in bacterial adhesion, antiphagocytosis, host immune system evasion, iron uptake, regulation, secretion system, and bacterial toxins production (Table 4).

Table 4. Predicted virulence factors in bacterial antagonists according to the virulence factor database (VFDB).

Predicted Virulence Factors	*B. pumilus*		*B. velezensis*	*P. chlororaphis*	*L. agricola*	
	202R2	293R14	219R3	R212R1	R242R3	250R3
Acid resistance	0	0	1	0	0	0
Adherence	2	2	2	73	3	5
Antimicrobial activity	0	0	0	6	0	0
Antiphagocytosis	1	1	2	24	2	1
Biofilm formation	0	0	0	4	0	0
Biosurfactant	0	0	0	1	0	0
Cell surface components	0	0	2	0	0	1
Copper uptake	0	0	0	1	0	0
Efflux pump	0	0	0	1	0	0
Enzyme	1	1	0	1	0	0
Glycosylation system	0	0	0	1	0	1
Immune evasion	10	11	18	8	4	1
Intracellular survival	0	0	0	0	1	1
Invasion	1	1	1	1	0	0
Iron acquisition	5	5	5	0	0	0
Iron uptake	2	2	1	31	7	7
Lipid and fatty acid metabolism	1	1	0	1	1	1
Magnesium uptake	0	0	0	1	0	0
Others	0	0	0	2	0	0
Peptidoglycan modification	1	1	0	0	0	1
Protease	0	0	0	2	0	0
Quorum sensing	0	0	0	5	0	0
Regulation	2	2	2	7	3	3
Secretion system	1	1	1	28	2	2
Serum resistance	0	0	0	1	0	0
Serum and immune evasion	0	0	0	0	1	0
Stress adaptation	0	0	1	4	1	1

Table 4. *Cont.*

Predicted Virulence Factors	*B. pumilus*		*B. velezensis*	*P. chlororaphis*	*L. agricola*	
	202R2	**293R14**	**219R3**	**R212R1**	**R242R3**	**250R3**
Surface protein anchoring	2	2	1	0	1	1
Toxin	1	2	2	8	3	6
Predicted VF genes	30	32	39	211	29	32
Total genes	3845	3842	4029	6212	4811	5020

4. Discussion

Each class of chemical fungicides against *Monilinia* spp. has a specific target [37–40], and pathogen resistance develops if used repeatedly [41,42]. Thus, fungicide rotation and combination strategies are essential in treating fungal diseases. A promising agrochemical protection strategy is microbial products and the search for new components for them [43]. The genetic diversity of microorganisms is infinite due to their high adaptability to the environment and the natural interaction between microorganisms. The multicomponent impact of antagonists prevents the pathogen from adapting [44]. This research showed that 8 out of 88 isolated microorganisms had strong antagonistic properties to *Monilinia* spp. pathogens (grow inhibition 45% to 85%) in the microbiota surrounding the plums in the rhizosphere or on the fruit surface (Figures 1 and 2).

According to WGS analysis, three microorganisms were identified as members of the *Bacillus* genus (*B. pumilus* 202R2 and 293R14, *B. velezensis* 219R3) (Table 2). *Bacillus* spp. is widely distributed worldwide and applied in various fields. The isolates R242R3 and 250R3 showed genetic identity with *L. agricola* (access. No. NZ_CP14476 in NCBI)—90.65 and 90.71%, respectively. A cutoff of 97–99% similarity is often used to distinguish species within bacterial taxonomy, but this varies based on the specific group of organisms being studied. This is a novel species of the *Lysinibacillus* genus, first isolated from farmland soil, identified and described in China in 2021 [45]. There are limitations with the reference genome for this species, which means that using it as the standard we cannot yet determine genetic variations. Thus, the one genotype (NZ_CP067341) as a reference genome might not represent the full genetic diversity of a species. We confirmed that both isolates identified in this study have 100% identity among 16s rRNA genes and assigned them to the *L. agricola* species. *Lysinibacillus* shares similarities with *Bacillus* species, but has a unique peptidoglycan composition and fatty acid profile [46]. Morphological characteristics of the isolated R242R3 and 250R3 distinguished them from the others as irregular in form and translucent in opacity (Table 1). Bigger genome sizes with less GC content and fewer gene percentages in the genomes have been identified among these genera in general genome features (Table 2). It is established that *L. agricola* isolates contained 180 and 156 ncRNA regions (R242R3 and 250R3, respectively), while the *Bacillus* genomes contained 16, 14, and 20 ncRNA regions. The ncRNA regions determine a higher complexity of the regulation system and thus better adaptation to stress, increased virulence, and more efficient metabolism in bacteria. *Bacillus* spp. and *Lysinibacillus* spp. have broader applications in agriculture, such as biofertilizers with PGP properties, biopesticides, biofungicides, and bioremediation [46]. *Bacillus* spp. and *Lysinibacillus* spp. are gram-positive and form endospores that can survive in a wide range of environmental conditions and can be formulated into stable dry powders as a product [47]. The gram-negative isolate R212R1 (Table 1) was identified as bacteria *P. chlororaphis* subsp. *chlororaphis* with the homology of 95.11%. *P. chlororaphis* is a plant-associated bacterium with a fast growth rate, wide usage, and various applications, including biocontrol activity, plant growth promotion, and secondary

metabolite production [48]. Two fungal isolates—(1)R293V2 and R293V5—were yeast-like fungi *A. pullulans*. This is a black yeast-like fungus of a ubiquitous genus that can survive in diverse environments [49]. *A. pullulans* are found in most phyllosphere and carposphere habitats and possess high antagonistic activity [50].

All isolated antagonists—*B. pumilus*, *B. velezensis*, *L. agricola*, *P. chlororaphis*, and *A. pullulans*—are known as species with antifungal capacity and positive effects on plant growth in agriculture [21,46,51–53]. There are several reported strains of *B. pumilus* that showed an antifungal effect on the mycelial growth of *M. fructigena* and *M. fructicola*, by up to ~60% in dual culture assays. *M. laxa* in the same study was inhibited only by up to 30% [21]. In this study, *B. pumilus* isolates showed a similar inhibition effect against *M. fructicola*, but it was stronger against *M. frutigena* and *M. laxa*. There were no reports of *B. velezensis* antagonism against brown rot pathogens, but it is indicated as a broad antagonistic spectrum against various phytopathogenic fungi [51]. In our research, *B. velezensis* 219R3 reached around an 80% antagonism level against all tested *Monilinia* species. *Lysinibacillus* species are known for antagonistic activities against numerous plant pathogens [46,54]. *L. agricola* isolates showed a similar pattern of antagonism against all *Monilinia* spp. pathogens in this study. *P. chlororaphis* is well known for inhibiting various phytopathogens (*Fusarium*, *Colletotrichum*, *Phytophthora*, *Pythium*, *Sclerotinia*, *Magnaporthe oryzae*, *Rhizoctonia*) [52]. *P. chlororaphis* R212R1 inhibition results were ~70% against different *Monilinia* spp. *A. pullulans* washed cells inhibited all three *Monilinia* species on nectarine fruits: *M. laxa* was suppressed completely, and *M. fructicola* and *M. fructigena* growth was reduced by 70–90% [53]. This does not fully align with the results obtained in this research, as *A. pullulans* (1)R293V2 and R293V5 inhibited *M. fructigena*'s growth by ~60%, and *M. fructicola*'s and *M. laxa*'s growth was inhibited by ~50%.

The genetic analysis revealed that identified microorganisms have great genetic potential in synthesizing antifungal compounds like lipopeptides and volatile organic compounds (Figure 3, Tables S1–S8). It was also characterized and confirmed by predicted genes related to PGP activity and antagonism (Table 3). The unique genetic setup of some species in *Bacillus* spp. enables them to produce bacilysin more efficiently than others [54,55]. Bacilysin synthesis is mainly determined by the bac operon and its role in converting prephenate to bacilysin. *B. velezensis* 219R3 was predicted with a high variety of secondary metabolites coding regions. It had 21 clusters, including NRPSs, transAT-PKS, NRP-metallophore, RiPP-like, PKS-like, and terpene. Some of them were identified as locillomycin, surfactin, fengycin, macrolactin H, bacillibactin, bacillaene, bacilysin, butirosin, difficidin, and pliplastin coding metabolites. Studies have reported inhibition of fungal growth using some of these substances through mechanisms such as the disruption of pathogen morphology and physiology [56]. *P. chlororaphis* R212R1 was predicted to synthesize phenazine and resorcinol. Phenazines are pigmented antimicrobial compounds [57]. Both molecules inhibit the growth of various phytopathogens [52]. Additionally, alkyl resorcinol (*dar* gene cluster) produced by *P. chlororaphis* isolate PCL 1606 promotes root colonization by this bacterium and functions antagonistically. They are part of the allelochemical plant-to-plant signaling machinery documented for rice and sorghum [58]. *A. pullulans* (1)R293V2 was predicted to have UNII-YC2Q1O94PT, which encodes melanin [59]. Another isolate, *A. pullulans* R293V5, was predicted with the synthesis of chaetoglobosin A. It was synthesized by *Chaetomium globosum* and has potential antifungal activity [60]. Plant growth-promoting traits might have indirect modes of action against *Monilinia* spp. pathogenesis. All eight isolates were predicted with phosphate, nitrogen metabolism, and IAA production (Table 3). PGP traits are common in the *B. pumilus*, *B. velezensis*, *L. agricola*, *P. chlororaphis*, and *A. pullulans* species [46,52,54,61–63] and improve plant metabolism, absorption, and adaptation. All identified isolates had coding genes for biofilm and VOCs

(2,3-butanediol, methanethiol, isoprene). In the previous study, the VOCs released by *B. amyloliquefaciens* FZB42 and the formation of biofilms by *B. velezensis* in the plant rhizosphere promoted growth and protected from infectious microbes through systemic resistance [47,64]. Only *B. velezensis* isolate and *A. pullulans* R293V5 were predicted to synthesize chitinase. Additionally, *B. velezensis* and *A. pullulans* R293V5 isolates were predicted with hydrolase activity. In another study, *A. pullulans* antagonistic yeast-like fungi showed enzymatic activity (chitinases, xylanase, urease) [65].

Virulence factors in biofungicides are essential against fungal pathogens. The predicted virulence factors according to VFDB were disclosed in our research (Tables 4 and S9–S11). The highest number of virulence factors (211) was found in the *P. chlororaphis* R212R1 genome. The majority (73) were related to adherence, which allows *P. chlororaphis* R212R1 to attach to plant surfaces (roots, leaves, or fungal pathogens). Immune evasion strategies present in three identified *Bacillus* isolates (202R2, 293R14, and R212R1) help bacteria avoid detection, resist immune attacks, and persist within the host. Virulence factors work by breaking down fungal structures, competing for resources, and boosting plant immunity [66]. The eight isolates identified in this study show promise as biocontrol strains for managing *Monilinia*-related infections. *B. velezensis* and *P. chlororaphis* isolates were predicted to have the highest number of secondary metabolites, which might be the reason for the most effective inhibition observed of selected pathogens. For precise application rates and conditions, further studies focusing on *Monilinia* spp. specifically in orchard trials are needed.

Supplementary Materials: The following supporting information can be downloaded at: https://www.mdpi.com/article/10.3390/microorganisms13040818/s1. Tables S1–S8: Predicted gene clusters involved in the synthesis of secondary metabolites. Tables S9–S11: Predicted virulence factors in isolates.

Author Contributions: Conceptualization, I.M. and A.K.; methodology, I.M., A.K. and B.F.; software, M.K., I.M. and A.K.; validation, A.K. and I.M.; investigation, I.M., A.K., G.P. and S.R.; resources, A.K., I.M., M.K. and B.F.; data curation, I.M. and A.K.; writing—original draft preparation, A.K.; writing—review and editing, I.M., M.K. and B.F.; visualization, A.K. and I.M.; supervision, I.M. and B.F. All authors have read and agreed to the published version of the manuscript.

Funding: This study was supported by the long-term research program 'Advances in genetics, biotechnology and breeding for improved plant diversity and technological innovations' implemented by Lithuanian Research Centre for Agriculture and Forestry.

Institutional Review Board Statement: Not applicable.

Informed Consent Statement: Not applicable.

Data Availability Statement: Data are contained within the article or Supplementary Materials.

Conflicts of Interest: The authors declare no conflicts of interest.

References

1. Pageni, B.B.; Lupwayi, N.Z.; Akter, Z.; Larney, F.J.; Kawchuk, L.M.; Gan, Y. Plant growth-promoting and phytopathogen-antagonistic properties of bacterial endophytes from potato (*Solanum tuberosum* L.) cropping systems. *Can. J. Plant Sci.* **2014**, *94*, 835–844. [CrossRef]
2. Gouda, S.; Das, G.; Sen, S.K.; Shin, H.S.; Patra, J.K. Endophytes: A treasure house of bioactive compounds of medicinal importance. *Front. Microbiol.* **2016**, *7*, 1538. [CrossRef]
3. Ghadamgahi, F.; Tarighi, S.; Taheri, P.; Saripella, G.V.; Anzalone, A.; Kalyandurg, P.B.; Catara, V.; Ortiz, R.; Vetukuri, R.R. Plant growth-promoting activity of *Pseudomonas aeruginosa* FG106 and its ability to act as a biocontrol agent against potato, tomato and taro pathogens. *Biology* **2022**, *11*, 140. [CrossRef] [PubMed]
4. Santoyo, G.; Moreno-Hagelsieb, G.; Orozco-Mosqueda Mdel, C.; Glick, B.R. Plant growth-promoting bacterial endophytes. *Microbiol. Res.* **2016**, *183*, 92–99. [CrossRef]

5. Li, N.; Wang, S.; Ma, L.; Liu, Y.; Xiu, Y.; Li, X. Phosphate-solubilizing capacity of two bacteria strains and its effect on maize growth and the phosphorus fractions in red soil. *J. Plant Nutr. Fertil.* **2021**, *27*, 275–283. [CrossRef]
6. Wang, Y.; Sun, Z.; Zhao, Q.; Yang, X.; Li, Y.; Zhou, H.; Zhao, M.; Zheng, H. Whole-Genome Analysis revealed the growth-promoting and biological control mechanism of the endophytic bacterial strain *Bacillus halotolerans* Q2H2, with strong antagonistic activity in potato plants. *Front. Microbiol.* **2024**, *14*, 1287921. [CrossRef]
7. Garzón-Posse, F.; Quevedo-Acosta, Y.; Mahecha-Mahecha, C.; Acosta-Guzmán, P. Recent progress in the synthesis of naturally occurring siderophores. *Eur. J. Org. Chem.* **2019**, *2019*, 7747–7769. [CrossRef]
8. Waksman, S.A.; Woodruff, B.H. The soil as a source of microorganisms antagonistic to disease-producing bacteria. *J. Bacteriol.* **1940**, *40*, 581–600.
9. Berendsen, R.L.; Vismans, G.; Yu, K.; Song, Y.; de Jonge, R.; Burgman, W.P. Disease-induced assemblage of a plant-beneficial bacterial consortium. *ISME J.* **2018**, *12*, 1496–1507. [CrossRef]
10. Babalola, O.O. Beneficial bacteria of agricultural importance. *Biotechnol. Lett.* **2010**, *32*, 1559–1570. [CrossRef]
11. Beneduzi, A.; Ambrosini, A.; Passaglia, L. Plant growth-promoting rhizobacteria (PGPR): Their potential as antagonists and biocontrol agents. *Genet. Mol. Biol.* **2012**, *35*, 1044–1051. [CrossRef] [PubMed]
12. Arrebola, E.; Tienda, S.; Vida, C.; de Vicente, A.; Cazorla, F.M. Fitness features involved in the biocontrol interaction of *Pseudomonas chlororaphis* with host plants: The case study of PcPCL1606. *Front. Microbiol.* **2019**, *10*, 719. [CrossRef] [PubMed]
13. Boro, M.; Sannyasi, S.; Chettri, D.; Verma, A.K. Microorganisms in biological control strategies to manage microbial plant pathogens: A review. *Arch. Microbiol.* **2022**, *204*, 666. [CrossRef] [PubMed]
14. Arrebola, E.; Jacobs, R.; Korsten, L. Iturin A is the principal inhibitor in the biocontrol activity of *Bacillus amyloliquefaciens* PPCB004 against postharvest fungal pathogens. *J. Appl. Microbiol.* **2010**, *108*, 386–395. [CrossRef]
15. Zeriouh, H.; Romero, D.; Garcia-Gutierrez, L.; Cazorla, F.M.; de Vicente, A.; Perez-Garcia, A. The Iturin-like lipopeptides are essential components in the biological control arsenal of *Bacillus subtilis* against bacterial diseases of cucurbits. *Mol. Plant-Microbe Interact.* **2011**, *24*, 1540–1552. [CrossRef]
16. Bonaterra, A.; Badosa, E.; Daranas, N.; Francés, J.; Roselló, G.; Montesinos, E. Bacteria as biological control agents of plant diseases. *Microorganisms* **2022**, *10*, 1759. [CrossRef]
17. Zhou, J.; Xie, Y.; Liao, Y.; Li, X.; Li, Y.; Li, S.; Ma, X.; Lei, S.; Lin, F.; Jiang, W.; et al. Characterization of a *Bacillus velezensis* strain isolated from *Bolbostemmatis rhizoma* displaying strong antagonistic activities against a variety of rice pathogens. *Front. Microbiol.* **2022**, *13*, 983781. [CrossRef]
18. Berrie, A.M.; Holb, I. Brown rot diseases. In *Compendium of Apple and Pear Diseases and Pests*, 2nd ed.; Sutton, T.B., Aldwinckle, H.S., Agnello, A.M., Walgenbach, J.F., Eds.; American Phytopathological Society: St Paul, MN, USA, 2014; pp. 43–45.
19. Tsalgatidou, P.C.; Boutsika, A.; Papageorgiou, A.G.; Dalianis, A.; Michaliou, M.; Chatzidimopoulos, M.; Delis, C.; Tsitsigiannis, D.I.; Paplomatas, E.; Zambounis, A. Global transcriptome analysis of the peach (*Prunus persica*) in the interaction system of fruit–chitosan–*Monilinia fructicola*. *Plants* **2024**, *13*, 567. [CrossRef]
20. Fenta, L.; Mekonnen, H. Microbial biofungicides as a substitute for chemical fungicides in the control of phytopathogens: Current perspectives and research directions. *Scientifica* **2024**, *2024*, 5322696. [CrossRef]
21. Hrustic, J.; Medic, O.; Beric, T.; Mihajlovic, M.; Milijaševic-Marčic, S.; Stankovic, S.; Pešic, B. Suppression of *Monilinia* brown rot by *Bacillus* spp. strains. *Agronomy* **2023**, *13*, 2839. [CrossRef]
22. Franco-Sierra, N.D.; Posada, L.F.; Santa-Maria, G.; Romero-Tabarez, M.; Villegas-Escobar, V.; Alvarez, J.C. *Bacillus subtilis* EA-CB0575 genome reveals clues for plant growth promotion and potential for sustainable agriculture. *Funct. Integr. Genom.* **2020**, *20*, 575–589. [CrossRef] [PubMed]
23. Coulson, T.J.D.; Patten, C.L. Complete genome sequence of *Enterobacter cloacae* UW5, a Rhizobacterium capable of high levels of Indole-3-acetic acid production. *Genome Announc.* **2015**, *3*, e00843-15. [CrossRef] [PubMed]
24. Asaf, S.; Khan, A.L.; Khan, M.A.; Al-Harrasi, A.; Lee, I.J. Complete genome sequencing and analysis of endophytic *Sphingomonas* sp. LK11 and its potential in plant growth. *3 Biotech* **2018**, *8*, 389. [CrossRef] [PubMed]
25. Iqbal, S.; Ullah, N.; Janjua, H.A. In vitro evaluation and genome mining of *Bacillus subtilis* strain RS10 reveals its biocontrol and plant growth-promoting potential. *Agriculture* **2021**, *11*, 1273. [CrossRef]
26. Kolytaitė, A.; Vaitiekūnaitė, D.; Antanynienė, R.; Baniulis, D.; Frercks, B. *Monilinia fructigena* suppressing and plant growth promoting endophytic *Pseudomonas* spp. bacteria isolated from plum. *Microorganisms* **2022**, *10*, 2402. [CrossRef]
27. Powers, E.M. Efficacy of the Ryu nonstaining KOH technique for rapidly determining Gram reactions of food-borne and waterborne bacteria and yeasts. *Appl. Environ. Microbiol.* **1995**, *61*, 3756–3758. [CrossRef]
28. Wick, R.R.; Judd, L.M.; Gorrie, C.L.; Holt, K.E. Unicycler: Resolving bacterial genome assemblies from short and long sequencing reads. *PLoS Comput. Biol.* **2017**, *13*, e1005595. [CrossRef]
29. Manni, M.; Berkeley, M.R.; Seppey, M.; Zdobnov, E.M. BUSCO: Assessing genomic data quality and beyond. *Curr. Protoc.* **2021**, *1*, e323. [CrossRef]

30. NCBI Resource Coordinators. Database resources of the National Center for Biotechnology Information. *Nucleic Acids Res.* **2018**, *46*, D8–D13. [CrossRef]
31. Kanehisa, M.; Goto, S. KEGG: Kyoto Encyclopedia of Genes and Genomes. *Nucleic Acids Res.* **2000**, *1*, 27–30. [CrossRef]
32. Blin, K.; Shaw, S.; Kloosterman, A.M.; Charlop-Powers, Z.; van Weezel, G.P.; Medema, M.H.; Weber, T. antiSMASH 6.0: Improving cluster detection and comparison capabilities. *Nucleic Acids Res.* **2021**, *48*, W29–W35. [CrossRef] [PubMed]
33. Alcock, B.P.; Huynh, W.; Chalil, R.; Smith, K.W.; Raphenya, A.R.; Wlodarski, M.A.; Edalatmand, A.; Petkau, A.; Syed, S.A.; Tsang, K.K.; et al. CARD 2023: Expanded curation, support for machine learning, and resistome prediction at the Comprehensive Antibiotic Resistance Database. *Nucleic Acids Res.* **2023**, *51*, D690–D699. [CrossRef] [PubMed]
34. Cosentino, S.; Voldby, L.M.; Møller, A.F.; Lund, O. PathogenFinder—Distinguishing friend from foe using bacterial whole genome sequence data. *PLoS ONE* **2013**, *8*, e77302. [CrossRef]
35. Liu, B.; Zheng, D.; Jin, Q.; Chen, L.; Yang, J. VFDB 2019: A comparative pathogenomic platform with an interactive web interface. *Nucleic Acids Res.* **2019**, *47*, D687–D692. [CrossRef]
36. Tang, D.; Chen, M.; Huang, X.; Zhang, G.; Zeng, L.; Zhang, G.; Wu, S.; Wang, Y. SRplot: A free online platform for data visualization and graphing. *PLoS ONE* **2023**, *18*, e0294236. [CrossRef]
37. Price, C.L.; Parker, J.E.; Warrilow, A.G.; Kelly, D.E.; Kelly, S.L. Azole fungicides—Understanding resistance mechanisms in agricultural fungal pathogens. *Pest. Manag. Sci.* **2015**, *71*, 1054–1058. [CrossRef]
38. Selim, R.E.; Khalil, M.S. Strobilurins: New group of fungicides. *J. Plant Sci. Phytopathol.* **2021**, *5*, 63–64. [CrossRef]
39. Chen, F.; Everhart, S.E.; Bryson, P.K.; Luo, C.; Song, X.; Liu, X.; Schnabel, G. Fungicide-induced transposon movement in *Monilinia fructicola*. *Fungal Genet. Biol.* **2015**, *85*, 38–44. [CrossRef]
40. Martini, C.; Mari, M. Monilinia fructicola, *Monilinia laxa* (Monilinia Rot, Brown Rot). In *Postharvest Decay*; Bautista-Baños, S., Ed.; Academic Press: Cambridge, MA, USA, 2014; Chapter 7; pp. 233–265, ISBN 9780124115521. [CrossRef]
41. Jayawardana, M.A.; Fernando, W.G.D. The mechanisms of developing fungicide resistance in *Fusarium graminearum* causing *Fusarium* head blight and fungicide resistance management. *Pathogens* **2024**, *13*, 1012. [CrossRef]
42. Luo, C.-X.; Schnabel, G. Adaptation to fungicides in *Monilinia fructicola* isolates with different fungicide resistance phenotypes. *Phytopathology* **2008**, *98*, 230–238. [CrossRef]
43. Van Lenteren, J.C.; Bolckmans, K.; Köhl, J. Biological control using invertebrates and microorganisms: Plenty of new opportunities. *BioControl* **2018**, *63*, 39–59. [CrossRef]
44. Shi, A.; Fan, F.; Broach, J.R. Microbial adaptive evolution. *J. Indust. Microbiol. Biotechnol.* **2022**, *49*, kuab076. [CrossRef]
45. Lu, J.R.; Liu, G.H. *Lysinibacillus agricola* sp. nov., isolated from soil. *Arch. Microbiol.* **2021**, *203*, 4173–4178. [CrossRef] [PubMed]
46. Jamal, Q.M.S.; Ahmad, V. *Lysinibacilli*: A biological factories intended for bio-insecticidal, bio-control, and bioremediation activities. *J. Fungi* **2022**, *8*, 1288. [CrossRef]
47. Rabbee, M.F.; Ali, M.S.; Choi, J.; Hwang, B.S.; Jeong, S.C.; Baek, K.H. *Bacillus velezensis*: A valuable member of bioactive molecules within plant microbiomes. *Molecules* **2019**, *16*, 1046. [CrossRef]
48. Liu, J.; Wang, X.; Dai, G.; Zhang, Y.; Bian, X. Microbial chassis engineering drives heterologous production of complex secondary metabolites. *Biotech. Adv.* **2022**, *59*, 107966. [CrossRef]
49. Samson, R.A.; Hoekstra, E.S.; Frisvad, J.C. *Introduction to Food and Airborne Fungi*, 7th ed.; Centralalbureau voor Schimmellcultures; Institute of the Royal Netherlands Academy of Arts and Sciences: Utrecht, The Netherlands, 2004; 389p.
50. Bozoudi, D.; Tsaltas, D. The multiple and versatile roles of *Aureobasidium pullulans* in the vitivinicultural sector. *Fermentation* **2018**, *4*, 85. [CrossRef]
51. Zhang, Y.; Li, Q.; Wang, C.; Liu, S. Transcriptomic and metabolomic analyses reveal the antifungal mechanism of the compound phenazine-1-carboxamide on *Rhizoctonia solani* AG1IA. *Front. Plant Sci.* **2022**, *13*, 1041733. [CrossRef]
52. Bertani, I.; Zampieri, E.; Bez, C.; Volante, A.; Venturi, V.; Monaco, S. Isolation and characterization of *Pseudomonas chlororaphis* strain ST9; *Rhizomicrobiota* and in planta studies. *Plants* **2021**, *10*, 1466. [CrossRef]
53. Mari, M.; Martini, C.; Guidarelli, M.; Neri, F. Postharvest biocontrol of *Monilinia laxa*, *Monilinia fructicola* and *Monilinia fructigena* on stone fruit by two *Aureobasidium pullulans* strains. *Biol. Contr.* **2012**, *60*, 132–140. [CrossRef]
54. Naureen, Z.; Rehman, N.U.; Hussain, H.; Hussain, J.; Gilani, S.A.; Al Housni, S.K.; Mabood, F.; Khan, A.L.; Farooq, S.; Abbas, G.; et al. Exploring the potentials of *Lysinibacillus sphaericus* ZA9 for plant growth promotion and biocontrol activities against phytopathogenic fungi. *Front. Microbiol.* **2017**, *8*, 1477. [CrossRef]
55. Islam, T.; Rabbee, M.F.; Choi, J.; Baek, K.H. Biosynthesis, molecular regulation, and application of bacilysin produced by *Bacillus* species. *Metabolites* **2022**, *27*, 397. [CrossRef] [PubMed]
56. Ye, Q.; Zhong, Z.; Chao, S.; Liu, L.; Chen, M.; Feng, X.; Wu, H. Antifungal effect of *Bacillus velezensis* ZN-S10 against plant pathogen *Colletotrichum changpingense* and its inhibition mechanism. *Int. J. Mol. Sci.* **2023**, *24*, 16694. [CrossRef] [PubMed]
57. Scales, B.S.; Dickson, R.P.; LiPuma, J.J.; Huffnagle, G.B. Microbiology, genomics, and clinical significance of the *Pseudomonas fluorescens* species complex, an unappreciated colonizer of humans. *Clin. Microbiol. Rev.* **2014**, *27*, 927–948. [CrossRef]

58. Anderson, A.J.; Young Cheol, K. Biopesticides produced by plant-probiotic *Pseudomonas chlororaphis* isolates. *Crop Prot.* **2018**, *105*, 62–69, ISSN 0261-2194. [CrossRef]
59. Jong, H.; Arshed, S.; Yu, J.; Cornish, D.; Vanneste, J.L.; Reglinski, T.; Elmer, P.A.G.; Templeton, M.D. A high-quality genome assembly for *Aureobasidium pullulans* CG163, the active ingredient in Aureo Gold, a bio-bactericide registered for control of bacterial canker of kiwifruit caused by *Pseudomonas syringae* pv. *actinidiae* Biovar 3. *PhytoFrontiers* **2024**, *4*, 486–490.
60. Cheng, M.; Zhao, S.; Liu, H.; Liu, Y.; Lin, C.; Song, J.; Thawai, C.; Charoensettasilp, S.; Yang, Q. Functional analysis of a chaetoglobosin A biosynthetic regulator in *Chaetomium globosum*. *Fungal Biol.* **2021**, *125*, 201–210. [CrossRef]
61. Pudova, D.S.; Toymentseva, A.A.; Gogoleva, N.E.; Shagimardanova, E.I.; Mardanova, A.M.; Sharipova, M.R. Comparative genome analysis of two *Bacillus pumilus* strains producing high level of extracellular hydrolases. *Genes* **2022**, *13*, 409. [CrossRef]
62. Dobrzyński, J.; Jakubowska, Z.; Dybek, B. Potential of *Bacillus pumilus* to directly promote plant growth. *Front. Microbiol.* **2022**, *13*, 1069053. [CrossRef]
63. Dobrzyński, J.; Jakubowska, Z.; Kulkova, I.; Kowalczyk, P.; Kramkowski, K. Biocontrol of fungal phytopathogens by *Bacillus pumilus*. *Front. Microbiol.* **2023**, *14*, 1194606. [CrossRef]
64. Rabbee, M.F.; Hwang, B.S.; Baek, K.H. *Bacillus velezensis*: A beneficial biocontrol agent or facultative phytopathogen for sustainable agriculture. *Agronomy* **2023**, *13*, 840. [CrossRef]
65. Zajc, J.; Cernosa, A.; Francesco, A.J.; Castoria, R.; Curtis, F.D.; Lima, G. Characterization of *Aureobasidium pullulans* isolates selected as biocontrol agents against fruit decay pathogens. *Fungal Genom. Biol.* **2020**, *10*, 163.
66. Liu, F.; Hu, M.; Tan, X.X.; Li, C.; Wang, S. Pseudomonas chlororaphis L5 and Enterobacter asburiae L95 biocontrol Dickeya soft rot diseases by quenching virulence factor modulating quorum sensing signal. *Microb. Biotechnol.* **2023**, *16*, 2145–2160. [CrossRef] [PubMed]

microorganisms

MDPI

Article

Synergistic Effect of Essential Oils and Rhamnolipid on *Xanthomonas citri* Subsp. *citri*

Maria Olimpia Pereira Sereia [1], Eduarda Araujo dos Santos [1], Lucas Prado Leite [2], Raphael Culim Neves [2], Vítor Rodrigues Marin [1], Henrique Ferreira [1], Jonas Contiero [2] and Daiane Cristina Sass [1,*]

[1] Department of General and Applied Biology, Institute of Biosciences, São Paulo State University (UNESP), Rio Claro 13506-900, Brazil; olimpia.sereia@unesp.br (M.O.P.S.); eduarda.araujo@unesp.br (E.A.d.S.); vitor.marin@unesp.br (V.R.M.); henrique.ferreira@unesp.br (H.F.)

[2] Institute of Research on Bioenergy, São Paulo State University (UNESP), Rio Claro 13506-900, Brazil; lp.leite@unesp.br (L.P.L.); raphael.culim@unesp.br (R.C.N.); jonas.contiero@unesp.br (J.C.)

* Correspondence: daiane.sass@unesp.br

Abstract: Citrus canker, caused by *Xanthomonas citri* subsp. *citri*, is a devastating disease that affects citrus production and trade worldwide. Traditional control methods, based on copper compounds, are effective but pose environmental and health risks due to their toxicity and potential for bioaccumulation. This study evaluates the synergistic potential of essential oils (EOs) and rhamnolipids as sustainable alternatives for disease management. Four EOS (citronella, palmarosa, geranium, and clove) were tested for their antibacterial activity. Citronella EO showed a 90% inhibitory concentration (IC 90) of 0.15% (*v*/*v*) and a minimum bactericidal concentration of 0.25% (*v*/*v*), while the other EOs showed IC 90 and bactericidal activity at 0.06% (*v*/*v*). Rhamnolipids (RHLs), biosurfactants produced by *Pseudomonas aeruginosa*, inhibited *X. citri* at a concentration of 0.3% (*v*/*v*). The combination of citronella EO and RHLs showed a synergistic effect, reducing the inhibitory concentration of citronella by 50% and that of RHLs by more than 90%. In addition, the combined formulation permeabilized more than 80% of bacterial membranes and reduced biofilm formation. In contrast, other oils tested in combination with rhamnolipid showed independent effects. These results indicate that EOs and rhamnolipids represent an environmentally safe strategy for the control of *X. citri* subsp. *citri* that overcomes the limitations of conventional methods while reducing environmental and health impacts.

Keywords: citrus canker; phytochemicals; biosurfactants; bioactive combination; sustainable agriculture

1. Introduction

Citrus canker, caused by the bacterium *Xanthomonas citri* subsp. *citri*, is a disease that severely affects commercially important citrus species, having impacts on fruit production and trade [1,2]. When the plant is infected, severe symptoms, such as leaf loss, premature fruit drop, and severe fruit discoloration, occur. Infection spreads rapidly in warm and humid weather conditions, resulting in defoliation and reduced fruit quality [3]. These effects not only undermine productivity, but also reduce the market value of the crop, resulting in economic losses for growers and the citrus industry as a whole. The ability of *X. citri* subsp. *citri* to form biofilms plays a central role in both its epiphytic and pathogenic forms [4]. Biofilm formation allows bacteria to adhere to and colonize leaf surfaces, establishing a stable niche that precedes the onset of visible disease symptoms [5,6]. In addition, the structured biofilm matrix provides protection against desiccation, ultraviolet radiation,

and antimicrobial agents, which together increase the fitness and ability of the pathogen to initiate successful infections [7]. Consequently, biofilms are not only survival strategies, but integral components of the disease cycle, underpinning the epidemiological success of *X. citri* subsp. *citri* in citrus-producing regions worldwide [5].

Traditionally, the control of this disease has relied on copper-based formulations, which, despite their efficacy, remain the main chemical control method for *X. citri* [2,8–13] However, the use of these formulations poses serious risks to human health and the environment, as copper is a bioaccumulative heavy metal with mutagenic and carcinogenic effects [14–16]. In addition, its application to soil can lead to the death of various organisms and disrupt entire ecosystems [17]. Considering this scenario, it is essential to search for effective and environmentally safe alternatives for the control of citrus canker. In this context, essential oils (EOs) have emerged as promising options due to their low toxicity to mammals and reduced environmental persistence due to their volatility [18]. In addition, they have demonstrated antibacterial activity against several bacterial species. For example, Xiao and coworkes identified 39 essential oils, including citronella, palmarosa, geranium, and clove, with antibacterial activity against *Staphylococcus aureus* in the stationary phase, a stage associated with persistent infections [19]. In the case of the genus *Xanthomonas*, studies also highlight the efficacy of EOs. Another study evaluated the antibacterial activity of essential oils from *Cymbopogon* species, such as citronella and palmarosa, against *X. citri* subsp. *citri*, highlighting their potential as natural alternatives for the disinfection of citrus fruits [20]. Complementarily, Nagy et al. investigated the antibacterial efficacy of essential oils, such as clove and citronella, against *Xanthomonas arboricola* pv. *pruni*, using microdilution and direct bioautographic assays, with clove oil showing particularly high efficacy [21]. These results reinforce the potential of EOs as sustainable tools for the management of diseases caused by pathogenic bacteria, highlighting their viability as natural alternatives for the control of citrus canker and similar diseases.

However, the industrial application of essential oils and their constituents as antimicrobial agents is limited mainly due to their hydrophobicity [22]. Therefore, it is crucial to develop appropriate formulations to allow their use on a commercial scale. In this sense, rhamnolipids, biosurfactants belonging to the class of glycolipids, have shown promise [23]. Synthesized mainly by the bacterium *Pseudomonas aeruginosa*, but also by other microorganisms, such as *Acinetobacter* sp. and *Enterobacter* sp. [19], rhamnolipids exhibit surfactant properties that remain stable over a wide range of pH levels and temperatures [23,24]. They also exhibit antimicrobial activity against fungi and bacteria, including *X. citri* [25–27]. In agriculture, rhamnolipids have been recommended for pathogen control in greenhouses as both as antimicrobial agents and as inducers of plant defense responses [26].

Recent studies have shown that, due to their excellent emulsifying properties, rhamnolipids can exhibit synergistic effects when combined with bioactive molecules, thereby enhancing biological activity [27,28]. For example, Haba et al. [28] demonstrated the synergistic effect of emulsions formed by rhamnolipids and four essential oils on *Staphylococcus aureus* and *Candida albicans*. However, to date, there is no information on the use of rhamnolipids as emulsifiers in essential oil formulations aimed at inhibiting *X. citri*.

Therefore, the aim of this study was to investigate the synergistic effect of citronella, palmarosa, geranium, and clove essential oils in combination with rhamnolipids, and to evaluate their respective activity against *X. citri* subsp. *citri.*

2. Materials and Methods

2.1. Bacterial Strains and Culture Conditions

The *X. citri* subsp. *citri* used in all experiments was the isolate WT306 (IBSBF 1594) obtained from the IBSBF Culture Collection Instituto Biológico (Campinas, São Paulo,

Brazil). The bacteria were grown in Nutrient Yeast Glycerol liquid medium (5 g L^{-1} of peptone, 3 g L^{-1} of yeast extract, 2% v/v of glycerol, and 20 g L^{-1} of bacteriological agar for solid media), at 29 °C ± 1 °C for 24–48 h with shaking at 200 rpm when necessary. The reagents used in the experiments, including resazurin dye, crystal violet, DAPI, and propidium iodide (PI) stains, as well as the Yeast Minimal Medium, were all commercially purchased from Sigma-Aldrich (Darmstadt, Hesse, Germany). The statistical analysis was performed using the GraphPad software Prism v.6 (GraphPad, San Diego, CA, USA).

2.2. Essential Oils and Rhamnolipid

The essential oils (EOs) of citronella, palmarosa, geranium, and clove were obtained commercially from the company OSHADI® (lot: 2023-001) (Colombo, Paraná, Brazil), and the rhamnolipids were prepared by the research group of Prof. Dr. Jonas Contiero, as described in the literature [25,29], using *Pseudomonas aeruginosa* LBI 2A1 from the random mutant bank at the Laboratory of Industrial Microbiology, Department of General and Applied Biology, UNESP, Rio Claro, São Paulo State, Brazil.

2.3. GC-MS Analysis

To characterize the chemical composition of EOs, all samples were analyzed by gas chromatography-mass spectrometry (GC-MS) using the methodology by Marin et al. [30]. GC-MS was performed using a Shimadzu GCMS-QP2010 ULTRA (Kyoto, Japan) with an Rtx-5MS capillary column (5% phenyl, 95% dimethylpolysiloxane) (Restek, Bellefonte, PA, USA) (30 m × 0.25 mm, 0.25 μm film). Helium was used as the carrier gas (1 mL·min^{-1}), with a 1:10 split injection. The injector and interface temperatures were 250 °C and 260 °C, respectively. The oven temperature was programmed from 60 °C (2 min hold) to 200 °C at 4 °C·min^{-1}, then to 260 °C at 6 °C·min^{-1} (10 min hold) [30]. The ionization source temperature was 280 °C, using the full-scan acquisition mode (70 eV). Compounds were identified using the National Institute of Standards and Technology (NIST) 11.0 EPA/NIH mass spectral library.

2.4. Bacterial Growth Inhibition

The evaluation of the inhibitory activity of *X. citri* subsp. *citri* by essential oils (EOs) and rhamnolipids alone was performed using the Resazurin Microtiter Assay Plate (REMA) technique of Palomino et al. [31]. This method, which indirectly measures cellular respiratory activity, allowed the precise determination of the inhibitory concentrations of the compounds. The tests were performed in 96-well plates, with at least three replicates per compound. Each well received the tested compounds at initial concentrations of 100 μg/mL, reduced by serial dilutions of 1/2. Bacteria were added in the appropriate medium at a concentration of 10^5 cells/well, in a total volume of 100 μL per well. Controls included: negative (medium without compound), positive (kanamycin), and vehicle control (e.g., DMSO 1%). After preparation, the plates were incubated, followed by the addition of resazurin (0.001%). Fluorescence was measured in the Synergy H1 reader (BioTek, Winooski, VT, EUA) with excitation/emission filters at 530/590 nm. The results are expressed as a percentage of cell growth inhibition, with the data processed using GraphPad Prism software (version 6).

This model was used to determine the minimum inhibitory concentration required to inhibit 90% of cell growth (IC 90) and the bactericidal concentration, the minimum bactericidal concentration (MBC), defined as the lowest concentration of an antimicrobial agent required to eliminate 99.9% of the initial bacterial population [32–34]. All experimental procedures were performed in triplicate to ensure reproducibility.

2.5. Synergism

The combined antibacterial activity of citronella essential oil and rhamnolipid was evaluated using the checkerboard microdilution assay according to the methodology described by Bellio et al. [35]. Stock solutions of both compounds were prepared at twice the minimum inhibitory concentration required to inhibit 90% of bacterial growth (2 × IC 90). The EO was serially diluted along the rows, while the rhamnolipid was diluted along the columns of a 96-well microplate. The outer columns (1 and 12) were filled only with NYG culture medium to minimize evaporation effects and were excluded from the analysis.

A standardized bacterial suspension of *X. citri* subsp. *citri* was adjusted to an optical density of 0.04 at 600 nm, equivalent to approximately 10^8 CFU/mL, and then diluted 1:10 in the NYG medium. Each well received 10 µL of the bacterial suspension, resulting in a final concentration of 10^5 cells/well. The microplates were incubated at 29 ± 1 °C for 16 h. After incubation, resazurin (0.015 µg·mL^{-1} final concentration) was added to each well, and the plates were further incubated for 2 h to assess bacterial viability. Fluorescence readings were performed using a Synergy H1 microplate reader (BioTek). All experiments were performed in triplicate.

The synergistic effect was determined by calculating the Fractional Inhibitory Concentration Index (FICI), defined as the sum of the individual Fractional Inhibitory Concentrations (FICs) of the compounds in the combination [36]. The FICI was calculated according to the following formula:

$$\text{FICI} = \text{FIC A} + \text{FIC B} = \frac{\text{IC 90 A combined}*}{\text{IC 90 A alone}} + \frac{\text{IC 90 B combined}*}{\text{IC 90 B alone}}$$

* IC 90 A combined: Refers to the concentration of compound A in combination with compound B required to inhibit 90% of bacterial growth.
* IC 90 B combined: Refers to the concentration of compound B combined with compound A required to inhibit 90% of bacterial growth.

The interaction of the combination of two substances was defined as a synergistic effect if the FIC index was $\leq$0.5, additive if 0.5 < FICI < 1, indifferent if 1 < FICI $\leq$ 4, and antagonistic if FICI > 4.

The concentrations selected for subsequent analyses were based on the combinations that showed a synergistic effect, as determined by the FICI values. Among the synergistic interactions observed, the combination with the lowest effective concentrations of both compounds was prioritized. This approach is consistent with the primary objective of this study, which is to maximize antibacterial efficacy while minimizing the required concentrations of the active compounds, thereby reducing potential cytotoxicity, environmental impact, and formulation costs.

2.6. Cell Membrane Permeabilization

The live and dead microscopy assay was performed according to the methodology described by Zamuner et al. [37] to evaluate the mechanism of action of synergistic combinations against *X. citri* subsp. *citri*. Cells were exposed to the compounds according to the REMA protocol, with 10^5 cells in 100 µL of culture in 1.5 mL microtubes. After the incubation period, the exposure was interrupted by diluting the samples (1:10) in 0.85% saline solution, followed by centrifugation at 2500× *g* for 5 min and discarding the supernatant. The cells were resuspended in 0.85% saline solution, and 10 µL of the suspension was applied to agarose-coated slides for observation.

DAPI staining was used to detect changes in the organization and distribution of the bacterial nucleoid [37]. DAPI penetrates cells with intact cytoplasmic membranes, whereas propidium iodide stains cells with damaged membranes. Cells with permeabilized

membranes were stained red (propidium iodide) while cells with intact membranes were artificially blue-stained (DAPI). Visualizations were performed using an Olympus BX-61 (Bridgewater, NJ, EUA) fluorescence optical microscope, with images captured by an OrcaFlash 2.8 camera Hamamatsu (Bridgewater, NJ, EUA) and processed using CellSens Dimension 1.18 (Olympus) software (Hachioji, Tokyo, Japan).

2.7. Effect of Bioactive Combinations on Biofilm Production by X. citri Subsp. citri

The biofilm assay was performed using the method of Malamud et al. [38], to quantify biofilms formed in 96-well plates. *X citri* subsp. *citri* colonies were grown in NYG medium, adjusted to an OD600 of 0.4, and diluted in Yeast Minimal Medium (YMM) with compounds at concentrations of 50 and 25 μg/mL. After incubation at 29 °C for 72 h, the biofilm was stained with crystal violet (CV), solubilized with 70% ethanol, and the absorbance measured at 590 nm. Biofilm formation indices were calculated and the data normalized in JASP software v. 0.14.1 [39].

2.8. Time-Kill Assay

The time-kill assay described by Gerits et al. [40] was performed using essential oil (EO) and rhamnolipid at a synergistic combination concentration of 1× IC 90, 0.002% (*v*/*v*) rhamnolipid and 0.075% citronella (*v*/*v*), 2× IC 90, 0.004% (*v*/*v*) rhamnolipid and 0.15% citronella (*v*/*v*), and 4× IC 90, 0.008% (*v*/*v*) rhamnolipid and 0.3% citronella (*v*/*v*). *X. citri* was inoculated in NYG medium at a concentration of 10^8 CFU/mL and incubated on an orbital shaker at 29 °C for 24 h. After the incubation period, 100 μL aliquots were taken from each sample at different time intervals (0, 1, 2, 4, 6, 24, and 48 h). Serial dilution was then performed and a plate counting technique was used to determine the number of viable cells. A bacterium inoculated in NYG without the addition of bioactives was used as a control. All experiments were performed in triplicate.

2.9. Statistical Analysis

The REMA assay for the crude extract was performed in triplicate in three independent experiments, with bacterial growth inhibition measured through fluorescence. Data analysis, including the construction of dose–response curves and the determination of IC 90 values along with their 95% confidence intervals (95% CIs), was performed using GraphPad Prism software. A significance level of $p < 0.05$ was used. To evaluate the inhibitory activity of the fractions, a single-replicate screening was performed. Microscopy results were evaluated using Brown–Forsythe and Welch ANOVA to detect significant differences among the treatment groups ($p < 0.05$). Percentage of permeabilized cells was determined by analyzing 200 cells per treatment in duplicate experiments performed on two different days. Biofilm data were evaluated using the unpaired *t*-test and Welch's ANOVA to determine significant differences ($p < 0.05$). All experiments were conducted in three independent replicates. Two-way ANOVA analysis was performed to examine statistical differences between treatments and time, at the 95% confidence level. Tukey's post hoc test (95% confidence interval) was used to examine the relationships between treatments at a single time point and between treatments at all time points.

3. Results

3.1. Bacterial Growth Inhibition

The inhibitory activity of the isolated EOs and rhamnolipids against *X. citri* subsp. *citri* was evaluated, and the results of these individual evaluations were used to prepare mixtures for inhibitory activity. The results obtained with the REMA assay for essential oils and rhamnolipids are shown in Table 1.

Table 1. Inhibitory concentrations 90% (IC 90) and minimum bactericidal concentrations (MBCs) for samples against *X. citri* subsp. *citri* in % (*v*/*v*).

Samples	IC 90	MBC
Palmarosa	0.06	0.06
Citronella	0.15	0.25
Geranium	0.06	0.06
Clove	0.06	0.06
Rhamnolipids	0.3	0.5

3.2. GC-MS Analysis

The four essential oils (EOs) studied, palmarosa (*Cymbopogon martinii),* citronella (*Cymbopogon nardus*), geranium (*Pelargonium roseum*), and clove (*Syzgium aromaticum/Eugenia caryophyllata*), were obtained commercially, and their composition was confirmed by analysis using the gas chromatography-mass spectrometry (GC-MS) technique (Tables 2–5). The sum of the identified compounds corresponds to 100% of the composition of each oil.

Table 2. Results obtained by GC/MS chromatographic analysis for palmarosa oil.

Compounds	Ret. Time	Height %	Area %
β-Myrcene	4.282	1.65	1.08
β-cis-Ocimene	5.142	3.56	2.46
Linalool	6.057	4.75	3.02
Geraniol	9.258	61.09	71.2
Citral	9.611	1.68	1.16
Neryl acetate (Z)	11.999	24.84	19.17
Caryophyllene	13.063	2.43	1.91
Total			100

Table 3. Results obtained by GC/MS chromatographic analysis for citronella oil.

Compounds	Ret. Time	Height %	Area %
Sulcatone	4.211	2.00	0.99
Myrcene	4.284	1.94	0.59
D-Limonene	4.927	2.45	3.61
Linalol	6.057	2.04	1.79
Citronellal	7.099	2.32	7.78
Cis-2-Decen-1-ol	8.156	2.08	0.59
Citronellol	8.625	2.23	6.33
Citral (Z)	8.992	2.43	9.48
Geraniol	9.239	3.16	43.68
Citral (E)	9.614	2.46	13.53
Citronellyl acetate	11.315	2.30	1.75
Neryl Acetate (Z)	11.992	2.36	4.74
Caryophyllene	13.062	2.61	3.42
Γ-Muurolene	15.034	2.59	1.72
Total			100

In the palmarosa essential oil, the main constituents were geraniol (71%) and neryl acetate (19.17%). For citronella, geraniol (43%) and citral (E) (13.53%) stood out. Geranium oil presented 21 compounds, the most abundant being citronellol (34.52%), geraniol (Z) (15.73%), and citronellyl formate (11.02%). In clove, the main compounds were chavibetol (63.84%) and eugenol acetate (30.86%).

Table 4. Results obtained by GC/MS chromatographic analysis for geranium oil.

Compounds	Ret. Time	Height %	Area %
Linalool	6.060	6.46	5.2
Rose Oxide (E)	6.661	0.66	0.54
(+)-Isomenthone (Cis)	7.253	4.75	4.19
(+)-Isomenthone (Trans)	7.481	4.65	4.28
Citronellol	8.643	31.52	34.63
Citral	8.994	0.6	0.51
Geraniol (Z)	9.218	16.48	15.73
Citronellyl formate	9.648	10.97	11.02
Geranyl Bromide	10.247	3.75	3.48
2,6-Octadiene, 2,6 dimethyl	11.319	0.62	0.53
α-Copaene	12.056	0.7	0.61
β-Bourbonene	12.285	1.58	1.48
Caryophyllene	13.066	1.32	1.26
Citronellyl propionate	13.271	0.81	0.77
β-Bisabolene	13.949	0.93	0.95
Citronellyl butyrate	15.073	0.82	0.66
γ-Muurolene	15.190	1.53	1.87
Geranyl isobutyrate	15.748	1.01	0.9
Phenylethyl tiglate	16.420	1.32	1.34
epi-γ-Eudesmol	17.307	6.5	7.33
Geranyl tiglate	18.589	1.37	1.31
Total			100

Table 5. Results obtained by GC/MS chromatographic analysis for clove oil.

Compounds	Ret. Time	Height %	Area %
Chavibetol	11.617	58.99	63.84
Caryophyllene	13.071	6.64	5.3
Eugenol Acetate	15.175	34.37	30.86
Total			100

3.3. Synergism

The checkerboard assay was used to evaluate the synergistic effect of rhamnolipid in combination with the four oils in vitro. In order to calculate the Fractional Inhibitory Concentration Index (FICI), only those results were considered that showed an inhibition of bacterial growth greater than 90%. Table 6 shows the results obtained in the experiments using rhamnolipid with citronella, palmarosa, geranium, and clove. According to the results obtained by calculating the FICI, a synergistic effect can be observed between citronella essential oil–rhamnolipid ($\leq$0.5), and for the other oils an additive effect is demonstrated (0.5 < FICI < 1) between the substances tested. All experiments were carried out in triplicate.

Table 6. Fractional Inhibitory Concentration Index (FICI) of the combination between essential oils and rhamnolipid against *X. citri* subsp. *citri*, in % (*v*/*v*).

Essential Oils	RHL *							
	0.002	**0.004**	**0.009**	**0.018**	**0.030**	**0.075**	**0.15**	**0.3**
Citronella								
0.15	1	1	1	1	1	1	1	2
0.075	0.5	0.5	0.5	0.6	0.6	0.7	1	1.5
0.03							0.7	1.2
0.018							0.6	1.1

Table 6. *Cont.*

Essential Oils	RHL *							
	0.002	**0.004**	**0.009**	**0.018**	**0.030**	**0.075**	**0.15**	**0.3**
Palmarosa								
0.06	1	1	1	1	1	1	1	2
0.03							1	1.5
0.015							0.7	1.2
0.0075							0.6	1.1
Geranium								
0.06	1	1	1	1	1	1	1	2
0.03							1	1.5
0.015								1.2
0.0075								1.1
Clove								
0.06	1	1	1	1	1	1	1	2
0.03							1	1.5
0.015								1.2
0.0075								1.1

* Rhamnolipid = RHL.

3.4. Cell Membrane Permeabilization

After obtaining the synergistic combinations, a live and dead microscopy assay was performed to evaluate their mechanism of action against *X. citri* subsp. *citri*. For this assay, the synergistic combination with the lowest concentrations of both components was selected: 0.075% (*v*/*v*) citronella essential oil and 0.002% (*v*/*v*) rhamnolipid. The microscopic results are shown in Figures 1 and 2. In Figure 1, after 15 min of treatment, more than 60% of the cells show permeabilized membranes, a percentage that increases to 80% after 30 min. In Figure 2, the fluorescence micrographs show that the staining of bacterial cells treated with the synergistic combination is similar to that of the positive control, indicating an effect on cell permeabilization.

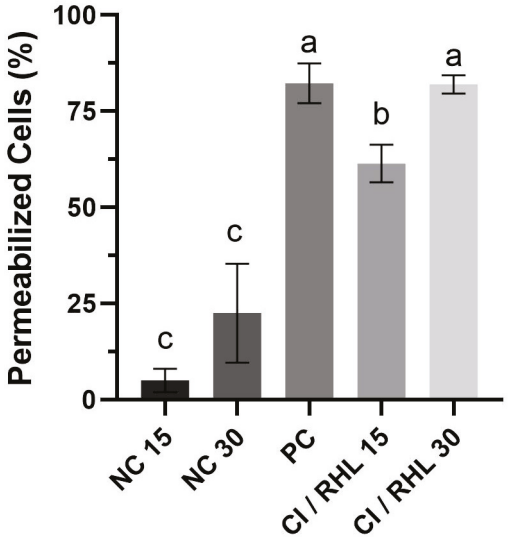

Figure 1. Percentage of *X. citri* subsp. *citri* with permeabilized cell membranes after treatment with citronella essential oil and rhamnolipid. CI: citronella essential oil; RHL: rhamnolipid; NC: negative control; PC: positive control. Error bars represent the standard deviation of the mean. Numbers 15 and 30 represent the duration of exposure to each treatment in minutes. Bars represent the mean of each treatment and whiskers represent the standard deviation. Letters (a), (b), and (c) represent statistically similar groups (p value > 0.05) according to the Brown–Forsythe and Welch ANOVA. A total of 200 cells were analyzed per treatment (n = 200).

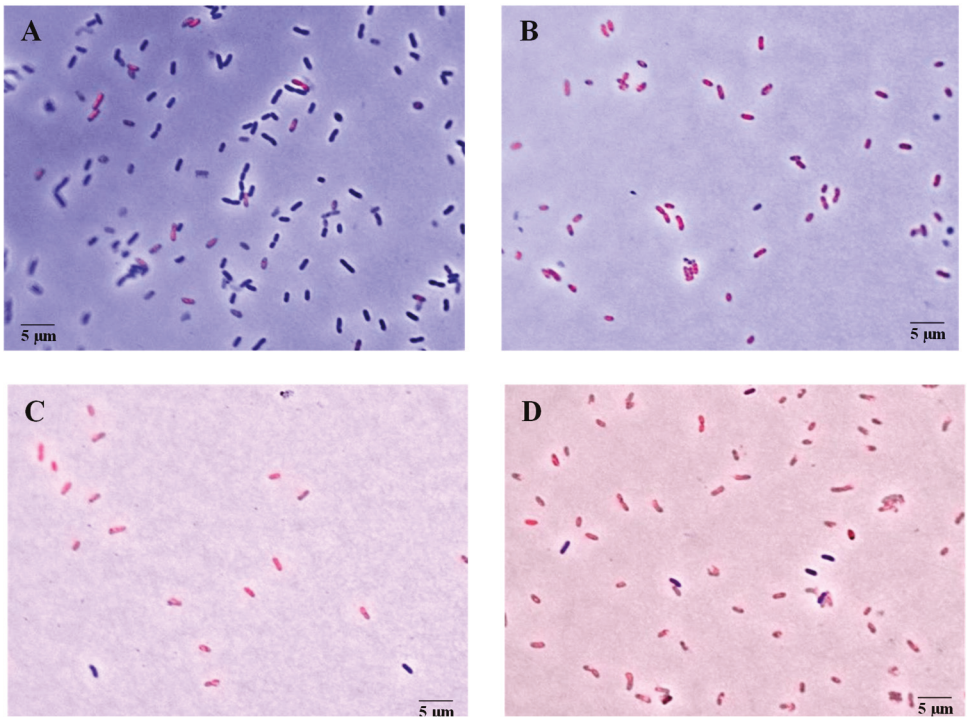

Figure 2. Fluorescence micrographs obtained during the live and dead assay with *X. citri* subsp. *citri* cells after 15 and 30 min of contact with the synergistic combination of 0.075% (*v*/*v*) citronella essential oil and 0.002% (*v*/*v*) rhamnolipid. (**A**): Negative control after 30 min; (**B**): Positive control after 30 min; (**C**,**D**): Cells treated with the combination of citronella essential oil and rhamnolipid after 15 and 30 min, respectively. Cells with permeabilized membranes are stained red, while cells with intact membranes are stained blue. Scale bar: 5 µm. Magnification of ×100.

3.5. Effect of Synergic Combination on Biofilm Production

This assay was used to evaluate whether synergistic combinations act as an anti-biofilm by reducing virulence expression and biofilm formation [41,42]. The results of the biofilm assay shown in Figure 3 indicate that the synergistic concentrations of citronella oil 0.075% (*v*/*v*) and rhamnolipid 0.002% (*v*/*v*) evaluated are effective in reducing bacterial biofilm formation.

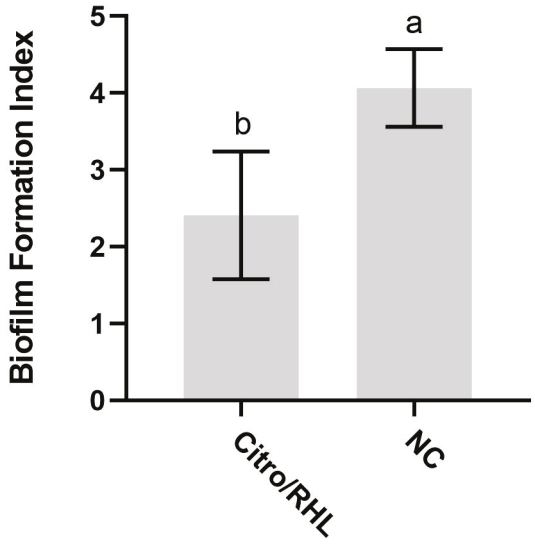

Figure 3. Biofilm formation index by *X. citri* subsp. *citri* bacteria in the presence of the synergistic combination of citronella essential oil and rhamnolipid. Biofilm formation index (absorbance:

590 nm/O.D. 600 nm). Negative control (NC). Treatments with citronella essential oil (EO) and rhamnolipid; concentration of 0.075% citronella and 0.002% RHL (*v*/*v*) (Citrol/RHL). Error bars represent the standard deviation of the mean. Letters (a) and (b) represent statistically similar groups (*p*-value > 0.05) according to the unpaired *t*-test and Welch's ANOVA.

3.6. Time-Kill Assay

The time-kill assay was used to analyze the elimination rate of the components of the synergistic combination at a concentration of 0.075% (*v*, *v*) citronella essential oil and 0.002% (*v*, *v*) rhamnolipid, using the IC 90, 2× IC 90 and 4× IC 90 values show in Figure 4.

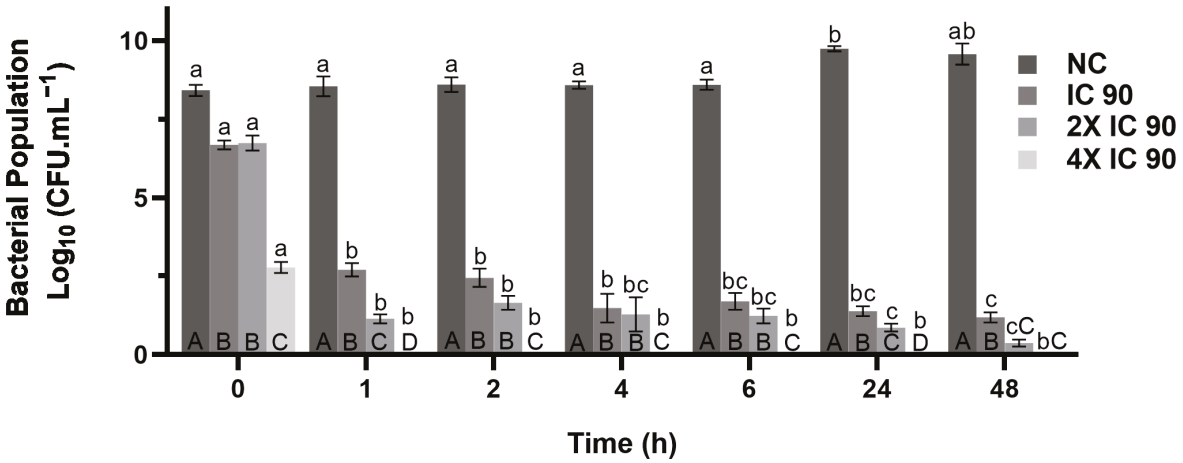

Figure 4. Time-kill kinetics of *X. citri* subsp. *citri* bacteria in the presence of the synergistic combination of citronella essential oil and rhamnolipid. IC 90 concentration of 0.075% citronella and 0.002% RHL (*v*/*v*). NC represents the negative control. Error bars represent the standard deviation of the mean. All the data are presented as the mean ± SD of independent experiments. Capital letters (e.g., A, B, C and D indicate statistical similarities between treatments within a time point; lower-case letters (e.g., a, b and c) indicate statistical similarities in a treatment across time points.

The synergistic combination reduced bacterial growth. Both the time (hours) and concentration variables (IC90, 2× IC90 and 4× IC90) had a significant effect on the number of cells recovered after exposure to the compound. The applied concentration was the dominant factor, accounting for 83% of the variation observed, while the hours of exposure accounted for 10% of the variation. At 1× IC 90, there was a bactericidal reduction of 5.55 $\log_{10}$ CFU/mL after 1 h compared to the negative control. The 4× the IC90 treatments differed from any other treatment in all time periods, except for cells treated with 2× IC90 at 48 h, where no cells were recovered. After 1 h of exposure, no cells were recovered when treated with 4× the IC90. All concentrations showed significant differences in the number of cells recovered compared to the controls at all time points.

4. Discussion

The results demonstrate the antimicrobial activity of rhamnolipid and the four essential oils against *X. citri* subsp. *citri*. Both the essential oils and rhamnolipid exhibited low inhibitory concentration 90% and minimal bactericidal concentration values, reinforcing their antimicrobial efficacy.

Previous studies indicate that essential oils such as palmarosa, clove, and geranium have an IC 90 of 1% against *Bacillus subtilis*, a Gram-positive bacterium [43]. However, in the present study, the same oils were even more effective against *X. citri* subsp. *citri*, achieving 90% inhibition at only 0.006%. This performance highlights the exceptional antimicrobial potency of these oils at extremely low concentrations. Similarly, citronella oil showed an IC 90 of 0.15% against *X. citri* subsp. *citri*, and Cerri and Esmerino reported an

IC 90 of 0.1% against *S. aureus*, *Escherichia coli*, and *C. albicans* [44]. These data suggest that citronella has a broad spectrum of antimicrobial activity, although there are variations in the concentrations that can inhibit different species.

The chemical composition of the essential oils may explain these differences in antimicrobial activity. Palmarosa essential oil contains geraniol and neryl acetate as its major compounds (Table 2). Geraniol, a monoterpene with well-documented antimicrobial activity, disrupts the integrity of the bacterial cell membrane, increasing its permeability and leading to cell lysis [45]. Neryl acetate, although less studied, also as antimicrobial activity and may potentiate the effect of geraniol [46].

Geranium oil contains citronellol and geraniol. Citronellol, like geraniol, is a monoterpene with antimicrobial properties often associated with bacterial cell membrane disruption [47]. The synergy between these compounds may enhance their effectiveness, further disrupting the cell membrane and inhibiting microbial growth [48].

Clove essential oil presented chavibetol and eugenol acetate as major compounds. Chavibetol, a phenylpropanoid, showed antimicrobial activity, mainly against Gram-positive bacteria, by inhibiting essential enzymes and compromising the integrity of the cell membrane [49]. Eugenol acetate, a derivative of eugenol, is also widely recognized for its ability to destabilize cell membranes and inhibit enzymes critical for microbial metabolism [50].

Finally, citronella oil, which is composed primarily of geraniol and citral, stands out for its antimicrobial potential. Citral is known for its high antibacterial activity, and geraniol enhances antibacterial activity, especially when combined with other antimicrobial agents. Studies indicate that essential oils rich in citral and geraniol have activity against *X. citri* subsp. *citri*, with citral being the component with the greatest antibacterial efficacy among those tested [36].

Rhamnolipid showed an IC 90 of 0.3% against *X. citri* subsp. *citri*, which is consistent with the values reported for other microorganisms, including the Gram-positive bacteria *S. aureus*, *Bacillus cereus*; the Gram-negative bacteria *Enterobacter cloacae*, *Proteus mirabilis*; and the fungi *C. albicans*, *Aspergillus niger* [51]. These results underscore the efficacy of essential oils and rhamnolipid as viable and sustainable alternatives for the control of *X. citri* subsp. *citri*.

After determining the antibacterial concentration of each essential oil and rhamnolipid, the checkerboard assay was performed to evaluate the synergistic effect between the two compounds. From the results, the FICI was calculated and the synergistic effects were identified only for concentrations that resulted in values equal to or less than 0.5 [52]. Citronella essential oil, in combination with rhamnolipid, stood out with three synergistic interactions, as evidenced by a reduction in the 90% inhibitory concentration of both compounds when used together. The IC 90 of citronella essential oil was reduced by half, reaching 0.075% (v/v), while rhamnolipid showed even more pronounced reductions, with IC 90s of 0.009%, 0.004%, and 0.002% (v/v).

For the other essential oils with rhamnolipids, there was no synergy, but presented an additive effect, or independent effects ($0.5 < \text{ICIF} \leq 1$), characterized by results equal to the sum of the individual effects of the compounds. This indicates that, although there is no potentiation, the compounds act independently, without antagonism [53].

Haba et al. [28] found that rhamnolipid-based emulsions increased the availability and antimicrobial efficacy of essential oils extracted from *Melaleuca alternifolia*, *Cinnamomum verum*, *Origanum compactum*, and *Lavandula angustifolia*, against *C. albicans* and methicillin-resistant *Staphylococcus aureus* (MRSA). These results support the potential of rhamnolipids to enhance the antimicrobial properties of essential oils.

However, studies investigating the synergistic combination of essential oils with rhamnolipids, especially against *X. citri* subsp. *citri*, are extremely scarce in the literature. Most of the available research focuses on associations between essential oils and antibacterials or antibiotics and other chemical substances. In this context, the data obtained in this project stand out as original and innovative, filling an important gap in the scientific field.

The results presented in Figures 1 and 2 indicate a significant membrane-disrupting effect resulting from the combined application of citronella essential oil and rhamnolipid. The uptake of propidium iodide by the treated cells—indicated by the reddish fluorescence—indicates a loss of membrane integrity, a hallmark of bacterial cell death. Notably, as shown in Figure 3, over 60% of the cells exhibited permeabilized membranes within 15 min of treatment, with this percentage increasing to approximately 80% after 30 min. This time-dependent increase in membrane permeabilization reinforces the bactericidal potential of the formulation and highlights the importance of exposure time in enhancing antimicrobial efficacy.

The efficacy of citronella essential oil may be attributed, at least in part, to its major constituents, such as geraniol and citral. Previous studies have reported that citral disrupts the bacterial cell envelope and alters cytoplasmic density, thereby compromising structural and functional cellular integrity [36]. In this context, the observed effects may be explained by a synergistic interaction between the membrane-solubilizing properties of rhamnolipids and the structure-disrupting effects of citral, resulting in increased membrane permeability and, consequently, increased bacterial susceptibility.

Marin et al. [20] found that essential oils, especially from the *Cymbopogon* species, have antimicrobial activity against *X. citri* subsp. *citri*. Studies have shown that the active compounds present in EOs promote the disruption of the integrity of the bacterial cell membrane. Components such as terpenoids and phenols can interact with membrane lipids, increasing their permeability. This action results in the loss of ions, amino acids, and other essential metabolites, leading to cell death [20]. For example, the essential oil of *Amomum villosum* à Lour affected the membrane of *S. aureus*, resulting in the leakage of intracellular substances [54]. Studies also show that rhamnolipids have antibacterial properties when they interact with bacterial cell membranes, disrupting the cell membrane and leading to increased membrane permeability [55].

The results of the biofilm assay show that the evaluated synergistic concentrations of citronella oil 0.075% (*v*/*v*) and rhamnolipid 0.002% (*v*/*v*) have an effect on reducing bacterial biofilm formation. This reduction was greater than the growth shown in the negative control, indicating that the combination of compounds enhanced the antimicrobial activity by directly interfering with the mechanisms involved in biofilm formation and maintenance.

The essential oil of *C. nardus* (citronella) and its major component, geraniol, have been shown in the literature to inhibit biofilm formation and reduce *S. aureus* biofilm biomass. This antibiofilm activity is critical for preventing chronic infections and increasing the efficacy of antibacterial treatments [56]. In studies comparing citronella oil to commercial mouthwashes, citronella demonstrated superior efficacy in inhibiting the biofilm formation of *S. aureus* and *C. albicans*. Citronella oil resulted in greater microbial reduction and exhibited less cytotoxic effects compared to commercial solutions, making it a promising alternative for biofilm control [57]. The interaction between rhamnolipids and biofilm layers involves changes in surface free energy and surface charge. Rhamnolipids reduce the negative charge of the surface by removing negatively charged substances, such as humic-like substances, proteins, and fulvic acids. This leads to a reduction in the concentrations of carbohydrates and proteins in the EPS, which are essential for biofilm integrity [58].

In the time-kill assay (Figure 4), the exposure of *X. citri* subsp. *citri* to IC 90 resulted in a reduction in the bacterial population to less than half of the initial value within one

hour. Note that increasing the concentration to 4× IC 90 accelerated bacterial elimination, reaching zero contamination within 1 hour and maintaining it for 48 h. Studies have also reported a similar effect, with citral and geraniol compounds in citronella oil eradicating *X. citri* subsp. *citri* within 30 min [36]. Thus, the results for IC 90, 2× IC 90 and 4× IC 90 after 1 h of contact confirm bactericidal activity, defined as a reduction of $\geq$3 $\log_{10}$ CFU/mL ($\geq$99.9%), while bacteriostatic activity corresponds to a reduction of <3 $\log_{10}$ CFU/mL [59–61].

Despite the promising in vitro antibacterial activity of the combination of rhamnolipid and citronella essential oil against *X. citri* subsp. *citri*, translating these findings into large-scale agricultural applications presents significant challenges. While these natural compounds offer an environmentally sound alternative to traditional copper-based bactericides, their economic viability remains uncertain [11].

The commercial feasibility of biosurfactants and essential oils in agriculture depends on several factors, including production cost, formulation stability, and shelf life [62]. For example, rhamnolipids, while effective, require optimized fermentation processes to reduce costs [63], while essential oils are limited by volatility and degradation under field conditions [62]. In addition, synergistic interactions that reduce the required concentration of active compounds need to be confirmed in real-world settings, where environmental factors can reduce efficacy.

Furthermore, the adoption of biobased alternatives in citrus canker management programs depends not only on efficacy, but also on cost competitiveness. Small-scale laboratory successes do not always translate into economically viable large-scale applications, as has been seen with other biocontrol agents [64]. Therefore, future research should prioritize field trials that evaluate long-term performance, formulation stability, and cost-effectiveness to determine whether rhamnolipid–essential oil combinations can be integrated into sustainable citrus production systems.

5. Conclusions

This study demonstrates the potential of essential oils and rhamnolipids as sustainable alternatives for the control of citrus canker, caused by *X. citri* subsp. *citri*. The evaluated EOs, citronella, palmarosa, geranium, and clove, showed antibacterial activity against *X. citri* subsp. *citri*. Rhamnolipids also showed antimicrobial activity, reinforcing their role as a viable alternative to traditional copper-based treatments. The synergistic combination of citronella oil with rhamnolipids was particularly effective, as this synergistic mixture not only permeabilized bacterial cell membranes, but also inhibited biofilm formation, a critical factor in bacterial virulence and persistence. Of particular note was highlighting the time required to eliminate the bacterial population rate, resulting in total death within a few hours.

Therefore, the results of this study provide a basis for the development of sustainable antimicrobial formulations for agricultural use. By reducing the reliance on copper-based products that pose environmental and health risks, the use of EOs and rhamnolipids offers a safer and more environmentally friendly treatment approach to disease control.

Author Contributions: Methodology, M.O.P.S., E.A.d.S., L.P.L., R.C.N., V.R.M. and J.C.; Software, H.F.; Formal analysis, M.O.P.S. and D.C.S.; Investigation, M.O.P.S. and D.C.S.; Resources, D.C.S.; Writing—original draft, M.O.P.S.; Writing—review and editing, H.F., J.C. and D.C.S. All authors have read and agreed to the published version of the manuscript.

Funding: This study was supported and financed by the National Council for Scientific and Technological Development—Brazil (CNPq) (process no. 404366/2023-6; 309024/2023-4) and the São Paulo Research Foundation (FAPESP) (grant number 2023/13083-3).

Institutional Review Board Statement: Not applicable.

Informed Consent Statement: Not applicable.

Data Availability Statement: The original contributions presented in this study are included in the article. Further inquiries can be directed to the corresponding author.

Conflicts of Interest: The authors declare no conflicts of interest.

References

1. Naqvi, S.A.H.; Wang, J.; Malik, M.T.; Umar, U.U.D.; Ateeq-Ur-Rehman; Hasnain, A.; Sohail, M.A.; Shakeel, M.T.; Nauman, M.; Hafeez-ur-Rehman; et al. Citrus Canker-Distribution, Taxonomy, Epidemiology, Disease Cycle, Pathogen Biology, Detection, and Management: A Critical Review and Future Research Agenda. *Agro* **2022**, *12*, 1075. [CrossRef]
2. Ference, C.M.; Gochez, A.M.; Behlau, F.; Wang, N.; Graham, J.H.; Jones, J.B. Recent Advances in the Understanding of *Xanthomonas citri* subsp. *citri* Pathogenesis and Citrus Canker Disease Management. *Mol. Plant Pathol.* **2018**, *19*, 1307–1325. [CrossRef]
3. Ali, S.; Hameed, A.; Muhae-Ud-Din, G.; Ikhlaq, M.; Ashfaq, M.; Atiq, M.; Ali, F.; Zia, Z.U.; Naqvi, S.A.H.; Wang, Y. Citrus Canker: A Persistent Threat to the Worldwide Citrus Industry—An Analysis. *Agronomy* **2023**, *13*, 1112. [CrossRef]
4. Rigano, L.; Siciliano, F.; Enrique, R.; Sendín, L.; Filippone, P.; Torres, P.; Qüesta, J.; Dow, M.; Castagnaro, A.; Vojnov, A.; et al. Biofilm formation, epiphytic fitness, and canker development in *Xanthomonas axonopodis* pv. *citri*. *Mol. Plant Microbe Interact.* **2007**, *20*, 1222–1230. [CrossRef]
5. Ficarra, F.; Grandellis, C.; Galván, E.; Ielpi, L.; Feil, R.; Lunn, J.; Gottig, N.; Ottado, J. *Xanthomonas citri* ssp. *citri* requires the outer membrane porin OprB for maximal virulence and biofilm formation. *Mol. Plant Pathol.* **2017**, *18*, 720–733. [CrossRef] [PubMed]
6. Li, J.; Wang, N. The *wxacO* gene of *Xanthomonas citri* ssp. *citri* encodes a protein with a role in lipopolysaccharide biosynthesis, biofilm formation, stress tolerance and virulence. *Mol. Plant Pathol.* **2011**, *12*, 381–396. [CrossRef] [PubMed]
7. Li, J.; Wang, N. Foliar application of biofilm formation-inhibiting compounds enhances control of citrus canker caused by *Xanthomonas citri* subsp. *citri*. *Phytopathology* **2014**, *104*, 134–142. [CrossRef]
8. Behlau, F. An overview of citrus canker in Brazil. *Trop. Plant Pathol.* **2020**, *46*, 441–452. [CrossRef]
9. Fan, X.; Saleem, T.; Zou, H. Copper resistance mechanisms in plant pathogenic bacteria. *Phytopathol. Mediterr.* **2022**, *61*, 129–138. [CrossRef]
10. Dewdney, M.M.; Graham, J.H. Florida citrus pest management guide: Citrus canker. *Univ. Fla. IFAS Ext.* **2019**, PP-182/CG040. [CrossRef]
11. Behlau, F.; Belasque, J.; Graham, J.H.; Leite, R.P. Effect of Frequency of Copper Applications on Control of Citrus Canker and the Yield of Young Bearing Sweet Orange Trees. *Crop Prot.* **2010**, *29*, 300–305. [CrossRef]
12. Areas, M.S.; Gonçalves, R.M.; Soman, J.M.; Souza Filho, R.C.; Gioria, R.; Da Silva Junior, T.A.F.; Maringoni, A.C. Resistance of Xanthomonas euvesicatoria Strains from Brazilian Pepper to Copper and Zinc Sulfates. *An. Acad. Bras. Ciênc.* **2018**, *90*, 2375–2380. [CrossRef] [PubMed]
13. Lopes, S.A.; Quezado-Soares, A.M. Bacterial diseases of tomato. In *Disease Control in Vegetable Crops*; Zambolim, L., Vale, F.X.R., Costa, H., Eds.; UFV Press: Chilliwack, BC, Canada, 2000; pp. 754–784.
14. Kazeminezhad, I.; Mosivand, S. Elimination of copper and nickel from wastewater by electrooxidation method. *J. Magn. Magn. Mater.* **2017**, *422*, 84–92. [CrossRef]
15. Macomber, L.; Imlay, J.A. The Iron-Sulfur Clusters of Dehydratases Are Primary Intracellular Targets of Copper Toxicity. *Proc. Natl. Acad. Sci. USA* **2009**, *106*, 8344–8349. [CrossRef]
16. Chillappagari, S.; Seubert, A.; Trip, H.; Kuipers, O.P.; Marahiel, M.A.; Miethke, M. Copper Stress Affects Iron Homeostasis by Destabilizing Iron-Sulfur Cluster Formation in *Bacillus subtilis*. *J. Bacteriol.* **2010**, *192*, 2512–2524. [CrossRef]
17. Martinez, J.G.; Paran, G.P.; Rizon, R.; De Meester, N.; Moens, T. Copper effects on soil nematodes and their possible impact on leaf litter decomposition: A microcosm approach. *Eur. J. Soil Biol.* **2016**, *73*, 1–7. [CrossRef]
18. Isman, M.B.; Miresmailli, S.; Machial, C. Commercial Opportunities for Pesticides Based on Plant Essential Oils in Agriculture, Industry, and Consumer Products. *Phytochem. Rev.* **2011**, *10*, 197–204. [CrossRef]
19. Xiao, S.; Cui, P.; Shi, W.; Zhang, Y. Identification of Essential Oils with Activity against Stationary Phase *Staphylococcus aureus*. *BMC Complement. Med. Ther.* **2020**, *20*, 99. [CrossRef] [PubMed]
20. Marin, V.R.; Zamunér, C.F.C.; Santos, E.A.; Ferreira, H.; Sass, D.C. Essential Oils as Alternatives in the Control of Phytopathogens: A Systematic Review of the Last Five Years. *J. Essent. Oil-Bear. Plants* **2024**, *27*, 903–937. [CrossRef]
21. Nagy, T.; Tóth, M.; Papp, G.; Horváth, B.; Kocsis, B.; Kustos, I. Antibacterial Efficacy of Essential Oils against *Xanthomonas arboricola* pv. *pruni*: A Comparative Study. *Molecules* **2023**, *28*, 2345. [CrossRef]
22. Hyldgaard, M.; Mygind, T.; Meyer, R.L. Essential Oils in Food Preservation: Mode of Action, Synergies, and Interactions with Food Matrix Components. *Front. Microbiol.* **2012**, *3*, 12. [CrossRef]

23. Rooney, A.P.; Price, N.P.J.; Ray, K.J.; Kuo, T.M. Isolation and Characterization of Rhamnolipid-Producing Bacterial Strains from a Biodiesel Facility. *Microbiology* **2009**, *155*, 1028–1038. [CrossRef]
24. Lovaglio, R.B.; Dos Santos, F.J.; Jafelicci, M., Jr.; Contiero, J. Rhamnolipid Emulsifying Activity and Emulsion Stability: pH Rules. *Colloids Surf. B Biointerfaces* **2011**, *85*, 301–305. [CrossRef]
25. Yochikawa, J.T.H. Evaluation of Anti-Xanthomonas Citri Activity of Rhamnolipids Produced by Pseudomonas Aeruginosa. Bachelor's Thesis, São Paulo State University, Institute of Biosciences of Rio Claro, Rio Claro, Brazil, 2016.
26. Vatsa, P.; Sanchez, L.; Clement, C.; Baillieul, F.; Dorey, S. Rhamnolipid Biosurfactants as New Players in Animal and Plant Defense against Microbes. *Int. J. Mol. Sci.* **2010**, *11*, 5095. [CrossRef]
27. Abalos, A.; Pinazo, A.; Infante, M.R.; Casals, M.; García, F.; Manresa, A. Physicochemical and Antimicrobial Properties of New Rhamnolipids Produced by *Pseudomonas aeruginosa* AT10 from Soybean Oil Refinery Wastes. *Langmuir* **2001**, *17*, 1367–1371. [CrossRef]
28. Haba, E.; Bouhdid, S.; Torrego-Solana, N.; Marqués, A.; Espuny, M.; García-Celma, M.; Manresa, Á. Rhamnolipids as Emulsifying Agents for Essential Oil Formulations: Antimicrobial Effect against *Candida albicans* and Methicillin-Resistant *Staphylococcus aureus*. *Int. J. Pharm.* **2014**, *476*, 134–141. [CrossRef]
29. Salazar-Bryam, A.M.; Silva, V.L.; De Abreu, M.R.; Matos, R.S.; Da Rocha, M.A.G.; Neves, R.C.; Camargo-Mathias, M.I.; Von Zuben, C.J.; Lovaglio, R.B.; Contiero, J. Rhamnolipids and Essential Oils in the Control of Mosquito-Borne Tropical Diseases. *Appl. Microbiol. Biotechnol.* **2021**, *105*, 7505–7515. [CrossRef]
30. Marin, V.R.; Zamuner, C.F.C.; Hypolito, G.B.; Ferrarezi, J.H.; Alleoni, N.; Caccalano, M.N.; Ferreira, H.; Sass, D.C. Antibacterial activity of Cymbopogon species essential oils against *Xanthomonas citri* and their use in post-harvest treatment for citrus canker management. *Lett. Appl. Microbiol.* **2024**, *77*, ovae041. [CrossRef]
31. Palomino, J.C.; Martin, A.; Camacho, M.; Guerra, H.; Swings, J.; Portaels, F. Resazurin Microtiter Assay Plate: Simple and Inexpensive Method for Detection of Drug Resistance in *Mycobacterium tuberculosis*. *Antimicrob. Agents Chemother.* **2002**, *46*, 2720–2722. [CrossRef]
32. Rodríguez-Melcón, C.; Alonso-Calleja, C.; García-Fernández, C.; Carballo, J.; Capita, R. Minimum Inhibitory Concentration (MIC) and Minimum Bactericidal Concentration (MBC) for Twelve Antimicrobials (Biocides and Antibiotics) in Eight Strains of *Listeria monocytogenes*. *Biology* **2021**, *11*, 46. [CrossRef]
33. Parvekar, P.; Palaskar, J.; Metgud, S.; Maria, R.; Dutta, S. The minimum inhibitory concentration (MIC) and minimum bactericidal concentration (MBC) of silver nanoparticles against *Staphylococcus aureus*. *Biomater. Investig. Dent.* **2020**, *7*, 105–109. [CrossRef]
34. Liu, Y.; Moore, J.; Kolling, G.; McGrath, J.; Papin, J.; Swami, N. Minimum Bactericidal Concentration of Ciprofloxacin to *Pseudomonas aeruginosa* Determined Rapidly Based on Pyocyanin Secretion. *Sens. Actuators B Chem.* **2020**, *312*, 127936. [CrossRef]
35. Bellio, P.; Fagnani, L.; Nazzicone, L.; Celenza, G. New and simplified method for drug combination studies by checkerboard assay. *MethodsX* **2021**, *8*, 101543. [CrossRef]
36. Mirzaei-Najafgholi, H.; Tarighi, S.; Golmohammadi, M.; Taheri, P. The Effect of Citrus Essential Oils and Their Constituents on Growth of *Xanthomonas citri* subsp. *citri*. *Molecules* **2017**, *22*, 591. [CrossRef]
37. Zamuner, C.F.C.; Marin, V.R.; Dilarri, G.; Hypolito, G.B.; Sass, D.C.; Ferreira, H. Oregano essential oil and its main components Thymol and Carvacrol as alternatives to control citrus canker. *Front. Agron.* **2023**, *5*, 1148969. [CrossRef]
38. Malamud, F.; Torres, P.S.; Roeschlin, R.; Rigano, L.A.; Enrique, R.; Bonomi, H.R.; Castagnaro, A.P.; Marano, M.R.; Vojnov, A.A. The *Xanthomonas axonopodis* pv. *citri* flagellum is required for mature biofilm and canker development. *Microbiology* **2011**, *157*, 819–829. [CrossRef]
39. JASP Team. *JASP (Version 0.14.1) [Computer Software]*; JASP: Amsterdam, The Netherlands, 2020; Available online: https://jasp-stats.org/ (accessed on 10 October 2023).
40. Gerits, E.; Blommaert, E.; Lippell, A.; O'Neill, A.J.; Weytjens, B.; De Maeyer, D.; Fierro, A.C.; Marchal, K.; Marchand, A.; Chaltin, P. Elucidation of the mode of action of a new antibacterial compound active against *Staphylococcus aureus* and *Pseudomonas aeruginosa*. *PLoS ONE* **2016**, *11*, e0155139. [CrossRef]
41. Rasmussen, T.B.; Skindersoe, M.E.; Bjarnsholt, T.; Phipps, R.K.; Bisgaard, K.; Jensen, P.O.; Andersen, J.B.; Koch, B.; Larsen, T.O.; Hentzer, M.; et al. Identity and Effects of Quorum-Sensing Inhibitors Produced by *Penicillium* Species. *Microbiology* **2005**, *151*, 1325–1340. [CrossRef]
42. Liaqat, I.; Bachmann, R.T.; Edyvean, R.G.J. Type 2 Quorum Sensing Monitoring, Inhibition, and Biofilm Formation in Marine Microorganisms. *Curr. Microbiol.* **2014**, *68*, 342–351. [CrossRef]
43. Santamarta, S.; Aldavero, A.C.; Rojo, M.A. Essential Oil of Cymbopogon martini, Source of Geraniol, as a Potential Antibacterial Agent against *Bacillus subtilis*, a Pathogen of the Bakery Industry. *F1000Research* **2021**, *10*, 1027. [CrossRef]
44. Cerri, A.C.; Esmerino, L.A. Antimicrobial Activity and Antibiofilm Effect of Essential Oils: A Comparative Study. *Braz. J. Dev.* **2022**, *8*, 73850–73863. [CrossRef]
45. Sharma, Y.; Khan, L.A.; Manzoor, N. Anti-Candida activity of geraniol involves disruption of cell membrane integrity and function. *J. Mycol. Méd.* **2016**, *26*, 244–254. [CrossRef]

46. Zeferino, R.C.F. Synthesis of Geranyl Acetate and Neryl Acetate via Heterogeneous Catalysis with Ion Exchange Resin and Characterization of the Esters for Potential Applications as Antimicrobial Additives. Ph.D. Thesis, Federal University of Santa Catarina, Florianópolis, Brazil, 2021. Available online: https://repositorio.ufsc.br/handle/123456789/231154 (accessed on 10 October 2023).
47. Serero, A.; Bedrat, A.; Baulande, S.; Bastianelli, G.; Colavizza, D.; Desfougères, T.; Pignède, G.; Quipourt-Isnard, A.D.; Nicolas, A. Recombination in a sterile polyploid hybrid yeast upon meiotic Return-To-Growth. *Microb. Res.* **2021**, *250*, 126789. [CrossRef]
48. Bakkali, F.; Averbeck, S.; Averbeck, D.; Idaomar, M. Biological Effects of Essential Oils—A Review. *Food Chem. Toxicol.* **2008**, *46*, 446–475. [CrossRef]
49. Noorshilawati, A.A.; Nurul Asyiqin, A.H.B.; Nur Suraya, A.; Aiza, H. Evaluation of antibacterial activity of Piper betle leaf extracts against pathogen of soft rot disease. *IOP Conf. Ser. Earth Environ. Sci.* **2023**, *1182*, 012049. [CrossRef]
50. Marchese, A.; Barbieri, R.; Coppo, E.; Orhan, I.E.; Daglia, M.; Nabavi, S.F.; Nabavi, S.M. Antimicrobial Activity of Eugenol and Essential Oils Containing Eugenol: A Mechanistic Viewpoint. *Crit. Rev. Microbiol.* **2017**, *43*, 668–689. [CrossRef]
51. Abdel-Mawgoud, A.M.; Lépine, F.; Déziel, E. Rhamnolipids: Diversity of structures, microbial origins and roles. *Appl. Microbiol. Biotechnol.* **2010**, *86*, 1323–1336. [CrossRef]
52. Kim, J.Y.; Kim, J.Y.; Park, J.Y.; Kim, J.S.; Seo, M.K.; Shin, M.K.; Kim, J.H. Synergistic bactericidal effects of carvone and β-lactams against *Xanthomonas campestris* pv. *vesicatoria*. *Appl. Biol. Chem.* **2023**, *66*, 44. [CrossRef]
53. Côté, I.M.; Darling, E.S.; Brown, C.J. Interactions among ecosystem stressors and their importance in conservation. *Proc. R. Soc. B* **2016**, *283*, 20152592. [CrossRef]
54. Tang, C.; Chen, J.; Zhang, L.; Zhang, R.; Zhang, S.; Ye, S.; Zhao, Z.; Yang, D. Exploring the Antibacterial Mechanism of Essential Oils by Membrane Permeability, Apoptosis, and Biofilm Formation Combination with Proteomic Analysis against Methicillin-Resistant *Staphylococcus aureus*. *Int. J. Med. Microbiol.* **2020**, *310*, 151435. [CrossRef]
55. Bharali, P.; Saikia, J.; Ray, A.; Konwar, B. Rhamnolipid (RL) from *Pseudomonas aeruginosa* OBP1: A Novel Chemotaxis and Antibacterial Agent. *Colloids Surf. B Biointerfaces* **2013**, *103*, 502–509. [CrossRef]
56. Pontes, E.; Melo, H.; Nogueira, J.; Firmino, N.; De Carvalho, M.; Júnior, F.; Cavalcante, T. Antibiofilm Activity of the Essential Oil of Citronella (*Cymbopogon nardus*) and Its Major Component, Geraniol, on the Bacterial Biofilms of *Staphylococcus aureus*. *Food Sci. Biotechnol.* **2018**, *28*, 633–639. [CrossRef]
57. Cunha, B.; Duque, C.; Caiaffa, K.; Massunari, L.; Catanoze, I.; Santos, D.; De Oliveira, S.; Guiotti, A. Cytotoxicity and Antimicrobial Effects of Citronella Oil (*Cymbopogon nardus*) and Commercial Mouthwashes on *S. aureus* and *C. albicans* Biofilms on Prosthetic Materials. Arch. *Oral Biol.* **2019**, *109*, 104577. [CrossRef]
58. Kim, L.; Jung, Y.; Yu, H.; Chae, K.; Kim, I. Physicochemical Interactions between Rhamnolipids and *Pseudomonas aeruginosa* Biofilm Layers. *Environ. Sci. Technol.* **2015**, *49*, 3718–3726. [CrossRef]
59. NCCLS. *Methods for Determining Bactericidal Activity of Antimicrobial Agents: Approved Guideline M26-A*; National Committee for Clinical Laboratory Standards: Wayne, PA, USA, 1999.
60. Petersen, P.J.; Jones, C.H.; Bradford, P.A. In vitro Antibacterial Activities of Tigecycline and Comparative Agents by Time-Kill Kinetic Studies in Fresh Mueller-Hinton Broth. *Diagn. Microbiol. Infect. Dis.* **2007**, *59*, 347–349. [CrossRef]
61. Silva, F.; Lourenço, O.; Queiroz, J.; Domingues, F.C. Bacteriostatic versus Bactericidal Activity of Ciprofloxacin in *Escherichia coli* Assessed by Flow Cytometry Using a Novel Far-Red Dye. *J. Antibiot.* **2011**, *64*, 321–325. [CrossRef]
62. Pavela, R.; Benelli, G. Essential oils as ecofriendly biopesticides? Challenges and constraints. *Trends Plant Sci.* **2016**, *21*, 1000–1007. [CrossRef]
63. Henkel, M.; Geissler, M.; Weggenmann, F.; Hausmann, R. Production of microbial biosurfactants: Status quo of rhamnolipid and surfactin towards large-scale production. *Biotechnol. J.* **2017**, *12*, 1600561. [CrossRef]
64. Damalas, C.A.; Koutroubas, S.D. Current status and recent developments in biopesticide use. *Agriculture* **2018**, *8*, 13. [CrossRef]

microorganisms

MDPI

Article

Evaluation of Microbial Transplantation from High-Productivity Soil to Improve Soybean Performance in Less Productive Farmland

Danilo Tosta Souza [1,*], Aurélio Carneiro Soares Moreira [2], Hélio Danilo Quevedo [1] and André May [1]

[1] EMBRAPA Environment, Brazilian Agricultural Research Corporation, Jaguariúna 13918-110, SP, Brazil; hd.qvdo@gmail.com (H.D.Q.); andre.may@embrapa.br (A.M.)
[2] NOOA Agricultural Science and Technology, Patos de Minas 38700-970, MG, Brazil
* Correspondence: danilo_tosta@hotmail.com

Abstract: Microbial transplantation represents a sustainable strategy to address productivity gaps in agricultural soils by transferring microbiomes that enhance nutrient cycling, pathogen suppression, and stress tolerance. This study evaluates whether probiotic consortia from high-yield soybean soils (donor soil) could improve crop performance in less productive fields (recipient soil). We developed a host-adapted inoculant from soybean rhizospheres grown in donor soil and applied it to seeds at five concentrations (0.25–10 g/kg seed) in recipient soil, with untreated controls for comparison. To assess crop-specific microbial recruitment, we prepared a parallel bean-derived inoculant under identical conditions. Through 16S rRNA sequencing and growth/yield analysis, we found the following: (1) Distinct bacteriome assemblies between soybean- and bean-derived inoculants, confirming host specificity; (2) Successful enrichment of beneficial taxa (*Enterobacteriaceae* increased by 15–22%, *Rhizobiaceae* by 7–12%) despite native community resilience; and (3) Consistent yield improvement trends (4.8–6.2%), demonstrating potential to bridge productivity gaps. These results show that transplanted microbiomes can effectively modulate rhizosphere communities while maintaining ecological balance. This work establishes a scalable approach to address soil productivity limitations through microbiome transplantation. Future research should optimize (a) inoculant composition for specific productivity gaps; (b) delivery systems; and (c) compatibility with resident microbiomes, particularly in systems where niche-specific processes govern microbial establishment.

Keywords: agricultural productivity; beneficial bacteria; crop yield; inoculant application; microbial consortium; rhizosphere microbiome

1. Introduction

Crop productivity is intrinsically linked to soil health, with beneficial microorganisms playing a critical role in promoting plant growth and resilience [1]. In high-performing agricultural soils, diverse and robust microbial communities facilitate nutrient cycling, suppress pathogens, and enhance plant stress tolerance, contributing to greater productivity [2–4]. Conversely, soils with diminished microbial diversity or an imbalance in beneficial strains often experience reduced productivity and ecosystem stability, as microbial dysfunction can favor the occupation of niches by pathogenic organisms, despite some functional redundancy within soil communities [5–11].

Despite decades of intervention, productivity gaps between high-yield and marginal farmlands persist. Traditional approaches, such as chemical fertilization, often fail to sustain

long-term soil health due to nutrient leaching and disruption of the soil microbiome [6], while crop rotation alone cannot fully overcome microbial deficiencies in degraded soils [8]. These limitations highlight the urgent need for ecological alternatives capable of rebuilding soil functionality.

To address this agricultural productivity gap, microbial transplantation has emerged as a promising strategy, enabling the transfer of robust microbial consortia from healthy, high-performing soils to degraded or less productive areas, with studies demonstrating its success in restoring disease-suppressive soils through whole-community transfer [5]—a feat unattainable by single-strain inoculants prone to competitive exclusion [12]. Field studies in crops such as rice [13] and wheat [14] have demonstrated significant yield improvements following microbial transplantation. Indeed, this technique restores critical microbial functions, improving soil fertility and crop performance [1,15,16]. For instance, microbial consortia sourced from the rhizosphere of healthy plants have been shown to enrich soils with beneficial bacteria, such as Gammaproteobacteria, which contribute to plant protection and nutrient acquisition [5,11,17]. Similarly, soybean plant-derived microbial inoculants have demonstrated the ability to enhance crop yields and alleviate oxidative stress by positively influencing the plant microbiome [17–22].

The concept of microbial transplantation, originally explored in biomedicine and microbial ecology, now offers a scalable and sustainable solution for agricultural soil restoration [23]. By introducing complex microbial communities from donor to recipient soils, this method re-establishes microbial balance, promotes plant health, and restores fertility while providing natural disease resistance [1,11]. Advances in genomic sequencing, bioinformatics, and biotechnology further enhance the precision and efficacy of this approach [2]. High-throughput 16S rRNA sequencing enables the identification of keystone taxa [2], while metagenomic tools facilitate the design of consortia targeting specific functional traits [18]. These technologies address prior limitations by (1) mapping host–microbe interactions critical for transplantation success [16]; and (2) predicting ecological outcomes through network analysis [15], thereby optimizing both ecological and economic benefits.

Despite these advancements, challenges remain in effectively delivering microbial consortia. Integrating these inoculants with existing agricultural inputs, such as fertilizers, requires further research to maximize their efficacy [24,25]. Moreover, traditional single-species inoculants are often less effective than complex consortia capable of addressing multiple soil health challenges [12,26]. Supposedly, specialist microbes, strains well-adapted to the plant system, emerge as a solution to improve inoculant effectiveness, as they are more likely to establish in the rhizosphere, interact beneficially with native communities, and provide targeted benefits to plant growth and health [1,3,4,7,16,18,27].

Building on these principles, the present study develops a microbial consortium inoculant derived from the rhizosphere and rhizoplane of soybean plants grown under controlled mesocosm conditions using soil from a high-productivity soybean field. The objective was to determine whether these well-adapted microbial consortia could enhance seedling growth in fields with historically lower soybean productivity. Based on the principle that microbial diversity and abundance are key drivers of soil fertility [1,6,8,9,18], we hypothesized that transferring these consortia from productive to less productive soils would increase the abundance of beneficial microbial groups, thereby promoting seedling development.

To test this hypothesis, we characterized the soybean-associated bacteriome using 16S rRNA gene sequencing and evaluated the impact of microbial inoculation on rhizosphere composition and seedling growth. Our findings show that microbial transplantation from high-productivity areas can modestly improve yields and selectively alter the rhizosphere composition of less productive soils, without disrupting the overall microbial community

structure. However, the effectiveness of microbial inoculants depends on environmental factors, soil properties, and interactions with native microbial communities. This study highlights the potential of microbial transplantation as a sustainable agricultural strategy while underscoring the need for further research into delivery mechanisms and interactions with native microbes to optimize its application in diverse agricultural systems.

2. Materials and Methods

2.1. Soil Sampling

Soil samples were collected in two agricultural fields. The first one is located in the municipality of Castro (24°47′57.4″ S and 49°53′16.7″ W), in the state of Paraná (PR), Brazil. The predominant soil type is Inceptisol (Soil Classification System), and the climate is classified as Cfb (subtropical humid with mild summers—Köppen classification) with an annual average air temperature of 16.8 °C and precipitation of 1553 mm. In this agricultural field, a no-till system was established more than 40 years ago. Crop rotation in this area includes soybeans, corn, wheat, and oats plus an annual application of swine manure. This first area was here considered a field of high soybean productivity, with an average of 5100 kg ha^{-1}.

The second field is located in the municipality of Patos de Minas (18°52′31.5″ S and 46°37′45.1″ W), in the state of Minas Gerais, Brazil. The predominant soil type is Oxisols, and the climate is classified as Aw (tropical savanna climate with dry winters) with an annual average air temperature of 21.1 °C and precipitation of 1400 mm. In this area, a no-till system was established 42 years ago, and crop rotation includes soybeans and corn. Due to historically lower agricultural productivity compared to the first field (4320 kg ha^{-1}), soil samples from this area were classified as a less productive soybean farmland.

Soil samples were taken after harvesting in 2018. For this, the litter layer was first removed and then soil samples were taken from the 0–20 cm topsoil layer and determined as bulk soil. Rhizosphere soil samples from many soybean plants were also collected. In total, 70 soil samples (35 bulk soil and 35 rhizosphere soil; ~1.5 kg of soil per sample) were collected in a zigzag pattern across an area of 2 ha totaling 100 kg of soil collected from the first site. The second site (less productive field) was sampled following identical procedures to Site 1, though with a reduced sample number. All samples from both sites were transported within 8 h in sterile, thermally insulated stainless steel containers maintained at ambient temperature (25 ± 2 °C, monitored with calibrated data loggers) to ensure microbial integrity during transit to the Brazilian Agricultural Research Corporation (Embrapa Meio Ambiente), located in Jaguariúna, São Paulo, Brazil. Upon arrival, samples were immediately stabilized at 20 °C and processed within 48 h. Figure 1 provides detailed information on the main chemical properties of the soils and the localization of the sampling sites.

2.2. Construction of the Clonal Garden and Inoculant Preparation

In the laboratory, soil samples from a highly productive soybean field (bulk and rhizosphere soil) were mixed to create a homogeneous sample, which served as the donor soil for the total intraspecific microbial community in a mesocosm bioassay. Both rhizospheric and bulk soil microbiomes are critical to plant health and agricultural productivity [28]. Consequently, we combined these to capture the complete microbial community for formulating a specific consortium adapted to the plant environment and aimed at enhancing soybean productivity.

	Patos de Minas	Castro
pH ($CaCl_2$)	5.84	6.8
Organic matter (g dm^{-3})	30	69
Exchangeable P (mg dm^{-3})	9.59	162
Exchangeable K (mmol$_c$ dm^{-3})	8.65	5
Exchangeable Ca (mmol$_c$ dm^{-3})	34	132
Exchangeable Mg (mmol$_c$ dm^{-3})	14.8	63
Potential acidity (H + Al; mmol$_c$ dm^{-3})	28.9	18
Cation exchange capacity (mmolc dm^{-3})	86.4	218
Base saturation (%)	66.5	92

Figure 1. Image sourced from Google Earth showing the sampling locations and soil chemical properties of high-productivity soybean fields in Castro, PR, and low-productivity fields in Patos de Minas, MG. The map indicates Embrapa Meio Ambiente, where greenhouse experiments were conducted.

This experiment, referred to as the "clonal garden", involved the multiplication and natural recruitment of microbial biomass within the soybean rhizosphere under controlled environmental conditions. The study was conducted in greenhouse seedling benches using the soybean cultivar TEC 7022 IPRO. Each seedling bench (2 m in length, 1 m in width, and 0.3 m in depth) was filled with a reactional mixture of donor soil. Soybean seeds (100 seeds per m^2) were sown, and two identical seedling benches were established as technical replicates, each containing 600 L of standardized substrate.

The substrate was homogenized using a concrete mixing machine and consisted of five parts expanded clay to one part by volume of peat (SEDA line of the Legro group, Helmond, The Netherlands). To this, 25 g of Potasil (Yoorin group, Pocos de Caldas, Brazil), 25 g of phosphate fertilizer from Yoorin, and 2 g of dolomitic limestone were added. Donor soil (2 kg per m^2 of the clonal garden) was broadcast onto the final mixture in the seedbeds.

The experiment was maintained at 28/19 °C (day/night) with a 12 h photoperiod. Soil moisture in the clonal garden was adjusted regularly using an aqueous solution prepared by inundating 10 kg of donor soil with water, vigorously agitating the mixture, decanting it for 2 min, and filtering through a clean cloth. The resulting liquid, enriched with microbes and nutrients, was applied via fertigation at a rate of 100 mL per m^2.

After 21 days, the roots of healthy soybean plants, containing the rhizoplane and rhizosphere, were harvested and ground into a homogeneous black powder. This powder,

containing the microbial consortium, was dehydrated in a forced air-drying oven at 28 °C for 7 days. The resulting microbial consortium inoculant was stored in hermetically sealed plastic bags at room temperature for later use.

To confirm the specificity of the microbial consortium inoculant derived from soybean plants, a bean-based inoculant was included as a control. Prepared under identical conditions using the bean cultivar Campos Gerais, this control provided the basis for evaluating differences in bacterial composition between the two inoculants, as detailed in the next section.

2.3. Inoculant Application and Seedling Growth Measures

The field experiment was conducted on low-productivity soybean farmland in Patos de Minas, MG. The study employed a randomized complete block design (RCBD) with six treatments and six repetitions (i.e., six blocks, each containing all six treatments). Treatments included five doses of the microbial consortium inoculant (0.25, 0.50, 0.75, 1.00, and 10.0 g per kg of soybean seed) and a non-inoculated control. The 10.0 g/kg dose was included as an extreme test case to evaluate potential saturation effects or dose-dependent responses, given that lower doses (0.25–1.00 g/kg) reflect typical agronomic ranges of biofertilizers. Each experimental unit consisted of five 6 m rows spaced 0.5 m apart (total area 15 m^2), with the central three rows (excluding 0.5 m at each end) serving as the 7.5 m^2 useful area to minimize edge effects. Standard crop management practices included fertilization with 100 kg ha^{-1} of MAP applied at planting and 400 kg ha^{-1} of a 30-00-20 (N-P_2O_5-K_2O) formulation applied at the V4 growth stage. Weed, insect, and disease management followed Embrapa's recommendations to ensure these factors did not limit the experiment.

The microbial consortium inoculant was then transferred to soybean seeds to evaluate its efficacy in seedling growth and impact on the rhizosphere when grown in an agriculture field with a history of low soybean productivity. The inoculant was applied to the seeds before sowing by microbiolization, according to the proposed doses. The inoculant was dispersed in 100 mL of water for each kg of soybean seeds, being applied by spraying and mixing in a concrete mixer. The microbiolized seeds were stored for a period of 2 h to ensure greater contact between microbes and seeds, and afterward, they were immediately sown. The rhizosphere microbiome was collected 90 days after planting in the field, at the R_2 flowering stage. Grains were harvested to measure agricultural productivity at the end of the soybean crop cycle from a 7.5 m^2 area in the central part of the plot.

In addition to assessing grain yield in open fields, seedling growth parameters (plant height, root and shoot dry mass) were evaluated in a greenhouse experiment. The experimental setup involved growing soybean seeds in soil from the field with a history of low soybean productivity and comparing it to the same soil treated with varying doses of soybean-based inoculant applied to microbiolized seeds. This greenhouse experiment was carried out for 21 days in 5 kg pots using natural soil (not autoclaved). The data obtained for seedling growth parameters were compared using one-way analysis of variance (ANOVA) with the F test applied at a probability level of 10%, and grain yield data were compared using regression analysis as described in the Supplementary Materials. All statistical analyses were performed using R software version 4.0.3.

2.4. DNA Extraction and Sequencing

Total DNA from each soil sample was extracted using the DNeasy Power Lyzer Power Soil DNA Isolation Kit (Qiagen Inc., Valencia, CA, USA) following the manufacturer's instructions. DNA quality and quantity were assessed using NanoDrop 1000

spectrophotometry (Thermo Scientific, Waltham, MA, USA) and 1% sodium boric acid agarose gel electrophoresis.

Taxonomical profiling was performed using amplicon sequencing targeting the V3-V4 region of the bacterial 16S rRNA gene. Sequencing was conducted at the GoGenetic Facility, located in the municipally of Curitiba, State of Paraná, Brazil. For RNA-seq analysis, we selected the 1.00 g/kg seed inoculant dose based on its superior phenotypic performance—most notably, an increased flower count—observed during preliminary evaluations. Six biological replicates were collected, one from each experimental block, to capture field-scale variability. Identical sampling procedures were applied to both treated and untreated plants. A total of 25 DNA sample libraries were prepared to characterize the bacterial consortia: 4 libraries originating from the donor soil (native soil from the field with a history of high soybean productivity); 6 libraries of soybean inoculant produced by growing soybean plants in the donor soil (a bioproduct developed in this study using the clonal garden technique); 6 libraries from the soybean rhizosphere in farmland that is historically less productive (untreated recipient soil); 6 libraries from the soybean rhizosphere in less productive farmland treated with the donor soil-derived soybean inoculant (treated recipient soil); and 3 libraries of bean-based inoculant produced by growing bean plants in the donor soil (developed using the clonal garden technique).

The libraries were prepared using the Miseq Reagent Kit v3 (Illumina, San Diego, CA, USA), following the manufacturer's instructions for the Illumina MiSeq platform (2×250 bp paired-end). Primers and reaction conditions used for amplification are described in Supplementary Materials.

2.5. Bacterial Community Analysis

The bacterial 16S rRNA sequences were processed using QIIME 2 (version 2020.11). First, the sequences were demultiplexed and quality control was carried out with DADA2 [29], using the consensus method to remove any remaining chimeric and low-quality sequences. Afterward, singletons, doubletons, chloroplast, and mitochondria sequences were removed from further analysis. Taxonomic classification was performed using a pre-trained classifier (silva-132-99-515-806-nb-classifier.qza) based on the SILVA database (v132) at 99% similarity [30], and the generated matrices were used for statistical analyses. The sequences are deposited in the NCBI database under the accession number PRJNA1259697.

To determine whether the bacterial community structure among treatments was significantly different from each other, we used Principal Coordinates Analysis (PCoA) followed by an ADONIS permutation-based statistical test in vegan-R with the weighted UniFrac distances matrix. The observed OTUs (Richness) and Shannon alpha diversity index were calculated based on the OTU table using base-R statistical packages and compared using Tukey's HSD test. To compare the differential abundance of bacteria among treatments, the OTU table was used as input in the software Excel. *p*-values were calculated based on a two-sided Welch's t-test with correction using Benjamini–Hochberg FDR.

3. Results

3.1. Definition of Terms

In this study, donor soil refers to soil collected from a highly productive soybean farmland, serving as the source of beneficial microbial communities for inoculant preparation. Recipient soil refers to soil from less productive soybean farmland, targeted for microbial enrichment through inoculation. The terms treated and untreated soils refer to recipient soils that either received or did not receive the microbial consortium inoculant, respectively. Similarly, treated and untreated plants refer to soybean plants grown in these respective

soils. The terms bean inoculant and soybean inoculant refer to microbial preparations derived from the rhizosphere and rhizoplane microbiomes of bean and soybean plants, respectively, collected from the donor soil. These inoculants were developed using a clonal garden strategy to ensure consistency and standardization, facilitating the inoculation of probiotic microbial strains as a consortium. Figure 2 presents the workflow for preparing inoculants using the clonal garden technique and transferring microbial consortia from high-productivity to less productive soybean farmland.

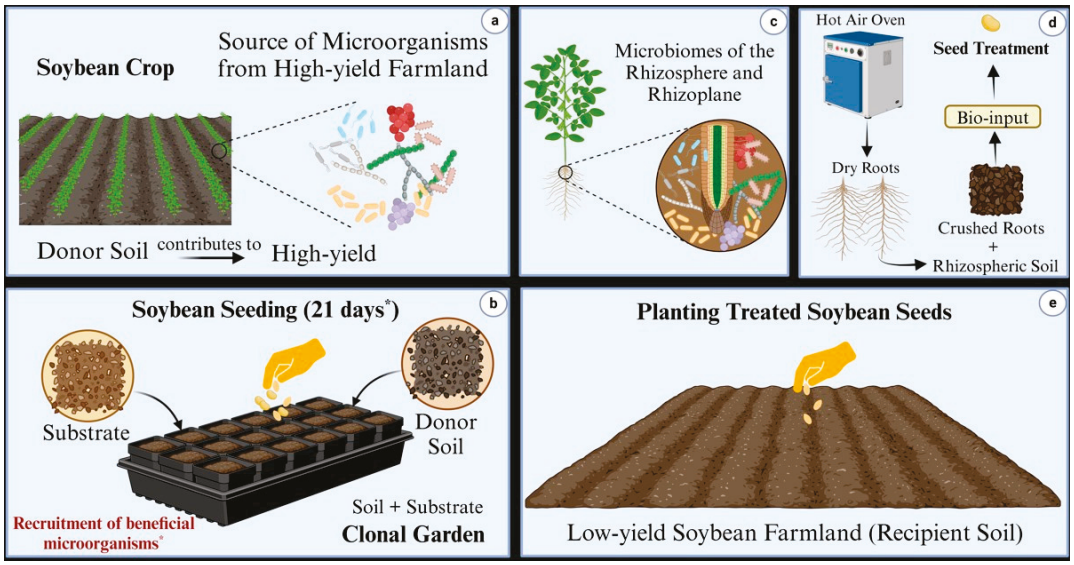

Figure 2. Illustrative scheme depicting the workflow for preparing inoculants. (**a**) Soil from high-yield farmland served as a donor of beneficial microbes. (**b**) Soybean plants were cultivated in a clonal garden containing donor soil to recruit key microbiomes, which formed the microbial consortium inoculant. The asterisk (*) indicates that plants grew for 21 days to recruit beneficial microorganisms. (**c**,**d**) The inoculants were prepared as a black powder by collecting, crushing, and dehydrating rhizosphere and rhizoplane samples. (**e**) Plants treated with the inoculant were grown in low-yield farmland to enhance productivity and microbial diversity. Results were compared with untreated plants.

3.2. Alpha-Diversity Analysis

The alpha-diversity analysis revealed distinct bacterial characteristics among the inoculants, donor soil, and recipient soils. The soybean inoculant exhibited significantly lower species richness (Chao1, $p = 0.003$) and diversity (Shannon, $p = 0.008$) than the donor soil (Figure 3). Conversely, species richness between the donor soil and untreated plants grown in the recipient soil was statistically similar (Chao1, $p = 0.21$). However, differences in diversity, as indicated by the Shannon ($p = 0.015$) and Simpson ($p = 0.021$) indices, were evident. These discrepancies likely resulted from variations in edaphoclimatic conditions, as the soils sampled from different regions exhibited limited species overlap. Moreover, the higher diversity observed in the donor soil may be attributed to its composition, which included homogenized bulk soil and soybean rhizosphere samples collected from high-productivity fields. In contrast, the untreated plants represented rhizosphere communities derived exclusively from less productive soils.

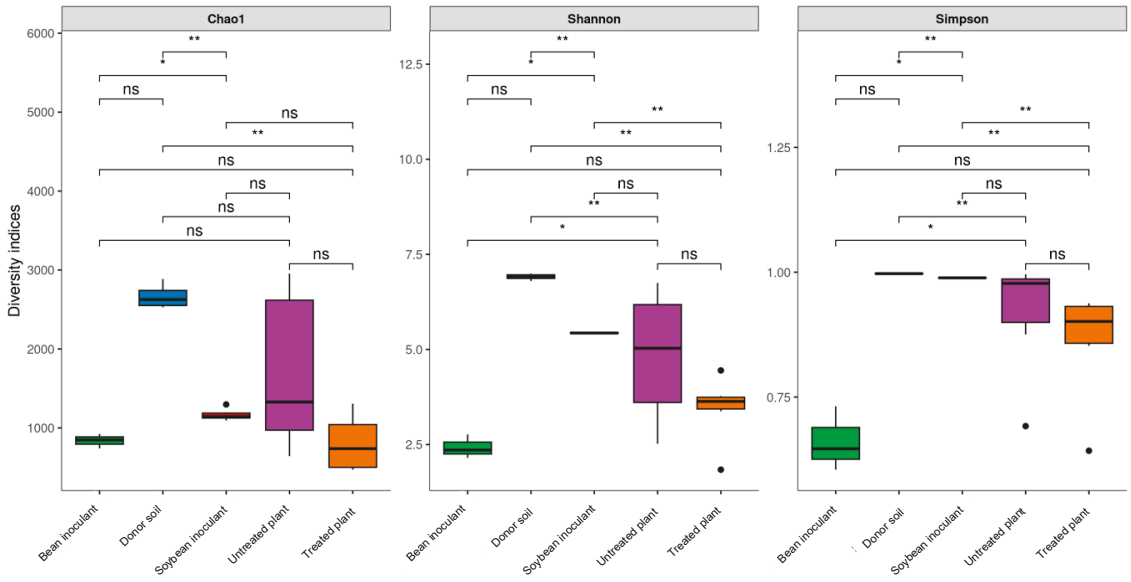

Figure 3. Alpha-diversity measures (Chao1, Shannon, and Simpson indices) of bacterial 16S rRNA amplicons across different sample types: donor soil (highly productive soybean farmland soil), soybean inoculant (microbial preparations from the rhizosphere and rhizoplane of soybean cultivated in donor soil), bean inoculant (microbial preparations from the rhizosphere and rhizoplane of bean cultivated in donor soil), untreated plant (soybean rhizosphere from a less productive field without soybean inoculant application), and treated plant (soybean rhizosphere from a less productive field with soybean inoculant application). Asterisks denote significant differences between treatments (Tukey's test, $p < 0.05$ *, $p < 0.01$ **). "ns" indicates non-significant differences.

Significant disparities in richness (Chao1, $p = 0.008$) and diversity (Shannon, $p = 0.013$) indices were also observed between the soybean and bean inoculants. Interestingly, the microbial communities inherent to inoculant constituents, such as peat-derived microbes, minimally impacted the bacterial composition. These findings emphasize the dominant role of host plants in shaping bacterial communities, even when grown under identical soil conditions.

No significant differences in richness (Chao1, $p > 0.40$) or diversity (Shannon/Simpson, $p > 0.35$) were observed between: (1) soybean inoculant and untreated groups, or (2) treated versus untreated plants (Figure 3). While the inoculant itself showed higher diversity (Shannon $p = 0.008$; Simpson $p = 0.012$) than field samples, it did not significantly alter overall rhizosphere diversity (all $p > 0.05$). Notably, both untreated and treated samples demonstrated increased variability in richness and diversity, as illustrated by alpha-diversity graphs (Figure 3). This variability likely reflected the effects of spatial and soil heterogeneity in open agricultural fields, which differentially shaped microbial dispersion across microhabitats.

3.3. Beta-Diversity and Taxonomic Composition

Principal Coordinate Analysis (PCoA) demonstrated significant compositional differences between donor soil and inoculant samples (PERMANOVA: $p = 0.001$), with soybean and bean inoculants forming distinct clusters ($p = 0.003$) that reflected host-specific recruitment during preparation. In contrast, field-grown plants showed remarkable community stability, with no significant differences between treated and untreated groups ($p = 0.34$; Figure 4). Beta-diversity metrics quantitatively supported these patterns: weighted UniFrac distances were 4-fold greater between donor soil and field plants (0.72 ± 0.03) than between treated and untreated plots (0.18 ± 0.02). Variance partitioning confirmed soil origin (donor vs. recipient) as the dominant structuring factor ($R^2 = 0.38$, $p = 0.001$), while inoculation

accounted for minimal variation ($R^2 = 0.05$, $p = 0.21$). Together, these results demonstrate that while the clonal garden technique successfully generated host-specific inoculants, their application failed to enhance overall rhizosphere diversity in treated plants.

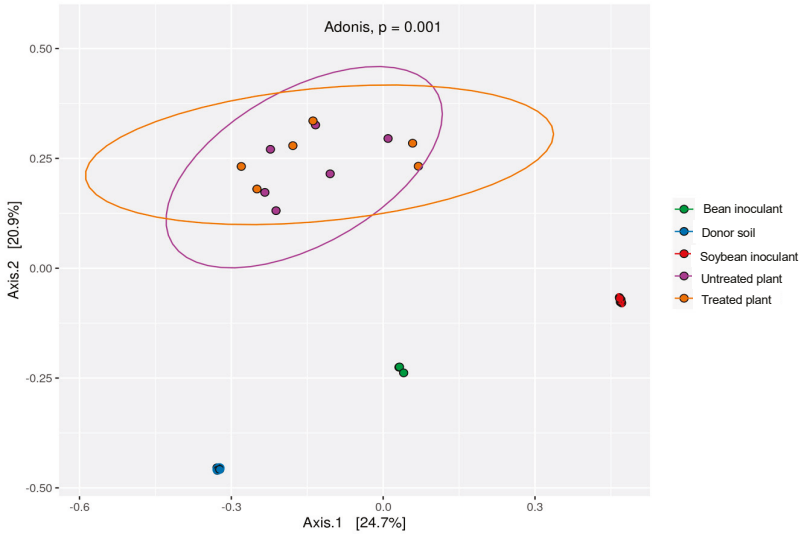

Figure 4. Principal Coordinate Analysis (PCoA) of bacterial communities at 99% similarity, based on 16S rRNA sequences using unweighted UniFrac distances. ADONIS test reveals distinct differences between donor soil and inoculants, with similarities between untreated and treated plants.

In Figure 5, despite some proportional differences in group abundances, bacterial profiles in untreated and treated samples exhibited similarity, as previously demonstrated. Untreated samples contained an average of 29 phyla, with Proteobacteria (49%), Actinobacteriota (19%), Firmicutes (18%), Bacteroidota (4%), Acidobacteriota (2%), Gemmatimonadota (2%), Planctomycetota (1%), and Chloroflexota (1%), each accounting for more than 1% of operational taxonomic unit (OTU) relative abundance. Similarly, treated samples averaged 26 phyla, dominated by Proteobacteria (58%), Firmicutes (28%), Actinobacteria (10%), and Bacteroidota (1%), each exceeding 1% of OTUs. The phyla detected at less than 1% in both untreated and treated samples were categorized as components of the rare biosphere.

The soybean-derived inoculant exhibited a distinct metataxonomic profile compared to the donor soil. Proteobacteria predominated in the inoculant accounting for 77% of observed OTUs across 21 bacterial phyla. This was in sharp contrast to the donor soil, where Proteobacteria represented only 24% of OTUs across a more diverse spectrum of 30 phyla. Other significant phyla in the soybean inoculant included Bacteroidota (9%), Actinobacteriota (7%), and Firmicutes (5%). Conversely, the donor soil exhibited higher relative abundances of Chloroflexota (6%), Acidobacteriota (4%), Gemmatimonadota (3%), Planctomycecota (3%), and Myxococcota (1%), which collectively contributed less than 1% of the reads in the soybean inoculant.

On the other hand, the bean-based inoculant was similarly dominated by Proteobacteria (75%) but included a higher proportion of Actinobacteriota (14%) alongside Firmicutes (4%) and Bacteroidota (2%). This inoculant comprised 22 bacterial phyla, including Nitrospinota, a group absent in the donor soil but detected as part of the rare biosphere within the inoculant. The appearance of Nitrospinota suggests its origin from external sources, such as the peat used in the formulation or the seeds of the bean cultivar Campos Gerais. However, its absence in the donor soil and other samples may also reflect technical limitations in sequencing, particularly in detecting low-abundance taxa associated with the rare biosphere.

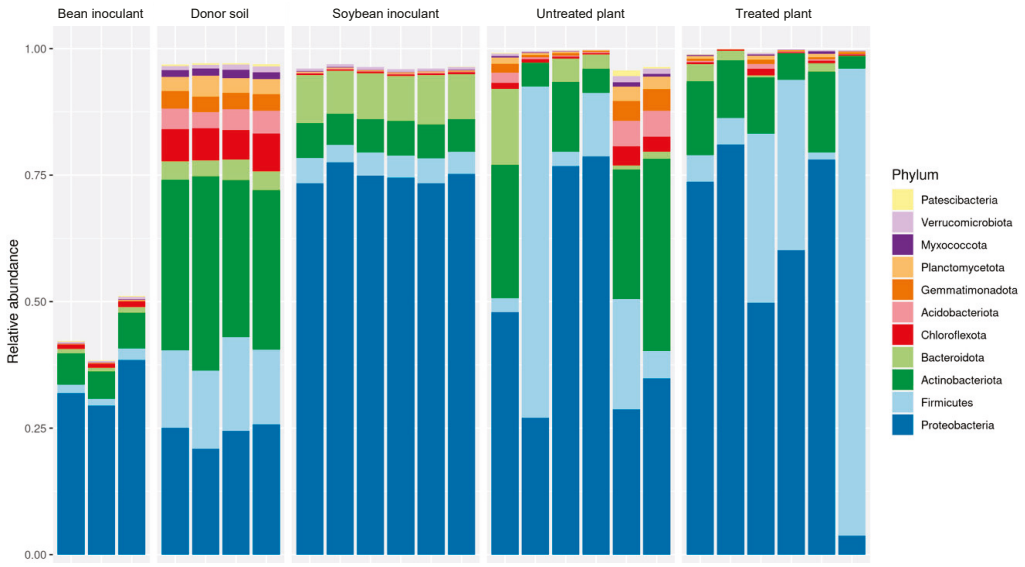

Figure 5. Taxonomic assignments at the phylum level showing the relative abundance (%) of the 16S rRNA gene sequences from different sample types: *bean inoculant* (microbial preparations from the rhizosphere and rhizoplane of bean cultivated in donor soil), *donor soil* (highly productive soybean farmland soil), *soybean inoculant* (microbial preparations from the rhizosphere and rhizoplane of soybean cultivated in donor soil), *untreated plant* (soybean rhizosphere from a less productive field without soybean inoculant application), and *treated plant* (soybean rhizosphere from a less productive field with soybean inoculant application).

In this study, the methodology involving a clonal garden and inoculant preparation from the soybean rhizosphere and rhizoplane revealed the absence of several bacterial groups in the inoculants, including Methylomirabilota, Dormibacterota, Elusimicrobiota, candidatus 4484-113, Deinococcota, Tectomicrobia, Halobacteriota, Fibrobacterota, and Eisenbacteria. This absence was likely due to the rhizosphere's recruitment of a highly specialized bacterial community predominantly composed of Proteobacteria, Bacteroidota, Actinobacteriota, and Firmicutes.

Interestingly, many phyla undetected in the inoculants were naturally present in both the donor and recipient soil samples. However, certain groups, such as Tectomicrobia, Halobacteriota, Fibrobacterota, and Eisenbacteria remained undetected in the recipient soil. These findings suggest that the phyla absent from both the recipient soil and inoculants may naturally occur only in the donor soil, as soybean plants failed to recruit these groups in the rhizosphere.

3.4. Deeper-Level Taxonomic Analysis

Taxonomic analysis at the order level revealed statistically significant changes in specific bacterial taxa following inoculation ($p < 0.05$ for all reported groups), despite overall community stability (PERMANOVA $p = 0.34$). Key taxonomic orders driving the differentiation of the samples, as shown in Figure 6A, include Rhizobiales, Enterobacterales, Pseudomonadales, Actinomycetales, Streptomycetales, Bacillales, Lactobacillales, Burkholderiales, Propionibacteriales, Sphingobacteriales, and Xanthomonadales, all with relative abundances exceeding 5% across the dataset.

More detailed family-level analysis (Figure 6B) demonstrated specific enrichment of plant-growth-promoting taxa in treated plants, most notably *Enterobacteriaceae* (22.3% increase, $p = 0.008$)—known for nitrogen fixation and phytohormone production—and *Rhizobiaceae* (15.7% increase, $p = 0.012$), which are essential for soybean nodulation. These beneficial increases coincided with reductions in native soil-adapted taxa, including *Micrococcaceae* (11.2% decrease, $p = 0.021$) and stress-tolerant *Sphingobacteriaceae* (8.5% decrease,

q = 0.038), suggesting competitive displacement of some native specialists. The treatment also enhanced other functionally important families like Pseudomonadaceae, *Xanthobacteraceae*, *Moraxellaceae*, *Bacillaceae*, *Streptococcaceae*, and *Planococcaceae* ($p < 0.05$), while reducing abundance of *Beijerinckiaceae* and *Burkholderiaceae*.

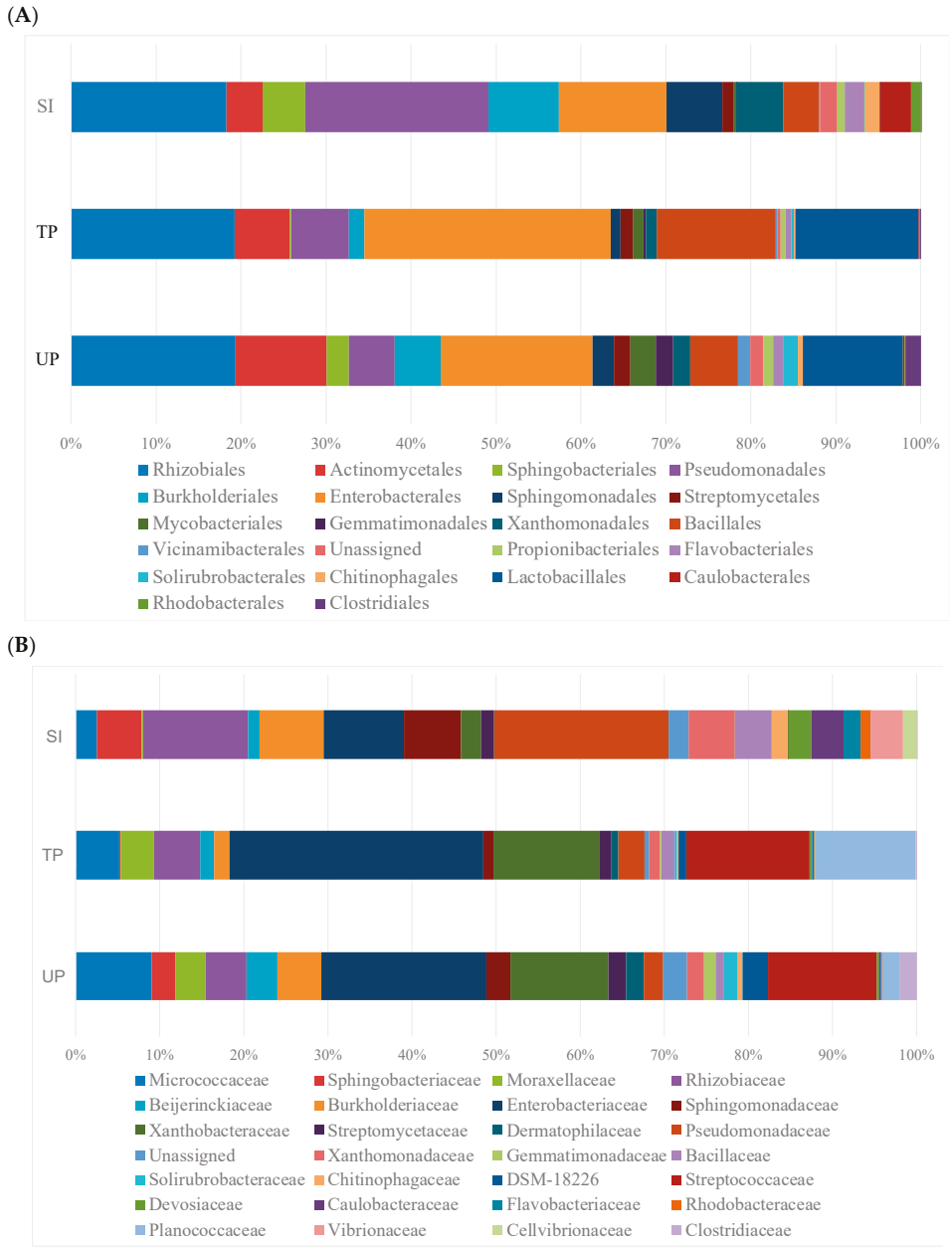

Figure 6. Distribution of the most abundant bacterial at the order (**A**) and family (**B**) levels based on the 16S rRNA gene sequences from different sample types: soybean inoculant, SI (microbial preparations from the rhizosphere and rhizoplane of soybean cultivated in donor soil); treated plants, TP (soybean rhizosphere from a less productive field with soybean inoculant application); and untreated plants, UP (soybean rhizosphere from a less productive field without soybean inoculant application).

The selective establishment of inoculated beneficial taxa without broader community disruption implies a balanced trade-off: the treatment successfully enriched key functional groups while the resident microbiome's resilience prevented complete restructuring. The maintenance of the overall community structure despite these taxon-specific changes highlights two key findings: (1) the remarkable resilience of established soil microbiomes

after 90 days of succession and (2) the ability to selectively enhance beneficial taxa without disrupting critical soil functions.

3.5. Greenhouse Experiment and Agricultural Productivity in the Field

A greenhouse experiment evaluated the performance of soybean plants after the incorporation of soybean inoculant sourced from highly productive to less productive soybean fields. The results indicate no significant differences in germination percentage, plant height, root dry mass, or shoot dry mass between treated and untreated plants (Table 1). Visual observations supported these findings, suggesting that transplanting microbiomes from a high agricultural productivity area to a less productive area, using the study's methodology, did not effectively promote soybean growth. It is worth noting, however, that the study's duration (21 days post-inoculation) may not capture short- or long-term effects on soil microbiome and plant growth.

Table 1. Effects of a microbial consortium inoculant, derived from soybean plants cultivated in a high-productivity field, on soybean development in less productive soil. Growth parameters, including germination rate, plant height, root dry mass, and shoot dry mass, were evaluated in a greenhouse pot experiment. Each treatment included six biological replicates (n = 6).

Seedling Properties	**Inoculant Doses (g kg^{-1} of Seeds)**					
	0.0	**0.25**	**0.50**	**0.75**	**1.0**	**10.0**
Germination (%)	93.3 ± 10.3	83.3 ± 15.1	73.3 ± 16.3	90.0 ± 11.0	90.0 ± 11.0	83.3 ± 23.4
Plant height (cm)	15.7 ± 1.4	15.7 ± 1.1	15.7 ± 1.5	16.0 ± 0.6	16.1 ± 1.1	15.3 ± 1.3
Root dry weight (g pL^{-1})	0.156 ± 0.012	0.171 ± 0.023	0.134 ± 0.044	0.155 ± 0.028	0.137 ± 0.028	0.150 ± 0.028
Shoot dry weight (g pL^{-1})	0.35 ± 0.03	0.37 ± 0.02	0.37 ± 0.03	0.38 ± 0.04	0.35 ± 0.06	0.36 ± 0.02

In terms of soybean agricultural productivity (kg ha^{-1}), although non-significant, a marginal increase of 240 kg ha^{-1} (4.8–6.2%, p = 0.08) post-transplantation was noted in variable dosages, indicating potential benefits on crop yield (Figure 7).

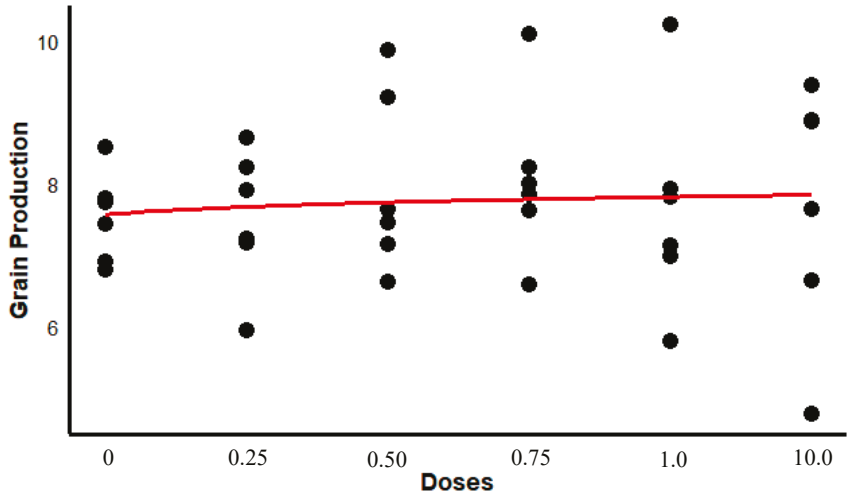

Figure 7. Response curve showing soybean grain yield as a function of microbial consortium inoculant applied to seeds before sowing. Five different dosages of inoculant (0.25, 0.50, 0.75, 1.00, 10.0 g of inoculant per Kg of soybean seed) were tested (treated plants), along with a control group without inoculant (untreated plants).

4. Discussion

This study addresses current agricultural challenges by leveraging microbiological interventions to promote sustainable crop production. Specifically, we aimed to improve soil health and plant productivity by transferring microbial consortia from the rhizosphere and rhizoplane of soybeans grown in high-productivity fields to lower-productivity farmland. As highlighted by Moretti et al. [4], inoculation significantly impacts bacterial communities, with more pronounced effects on rhizofertility than on archaeal or fungal communities. Bacteria were prioritized in this study due to their sensitivity to microbiological interventions and their role as key indicators of soil health and rhizosphere modulation. They also dominate crucial plant-growth-promoting functions—such as nitrogen fixation and phosphorus solubilization—respond rapidly to inoculation and have well-established detection methods. Although archaea and fungi also contribute to soil health, their slower dynamics made bacteria more suitable for this proof-of-concept study evaluating the immediate effects of microbial transfer. Using 16S rRNA gene sequencing, we profiled bacterial communities in inoculated and non-inoculated plants, as well as in the microbial consortia used for inoculation, providing a robust framework to assess inoculation efficacy in modulating the soybean rhizosphere.

The rhizosphere is a dynamic environment shaped by interactions between specialist and generalist microbes, both of which are critical for plant health and soil function [1,7,16,28]. Specialist taxa, such as soybean-associated *Rhizobiaceae*, often form host-specific mutualisms, while generalists like *Pseudomonadaceae* thrive across diverse environments due to their metabolic versatility [1,10,28]. In our study, bacterial community composition and diversity indices differed significantly between the two soils, likely due to contrasting edaphoclimatic conditions [31,32]. These conditions influenced the success of microbial transfer: *Rhizobiaceae* abundance increased by 15.7% in inoculated soils ($p = 0.012$), likely driven by host-specific interactions, while generalist taxa showed variable establishment. Soil origin explained a substantial portion of microbial variance ($R^2 = 0.38$, $p = 0.001$), while inoculation accounted for a smaller effect ($R^2 = 0.05$), underscoring both the resilience of native microbial communities and the importance of matching inoculant traits to soil compatibility [33]

Traditional inoculants, typically composed of one or a few microbial strains, often yield inconsistent results due to the complexity and competitiveness of soil microbiomes [11,12]. In contrast, indigenous microbial consortia—microbes naturally adapted to local soils and host plants—offer a promising alternative to enhance crop resilience and productivity [3,11,16,22]. This strategy has proven effective in diverse fields, including human health, ecosystem restoration, and soybean cultivation [3,5,11,23]. Following this approach, we employed the "clonal garden" technique to develop a microbial consortium specifically enriched for soybean-associated microbes from high-productivity soils. This method targets locally adapted microbial species, potentially offering advantages over more generalized native inoculants. Furthermore, combining the microbial material with peat and fertilizer may have introduced rare groups such as Nitrospinota, involved in nitrite oxidation and nitrogen cycling [24,25,34]. However, this group was detected only in bean inoculants, highlighting rhizosphere selectivity.

Differences between bean- and soybean-derived inoculants likely reflect rhizosphere-specific recruitment processes shaped by plant genotype, root exudates, soil properties, and developmental stage [7,35,36]. Notably, the inoculant was derived from 21-day-old soybean plants, while rhizosphere samples in the recipient soils were collected at 90 days post-sowing. This temporal mismatch may have influenced microbial dynamics, as recruitment patterns evolve during plant development [32]. Although not directly tested, our

findings suggest that future studies should align inoculation timing with plant phenology to maximize microbial establishment and function.

Consistent with Mendes et al. [1], our results reinforce the rhizosphere as a central interface for plant–microbe interactions. Transferring microbiota from high- to low-productivity soils modulated specific microbial taxa and led to modest improvements in plant performance. Similar outcomes have been reported in other crops: rice fields receiving microbiota from high-productivity soils showed improved nitrogen use efficiency [13], and wheat experienced 8–12% yield gains after rhizosphere transplantation [14]. Nevertheless, the variability in outcomes—including our own—highlights the importance of soil type, environmental context, and inoculant composition [4,11,17,27,36].

Contrary to expectations, treated plants did not fully reflect the diversity present in the inoculant, likely due to competitive exclusion and ecological filtering favoring native taxa [7,8]. For instance, although Proteobacteria dominated the inoculant, they showed limited establishment in the treated soils, emphasizing the selective nature of rhizosphere colonization [7]. While the inoculant enriched certain beneficial taxa, it did not significantly alter the overall community structure. This is supported by stable alpha-diversity indices (Shannon $p = 0.38$; Simpson $p = 0.41$), minimal beta-diversity shifts (PCo2 variance = 6.2%), and a high degree of shared ASVs (78%) between treated and control samples. These findings suggest that inoculants can enhance specific microbial groups while preserving core microbiome resilience over a 90-day period.

This pattern aligns with concepts from microbial invasion ecology, where introduced taxa often occupy narrow ecological niches without disrupting resident communities [37,38]. The observed "priority effect" allows introduced microbes to persist by exploiting underutilized metabolic functions without inducing competitive displacement [39]. Our data support the stochastic niche occupancy model [40], where introduced and native microbes coexist through niche partitioning, metabolic complementarity, and neutral interactions. These findings mirror observations in other cropping systems where successful inoculants supplement, rather than replace, indigenous microbiota [41]. Considering the temporal and spatial variability of field conditions, future research should prioritize stage-specific sampling to determine optimal inoculation windows—particularly early in development, when microbial communities may be more receptive to modulation.

Further taxonomic analysis revealed enrichment of beneficial bacterial families, such as *Enterobacteriaceae* and *Rhizobiaceae*, in inoculated rhizospheres. This agrees with previous studies showing targeted increases in growth-promoting genera like *Enterobacter*, *Pseudomonas*, and *Xanthomonas* [11]. However, concurrent declines in other microbial groups indicate that the inoculant exerted a selective rather than broad-spectrum effect on community composition. These findings are consistent with research suggesting that microbial inoculants shift microbial balances but do not necessarily confer universal benefits [7,42,43]. In our greenhouse experiment, no significant differences in seedling growth were observed between treatments, possibly due to the short trial duration (21 days), which may have been insufficient to detect plant-level impacts. Nevertheless, the marginal 6.2% increase in soybean yield observed under field conditions suggests that microbial transfers may confer agronomic benefits under more variable and stressful environments. Given that traditional plant breeding typically achieves annual yield gains of 1–2% [44], a single microbial intervention yielding over 6% is notable.

The contrasting results between greenhouse and field trials underscore the importance of environmental context in determining inoculant efficacy. In the controlled greenhouse setting, microbial activity may have been constrained by stable conditions. In contrast, the 90-day field trial introduced abiotic variability (e.g., temperature, moisture, and nutrient fluctuations), creating ecological niches that may have favored the activity and persistence

of introduced microbes. The extended timeframe also allowed for more sustained interactions between the microbiome and plant physiology—critical elements often absent in short-term studies.

These results suggest that microbial inoculants act more effectively as buffers against environmental stress rather than as direct growth stimulants. This is consistent with meta-analyses showing that co-inoculation often yields modest or inconsistent results unless closely matched to specific environmental conditions [43]. Still, emerging evidence demonstrates considerable yield improvements in soybean and other crops when inoculants are ecologically tailored [4,22,29,45]. Our findings contribute to this growing body of evidence by demonstrating that intraspecific microbial transfers can enhance rhizosphere function and support crop performance in marginal soils.

Overall, our results highlight the importance of long-term, field-based studies that capture environmental variability across full crop cycles. They also suggest a dual mechanism: while soil fertility parameters establish the fundamental productivity potential, microbial consortia can provide incremental yield improvements by optimizing nutrient use efficiency and stress tolerance. This synergistic effect implies that microbial transplantation should be viewed as a complement to—rather than replacement for—balanced fertilization in low-fertility soils. Future research should focus on optimizing inoculant formulation, application timing, and delivery strategies—particularly for degraded or low-fertility soils. These efforts should be grounded in ecological principles such as niche complementarity and host–microbe specificity to improve inoculant persistence and function in diverse agroecosystems.

5. Conclusions

This study demonstrates the feasibility and potential of using host-adapted microbial consortia derived from high-productivity soybean soils to enhance crop performance in less fertile farmland. The inoculant selectively enriched beneficial bacterial families such as *Enterobacteriaceae* and *Rhizobiaceae*, which are associated with nutrient acquisition and nodulation. Importantly, these changes occurred without disrupting the broader rhizosphere microbial community, indicating a balanced integration with native soil microbiota. While short-term greenhouse trials showed limited plant growth responses, field experiments revealed a modest yield increase of 4.8–6.2%, suggesting that microbial transplantation may confer agronomic benefits under real-world environmental conditions. These findings support the concept that microbial inoculants can function more effectively as resilience-enhancing agents than as direct growth stimulants.

To fully realize the agronomic potential of microbiome transplantation, long-term, multi-site field trials should be conducted across diverse agroecological zones and cropping systems. Such trials should assess microbial persistence, functional stability, and crop performance across complete growth cycles, while also evaluating interactions with soil type, climate variability, and crop management practices. In particular, future work should explore the synchronization of inoculation with crop phenological stages to optimize plant–microbe interactions and improve microbial establishment. Furthermore, integrating microbial inoculants with existing fertilization strategies may offer synergistic benefits, particularly in nutrient-poor soils. Collectively, these efforts will be essential to refining inoculant composition, formulation, and delivery methods, thereby enhancing the ecological compatibility and efficacy of microbiome-based solutions for sustainable agriculture.

Supplementary Materials: The following supporting information can be downloaded at: https://www.mdpi.com/article/10.3390/microorganisms13061177/s1. File S1: Supplementary Material. References [46–50] are cited in the Supplementary Materials.

Author Contributions: Conceptualization, A.M.; Methodology, A.M.; Software, H.D.Q.; Resources, A.M.; Data curation, D.T.S. and H.D.Q.; Writing—original draft, D.T.S.; Writing—review & editing, A.C.S.M., H.D.Q. and A.M.; Visualization, A.C.S.M.; Supervision, A.M.; Project administration, A.M.; Funding acquisition, A.M. All authors have read and agreed to the published version of the manuscript.

Funding: This work was made possible thanks to the financial support of Nooa Agricultural Science and Technology and FAPED/CNPMA/Curimbaba 1154-21300.230006-3.

Data Availability Statement: The original contributions presented in this study are included in the article/Supplementary Materials. Further inquiries can be directed to the corresponding author.

Acknowledgments: The authors thank Nooa Agricultural Science and Technology for supporting this work. Thanks to the farmer Jan Haajes from Castro, Paraná, for kindly providing the agricultural soil from his productive field.

Conflicts of Interest: Author Aurélio Carneiro Soares Moreira was employed by the company NOOA. The remaining authors declare that the research was conducted in the absence of any commercial or financial relationships that could be construed as a potential conflict of interest.

References

1. Mendes, R.; Garbeva, P.; Raaijmakers, J.M. The Rhizosphere Microbiome: Significance of Plant Beneficial, Plant Pathogenic, and Human Pathogenic Microorganisms. *FEMS Microbiol. Rev.* **2013**, *37*, 634–663. [CrossRef] [PubMed]
2. Chaparro, J.M.; Sheflin, A.M.; Manter, D.K.; Vivanco, J.M. Manipulating the Soil Microbiome to Increase Soil Health and Plant Fertility. *Biol. Fertil. Soils* **2012**, *48*, 489–499. [CrossRef]
3. Bziuk, N.; Maccario, L.; Sørensen, S.; Schikora, A.; Smalla, K. Barley Rhizosphere Microbiome Transplantation—A Strategy to Decrease Susceptibility of Barley Grown in Soils with Low Microbial Diversity to Powdery Mildew. *Front. Microbiol.* **2022**, *13*, 830905. [CrossRef]
4. Moretti, L.G.; Crusciol, C.A.C.; Leite, M.F.A.; Momesso, L.; Bossolani, J.W.; Costa, O.Y.A.; Hungria, M.; Kuramae, E.E. Diverse Bacterial Consortia: Key Drivers of Rhizosoil Fertility Modulating Microbiome Functions, Plant Physiology, Nutrition, and Soybean Grain Yield. *Environ. Microbiome* **2024**, *19*, 50. [CrossRef]
5. Mendes, R.; Kruijt, M.; De Bruijn, I.; Dekkers, E.; Van Der Voort, M.; Schneider, J.H.; Piceno, Y.M.; DeSantis, T.Z.; Andersen, G.L.; Bakker, P.A.; et al. Deciphering the Rhizosphere Microbiome for Disease-Suppressive Bacteria. *Science* **2011**, *332*, 1097–1100. [CrossRef]
6. Rodrigues, J.L.; Pellizari, V.H.; Mueller, R.; Baek, K.; Jesus, E.D.C.; Paula, F.S.; Mirza, B.; Hamaoui, G.S.; Tsai, S.M.; Feigl, B.; et al. Conversion of the Amazon Rainforest to Agriculture Results in Biotic Homogenization of Soil Bacterial Communities. *Proc. Natl. Acad. Sci. USA* **2013**, *110*, 988–993. [CrossRef]
7. Philippot, L.; Raaijmakers, J.; Lemanceau, P.; Putten, W. Going Back to the Roots: The Microbial Ecology of the Rhizosphere. *Nat. Rev. Microbiol.* **2013**, *11*, 789–799. [CrossRef]
8. Mendes, L.W.; de Lima Brossi, M.J.; Kuramae, E.E.; Tsai, S.M. Land-Use System Shapes Soil Bacterial Communities in Southeastern Amazon Region. *Appl. Soil Ecol.* **2015**, *95*, 151–160. [CrossRef]
9. Santos, M.D.S.; Kavamura, V.N.; Reynaldo, E.F.; Souza, D.T.; Da Silva, E.H.F.M.; May, A. Bacterial Structure of Agricultural Soils with High and Low Yields. *J. Plant Pathol. Microbiol.* **2017**, *8*, 1000405. [CrossRef]
10. Schlatter, D.; Kinkel, L.; Thomashow, L.; Weller, D.; Paulitz, T. Disease Suppressive Soils: New Insights from the Soil Microbiome. *Phytopathology* **2017**, *107*, 1284–1297. [CrossRef]
11. May, A.; Coelho, L.; Pedrinho, A.; Batista, B.; Mendes, L.; Mendes, R.; Morandi, M.; Barth, G.; Viana, R.; Vilela, E. The Use of Indigenous Bacterial Community as Inoculant for Plant Growth Promotion in Soybean Cultivation. *Arch. Agron. Soil Sci.* **2021**, *69*, 135–150. [CrossRef]
12. Van Veen, J.A.; van Overbeek, L.S.; van Elsas, J.D. Fate and Activity of Microorganisms Introduced into Soil. *Microbiol. Mol. Biol. Rev.* **1997**, *61*, 121–135. [CrossRef]
13. Shi, Y.-C.; Zheng, Y.-J.; Lin, Y.-C.; Huang, C.-H.; Shen, T.-L.; Hsu, Y.-C.; Lee, B.-H. Investigation of the Microbial Diversity in the *Oryza sativa* Cultivation Environment and Artificial Transplantation of Microorganisms to Improve Sustainable Mycobiota. *J. Fungi* **2024**, *10*, 412. [CrossRef]
14. Khatri, S.; Bhattacharjee, A.; Shivay, Y.S.; Sharma, S. Transplantation of Soil from Organic Field Confers Disease Suppressive Ability to Conducive Soil. *World J. Microbiol. Biotechnol.* **2024**, *40*, 112. [CrossRef]

15. Cordovez, V.; Dini-Andreote, F.; Carrión, V.J.; Raaijmakers, J.M. Ecology and Evolution of Plant Microbiomes. *Annu. Rev. Microbiol.* **2019**, *73*, 69–88. [CrossRef]
16. Qiu, Z.; Egidi, E.; Liu, H.; Kaur, S.; Singh, B.K. New Frontiers in Agriculture Productivity: Optimised Microbial Inoculants and In Situ Microbiome Engineering. *Biotechnol. Adv.* **2019**, *37*, 107371. [CrossRef]
17. Bradáčová, K.; Sittinger, M.; Tietz, K.; Neuhäuser, B.; Kandeler, E.; Berger, N.; Ludewig, U.; Neumann, G. Maize Inoculation with Microbial Consortia: Contrasting Effects on Rhizosphere Activities, Nutrient Acquisition and Early Growth in Different Soils. *Microorganisms* **2019**, *7*, 329. [CrossRef]
18. Arif, I.; Batool, M.; Schenk, P. Plant Microbiome Engineering: Expected Benefits for Improved Crop Growth and Resilience. *Trends Biotechnol.* **2020**, *38*, 1385–1396. [CrossRef]
19. Moretti, L.; Crusciol, C.; Bossolani, J.; Momesso, L.; Garcia, A.; Kuramae, E.; Hungria, M. Bacterial Consortium and Microbial Metabolites Increase Grain Quality and Soybean Yield. *J. Soil Sci. Plant Nutr.* **2020**, *20*, 1923–1934. [CrossRef]
20. May, A.; Coelho, L.F.; da Silva, E.H.F.M.; Junior, N.A.V.; da Silva Viana, R.; Verdial, M.; Gonzaga, A.R.; Boratto, V.N.M.; Boratto, I.V.; Carvalho, P. Use of Plant Extracts from Healthy Soybean and Potato Plants for Treatments of Plants of the Same Species. *Res. Soc. Dev.* **2021**, *10*, e225101220351. [CrossRef]
21. May, A.; Silva, E.H.F.M.D.; Vieira Junior, N.A.; Vilela, E.S.D.; Santos, M.D.S.D.; Coelho, L.F.; Pedrinho, A.; Batista, B.D.; Viana, R.D.S. Soybean Extracts Can Improve Plant Development. *Sci. Agric.* **2022**, *80*, e20210102. [CrossRef]
22. Smirnova, I.; Sadanov, A.; Baimakhanova, G.; Faizulina, E.; Tatarkina, L. Use of a Consortium of Agronomically Important Microorganisms for Growing Soybean (*Glycine max* L.). *Open Agric. J.* **2023**, *17*, e187433152302140. [CrossRef]
23. Khoruts, A.; Dicksved, J.; Jansson, J.K.; Sadowsky, M.J. Changes in the Composition of the Human Fecal Microbiome after Bacteriotherapy for Recurrent *Clostridium difficile*-Associated Diarrhea. *J. Clin. Gastroenterol.* **2010**, *44*, 354–360. [CrossRef] [PubMed]
24. Miljakoviae, D.; Marinkoviæ, J.; Đorđeviæ, V.; Vasiljeviæ, M.; Tintor, B.; Jaæimoviæ, S.; Ristiæ, Ž. Integrated Use of Consortia-Based Microbial Inoculants and Nutrient Complex Stimulates the Rhizosphere Microbiome and Soybean Productivity. *Legume Res.—Int. J.* **2023**, *47*, 120–125. [CrossRef]
25. Tshering, K.; Rengel, Z.; Storer, P.; Solaiman, Z.M. Microbial Consortium Inoculum with Rock Minerals Increased Wheat Grain Yield, Nitrogen-Use Efficiency, and Protein Yield Due to Larger Root Growth and Architecture. *Agronomy* **2022**, *12*, 2481. [CrossRef]
26. Singh, V.; Kumar, B. A Review of Agricultural Microbial Inoculants and Their Carriers in Bioformulation. *Rhizosphere* **2024**, *29*, 100843. [CrossRef]
27. Lopes, M.; Dias-Filho, M.; Gurgel, E. Successful Plant Growth-Promoting Microbes: Inoculation Methods and Abiotic Factors. *Front. Sustain. Food Syst.* **2021**, *5*, 606454. [CrossRef]
28. Bever, J.D.; Mangan, S.A.; Alexander, H.M. Maintenance of Plant Species Diversity by Pathogens. *Annu. Rev. Ecol. Evol. Syst.* **2015**, *46*, 305–325. [CrossRef]
29. Callahan, B.J.; McMurdie, P.J.; Rosen, M.J.; Han, A.W.; Johnson, A.J.A.; Holmes, S.P. DADA2: High-Resolution Sample Inference from Illumina Amplicon Data. *Nat. Methods* **2016**, *13*, 581–583. [CrossRef]
30. Quast, C.; Pruesse, E.; Yilmaz, P.; Gerken, J.; Schweer, T.; Yarza, P.; Glöckner, F.O. The SILVA Ribosomal RNA Gene Database Project: Improved Data Processing and Web-Based Tools. *Nucleic Acids Res.* **2012**, *41*, D590–D596. [CrossRef]
31. Fulthorpe, R.R.; Roesch, L.F.; Riva, A.; Triplett, E.W. Distantly Sampled Soils Carry Few Species in Common. *ISME J.* **2008**, *2*, 901–910. [CrossRef] [PubMed]
32. Fernandez-Gnecco, G.; Smalla, K.; Maccario, L.; Sørensen, S.; Barbieri, P.; Consolo, V.; Covacevich, F.; Babin, D. Microbial Community Analysis of Soils under Different Soybean Cropping Regimes in the Argentinean South-Eastern Humid Pampas. *FEMS Microbiol. Ecol.* **2021**, *97*, fiab007. [CrossRef] [PubMed]
33. Mallon, C.A.; Poly, F.; Le Roux, X.; Marring, I.; van Elsas, J.D.; Salles, J.F. Resource pulses can alleviate the biodiversity–invasion relationship in soil microbial communities. *Ecol. Lett.* **2015**, *18*, 1310–1319. [CrossRef] [PubMed]
34. Kop, L.F.; Koch, H.; Jetten, M.S.; Daims, H.; Lücker, S. Metabolic and Phylogenetic Diversity in the Phylum Nitrospinota Revealed by Comparative Genome Analyses. *ISME Commun.* **2024**, *4*, ycad017. [CrossRef]
35. Dos Santos, J.A.F.; do Nascimento, A.F.; Rempel, D.M.; Ferreira, A. Changes in Bacterial Communities Induced by Integrated Production Systems and the Phenological Stages of Soybean. *Sci. Total Environ.* **2024**, *912*, 168626. [CrossRef]
36. Hashmi, I.; Paul, C.; Al-Dourobi, A.; Sandoz, F.; Deschamps, P.; Junier, T.; Junier, P.; Bindschedler, S. Comparison of the Plant Growth-Promotion Performance of a Consortium of Bacilli Inoculated as Endospores or as Vegetative Cells. *FEMS Microbiol. Ecol.* **2019**, *95*, fiz147. [CrossRef]
37. Carlström, C.I.; Field, C.M.; Bortfeld-Miller, M.; Müller, D.B.; Vorholt, J.A. Synthetic Microbiota Reveal Priority Effects and Keystone Strains in the Arabidopsis Phyllosphere. *Nat. Ecol. Evol.* **2019**, *3*, 1445–1454. [CrossRef]
38. Mallon, C.A.; Le Roux, X.; van Doorn, G.S.; Dini-Andreote, F.; Poly, F.; Salles, J.F. The Impact of Failure: Unsuccessful Bacterial Invasions Steer the Soil Microbial Community Away from the Invader's Niche. *ISME J.* **2018**, *12*, 728–741. [CrossRef]

39. Fukami, T. Historical Contingency in Community Assembly: Integrating Niches, Species Pools, and Priority Effects. *Annu. Rev. Ecol. Evol. Syst.* **2015**, *46*, 1–23. [CrossRef]
40. Nemergut, D.R.; Schmidt, S.K.; Fukami, T.; O'Neill, S.P.; Bilinski, T.M.; Stanish, L.F.; Knelman, J.E.; Darcy, J.L.; Lynch, R.C.; Wickey, P.; et al. Patterns and Processes of Microbial Community Assembly. *Microbiol. Mol. Biol. Rev.* **2013**, *77*, 342–356. [CrossRef]
41. Bashan, Y.; de-Bashan, L.E.; Prabhu, S.R.; Hernandez, J.-P. Advances in plant growth-promoting bacterial inoculant technology: Formulations and practical perspectives (1998–2013). *Plant Soil* **2014**, *378*, 1–33. [CrossRef]
42. Liu, F.; Hewezi, T.; Lebeis, S.; Pantalone, V.; Grewal, P.; Staton, M. Soil Indigenous Microbiome and Plant Genotypes Cooperatively Modify Soybean Rhizosphere Microbiome Assembly. *BMC Microbiol.* **2019**, *19*, 201. [CrossRef]
43. Zeffa, D.M.; Fantin, L.H.; Koltun, A.; de Oliveira, A.L.; Nunes, M.P.; Canteri, M.G.; Gonçalves, L.S. Effects of Plant Growth-Promoting Rhizobacteria on Co-Inoculation with Bradyrhizobium in Soybean Crop: A Meta-Analysis of Studies from 1987 to 2018. *PeerJ* **2020**, *8*, e7905. [CrossRef] [PubMed]
44. Specht, J.E.; Hume, D.J.; Kumudini, S.V. Soybean yield potential—A genetic and physiological perspective. *Crop Sci.* **1999**, *39*, 1560–1570. [CrossRef]
45. Moretti, L.G.; Lazarini, E.; Bossolani, J.W.; Parente, T.L.; Caioni, S.; Araujo, R.S.; Hungria, M. Can Additional Inoculations Increase Soybean Nodulation and Grain Yield? *Agron. J.* **2018**, *110*, 715–721. [CrossRef]
46. Caporaso, J.G.; Lauber, C.L.; Walters, W.A.; Berg-Lyons, D.; Lozupone, C.A.; Turnbaugh, P.J.; Fierer, N.; Knight, R. Global patterns of 16S rRNA diversity at a depth of millions of sequences per sample. *Proc. Natl. Acad. Sci. USA* **2011**, *108*, 4516–4522. [CrossRef]
47. Core Team, R. *R: A Language and Environment for Statistical Computing*; R Foundation for Statistical Computing: Vienna, Austria, 2025.
48. Levene, H. Contributions to probability and statistics. *Essays Honor Harold Hotell.* **1960**, *278*, 292.
49. Ripley, B.; Venables, W.; Bates, D.M.; Hornik, K.; Gebhardt, A.; Firth, D. Package 'stats'. R Foundation for Statistical Computing. 2021. Available online: https://CRAN.R-project.org (accessed on 13 January 2025).
50. Shapiro, S.S.; Wilk, M.B. An analysis of variance test for normality (Complete Samples). *Biometrika* **1965**, *52*, 591. [CrossRef]

microorganisms

MDPI

Article

Volatile Metabolome and Transcriptomic Analysis of *Kosakonia cowanii* Ch1 During Competitive Interaction with *Sclerotium rolfsii* Reveals New Biocontrol Insights

Yoali Fernanda Hernández Gómez [1,†], Jacqueline González Espinosa [1,†], Griselda Catalina Olvera Rivas [1], Jackeline Lizzeta Arvizu Gómez [2], José Humberto Valenzuela Soto [3], Miguel Angel Ramos López [1], Aldo Amaro Reyes [1], Eloy Rodríguez de León [1], Carlos Saldaña [4], José Luis Hernández Flores [5,*] and Juan Campos Guillén [1,*]

[1] Facultad de Química, Universidad Autónoma de Querétaro, Cerro de las Campanas S/N, Querétaro 76010, Mexico; yhernandez01@alumnos.uaq.mx (Y.F.H.G.); jaqui16.je@gmail.com (J.G.E.); golvera13@alumnos.uaq.mx (G.C.O.R.); miguel.angel.ramos@uaq.mx (M.A.R.L.); aldo.amaro@uaq.edu.mx (A.A.R.); eloy.q22@gmail.com (E.R.d.L.)
[2] Secretaría de Investigación y Posgrado, Centro Nayarita de Innovación y Transferencia de Tecnología (CENITT), Universidad Autónoma de Nayarit, Tepic 63173, Mexico; jackeline.arvizu@uan.edu.mx
[3] Centro de Investigación en Química Aplicada, Blvd. Enrique Reyna Hermosillo No. 140, Saltillo 25294, Mexico; humberto.valenzuela@ciqa.edu.mx
[4] Facultad de Ciencias Naturales, Universidad Autónoma de Querétaro, Av. De las Ciencias S/N, Querétaro 76220, Mexico; carlos.saldana@uaq.mx
[5] Centro de Investigación y de Estudios Avanzados del IPN, Irapuato 36824, Mexico
* Correspondence: jose.hernandezf@cinvestav.mx (J.L.H.F.); juan.campos@uaq.mx (J.C.G.)
† These authors contributed equally to this work.

Abstract

The volatile organic compounds (VOCs) produced by *K. cowanii* Ch1 play a significant role in the inhibition of the mycelial growth of phytopathogen strains. As a continuation of our previous studies, we aim to elucidate the mechanisms of the responses of *K. cowanii* Ch1 against *S. rolfsii* during a colonization competence interaction in the presence and absence of a mixture of bacterial VOCs under in vitro conditions. The results of this study showed that, in the absence of bacterial VOCs, *K. cowanii* Ch1 cannot compete against *S. rolfsii*, and the RNA-Seq analysis revealed the differential expression of genes related to the oxidative stress response in *K. cowanii* Ch1 for survival. However, in the presence of bacterial VOCs, an interesting phenotypical response was observed in *K. cowanii* Ch1, resulting in the mycelial growth inhibition of *S. rolfsii*. The upregulated genes were related to the siderophore-mediated iron transport system, zinc ion transport system, antibiotic biosynthesis monooxygenase, carbohydrate metabolism, polyketide synthase modules, and related proteins, and *katG* was probably related to the phenotype resulting in the formation of gas bubbles by *K. cowanii*. In addition, the VOC profile analyzed at 36 h for bacterial growth revealed a cocktail with an ability to increase the competence of *K. cowanii* Ch1 against *S. rolfsii* in vitro and in vivo. This study provides evidence regarding the key role that VOCs play during the colonization competition involving *K. cowanii* Ch1, the comprehension of which may enable the development of new biocontrol strategies.

Keywords: *K. cowanii* Ch1; *S. rolfsii*; RNA-Seq; colonization competence; VOC profile; biocontrol

1. Introduction

The genus *Kosakonia* is a member of the *Enterobacteriaceae* family [1]. The bacteria of this genus have a metabolic ability to grow as facultative anaerobes, are motile, grow in a wide range of temperatures, ferment various carbohydrates, and have been isolated from diverse ecological niches, which indicates that their metabolic potential in these environments enables competitive colonization against other microorganisms [2] or specific interactions with plant [3], animal [4], fungal [5], or insect hosts [6]. Some common species that reside in the rhizosphere, such as *K. oryzendophytica* YMA7 [7], *K. radicincitans* DSM 16656 [8,9], and *K. oryziphila* NP19 [10], which have been isolated from rice and wheat fields, show important plant growth-promoting traits, such as solubilizing phosphate and potassium, producing IAA and siderophores, and fixing nitrogen. Also, some strains such as *K. cowanii* Ch1 (isolated from chili powder) can produce volatile organic compounds (VOCs); in particular, these VOCs presented important effects on the mycelial growth inhibition of *Alternaria alternata* and *Sclerotium rolfsii*, with a mean rate of 70% under in vitro conditions [11]. Additionally, the *K. cowanii* Cp1 strain isolated from the seeds of *Capsicum pubescens* can produce VOCs during competitive colonization to reduce the soft rot caused by *Pectobacterium aroidearum* SM2 in economically important crops such as chili and tomato fruits [2]. Furthermore, a relevant study has demonstrated that, during the colonization of *K. radicincitans*, the acquisition of nutrients from the plant-beneficial fungus *Serendipita indica* can provide biofilm-based protection against the fungus-feeding bacterium *Collimonas fungivorans* [5]. Research on the colonization of *Anopheles gambiae* and *Glossina* sp. by *K. cowanii* Zambiae from the midgut and its correlation with the production of reactive oxygen intermediates and organic acids has demonstrated its metabolic potential to reduce *Plasmodium* and *Trypanosome* infection in the midgut of these insects [6,12].

Therefore, based on these research findings, a better understanding of the metabolic capabilities of the genus *Kosakonia* has revealed its great potential, not only in interactome systems [13], but also in biotechnological applications to produce important metabolites [14]. In this sense, more research is necessary to advance the knowledge on the bacterial ecological responses occurring during bacterial colonization through metabolomic, transcriptomic, and proteomic analyses under specific growth conditions, such as specific pH, temperature, nutrients, and CO_2 and O_2 concentrations, and in environmentally stressful conditions, such as microbial competence, VOC responses, and under toxic metabolites, in order to explore alternative metabolic pathways for the production of novel metabolites, thus providing a competitive advantage that is critical for the survival and colonization of *Kosakonia*.

In this sense, diverse studies have demonstrated the potential of VOCs, produced by an increasing number of microorganisms reported, as potent modulators of communication signals and for the biocontrol of phytopathogenic microorganisms based on their hazardous physical–chemical properties, which may affect cell integrity and the up/downregulation of gene expression related to diverse metabolic pathways, virulence, and alterations in the redox balance that compromise cell viability [15,16]. Therefore, the fact that important chemical classes of VOCs have been identified in *K. cowanii,* such as dodecanoic acid; 3-hydroxy ethanol; 1-butanol-3-methyl; acetaldehyde; butanoic acid, butyl ester; cyclodecane; 2-butanone, 3-hydroxy; disulfide, dimethyl; and pyrazine-2,5-dimethyl, with similar antimicrobial properties and conserved in phylogenetically different bacterial species suggests that there is probably a common competitive colonization strategy that affects the important metabolic functions of phytopathogenic microorganisms, which can eventually be implemented to mitigate the losses caused by microbial infections in crops [17].

Based on our previous study [11], it is imperative to determine whether *K. cowanii* Ch1 requires specific growth conditions or the production of VOCs as modulators of stress

responses during competitive interactions with *S. rolfsii*, which is a soil-borne fungus that causes different types of plant diseases, such as stem canker, damping off, crown and root rot, collar rot, foot rot, stem rot, or southern stem rot, in economically valuable crops and produces specialized structures called sclerotia, which enhance its spread in the field during the disease cycle and represent a significant challenge for disease control associated with this microorganism [18]. Therefore, these findings will provide new insights into the biocontrol of *S. rolfsii* or other fungal strain such as *A. alternata* in the field as an alternative of toxic chemical fungicides [17].

Therefore, the aim of this study was to determine whether (i) *K. cowanii* Ch1 can compete directly with *S. rolfsii*, (ii) if the presence of bacterial VOCs during bacteria–fungal interaction produce a beneficial competitive interaction to *K. cowanii* Ch1, and (iii) to determinate gene expression changes in *K. cowanii* Ch1 during microbial interaction. To achieve this aim, we conducted in vitro bacterial–fungal interaction assays to evaluate whether the presence of bacterial VOCs can enhance the efficiency of the colonization competence of *K. cowanii* Ch 1 to reduce mycelial growth. Additionally, we investigated the transcriptional profiling of *K. cowanii* Ch1 using RNA-Seq during these bacterial–fungal interactions for the elucidation of competence responses.

2. Materials and Methods

2.1. Bacterial–Fungal Interaction Assays

The fungal strains evaluated were *Sclerotium rolfsii* and *Alternaria alternata*, both of which present mycelial growth inhibition in response to the VOCs produced by *K. cowanii* Ch1, as well as *Fusarium oxysporum*, which presents VOC resistance in previous work [11]. These fungal strains were provided and identified by their morphological characteristics by the Laboratory of Plants and Agriculture Bio-technology at Queretaro University, Mexico. The fungal strains were grown in a potato dextrose agar (PDA) medium (Difco Laboratories, Detroit, MI, USA) and incubated at 28° for 5–7 days as per the requirements of each specific fungal strain. The bacterial strain used was *K. cowanii* Ch1 [11], and the bacterial strains used as controls for VOC production were *Bacillus altitudinis* CH05 [19], *Bacillus tropicus* CH13 [19], and *Pectobacterium aroidearum* SM2 [2], which were grown in a TSA medium (Difco Laboratories, Detroit, MI, USA) at 37 °C. For bacterial–fungal interaction assays, a double-compartment Petri dish chamber (9 cm) was used [11]. For the treatments, the lower part of the compartment was inoculated with 100 µL of each bacterial strain (1×10^8 CFU/mL) in the TSA medium (Difco Laboratories, Detroit, MI, USA) for VOC production, while in the upper compartment, the PDA medium (Difco Laboratories, Detroit, MI, USA) was inoculated with fungal strain disks (with a diameter of 7 mm). Around these fungal disks, 20 µL (1×10^8 CFU/mL) of *K. cowanii* Ch1 was inoculated. For the treatments without VOC production, the PDA medium (Difco Laboratories, Detroit, MI, USA) was inoculated with fungal strain disks, and 20 µL (1×10^8 CFU/mL) of *K. cowanii* Ch1 was inoculated around each of these fungal disks, while the lower compartment was not inoculated with any bacterial strains, such that VOC production was absent in that compartment. For the controls, each fungal disk and *K. cowanii* Ch1 (in the upper compartment) were grown with or without the production of bacterial VOCs (in the lower compartment). All double-compartment Petri dish chambers were sealed with parafilm and incubated at 28 °C, and measurements of the radial mycelial growth were performed every 24 h.

2.2. Analysis of VOCs Produced by Bacterial Strains via HS-SPME-GC-MS

The VOC profiles produced by the bacterial strains were evaluated at 24 h of growth in 50 mL of tryptone soy broth (TSB) medium at 28 °C and 120 rpm with an initial inoculum

of 1×10^4 CFU/mL. The characterization of VOCs was performed using a previously reported methodology [11], where the samples were incubated at 50 °C for one hour and then the VOCs were collected on a divinylbenzene/carboxen/polydimethylsiloxane fiber (DVB/CAR/PDMS, Supelco, Sigma-Aldrich, Visalia, CA, USA). After this, manual injection was carried out in splitless mode; the injection port and transfer line temperature were set to 250 °C using a 7820A GC with a 5975C MSD (Agilent Technologies, Inc., Santa Clara, CA, USA) and HP-5MS 30 m, 0.25 mm, and 0.25 μm GC Column Capillaries (Agilent Technologies Inc., Santa Clara, CA, USA). The column oven was programmed at 40 °C, increasing to 180 °C at 5 °C/min and then at 20 °C/min to 260 °C, and held at that temperature for 5 min. Helium (99.999% purity) was used as the carrier gas with a flow rate of 1.0 mL/min. Mass spectrometry analyses were conducted at an electron energy of 70 eV and the m/z range was 33–500. Data were obtained and processed using the NIST/EPA/NIH Mass Spectra Library instrumental analysis software, version 2017, Antioch, CA, USA. For comparison of the VOCs between bacterial strains, the compounds with the highest relative abundance values (%) were plotted with the statistical R program (version 4.2.2) using ggplot2 and pheatmap. Based on the VOC profiles detected using the described methodology, we tested the following synthetic VOCs to evaluate their phenotypical responses in *K. cowanii* Ch1 during its physical interaction with *S. rolfsii*. A Petri dish of 9 cm in diameter was used to place a sterile filter paper disk containing the synthetic VOCs, while another Petri dish with potato dextrose agar (PDA) medium (Difco Laboratories, Detroit, MI, USA) was co-inoculated with the bacteria-fungal strain. The volume of each VOC used was as follows: acetoin of 100 μL (≥95%, Sigma-Aldrich, USA), 2,5-Dimethyl pyrazine of 50 μL (98%, Sigma-Aldrich, USA), ethanol of 200 μL (≥99.5%, Sigma-Aldrich, USA), cyclododecane of 50 μL (a solution prepared with 20 mg cyclododecane dissolved in 1 mL of hexane), and benzaldehyde of 20 μL (97%, Sigma-Aldrich, USA).

2.3. Evaluation of Cell-Free Filtrates in In Vitro and In Vivo Competitive Colonization Interaction Essays

K. cowanii Ch1 was grown for 48 h on the tryptic soy broth medium (Difco Laboratories; Detroit, MI, USA) at 28 °C and 100 rpm for 48 h. Cell-free filtrates were obtained at 12, 24, 36, and 48 h of growth via centrifugation and filtration with 0.22 μm pore-size disposable filters (Corning Incorporated, Corning, NY, USA). To evaluate the cell-free filtrates in vitro, first, the fungal mycelium disk and *K. cowanii* Ch1 inoculated around it were grown in the potato dextrose agar (PDA) medium (Difco Laboratories, Detroit, MI, USA) for 24 h at 28 °C. After this period of incubation, 50 μL of each cell-free filtrate was added around the mycelium disks every 12 h for 2 days, and the results were recorded on the 5th day. As a control, a fungal mycelium disk was grown in the PDA medium (Difco Laboratories, Detroit, MI, USA). From these experiments, the cell-free filtrate at 36 h showed the highest mycelium growth inhibition and was used for in vivo experiments. The VOC profile produced at 36 h was analyzed according to the methodology described in Section 2.2 and compared with the VOC profile obtained at 24 h for *K. cowanii* Ch1. To evaluate the cell-free filtrates in vivo, bacterial–fungal competitive colonization interaction assays were performed on fruits of the serrano chili (*Capsicum annuum* L.) to assess the potential of *K. cowanii* Ch1 against *S. rolfsii* in reducing infection symptoms. The serrano chili fruits were surface sterilized as previously reported [2], then punctured with a sterile toothpick and inoculated with 10 μL of *K. cowanii* Ch1 suspension at a concentration of 1×10^8 CFU/mL; this assay was performed in triplicate. After bacterial inoculation, three mature melanized sclerotia were inoculated at the same point. The controls were inoculated only with mature melanized sclerotia. To determine whether cell-free filtrates possessed activity against fungal growth and reduce infection, the chili fruits were inoculated with sclerotia or co-inoculated with

sclerotia–bacteria and incubated at 28 °C for 24 h. After this period of incubation, a 20 µL volume of cell-free filtrates was applied during bacterial–fungal treatments of infections at 12, 24, and 36 h. The inoculated chili fruits were placed inside an airtight container at 28 °C. The infection of *S. rolfsii* in chili fruits was observed as macerated tissue and the diameter was registered in millimeters for comparison with the control and treatments.

2.4. RNA Isolation

Based on the results of microbial interaction obtained, we decided to use the bacterial cells at 36 h of interaction, because we could recover the bacterial colony for the RNA-Seq analysis; beyond 36 h, a thick mycelium was established in the absence of bacterial VOCs, which made bacterial recovery difficult in comparison. The bacterial cells representing technical duplicates of treatments in (1) the absence of bacterial VOCs, and (2) the presence of bacterial VOCs and control (*K. cowanii* Ch1 growth in the absence of VOCs) were scraped into 800 µL of RNA Shield™ reagent (Zymo Research, Irvine, CA, USA), resuspended, and briefly vortexed, before being stored at 5 °C. The total RNA was purified using the Quick-RNA™ Miniprep Plus Kit, following the manufacturer's instructions (Zymo Research, Irvine, CA, USA).

2.5. RNA-Seq Library Preparation

RNA samples were sent to Zymo Research, Irvine, CA, USA, for total RNA-Seq service. Libraries were constructed from the total RNA samples. Libraries were prepared using the Zymo-Seq RiboFree Total RNA Library Prep Kit™, according to the manufacturer's instruction manual. Briefly, RNA was reverse transcribed into cDNA, which was followed by ribosomal RNA depletion. After that, a partial P7 adapter sequence was ligated at the 3′ end of cDNAs, followed by second-strand synthesis and partial P5 adapter ligation to the 5′ end of the double-stranded DNA. Lastly, libraries were amplified to incorporate full-length adapters under the following conditions: initial denaturation at 95 °C for 10 min; 10–16 cycles of denaturation at 95 °C for 30 s, annealing at 60 °C for 30 s, and extension at 72 °C for 60 s; and final extension at 72 °C for 7 min. Successful library construction was confirmed with Agilent's D1000 ScreenTape Assay on TapeStationc (Agilent Technologies, Inc., Santa Clara, CA, USA). The RNA-Seq libraries were sequenced on an Illumina NovaSeq to a sequencing depth of at least 30 million read pairs (150 bp paired-end sequencing) per sample.

2.6. RNA-Seq Data Bioinformatics Analysis

RNA-Seq data were analyzed at Zymo Research using the RNA-Seq pipeline adapted from the nf-core/rnaseq pipeline v1.4.2 (https://github.com/nf-core/rnaseq, accessed on 11 November 2024). The pipelines were built using Nextflow [20]. Briefly, the quality control of raw reads was carried out using FastQC v0.11.9 [21]. Adapter and low-quality sequences were trimmed from raw reads using Trim Galore! v0.6.6 [21]. Trimmed reads were aligned to the reference genome of *K. cowanii* Ch1 (genome accession number at NCBI: JAUDFU000000000) using STAR v2.6.1d [22]. BAM file filtering and indexing were carried out using SAMtools v1.9 [23]. RNAseq library quality control was implemented using RSeQC v4.0.0 and QualiMap v2.2.2-dev [24,25]. Duplicate reads were marked using Picard tools v2.23.9 [26]. Library complexity was estimated using Preseq v2.0.3 [27]. Duplication rate quality control was performed using dupRadar v1.18.0 [28,29]. Differential gene expression analysis was completed using DESeq2 v1.28.0 with a padJ of $\leq$0.05, where the mean transformed read counts of genes, to normalize sequencing depth and RNA composition, was used in DESeq2. The similarities (Pearson correlation coefficient) between samples were calculated using the normalized and 'rlog' transformed read counts of all genes via DESeq2. Also, multidimensional scaling was conducted to visualize the distance/similarity between samples [30]. Quality control and analysis result plots were

visualized using MultiQC v1.9 [31]. Functional enrichment analysis was achieved with ShinyGO 0.80 [32], in which genes with a fold change of >1.0 and an FDR of <0.05 present in the pathway database in the Local Network Cluster (STRING) were considered as highly differentially expressed. The raw data has been deposited in the NCBI SRA database with the BioProject accession number PRJNA1276248.

2.7. Statistical Analysis

At least three technical replicates of in vitro and in vivo competitive colonization interaction assays were carried out for statistical analysis. The equation ICM = [(C) − (T)/C] × 100% was used to analyze the growth percentage of the controls (C) and treatments in the presence or absence of VOCs in vitro or in vivo experiments to determine the infection percentage (T), and the data were analyzed using Minitab version 18.0. Means with ±standard error were analyzed via one-way ANOVA ($p < 0.05$).

3. Results

3.1. Bacterial–Fungal Interaction Assays

K. cowanii Ch1 can produce VOCs with antifungal activity, and its effects were evaluated on the mycelial growth in *S. rolfsii*. The result showed an inhibition with a mean rate of 80 ± 5% ($p < 0.05$) at 72 h when compared with the control (Figure 1A,B). With this result in mind, we decided to test whether *K. cowanii* Ch1 competed against *S. rolfsii* during a physical interaction and reduced the mycelial growth; thus, we conducted an assay where *K. cowanii* Ch1 was grown around a mycelial disk of *S. rolfsii*. As indicated in Figure 1, contrary to the first experiment conducted, *K. cowanii* Ch1 did not affect the mycelial growth and *S. rolfsii* outgrew the bacterial colony (Figure 1C, indicated by an arrow). Therefore, we decided to test whether, for an attenuated mycelial growth disturbed probably by oxidative stress caused by bacterial VOCs, *K. cowanii* Ch1 had a major effect in reducing the mycelial growth during physical interactions. Surprisingly, the metabolic response of *K. cowanii* Ch1, through the growth around the mycelial fungal disk, was evident, with gas bubble production being observed; indeed, the complete mycelial growth inhibition was observed, as indicated in Figure 1D. This phenotypical trait was not observed in the bacterial colony in the presence of VOCs (Figure 1E).

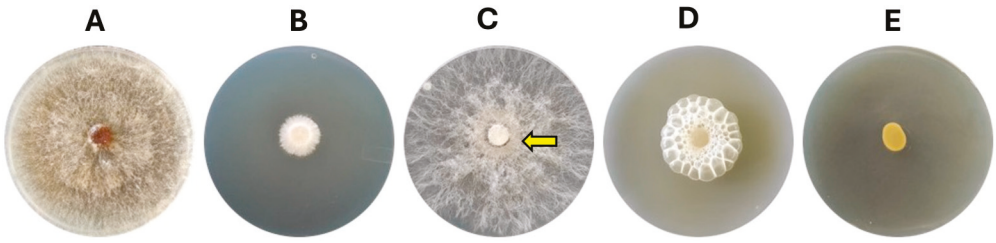

Figure 1. Microbial interaction assays. (**A**) *S. rolfsii* was grown in a PDA medium. (**B**) *S. rolfsii* was grown in the presence of bacterial VOCs, where mycelial growth was affected. (**C**) *K. cowanii* Ch1 grew around the mycelial disk in the absence of bacterial VOCs and (**D**) *K. cowanii* Ch1 grew around the mycelial disk in the presence of bacterial VOCs. The arrow in (**C**) indicates that *S. rolfsii* has outgrown the bacterial colony in the absence of VOCs, while in the presence of VOCs (**D**), gas bubbles were produced by *K. cowanii* Ch1. (**E**) As a control, the bacterial colony was grown in the presence of VOCs. The images were taken at 72 h.

Based on these results, we decided to evaluate whether the additional fungal strains would have similar metabolic responses, or whether they were exclusively produced by *S. rolfsii*. Thus, we tested *A. alternata*, a fungal strain also sensitive to VOCs produced by *K. cowanii* Ch1, and it showed a mean rate of mycelial growth inhibition of 70 ± 5% ($p < 0.05$) compared with that of the control. A similar metabolic response was observed in the

presence of VOCs with the production of gas bubbles by *K. cowanii* Ch1 (Figure 2, indicated by an arrow), but not in the absence of VOCs. Both conditions showed mycelial growth inhibition as indicated in Figure 2. On the other hand, *F. oxysporum*, a fungal strain with resistance to VOCs produced by *K. cowanii* Ch1, showed a mean rate of mycelial growth inhibition of 10 ± 5% ($p < 0.05$) compared with that of the control; the production of gas bubbles by *K. cowanii* Ch1 was not observed in the presence of VOCs, and the mycelium outgrew the bacterial colony without affectation (Figure 2, indicated by an arrow). This result indicated that *F. oxysporum* possessed different mechanisms of resistance to VOCs produced by *K. cowanii* Ch1, and that sensitive fungal strains probably produce important molecules in response to oxidative stress, which could compromise their cell viability.

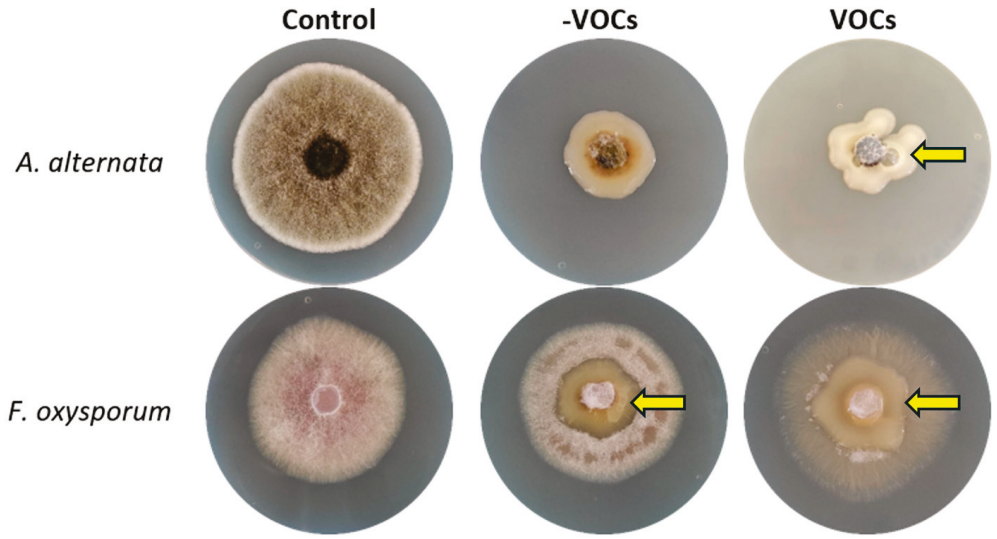

Figure 2. Evaluation of *K. cowanii* Ch1 against *A. alternata* and *F. oxysporum*. Fungal strains were grown under the presence or absence of VOCs produced by *K. cowanii* Ch1. In both conditions, *K. cowanii* Ch1 was grown around the mycelial disks. The arrow shows the gas bubbles produced with *A. alternata*. However, for *F. oxysporum*, the arrows indicate that the mycelium outgrew the bacterial colony. Controls indicate the fungal strains' growth without VOCs.

With these evident results—and the fact that sensitive fungal strains had similar oxidative stress responses under these bacterial VOCs—we decided to test whether *K. cowanii* Ch1 produced specific VOCs compared with other bacterial strains that produced some common VOCs with a similar effect on the mycelial growth inhibition of *S. rolfsii*. Therefore, we evaluated the VOCs produced by *B. altitudinis* CH05, *B. tropicus* CH13, and the phytopathogen *P. aroidearum* SM2. The results shown in Figure 3 revealed similar results in *S. rolfsii* under this mixture of VOCs produced in all bacterial strains, as well as the phenotypical response of gas bubble production in *K. cowanii* Ch1 when it grew around the mycelial disks. However, an increased response was observed with the VOCs produced by *K. cowanii* Ch1 (Figure 3A) and *P. aroidearum* SM2 (Figure 3D). Additionally, complete mycelial growth inhibition was observed under these conditions.

3.2. Identification of VOCs Using HS-SPME-GC-MS

We compared the VOCs produced at 24 h by the bacterial strains to identify some common molecules (Figure 4 and Table S1). A total of 53 compounds were detected and plotted in Figure 4, which were classified as alcohols (18.10%), aldehydes (7.56%), acids (16.50%), pyrazines (15.28%), ketones (7.87%), hydrocarbons (7.44%), thiols (1.13%), and other compounds (24.75%). The molecules with a high relative abundance in *B. tropicus* CH13 were acetoin (32.77%), 2,5-Dimethyl pyrazine (12.33%), 2,3-Butanedione (10.38%), and Nonanoic acid (6.53%); in *B. altitudinis* CH05 were 2,5-Dimethyl pyrazine (13.31%),

Acetoin (11.9%), Nonanoic acid (6.72%), and 3-methyl-1-Butanol (4.43%); in *P. aroidearum* SM2 were 2-Ethylhexyl salicylate (5.65%), 2,5-Dimethyl pyrazine (4.99%), 1-Decene (4.93%), and Butanoic acid, butyl ester (4.25%); and in *K. cowanii* Ch1 were acetoin (13.52%), 2,5-Dimethyl pyrazine (6.47%), Ethanol (5.56%), and 3-methyl-1-Butanol (4.85%). Based on the profiles of the VOCs and whether some of them can cause oxidative stress in *S. rolfsii*, we decided to use acetoin, 2,5-Dimethyl pyrazine, ethanol, cyclododecane, and benzaldehyde to test the bacterial–fungal interactions as above, but the phenotypical response in *K. cowanii* Ch1 was not observed; thus, the complex mixture of VOCs probably had multiple targets in the cells to cause oxidative stress (Figure S1).

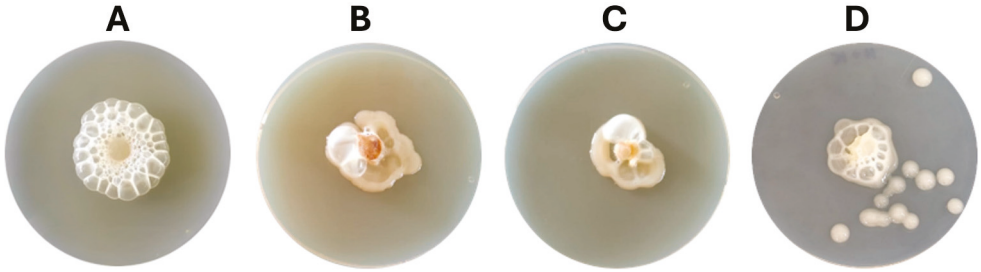

Figure 3. Evaluation of VOCs produced by bacterial strains. VOCs produced by (**A**) *K. cowanii* Ch1, (**B**) *B. altitudinis* CH05, (**C**) *B. tropicus* CH13, and (**D**) *P. aroidearum* SM2. In all conditions, *K. cowanii* Ch1 was grown around mycelial disks of *S. rolfsii*.

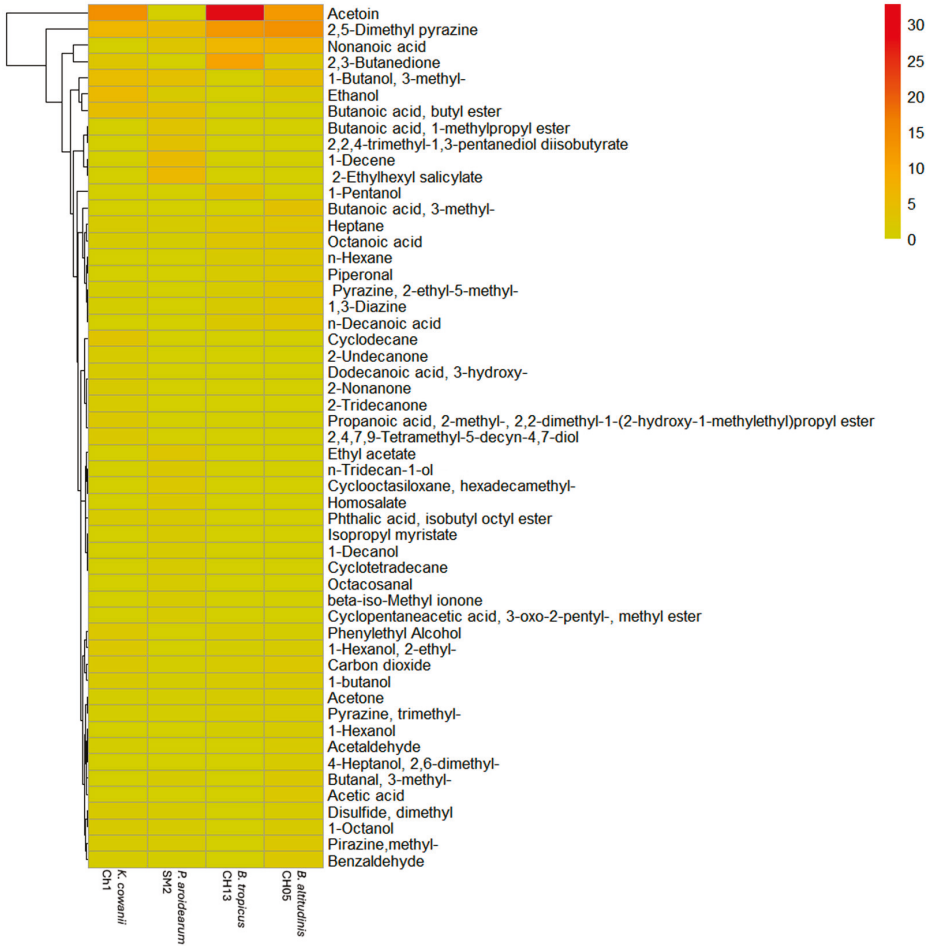

Figure 4. Relative percentages of the different classes of VOCs produced in the bacterial strains at 24 h. The bar color represents the relative abundance based on the relative peak area (%) detected in the HS-SPME-GC-MS analysis.

3.3. In Vitro and In Vivo Evaluation of Cell-Free Filtrates

Based on the microbial interaction in the presence of VOCs (Figure 1), we decided to evaluate cell-free filtrates from *K. cowanii* Ch1 obtained during the different bacterial growth time periods and applied directly on the physical interaction between the mycelium disk and the bacteria growth on the PDA medium to determine its response to the inhibition of mycelium growth in vitro (Figure 5A). We observed that the cell-free filtrate obtained at 36 h of bacterial growth showed an important mycelial inhibition capacity compared with the control and the other cell-free filtrates (12, 24 and 48 h) recorded on the 5th day of the experiment. Thus, we decided to evaluate this cell-free filtrate (36 h) on the bacterial–fungal competitive colonization interaction on fruits of the serrano chili (*Capsicum annuum* L.) to determine the potential of *K. cowanii* Ch1 to reduce infection symptoms caused by *S. rolfsii* (Figure 5B). When *K. cowanii* Ch1 was co-inoculated with *S. rolfsii* (T1), an evident infection symptom was observed with a diameter of 1.8 ± 0.2 cm, similar to the control with a diameter of 2.2 ± 0.3 cm. In treatment T2, the cell-free filtrate (F36 h) showed a reduction in infection symptoms of nearly 50% (1.06 ± 0.8 cm). When both microorganisms were co-inoculated and treated with a cell-free filtrate (T3), a reduction of 80% of infection symptoms was observed (0.5 ± 0.2 cm) compared with the control. These results mean that biomolecules produced around 36 h of bacterial growth can inhibit mycelial growth, but in the presence of bacteria, additional metabolic activity during competitive colonization can increase major fungal inhibition.

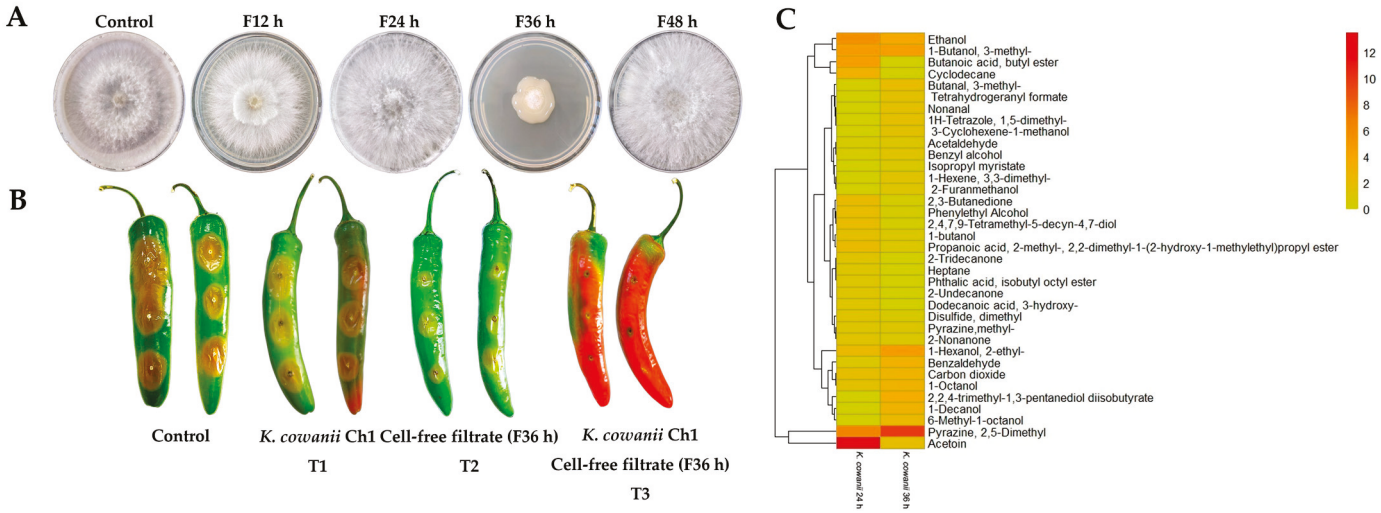

Figure 5. The in vitro and in vivo evaluation of cell-free filtrates. Cell-free filtrates obtained at 12, 24, 36, and 48 h of bacterial growth were added during fungi–bacteria interaction (**A**). (**B**) Colonization competence between both microorganisms was evaluated in chili fruits (T1). Cell-filtrate obtained at 36 h was evaluated against *S. rolfsii* (T2) and T3 is the co-inoculation of both microorganisms treated with the cell-free filtrates (F36 h). Control was inoculated only with *S. rolfsii*. Results in (**A**) were recorded on the 5th day of mycelial growth, and results in (**B**) were recorded on the 4th day of the experiment. (**C**) A comparison of VOC profiles produced at 24 h and 36 h in *K. cowanii* Ch1. The bar color represents the relative abundance based on the relative peak area (%) detected in the HS-SPME-GC-MS analysis.

To adequately understand the differences between cell-free filtrates, we decided to analyze the VOC profile at 36 h of bacterial growth. The comparative results of the VOCs produced at 36 h and 24 h of bacterial growth showed important differences in the VOC chemical classes (Figure 5C and Table S2). For example, Butanoic acid, butyl ester; 2-Undecanone; Cyclodecane; 2-Tridecanone; Dodecanoic acid, 3-hydroxy-; Heptane; and Phthalic acid, isobutyl octyl ester were absent at 36 h. Other chemicals, such as Ethanol; 2,3-

Butanedione; 1-butanol; acetoin; Phenylethyl Alcohol; Disulfide, dimethyl; 2-Nonanone; Propanoic acid, 2-methyl-, 2,2-dimethyl-1-(2-hydroxy-1-methylethyl)propyl ester; and 2,4,7,9-Tetramethyl-5-decyn-4,7-diol were reduced considerably at 36 h. The chemical compounds that increased or were synthetized de novo with a high relative abundance in percentage were Pyrazine, 2,5-Dimethyl; 1-Decanol; 2,2,4-trimethyl-1,3-pentanediol diisobutyrate; Isopropyl myristate; Acetaldehyde; Butanal, 3-methyl-; Benzaldehyde; 1-Octanol; 1-Hexanol, 2-ethyl-; Nonanal; 1-Hexene, 3,3-dimethyl-; 6-Methyl-1-octanol; Tetrahydrogeranyl formate; 1H-Tetrazole, 1,5-dimethyl-; 2-Furanmethanol; 3-Cyclohexene-1-methanol; and Benzyl alcohol. Therefore, the observed differences in the composition and concentrations of the VOCs at different time periods of bacterial growth are important research findings, as VOCs could have a major impact on microbial interactions and colonization competence.

3.4. RNA Sequencing Analysis in K. cowanii Ch1

According to the results obtained in Figure 1C,D, and in order to gain insight into the competence mechanism of *K. cowanii* Ch1 against *S. rolfsii*, the bacterial–fungal interaction assays in the presence or absence of VOCs were performed to study the bacterial transcriptome at 36 h of the interaction. By this time, the initial mycelium had outgrown the bacterial colony in the absence of VOCs, and we could recover the bacterial colony for the RNA-Seq analysis; beyond 36 h a thick mycelium was established, which made bacterial recovery difficult. Approximately 47.50 million paired-end sequence reads were generated from each duplicate technical condition and the percentage of reads successfully mapped against the reference genome were from 24.3% to 98.9% (Table S3). The similarities between samples are visualized in the form of a heatmap in Supplementary Figure S2 and the mean transformed read counts of genes is shown in Supplementary Figure S3. The general statistics of differentially expressed genes in pairwise comparisons (adjusted *p*-values of <0.05) showed that, in the absence of VOCs, 388 genes were upregulated, and 269 genes were downregulated (Figure 6A), with 3796 genes that were not differentially expressed. However, in the presence of VOCs, 35 genes were upregulated, and 4 genes were downregulated (Figure 6B), with 4414 genes that were not differentially expressed.

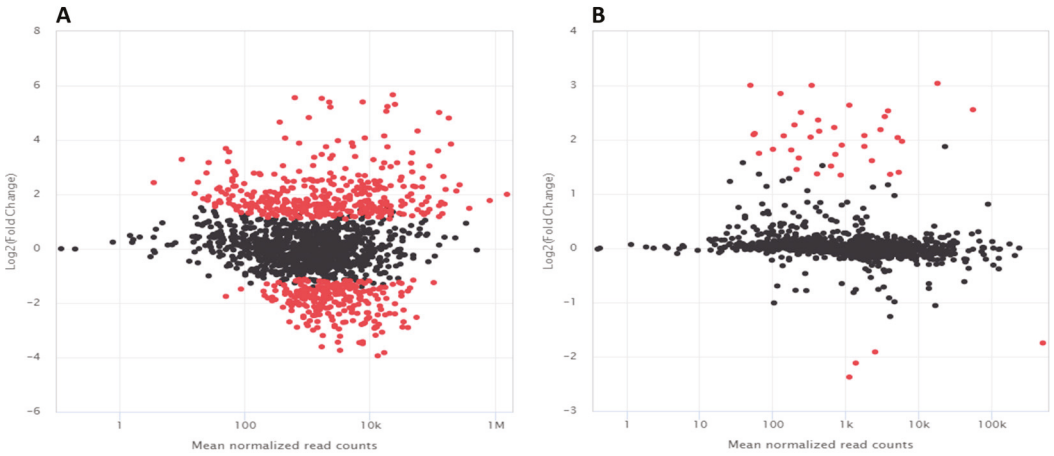

Figure 6. The MA plot visualization of differential gene expression in *K. cowanii* Ch1. Differentially expressed genes in pairwise comparisons during bacterial–fungal interactions in the absence of VOCs (**A**) and in the presence of VOCs (**B**). These conditions were compared with *K. cowanii* Ch1 grown in the absence of VOCs as a control. Expression levels are shown on X-axis, while log2 of fold changes are shown on Y-axis. Red dots represent differentially expressed genes (adjusted *p*-values of <0.05). Black dots represent non-differentially expressed genes. The shrinkage of effect size was carried out using the 'ashr' method in DESeq2.

3.5. Differentially Expressed Genes in K. cowanii Ch1 in Absence of VOCs

According to the differentially upregulated genes in *K. cowanii* Ch1, gene ontology (GO) enrichment analysis was carried out, and the top enriched pathways were listed in Figure 7A. During this microbial competence interaction, 19 top pathways were identified, and diverse genes were related to the stress responses, which indicated that *K. cowanii* Ch1 was under very stressful conditions when interacting with the fungal strain. Important key transcriptional regulators were detected, such as the yqjI gene (with a more than four-fold change), which is related to iron homeostasis. Furthermore, the feoC gene was upregulated by two-fold, which is related to the mediation of ferrous iron [Fe(II)] import. The redox-sensitive transcriptional regulators soxRS and qorR were upregulated, with a >1.5-fold change. The phoP gene was upregulated by two-fold, which is related to virulence, Mg^{2+} homeostasis, and resistance to a variety of antimicrobial agents, including acidic pH and cationic antimicrobial peptides. The zntR gene was upregulated by two-fold, which is related to the control of cellular Zn(II) status. The ydcI gene was upregulated by two-fold, which is a LysR family transcriptional regulator related to pH homeostasis. The anaerobic nitric oxide reductase transcription regulator norR gene was upregulated by two-fold, which encodes a σ^{54}-dependent regulatory protein that senses nitric oxide to activate detoxification genes. The response regulator creB gene was upregulated by nearly two-fold, which is part of a two-component signal transduction system CreBC (for carbon source responses), which is a global sensing and regulation system that controls the expression of genes involved in a variety of functions, including the enzymes of intermediary catabolism. The LysR family transcriptional regulator yeiE was upregulated, which is related to the regulation of flagellum-mediated motility. The transcriptional regulator slyA was upregulated, which is involved in the regulation of genes that are important for bacterial virulence and stress response. The iron–sulfur cluster regulator iscR gene is a sensor of cellular [Fe-S] levels and a global transcription regulator for [Fe-S] homeostasis under stressful conditions.

Following these routes of the oxidative stress defense system and the activation of diverse genes by these key transcriptional regulators, diverse pathways were observed (Figure 7A). Some of them were related to the siderophore-mediated iron transport, and these genes were upregulated with a >1.5-fold change, such as entCF that encodes synthetases for the biosynthesis of enterobactin. Enterobactin recognition and transport are represented by upregulated genes such as fepBCD, tonB, exbBD, and fes. Additionally, the ferrous iron transport system was represented by upregulated genes such as feoAB. Genes that encode for oxidative enzymes were upregulated with a >1.5-fold change and included 2-Oxobutyrate oxidase (ID QU629_RS16930), Ferric reductase (fhuF), Alkyl hydroperoxide reductase protein C (ahpC), NAD-dependent glyceraldehyde-3-phosphate dehydrogenase (gapA), Peptide-methionine (S)-S-oxide reductase (msrA), Ribonucleotide reductase of class III (nrdG), Thiol peroxidase (tpx), Oxidoreductase (ID QU629_RS03245), and other important genes (Table S2). The genes upregulated with a >1.5-fold change that prevented protein misfolding and aggregation were represented by the multiple stress resistance protein BhsA (bhsA), 16 kDa heat shock protein AB (ibpAB), heat shock protein GrpE (grpE), chaperone protein ClpB (ATP-dependent unfoldase) (clpB), chaperone protein DnaJK (dnaJK), heat shock protein 60 kDa family chaperone GroEL (groL), and HtrA protease/chaperone protein (degP). The cellular oxidant detoxification and glutathione metabolic process pathways were represented by Glutathione S-transferase (gstA), Thioredoxin 2 (trxC), and Glutaredoxin-like protein NrdH (nrdH). Endonuclease IV was upregulated with a 5-fold change. Downregulated genes related to important transporters, membrane proteins, motility, signal regulation, and metabolism were detected (Table S4).

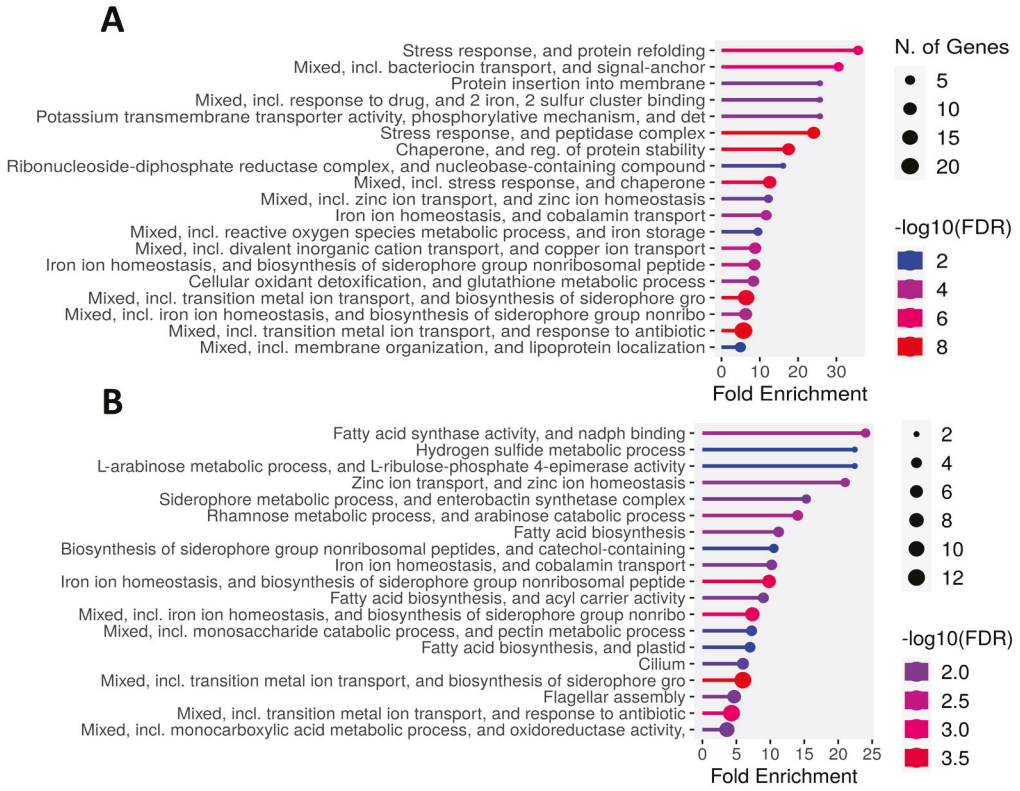

Figure 7. Gene ontology (GO) enrichment. Pathways detected for microbial interaction in the absence of VOCs (**A**) and in the presence of VOCs (**B**). Genes with a fold change of >1.0, an FDR of <0.05, and present in the pathway database, the Local Network Cluster (STRING), were considered as highly differentially expressed.

3.6. Differentially Expressed Genes in K. cowanii Ch1 in Presence of VOCs

Based on the evident phenotype shown by *K. cowanii* Ch1 under the presence of VOCs (Figure 1D), the RNA-Seq analysis revealed that, during its microbial competence interaction, 19 top pathways were identified (Figure 7B, Table S5). Also, and probably related to the phenotype of bubble gas of *K. cowanii* Ch1, the gene katG that encodes for a catalase is upregulated by 2.7-fold. This means, under this specific competence interaction, a probable hypothesis is that fungal strains may produce hydrogen peroxide (H_2O_2) as a VOC stress response. Therefore, the antioxidant systems that remove H_2O_2 are activated in *K. cowanii* Ch1. In addition, stress response genes were identified in the metal transportation mechanisms, with a >1.0-fold change in gene upregulation, siderophore-mediated iron transport system (entS, entCF, fepBDG, tonB, exbBD and fes) and ferrous iron transport system (feoAB, efeOU). The zinc ion transport system and homeostasis were represented by genes upregulated with a >1.0-fold change, such as znuABC. Protein misfolding and aggregation were represented by the 16 kDa heat shock protein AB (ibpAB). The flagellar assembly genes detected were flhACD, flgCDEFGHI, and filFN. Genes related to the production of biomolecules with antimicrobial responses were detected, such as antibiotic biosynthesis monooxygenase (ID QU629_RS21570), which was upregulated with a 2.1-fold change; furthermore, polyketide synthase modules and related proteins (ID QU629_RS05045) were upregulated with a 1.7-fold change. Additional upregulated and downregulated genes related to membrane proteins, signal regulation, and metabolism were detected (Table S5).

4. Discussion

Understanding the beneficial bacterial responses during the colonization competition against phytopathogenic microorganisms could be crucial not only for elucidating genetic mechanisms during microbial interactions, but also for developing effective strategies that could enhance the metabolic abilities and eventually be applied to reduce disease symptoms in crops in agricultural systems, as an alternative to the use of undesirable chemical fungicides [17]. The increased research interest for identifying colonization factors (CFs) in specific ecological niches has allowed for the development of diverse methodology approaches [33]; however, significant challenges remain to be overcome. Therefore, in this study, we hypothesized that the VOCs produced by *K. cowanii* Ch1 could be modulators of stress responses during the competitive colonization interaction against *S. rolfsii*. In this sense, we developed microbial interaction assays to overcome the challenges, and the results indicated potential key biological processes that may contribute to a better understanding of biocontrol.

Based on the microbial interaction assays and according to our results shown in Figure 1B, a mixture of VOCs represented by a diverse chemical class were identified (Figure 4), which were produced by *K. cowanii* Ch1 to arrest mycelial growth at a mean rate of 80 $\pm$ 5% ($p < 0.05$) in *S. rolfsii*. Thus, based on this bacterial trait, a possible alternative to biocontrol, for preventing fungal disease caused by *S. rolfsii,* could be devised. However, in agreement with the diverse research conducted in this field, the assays of inhibition of mycelial growth by the bacterial VOCs produced in vitro could be the first step to selecting potential microorganisms under controlled conditions; additional research is required to be conducted, as the experimental conditions may not be representative of real growth conditions. Diverse studies have also confirmed that environmental conditions, including pH, CO_2/O_2 levels, nutrients, temperature, humidity, growth stage, and interactions between microorganisms of different species, can influence the composition of these mixtures of volatiles produced by the studied microorganisms [34–37]. In this sense, our results clearly showed that, under the tested conditions, the profile of volatile compounds differed between bacterial species, and even closely related *Bacillus* strains produced different mixtures of volatile compounds. Some common molecules with different concentrations were analyzed at least at 24 h (Figure 4 and Table S1), and they had the ability to impact the inhibition of mycelial growth during the interaction between *K. cowanii* Ch1 and *S. rolfsii* (Figure 3). Also, both fungal strains *S. rolfsii* and *A. alternata* were sensitive to the VOCs produced by some of the tested bacterial strain as previously reported [11,19], while *F. oxysporum* showed resistance to these mixtures of volatiles, demonstrating different evolutionary mechanisms to counteract compounds with hazardous physical–chemical properties that may affect cell integrity and viability. Therefore, future perspectives on molecular processes and the comparison of mechanisms between sensitive and resistant fungal strains could provide us with possible new routes to design better strategies against these resistant strains.

Colonization competence evaluated between *K. cowanii* Ch1 and *S. rolfsii* (Figure 1C) in the absence of VOCs revealed an important finding for understanding why the *K. cowanii* Ch1 colony was outgrown by the mycelium of *S. rolfsii*. Under this microbial interaction condition, gene expression analysis showed that complex defense and repair mechanisms were induced by *K. cowanii* Ch1 to mitigate the oxidative stress induced by the mycelial growth (Figure 7A, Table S4). In this regard, the redox-sensitive transcriptional regulator SoxR (*soxR*) was induced by 2.2-fold, and its critical role in the defense system, under oxidative stress related to enteric bacteria, has been well studied [38,39]. When SoxR is activated through the oxidation of [2Fe-2S] clusters, it induces the expression of the *soxS* gene [39], a DNA-binding transcriptional dual regulator which, in our results, was induced by 1.5-fold, and has the ability to activate the transcription of diverse genes related

to the restoration of redox homeostasis and the repair of cellular damage induced by oxidative stress [38,39]. Protective mechanisms observed in *K. cowanii* Ch1 induced a 5.8-fold change in Endonuclease IV (QU629_RS04135), a DNA damage-specific endonuclease that is induced by oxidative stress in related enteric bacteria [40]. Molecular chaperones (*ibpAB*, *grpE*, *clpB*, *dnaJK*, *groL*, *degP*) were also upregulated, and they play a regulatory role in the folding of proteins, the intracellular transport of proteins, the repair and degradation of proteins, and the refolding of proteins during specific cell growth conditions, but were markedly upregulated by stress effectors [41]. The multiple stress resistance gene *bhsA* was induced by five-fold, which is a putative outer membrane protein that has been studied in *E. coli* and shown to influence biofilm formation through hydrophobicity and stress response [42]. The mechanisms of metal homeostasis were probably induced as metals are important antimicrobial effectors that resist cellular stress for survival; for example ZnuABC system was upregulated by five-fold, which indicates that ZnuABC is essential for zinc uptake and required as cofactor in catalytic sites of enzymes related with oxidative stress [43,44]. Additionally, the iron uptake systems (*fepBCD*, *tonB*, *exbBD*, *fes* and *feoAB*) and genes related to the production of siderophore enterobactin (*entCF*) to chelate and acquire iron were upregulated. Iron is an essential nutrient for the metabolism and growth of bacterial cells, but much attention has been paid during colonization competence and oxidative stress to understand these mechanisms of iron regulation [45]. In this sense, production of growth-inhibitory siderophores with compatible receptor for iron uptake has been studied as a mechanism against plant pathogens [46,47]. Based on the finding that the *asr* gene was upregulated by four-fold, and as diverse studies have confirmed its expression during the response to external acidity and for survival [48], it is probable that the mycelial growth of *S. rolfsii* could cause a lower pH through the production of organic acids that cause oxidative stress in *K. cowanii* Ch1 and generate oxidative stress responses. Upregulated spermidine export genes *mdtIJ* and spermidine N1-acetyltransferase (*speG*) are required probably for stress tolerance in *K. cowanii* Ch1 [49]. Cellular oxidant detoxification and glutathione metabolic processes, as important components of *K. cowanii* Ch1 for stress resistance and motility mechanisms that probably evade stressful conditions, were also upregulated. Important downregulated genes were detected as a response to reduce the number of diverse metabolic pathways for stress homeostasis in *K. cowanii* Ch1 (Table S4).

The gene expression analysis revealed that *K. cowanii* Ch1 had a different response in the presence of VOCs (Figure 6B). Only a set of 35 genes were significantly upregulated and 4 genes were significantly downregulated. Among these differentially expressed genes were *fes*, which encodes the enterobactin esterase enzyme that facilitates intracellular iron release, and genes that encode for siderophore-mediated iron transport (*fepBD*, *tonB*, *feoA*, *entS*, and *efeO*), which indicate the importance of this iron uptake system for enzymatic activities and cell viability in this condition [50]. In fact, the genes that encode for pyruvate formate-lyase (PFL) and pyruvate formate-lyase-activating enzyme (PFL-AE) that utilize iron–sulfur clusters were upregulated by three-fold (Table S5). Both of these enzymes are regulated under anaerobic conditions and play an important role in the supply of acetyl-CoA to the citric acid cycle during anaerobic glycolysis in *E. coli* and other facultative anaerobes [51]. Furthermore, two genes *gatYZ* that encode for D-tagatose 1,6-bisphosphate (TagBP)-specific aldolases and are involved in catabolism of galactitol [52] were upregulated. The upregulated genes related to carbohydrate transport systems provide energy to *K. cowanii* Ch1 and indicate its active metabolism during colonizing competence. Genes related to oxidative stress were upregulated, such as *ibpAB* that encodes a 16 kDa heat shock protein [41] and *trxC* that encodes a thioredoxin, which is a protein with a highly conserved active site sequence [(Cys-Gly-Pro-Cys)], with a key role in maintaining the thiol-disulfide redox potential [53]. An interesting gene that was upregulated was *katG*,

which encodes for the catalase–peroxidase KatG, and its catalase activity protects against peroxide-mediated oxidative damage in the cells by catalyzing the conversion of hydrogen peroxide to water and oxygen [54]. In this sense, the interpretation of bubble gas production during microbial interaction (Figure 1D) could be related to the KatG activity; however, the production of hydrogen peroxide by *K. cowanii* Ch1 during colonization competence remains to be investigated to understand its production as in other bacteria, as well as the role of KatG during colonization competence under the influence of VOCs [55]. In fact, in a study where *P. fluorescens* Pf0–1 was exposed to volatiles produced by *Collimonas pratensis*, *Serratia plymuthica*, *Paenibacillus* sp., and *Pedobacter* sp., the catalase was upregulated by >3-fold [56]. Another possibility is that hydrogen peroxide could be produced by *S. rolfsii* in response to volatiles produced by the bacterial strains (Figure 3). This hypothesis can be supported by the research work published in 2000 by Sideri and Georgiou [57], in which they demonstrated that hydrogen peroxide was produced by the phytopathogen *S. rolfsii* during its development and influenced the oxidative stress caused by growth factors such as light and iron. Another source of evidence is a study in which it was demonstrated that reactive oxygen species (ROS) were accumulated in *Sclerotinia sclerotiorum* hyphae cells when they were treated with VOCs produced by *Bacillus* endophyte strains as a mechanism of oxidative stress response [58]. Therefore, the presence of bacterial VOCs during the interaction between *K. cowanii* Ch1 and *S. rolfsii* could be a positive response for the biological processes of bacterial colonizing competence in at least the condition evaluated; however, the transcriptomic analysis was performed during the early stage of interaction, and this could be a limiting factor. Additional studies are necessary to understand this complex interactome and evaluate the potential production of biomolecules with antifungal properties under colonizing competence. In fact, some genes related to antimicrobial defense were upregulated in *K. cowanii* Ch1 (Table S5), like those that encode for antibiotic biosynthesis monooxygenase (QU629_RS21570), polyketide synthase modules, and related proteins, which are crucial in the synthesis of polyketides, an important class of secondary metabolites that provide certain survival advantages to diverse organisms [59]. Furthermore, the gene that encodes for the virulence factor VirK was upregulated by two-fold, which is a component of the chaperone pathways involved in the secretion systems to deliver virulence factors, such as the plasmid-encoded toxin in *E. coli* [60].

The differences in the phenotypical responses of *K. cowanii* Ch1 in the presence of VOCs produced by different bacterial strains (Figure 3), including the fungal responses during the interaction assays (Figure 2), appeared to reflect that the composition and concentrations of these mixtures of VOCs as well as their effects on gene expression (Figure 6) can potently modulate communication signals conserved during colonization competence in microorganisms [37]. Therefore, the evaluation of cell-free filtrates of *K. cowanii* Ch1 obtained at different growth time periods (Figure 5), and the important finding that the cell-free filtrate at 36 h, applied in the microbial interaction, caused mycelial growth inhibition in vitro and in vivo suggest that the VOC composition produced at a specific bacterial growth stage could be a key factor in determining the biological processes observed, indicating the importance of understanding its impact on competitors, particularly due to its ability to compromise cell viability and gene expression to reduce infection in chili fruit tissues. In this sense, marked differences were observed between the VOC profiles at 36 h compared to those at 24 h. Some common chemical compounds with potent antifungal activities that have been studied in other bacteria strains [37] were detected with high relative abundance, including Pyrazine, 2,5-Dimethyl; 1-Hexanol, 2-ethyl-; 3-methyl-1-Butanol; Ethanol; 2,2,4-trimethyl-1,3-pentanediol diisobutyrate; Benzaldehyde; 1-Decanol; 1-Octanol; and 6-Methyl-1-octanol. Finally, and in agreement with other studies, the mixtures of VOCs, produced by diverse bacterial strains isolated under specific conditions,

represent an important alternative for the biocontrol of phytopathogens [15–17]; therefore, our study proposes a cocktail with antimicrobial properties that contains a combination of the aforementioned chemical compounds detected in the HS-SPME-GC-MS analysis.

5. Conclusions

In conclusion, the results of this study demonstrated that, under the presence of bacterial VOCs during microbial interactions, *K. cowanii* Ch1 had better biocontrol ability to reduce mycelial growth in *S. rolfsii* in both in vitro and in vivo assays, likely by disrupting multiple metabolic pathways in *S. rolfsii* leading to compromised cell viability. Furthermore, the transcriptomic analysis revealed important upregulated genes, and also demonstrated an additional mechanism related to the production of polyketides; however, additional experimental research is needed to validate this mechanism. The mixture of VOCs identified at a specific growth stage of *K. cowanii* Ch1 provides future perspectives to enhance its metabolic ability for the potential development of an efficient biocontrol strategy as potent modulators of communication signals to promote the colonization competence in *K. cowanii* Ch1.

Supplementary Materials: The following supporting information can be downloaded at https://www.mdpi.com/article/10.3390/microorganisms13071483/s1: Table S1. Profile of volatile organic compounds detected in bacterial strains using HS-SPME-GC-MS. Table S2. Profile of volatile organic compounds detected in *K. cowanii* Ch1 at 24 h and 36 h of bacterial growth using HS-SPME-GC-MS. Table S3. RNA-Seq analysis from RNA samples. Table S4. Top differentially expressed genes in *K. cowanii* Ch1 during interaction with *S. rolfsii* in absence of VOCs. Table S5. Top differentially expressed genes in *K. cowanii* Ch1 during interaction with *S. rolfsii* in presence of VOCs. Figure S1. Evaluation of synthetic VOCs on interaction of *K. cowanii* Ch1 and *S. rolfsii* using a double-compartment Petri dish chamber. Figure S2. Similarities between samples. Larger values indicate higher similarity between samples. The similarities were calculated using normalized and 'rlog' transformed read counts of all genes using DESeq2. Figure S3. Scatter plot to visualize differential gene expression results. Mean transformed read counts of genes in one group are shown on X-axis while those in the other are shown on Y-axis. Red dots represent differentially expressed genes (adjusted p-values < 0.05).

Author Contributions: Y.F.H.G., J.G.E. and G.C.O.R.: methodology and software; J.L.A.G., J.H.V.S., M.A.R.L. and C.S.: validation and formal analysis; J.C.G., J.L.H.F., M.A.R.L., E.R.d.L. and A.A.R.: writing—review and editing; J.C.G., C.S., J.L.H.F. and A.A.R.: visualization, supervision, and project administration; J.C.G.: funding acquisition. All authors have read and agreed to the published version of the manuscript.

Funding: This research was partially funded by the Universidad Autónoma de Querétaro (FONFIVE-UAQ-2024; FOPER-2025).

Institutional Review Board Statement: Not applicable.

Informed Consent Statement: Not applicable.

Data Availability Statement: The data presented in this work are available from the corresponding authors upon request.

Acknowledgments: We thank SECIHTI for providing fellowships to Y.F.H.G. and J.G.E.

Conflicts of Interest: The authors declare no conflicts of interest.

References

1. Jan-Roblero, J.; Cruz-Maya, J.A.; Barajas, C.G. Chapter 12—Kosakonia. In *Beneficial Microbes in Agro-Ecology*; Amaresan, N., Annapurna, K., Sankaranarayanan, A., Senthil Kumar, M., Kumar, K., Eds.; Academic Press: Cambridge, MA, USA, 2020; pp. 213–231.

2. Mena Navarro, M.P.; Espinosa Bernal, M.A.; Martinez-Avila, A.E.; Aponte Pineda, L.S.; Montes Flores, L.A.; Chan Ku, C.D.; Hernández Gómez, Y.F.; González Espinosa, J.; Pacheco Aguilar, J.R.; Ramos López, M.Á.; et al. Role of Volatile Organic Compounds Produced by *Kosakonia cowanii* Cp1 during Competitive Colonization Interaction against *Pectobacterium aroidearum* SM2. *Microorganisms* **2024**, *12*, 930. [CrossRef]
3. Quintas-Nunes, F.; Rossi, M.J.; Nascimento, F.X. Genomic insights into the plant-associated lifestyle of *Kosakonia radicincitans* MUSA4, a diazotrophic plant-growth-promoting bacterium. *Syst. Appl. Microbiol.* **2022**, *45*, 126303. [CrossRef]
4. Mertschnigg, T.; Patz, S.; Becker, M.; Feierl, G.; Ruppel, S.; Bunk, B.; Spröer, C.; Overmann, J.; Zarfel, G. First Report of *Kosakonia radicincitans* Bacteraemia from Europe (Austria)—Identification and Whole-Genome Sequencing of Strain DSM 107547. *Sci. Rep.* **2020**, *10*, 1948. [CrossRef] [PubMed]
5. Sharma, S.; Compant, S.; Franken, P.; Ruppel, S.; Ballhausen, M.-B. It Takes Two to Tango: A Bacterial Biofilm Provides Protection against a Fungus-Feeding Bacterial Predator. *Microorganisms* **2021**, *9*, 1566. [CrossRef] [PubMed]
6. Weiss, B.L.; Maltz, M.A.; Vigneron, A.; Wu, Y.; Walter, K.S.; O'Neill, M.B.; Wang, J.; Aksoy, S. Colonization of the tsetse fly midgut with commensal Kosakonia cowanii Zambiae inhibits trypanosome infection establishment. *PLoS Pathog.* **2019**, *15*, e1007470. [CrossRef]
7. Sherpa, M.T.; Sharma, L.; Bag, N.; Das, S. Isolation, Characterization, and Evaluation of Native Rhizobacterial Consortia Developed From the Rhizosphere of Rice Grown in Organic State Sikkim, India, and Their Effect on Plant Growth. *Front. Microbiol.* **2021**, *12*, 713660. [CrossRef]
8. Remus, R.; Ruppel, S.; Jacob, H.-J.; Hecht-Buchholz, C.; Merbach, W. Colonization behaviour of two enterobacterial strains on cereals. *Biol. Fertil. Soils* **2000**, *30*, 550–557. [CrossRef]
9. Brock, A.K.; Berger, B.; Mewis, I.; Ruppel, S. Impact of the PGPB Enterobacter radicincitans DSM 16656 on growth, glucosinolate profile, and immune responses of Arabidopsis thaliana. *Microb. Ecol.* **2013**, *65*, 661–670. [CrossRef] [PubMed]
10. Thanwisai, L.; Siripornadulsil, W.; Siripornadulsil, S. *Kosakonia oryziphila* NP19 bacterium acts as a plant growth promoter and biopesticide to suppress blast disease in KDML105 rice. *Sci. Rep.* **2024**, *14*, 17944. [CrossRef]
11. González Espinosa, J.; Hernández Gómez, Y.F.; Javier Martínez, Y.; Flores Gallardo, F.J.; Pacheco Aguilar, J.R.; Ramos López, M.Á.; Arvizu Gómez, J.L.; Saldaña Gutierrez, C.; Rodríguez Morales, J.A.; García Gutiérrez, M.C.; et al. *Kosakonia cowanii* Ch1 Isolated from Mexican Chili Powder Reveals Growth Inhibition of Phytopathogenic Fungi. *Microorganisms* **2023**, *11*, 1758. [CrossRef]
12. Cirimotich, C.M.; Dong, Y.; Clayton, A.M.; Sandiford, S.L.; Souza-Neto, J.A.; Mulenga, M.; Dimopoulos, G. Natural microbe-mediated refractoriness to Plasmodium infection in Anopheles gambiae. *Science* **2011**, *332*, 855–858. [CrossRef] [PubMed] [PubMed Central]
13. Romano, I.; Ventorino, V.; Ambrosino, P.; Testa, A.; Chouyia, F.E.; Pepe, O. Development and Application of Low-Cost and Eco-Sustainable Bio-Stimulant Containing a New Plant Growth-Promoting Strain *Kosakonia pseudosacchari* TL13. *Front. Microbiol.* **2020**, *11*, 2044. [CrossRef] [PubMed]
14. Gao, H.; Lu, C.; Wang, H.; Wang, L.; Yang, Y.; Jiang, T.; Li, S.; Xu, D.; Wu, L. Production exopolysaccharide from Kosakonia cowanii LT-1 through solid-state fermentation and its application as a plant growth promoter. *Int. J. Biol. Macromol.* **2020**, *150*, 955–964. [CrossRef] [PubMed]
15. Montejano-Ramírez, V.; Ávila-Oviedo, J.L.; Campos-Mendoza, F.J.; Valencia-Cantero, E. Microbial Volatile Organic Compounds: Insights into Plant Defense. *Plants* **2024**, *13*, 2013. [CrossRef] [PubMed] [PubMed Central]
16. Tahir, H.A.S.; Ali, Q.; Rajer, F.U.; Shakeel, Q.; Gillani, W.; Binyamin, R.; Tayyab, H.M.A.; Khan, A.R.; Gu, Q.; Gao, X.; et al. Transcriptomic analysis of Ralstonia solanacearum in response to antibacterial volatiles of Bacillus velezensis FZB42. *Arch. Microbiol.* **2023**, *205*, 358. [CrossRef]
17. Beyari, E.A. Alternatives to chemical pesticides: The role of microbial biocontrol agents in phytopathogen management: A comprehensive review. *J. Plant Pathol.* **2025**, *107*, 291–314. [CrossRef]
18. Patra, G.K.; Acharya, G.K.; Panigrahi, J.; Mukherjee, A.K.; Rout, G.R. The soil-borne fungal pathogen *Athelia rolfsii*: Past, present, and future concern in legumes. *Folia Microbiol.* **2023**, *68*, 677–690. [CrossRef]
19. Espinosa Bernal, M.A.; Mena Navarro, M.P.; Arvizu Gómez, J.L.; Saldaña, C.; Ramos López, M.Á.; Amaro Reyes, A.; Escamilla García, M.; Pacheco Aguilar, J.R.; Moreno, V.P.; Rodríguez Morales, J.A.; et al. Biocontrol Activity of *Bacillus altitudinis* CH05 and *Bacillus tropicus* CH13 Isolated from *Capsicum annuum* L. Seeds against Fungal Strains. *Microorganisms* **2024**, *12*, 1943. [CrossRef]
20. Di Tommaso, P.; Chatzou, M.; Floden, E.W.; Barja, P.P.; Palumbo, E.; Notredame, C. Nextflow enables repro-ducible computational workflows. *Nat. Biotechnol.* **2017**, *35*, 316–319. [CrossRef]
21. Patel, H.; Ewels, P.; Peltzer, A.; Hammarén, R.; Botvinnik, O.; Sturm, G.; Davenport, C. nf-core/rnaseq: nf-core/rnaseq v3.0—Silver Shark (Version 3.0). Zenodo: 2020. Available online: https://zenodo.org/records/4323183 (accessed on 11 November 2024).
22. Dobin, A.; Davis, C.A.; Schlesinger, F.; Drenkow, J.; Zaleski, C.; Jha, S.; Batut, P.; Chaisson, M.; Gingeras, T.R. STAR: Ultrafast universal RNA-seq aligner. *Bioinformatics* **2013**, *29*, 15–21. [CrossRef]

23. Danecek, P.; Bonfield, J.K.; Liddle, J.; Marshall, J.; Ohan, V.; Pollard, M.O.; Whitwham, A.; Keane, T.; McCarthy, S.A.; Davies, R.M.; et al. Twelve years of SAMtools and BCFtools. *Gigascience* **2021**, *10*, giab008. [CrossRef]
24. Wang, L.; Wang, S.; Li, W. RSeQC: Quality control of RNA-seq experiments. *Bioinformatics* **2012**, *28*, 2184–2185. [CrossRef] [PubMed]
25. García-Alcalde, F.; Okonechnikov, K.; Carbonell, J.; Cruz, L.M.; Götz, S.; Tarazona, S.; Dopazo, J.; Meyer, T.F.; Conesa, A. Qualimap: Evaluating next-generation sequencing alignment data. *Bioinformatics* **2012**, *28*, 2678–2679. [CrossRef]
26. Broad Institute. *"Picard Toolkit." Broad Institute, GitHub Repository*; Broad Institute: Cambridge, MA, USA, 2019; Available online: http://broadinstitute.github.io/picard/ (accessed on 14 November 2024).
27. Daley, T.; Smith, A.D. Predicting the molecular complexity of sequencing libraries. *Nat. Methods* **2013**, *10*, 325–327. [CrossRef] [PubMed]
28. Sayols, S.; Scherzinger, D.; Klein, H. dupRadar: A Bioconductor package for the assessment of PCR artifacts in RNA-Seq data. *BMC Bioinform.* **2016**, *17*, 428. [CrossRef]
29. Liao, Y.; Smyth, G.K.; Shi, W. featureCounts: An efficient general purpose program for assigning sequence reads to genomic features. *Bioinformatics* **2014**, *30*, 923–930. [CrossRef] [PubMed]
30. Love, M.I.; Huber, W.; Anders, S. Moderated estimation of fold change and dispersion for RNA-seq data with DESeq2. *Genome Biol.* **2014**, *15*, 550. [CrossRef]
31. Ewels, P.; Magnusson, M.; Lundin, S.; Käller, M. MultiQC: Summarize analysis results for multiple tools and samples in a single report. *Bioinformatics* **2016**, *32*, 3047–3048. [CrossRef]
32. Ge, S.X.; Jung, D.; Yao, R. ShinyGO: A graphical gene-set enrichment tool for animals and plants. *Bioinformatics* **2020**, *36*, 2628–2629. [CrossRef]
33. Liu, M.; Blattman, S.B.; Takahashi, M.; Mandayam, N.; Jiang, W.; Oikonomou, P.; Tavazoie, S.F.; Tavazoie, S. Conserved genetic basis for microbial colonization of the gut. *Cell* **2025**, *188*, 2823–2824. [CrossRef]
34. Chandrasekaran, M.; Paramasivan, M.; Sahayarayan, J.J. Microbial volatile organic compounds: An alternative for chemical fertilizers in sustainable agriculture development. *Microorganisms* **2023**, *11*, 42. [CrossRef]
35. Weisskopf, L.; Schulz, S.; Garbeva, P. Microbial volatile organic compounds in intra-kingdom and inter-kingdom interactions. *Nat. Rev. Microbiol.* **2021**, *19*, 391–404. [CrossRef]
36. Schulz-Bohm, K.; Martín-Sánchez, L.; Garbeva, P. Microbial volatiles: Small molecules with an important role in intra- and inter-kingdom interactions. *Front. Microbiol.* **2017**, *8*, 2484. [CrossRef] [PubMed]
37. Grahovac, J.; Pajčin, I.; Vlajkov, V. Bacillus VOCs in the Context of Biological Control. *Antibiotics* **2023**, *12*, 581. [CrossRef] [PubMed]
38. Koo, M.S.; Lee, J.H.; Rah, S.Y.; Yeo, W.S.; Lee, J.W.; Lee, K.L.; Koh, Y.S.; Kang, S.O.; Roe, J.H. A reducing system of the superoxide sensor SoxR in Escherichia coli. *EMBO J.* **2003**, *22*, 2614–2622. [CrossRef]
39. Seo, S.W.; Kim, D.; Szubin, R.; Palsson, B.O. Genome-wide Reconstruction of OxyR and SoxRS Transcriptional Regulatory Networks under Oxidative Stress in *Escherichia coli* K-12 MG1655. *Cell Rep.* **2015**, *12*, 1289–1299. [CrossRef]
40. Chan, E.; Weiss, B. Endonuclease IV of Escherichia coli is induced by paraquat. *Proc. Natl. Acad. Sci. USA* **1987**, *84*, 3189–3193. [CrossRef] [PubMed]
41. Dubey, A.; Prajapati, K.S.; Swamy, M.; Pachauri, V. Heat shock proteins: A therapeutic target worth to consider. *Vet World* **2015**, *8*, 46–51. [CrossRef]
42. Zhang, X.S.; García-Contreras, R.; Wood, T.K. YcfR (BhsA) influences Escherichia coli biofilm formation through stress response and surface hydrophobicity. *J. Bacteriol.* **2007**, *189*, 3051–3062. [CrossRef]
43. Capdevila, D.A.; Wang, J.; Giedroc, D.P. Bacterial Strategies to Maintain Zinc Metallostasis at the Host-Pathogen Interface. *J. Biol. Chem.* **2016**, *291*, 20858–20868. [CrossRef]
44. Sullivan, M.J.; Terán, I.; Goh, K.G.; Ulett, G.C. Resisting death by metal: Metabolism and Cu/Zn homeostasis in bacteria. *Emerg. Top. Life Sci.* **2024**, *8*, 45–56. [CrossRef] [PubMed]
45. Ullah, I.; Lang, M. Key players in the regulation of iron homeostasis at the host-pathogen interface. *Front. Immunol.* **2023**, *14*, 1279826. [CrossRef] [PubMed]
46. Gu, S.; Wei, Z.; Shao, Z.; Friman, V.-P.; Cao, K.; Yang, T.; Kramer, J.; Wang, X.; Li, M.; Mei, X.; et al. Competition for iron drives phytopathogen control by natural rhizosphere microbiomes. *Nat. Microbiol.* **2020**, *5*, 1002–1010. [CrossRef]
47. Lyng, M.; Jørgensen, J.P.B.; Schostag, M.D.; Jarmusch, S.A.; Aguilar, D.K.C.; Lozano-Andrade, C.N.; Kovács, Á.T. Competition for iron shapes metabolic antagonism between Bacillus subtilis and Pseudomonas marginalis. *ISME J.* **2024**, *18*, wrad001. [CrossRef] [PubMed]
48. Seputiene, V.; Motiejūnas, D.; Suziedelis, K.; Tomenius, H.; Normark, S.; Melefors, O.; Suziedeliene, E. Molecular characterization of the acid-inducible asr gene of Escherichia coli and its role in acid stress response. *J. Bacteriol.* **2003**, *185*, 2475–2484. [CrossRef]

49. Nair, A.V.; Singh, A.; Devasurmutt, Y.; Rahman, S.A.; Tatu, U.S.; Chakravortty, D. Spermidine constitutes a key determinant of motility and attachment of Salmonella Typhimurium through a novel regulatory mechanism. *Microbiol. Res.* **2024**, *281*, 127605. [CrossRef]
50. Abergel, R.J.; Warner, J.A.; Shuh, D.K.; Raymond, K.N. Enterobactin protonation and iron release: Structural characterization of the salicylate coordination shift in ferric enterobactin. *J. Am. Chem. Soc.* **2006**, *128*, 8920–8931. [CrossRef]
51. Crain, A.V.; Broderick, J.B. Pyruvate formate-lyase and its activation by pyruvate formate-lyase activating enzyme. *J. Biol. Chem.* **2014**, *289*, 5723–5729. [CrossRef]
52. Dai, Y.; Zhang, J.; Zhang, T.; Chen, J.; Hassanin, H.A.M.; Jiang, B. Characteristics of a fructose 6-phosphate 4-epimerase from Caldilinea aerophila DSM 14535 and its application for biosynthesis of tagatose. *Enzym. Microb. Technol.* **2020**, *139*, 109594. [CrossRef]
53. Zeller, T.; Klug, G. Thioredoxins in bacteria: Functions in oxidative stress response and regulation of thioredoxin genes. *Naturwissenschaften* **2006**, *93*, 259–266. [CrossRef]
54. Uhlich, G.A. KatP contributes to OxyR-regulated hydrogen peroxide resistance in Escherichia coli serotype O157: H7. *Microbiology* **2009**, *155 Pt 11*, 3589–3598. [CrossRef] [PubMed]
55. Korshunov, S.; Imlay, J.A. Two sources of endogenous hydrogen peroxide in Escherichia coli. *Mol. Microbiol.* **2010**, *75*, 1389–1401. [CrossRef] [PubMed]
56. Garbeva, P.; Hordijk, C.; Gerards, S.; de Boer, W. Volatile-mediated interactions between phylogenetically different soil bacteria. *Front. Microbiol.* **2014**, *5*, 289. [CrossRef] [PubMed]
57. Sideri, M.; Georgiou, C.D. Differentiation and hydrogen peroxide production in Sclerotium rolfsii are induced by the oxidizing growth factors, light and iron. *Mycologia* **2000**, *92*, 1033–1042. [CrossRef]
58. Massawe, V.C.; Hanif, A.; Farzand, A.; Mburu, D.K.; Ochola, S.O.; Wu, L.; Tahir, H.A.S.; Gu, Q.; Wu, H.; Gao, X. Volatile Compounds of Endophytic Bacillus spp. have Biocontrol Activity Against Sclerotinia sclerotiorum. *Phytopathology* **2018**, *108*, 1373–1385. [CrossRef]
59. Singh, A.; Chaudhary, S.; Shankar, A.; Prasad, V. Chapter 13—Polyketide and Its Derivatives. In *New and Future Developments in Microbial Biotechnology and Bioengineering*; Singh, H.B., Gupta, V.K., Jogaiah, S., Eds.; Elsevier: Amsterdam, The Netherlands, 2019; pp. 219–227. [CrossRef]
60. Tapia-Pastrana, G.; Chavez-Dueñas, L.; Lanz-Mendoza, H.; Teter, K.; Navarro-García, F. VirK is a periplasmic protein required for efficient secretion of plasmid-encoded toxin from enteroaggregative Escherichia coli. *Infect. Immun.* **2012**, *80*, 2276–2285. [CrossRef]

microorganisms

MDPI

Article

Co-Application of Seaweed Extract (*Solieria filiformis*) and Silicon: Effect on Sporulation, Mycorrhizal Colonization, and Initial Growth of *Mimosa caesalpiniaefolia*

Isaac Alves da Silva [1], José Lucas Sousa de Andrade [2], Francisco Luan Almeida Barbosa [2], Murilo de Sousa Almeida [2], Marjory Lima Holanda Araújo [1], Adijailton Jose de Souza [3], Ademir Sergio Ferreira Araujo [4], Arthur Prudêncio de Araujo Pereira [2,*] and Kaio Gráculo Vieira Garcia [2]

[1] Biochemistry and Molecular Biology Department, Federal University of Ceará, Av. Mister Hull, 2977, Fortaleza 60440-900, Brazil; isaacalvesbiotec@gmail.com (I.A.d.S.); marjory.holanda@ufc.br (M.L.H.A.)
[2] Soil Science Department, Federal University of Ceará, Av. Mister Hull, 2977, Fortaleza 60021-970, Brazil; lucasphy2@gmail.com (J.L.S.d.A.); luan02101994@gmail.com (F.L.A.B.); sousamuriloalmeida@gmail.com (M.d.S.A.); kaiovieira@ufc.br (K.G.V.G.)
[3] Luiz de Queiroz College of Agriculture (ESALQ), University of São Paulo (USP), Piracicaba 13418-900, Brazil; adijailtonjsouza@alumni.usp.br
[4] Agricultural Science Center, Federal University of Piauí, Teresina 64049-550, Brazil; ademir@ufpi.edu.br
* Correspondence: arthur.prudencio@ufc.br; Tel.: +55-(85)-3366-9686

Abstract

Seaweed extracts (SEs) and silicon (Si) are known to enhance plant growth under adverse conditions. However, their combined effects on arbuscular mycorrhizal fungi (AMF) are not yet fully understood. This study evaluated the effect of the co-application of an SE and Si on the AMF spore abundance, mycorrhizal colonization, and early growth of *Mimosa caesalpiniaefolia*. Plants were grown in a greenhouse for 70 days in soil with or without an SE (*Solieria filiformis*) and three Si levels (0, 150, and 300 mg kg^{-1}). Growth parameters, AMF spore abundance, mycorrhizal colonization, and plant/soil chemical composition were assessed. SE and Si increased the plant height, stem diameter, number of leaves, and shoot dry mass, while higher Si levels reduced the root dry mass and length. Mycorrhizal colonization was highest (64%) at 150 mg kg^{-1} Si with SE, whereas AMF spore abundance decreased as Si increased. SE and 300 mg kg^{-1} Si raised the Si levels in the shoot, while root Si increased only at 300 mg kg^{-1} Si. Shoot Na increased at 300 mg kg^{-1} Si without SE, whereas K was highest at 150 mg kg^{-1} Si with SE. The soil pH, electrical conductivity, and Na increased at 300 mg kg^{-1} Si, while K and P decreased at this level without SE. These findings indicate that SE and Si co-application benefits early growth and may modulate mycorrhizal symbiosis, highlighting the importance of proper management to maximize plant and soil benefits.

Keywords: plant–soil interactions; arbuscular mycorrhizae; biostimulants; silicate; sustainable practices

1. Introduction

In agriculture, seaweed extracts (SEs) are widely used as biostimulants due to their complex composition, rich in polysaccharides such as laminarin, fucoidan, and alginate, which are predominant in brown macroalgae and extensively utilized in the formulation of these commercial extracts [1]. However, red macroalgae remain understudied for this purpose, with few reports in the literature regarding their biostimulant potential [2–4]. The

application of an SE, either to the soil or via foliar spraying, can increase chlorophyll content, optimize photosynthesis and nutrient uptake, and improve water retention, thus promoting the growth of various agricultural crops and ecologically important plant species [5].

The red macroalga *Solieria filiformis* presents a promising biochemical composition for use as a biostimulant, containing 65.8% (*w*/*w*) carbohydrates, 9.6% (*w*/*w*) proteins, 1.7% (*w*/*w*) lipids, 7.0% (*w*/*w*) moisture, and 15.9% (*w*/*w*) ash, in addition to being rich in essential minerals such as calcium (Ca), potassium (K), magnesium (Mg), and phosphorus (P), as well as micronutrients like boron (B), copper (Cu), iron (Fe), manganese (Mn), and zinc (Zn) [6,7]. Evidence suggests that SEs may also positively influence soil microbiota by stimulating beneficial microorganisms, such as arbuscular mycorrhizal fungi (AMF) [8,9].

AMF are known to form mutualistic relationships with nearly 90% of land plants [10], playing a crucial role in promoting the absorption of water and essential nutrients such as P and nitrogen (N), as well as other beneficial elements like silicon (Si). Moreover, these interactions improve the plant's ability to cope with both biotic and abiotic challenges [11–13], making AMF a valuable tool for sustainable agriculture. This is particularly relevant in degraded soils, which often exhibit low fertility and water scarcity. However, the effectiveness of mycorrhizal colonization depends on a complex signaling process between plant roots and AMF. In this context, flavonoids play an essential role as signaling molecules, activating spore germination and guiding hyphal growth toward roots [14].

Recently, various flavonoids have been identified in SEs, including hispidulin, as well as derivatives of gallocatechin and acacetin, which may stimulate mycorrhizal symbiosis [9]. Studies have demonstrated that SEs can promote AMF spore germination, hyphal growth, and accelerate mycorrhizal colonization. In *Medicago truncatula*, for instance, foliar application or immersion in SE resulted in the significantly higher expression of genes associated with the establishment of mycorrhizal symbiosis compared to controls [9].

Complementary to these effects, Si—an element widely distributed in the Earth's crust—has been recognized for its role in mitigating environmental stresses and enhancing plant performance within the soil–plant–environment system [15,16]. Although Si is not classified as an essential element, its application can strengthen plant resistance against drought, salinity, and heavy metal toxicity [17,18]. Studies indicate that Si supplementation improves physiological processes and stimulates plant growth, particularly under adverse conditions [19–21]. Moreover, Si appears to strengthen mycorrhizal relationships by boosting photosynthetic activity in plants, supplying extra carbon to the fungi and curtailing lignin production [21].

However, the interaction between Si and AMF may vary depending on plant species and environmental conditions. While some plants with high Si accumulation are not significantly affected by AMF presence, in other species, such as strawberry, Si application favors mycorrhizal colonization and stimulates fungal structure formation, as well as increases Si uptake after mycorrhization [22]. In another study, with *Leucaena leucocephala*, Si application also increased mycorrhizal colonization; however, AMF spore abundance in the soil decreased with increasing Si levels [23]. Thus, it remains unclear how Si regulates mycorrhizal symbiosis and plant growth, especially in species adapted to nutrient-poor and semi-arid soils, such as *Mimosa caesalpiniaefolia*.

M. caesalpiniaefolia is a fast-growing, perennial leguminous species native to the Caatinga biome, widely recognized for its ecological importance and functional traits. It is capable of establishing symbiotic associations with both AMF [24] and nitrogen-fixing bacteria known as rhizobia [25], which makes it particularly suitable for studies on the interactions between biostimulants, soil microbiota, and plant nutrition. Its high adaptability to the edaphoclimatic conditions of the Caatinga [26], along with its frequent use

in the recovery of degraded areas and agroforestry systems [27], reinforces its potential as a model species in sustainable land management strategies aimed at promoting soil health and resilience in semi-arid environments [28]. Beyond its ecological importance, *M. caesalpiniaefolia* exhibits significant agronomic value, serving multiple purposes such as forage for livestock, timber production, and green manure.

Although several studies have investigated the isolated effects of SEs and Si on plant growth, knowledge gaps remain regarding how the combined application of these inputs may influence mycorrhizal attributes and promote the development of plant species that have not been previously evaluated under this strategy. Thus, this study aims to evaluate the effect of the co-application of an SE (*S. filiformis*) and Si on mycorrhizal colonization, AMF sporulation, and the early growth of *M. caesalpiniaefolia*. We hypothesized that the combination of an SE (*S. filiformis*) and Si will promote increased mycorrhizal colonization, which in turn will stimulate AMF spore abundance in the soil, ultimately enhancing the growth of this species.

2. Materials and Methods

2.1. Study Area and Experimental Soil

The study was conducted in a greenhouse at the Department of Soil Science, Federal University of Ceará (UFC), located at the Pici Campus in Fortaleza, Ceará, Brazil (3°45′47″ S; 38°31′23″ W; 47 m altitude). According to the Köppen–Geiger classification, the region has a tropical climate with a dry winter (Aw), an average annual rainfall of 1600 mm, and a mean temperature of 27 °C [29]. Soil samples were collected from a depth of 0–20 cm in a native forest area within the Urban Agriculture Teaching and Research Center (NEPAU) at the UFC. The samples were passed through a 2 mm mesh sieve to remove coarse particles, homogenized, and stored in plastic bags. The chemical characterization of the soil was performed at the Soil, Water, and Plant Laboratory of the UFC following the methodology described by [30] (Table 1).

Table 1. Chemical and physical characterization of the soil collected from the Urban Agriculture Teaching and Research Center (NEPAU) at the UFC, Fortaleza, CE, Brazil.

pH	EC	Mg^{2+}	Na^{+}	K^{+}	H + Al	Al^{3+}	BS	AS	ESP
(H_2O)	(dS/m)			($cmol_c/kg$)			(%)	(%)	(%)
5.0	0.9	0.4	0.6	0.18	4.46	0.5	41	14	1
N	OM	P	Bulk Density	Coarse Sand	Fine Sand	Silt	Clay	Natural Clay	Textural Class
(g/kg)	(g/kg)	(mg/kg)	g/cm^3			(g/kg)			-
1.36	21.39	37	1.6	586	282	95	37	4	Loamy Sand

Note: EC = electrical conductivity, BS = base saturation percentage, AS = aluminum saturation percentage, ESP = exchangeable sodium percentage, OM = organic matter.

2.2. Seaweed Type and Production Process

The seaweed used in the extract was *S. filiformis*, a red algae species commonly found along the Brazilian coast. The *S. filiformis* used in this study was harvested from cultivation structures known as colonized modules, maintained at sea by the Flecheiras and Guajiru Seaweed Producers Association (APFG), in collaboration with the Algae Biotechnology and Bioprocess Laboratory (BioAP) of the Department of Biochemistry and Molecular Biology at the UFC. The collection site was on the western coast of Ceará, in the municipality of

Trairi, at Flecheiras Beach, Brazil. After collection, the algae were stored frozen in their natural state.

To produce the extract, 500 g of *S. filiformis* was ground in an electric mill with 2.5 L of distilled water for 1 min and 30 s. The mixture was then heated on a hot plate (MYLABOR-model AG-10 [https://www.lojanetlab.com.br, accessed 2 July 2025]) until it reached 80 °C and maintained at this temperature for 1 h under constant mechanical stirring at 140 RPM. As some water evaporated during heating, it was replenished to maintain the initial volume. The solution was subsequently filtered through a fine-mesh nylon fabric at 80 °C to prevent gelatinization, which could hinder the filtration process, given that gelation begins at 45 °C. The final filtrate was stored in a refrigerator for later application to the plants. A detailed characterization of the chemical composition of *S. filiformis* used in this study is available in [7].

2.3. Process and Experimental Design

The experiment followed a completely randomized design (CRD) in a 2 × 3 factorial arrangement, considering (i) the presence or absence of *S. filiformis* seaweed extract (SE) in the soil and (ii) three levels of silicon (0, 150, and 300 mg kg^{-1}). The study included 5 replicates per treatment, totaling 30 experimental units.

The soil was placed into 1 L pots, each containing 1 kg of substrate. To minimize drainage and nutrient leaching, the pots were lined with plastic bags. We chose to use non-sterilized soil in this experiment in order to maintain edaphic conditions as close as possible to those found in the natural environment. This approach aims to allow more representative microbial interactions, resulting in data with greater ecological relevance. Si was incorporated at three levels, 0, 150, and 300 mg kg^{-1}, using sodium silicate (Na_2SiO_3) as the source. The Si levels were selected based on previous studies by [23,31]. Following Si treatment, the soil underwent thorough homogenization and was incubated for ten days. The seaweed extract, supplied by the Algae Biotechnology and Bioprocess Laboratory at the UFC, was applied to the soil at a 10% (v/v) concentration. This concentration was selected based on prior studies [32,33] that demonstrated its effectiveness. Before sowing, *M. caesalpiniaefolia* seeds were exposed to 70% ethanol for 30 s to reduce surface tension, then disinfected using a 1% sodium hypochlorite solution for 10 min. Subsequently, the seeds were rinsed with sterile distilled water to eliminate any remaining hypochlorite residue [34]. Three seeds were planted per pot, and 10 days after seedling emergence, thinning was carried out to retain a single plant per pot. The soil was irrigated daily to maintain approximately 60% of field capacity. Field capacity was estimated based on the concept of total available water (TAW) described by [35], considering the soil bulk density, effective root zone depth, and typical water content values at field capacity and permanent wilting point for the soil type. Water replacement was performed daily using pot lysimeters to compensate for evapotranspiration losses. The experiment lasted for 70 days after sowing (DASs).

2.4. Plant Growth Parameters

At 70 DASs, the plants were collected, placed in paper bags, and dried in a forced-air oven (PROLAB-model SSDicr-150 [https://www.prolab.com.br, accessed 2 July 2025]) at 65 °C for three days to determine the shoot dry mass (SDM). The roots were rinsed with running water and dried following the same procedure to obtain the root dry mass (RDM). The plant height (H) was measured with a graduated ruler from the soil surface to the plant apex and expressed in centimeters. The root length (RL) was also measured with a graduated ruler from the soil insertion point to the root tip. The stem diameter (SD) was recorded 5 cm above the soil surface using a digital caliper (MTX-model 316119

[https://mtxtools.ru, accessed 2 July 2025]) and expressed in millimeters. The number of leaves (NL) was determined through direct counting and expressed as the NL per plant.

2.5. Quantification of Mycorrhizal Colonization and Spore Abundance

Mycorrhizal colonization (MC) was assessed by clearing the roots with a 10% potassium hydroxide (KOH) solution, as outlined by [36]. The samples were placed in open tubes containing a 10% KOH solution and subjected to a preheated water bath (MYLABOR-model SSDc-10 [https://www.lojanetlab.com.br, accessed 2 July 2025]) maintained at 80 °C for 1 h, with the solution being replaced every 20 min. After this period, the tubes were removed from the water bath, the KOH solution was discarded, and a 3% hydrogen peroxide (H_2O_2) solution was added. Subsequently, the roots were washed with distilled water. Following the clearing process, the roots were stained by adding a 5% acidified blue ink solution (Parker Quink [https://www.parkerpen.com, accessed 2 July 2025]) to the tubes, which were again placed in the water bath at 80 °C for 10 min, following the method by [37]. After staining, the samples were removed, washed with a 5% acetic acid solution, and stored in a preservative solution composed of equal volumes of glycerol, lactic acid, and distilled water (1:1:1 v/v). For microscopic analysis, slides were prepared with ten root fragments, each approximately 1 cm long, and examined using an optical microscope (BIOFOCUS-model Blue-1600 [https://www.ionlab.com.br, accessed 2 July 2025]). Mycorrhizal colonization (%) was assessed following the methodology described by [38].

The abundance of AMF spores in the soil (AS) was assessed using the wet sieving method, following the protocol described by [39]. For this, 100 g of soil from each sample was mixed with ~500 mL of water and blended at a high speed for 15 s in a Mondial Blender. The resulting suspension was then poured through a series of sieves with mesh sizes of 106 and 44 μm. All particles retained on the 44 μm sieve were collected and centrifuged with a 70% sucrose solution at 3500 rpm for 5 min. The AMF spores in suspension were filtered (44 μm mesh), rinsed with water, transferred to Petri dishes, and quantified by direct counting under a stereomicroscope (OLEN-model TECNIVAL-SQF-F [https://www.lojanetlab.com.br, accessed 2 July 2025]).

2.6. Silicon in Shoots and Roots and Phosphorus, Sodium, and Potassium in Shoots

The Si content in the roots and shoots of *M. caesalpiniaefolia* was extracted using 30% hydrogen peroxide and 50% sodium hydroxide. The samples were then placed in a water bath (MYLABOR-model SSDc-10 [https://www.lojanetlab.com.br, accessed 2 July 2025]) at 85 °C for 1 h until complete gas release occurred. Next, they underwent digestion in a semi-open Falcon tube using an autoclave (PHOENIX-model AV-75 [https://phoenix.ind.br, accessed 2 July 2025]) at 123 °C and 1.5 atm pressure for 1 h [40]. Si determination in plant tissues was performed through colorimetry at 410 nm, following the procedures described by [40]. The concentrations of P, sodium (Na), and K in the shoots of *M. caesalpiniaefolia* were extracted using 1 mol L^{-1} HCl [30]. P was determined by colorimetry (KASVI-model K37-VIS [https://kasvi.com.br, accessed 2 July 2025]) at a wavelength of 660 nm, while Na and K were analyzed using flame photometry (DIGIMED-model DM-62 [https://www.digimed.ind.br, accessed 2 July 2025]) [30].

2.7. Soil Chemical Analysis

Electrical conductivity (EC) and soil solution pH were measured in water (1:2.5 soil-to-distilled water ratio). The pH was determined using a potentiometer (R-TEC-7/2-MP Tecnal [https://tecnal.com.br, accessed 2 July 2025]), while EC was measured with a conductivity meter (DDS-11C MFC:2409087 Meter [https://impac.com.br, accessed 2 July 2025]) [30]. Soil Si content was extracted using a 0.5 M acetic acid solution and quantified by colorime-

try (KASVI-model K37-VIS [https://kasvi.com.br, accessed 2 July 2025]) at a wavelength of 660 nm, following the procedures described by [41]. Soil P content was extracted using Mehlich 1 solution (0.05 mol L^{-1} HCl and 0.0125 mol L^{-1} H_2SO_4) and determined by colorimetry (KASVI-model K37-VIS [https://kasvi.com.br, accessed 2 July 2025]) at a wavelength of 660 nm. Na and K were extracted using 1N ammonium acetate and determined by flame photometry (DIGIMED-model DM-62 [https://www.digimed.ind.br, accessed 2 July 2025]) [30].

2.8. Statistical Analysis

Statistical analyses were conducted to assess the data distribution and variance homogeneity. Normality was evaluated using the Shapiro–Wilk test, and Levene's test was applied to verify the homogeneity of variances. When the data met the normality assumption and exhibited homogeneous variances, a two-way analysis of variance (ANOVA) was performed using the F test ($p \leq 0.05$). When significant differences were detected, mean comparisons were conducted using the Scott–Knott test ($p \leq 0.05$). All statistical analyses were performed using the AgroEstat software (version 1.1.0.712).

3. Results

3.1. Plant Growth

Plants of M. caesalpinifolia Benth. exhibited improved growth with the application of *S. filiformis* seaweed extract and Si (Figure 1). The application of *S. filiformis* seaweed extract increased the shoot dry mass production, plant height, stem diameter, and leaf number, regardless of Si levels. Additionally, at Si levels of 150 and 300 mg kg^{-1}, these variables increased regardless of the application of *S. filiformis* seaweed extract (Figure 2A,C,E,F). On the other hand, the absence of Si application resulted in higher root dry mass production and root length (Figure 2B,D).

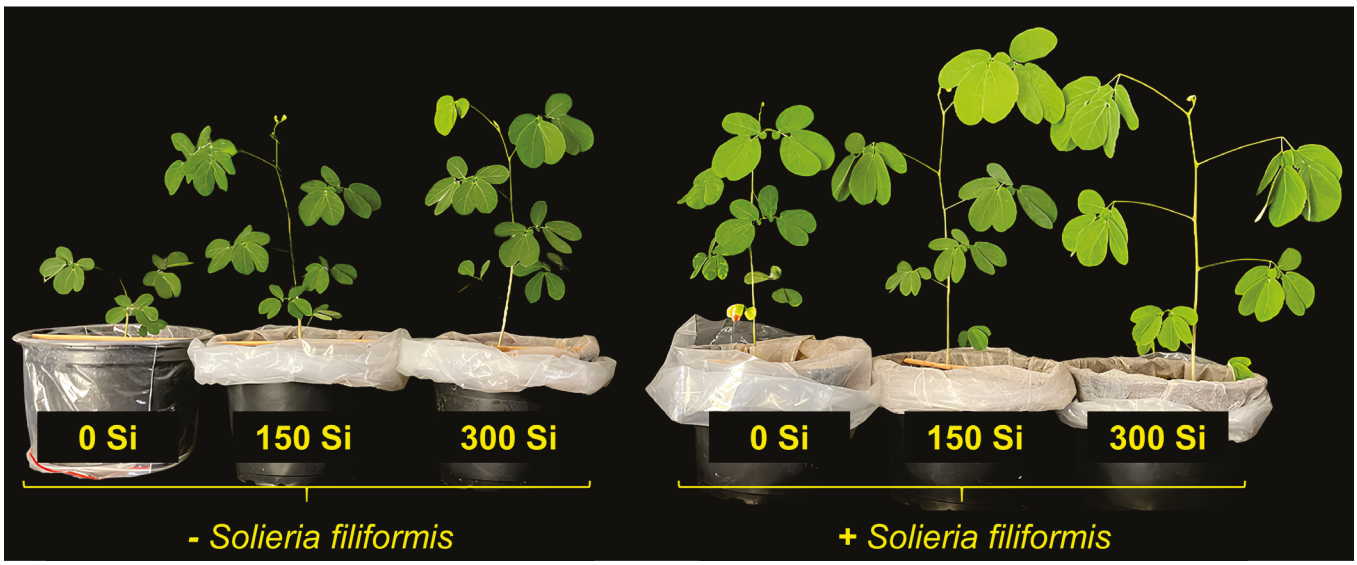

Figure 1. Growth of *M. caesalpiniaefolia* plants in the absence (−*S. filiformis*) and presence (+*S. filiformis*) of *S. filiformis* seaweed extract, under three levels of Si applied to the soil (0 mg kg^{-1}, 150 mg kg^{-1}, and 300 mg kg^{-1}).

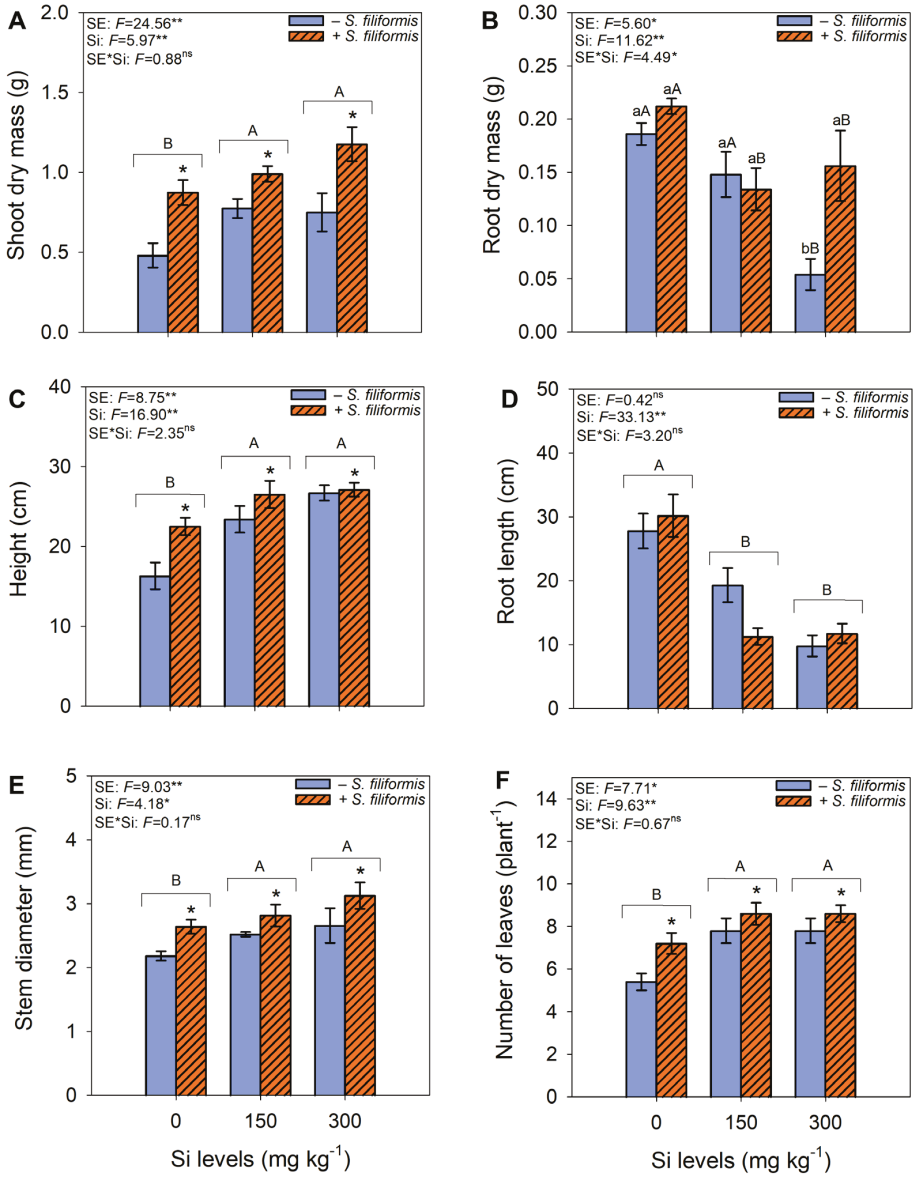

Figure 2. Growth parameters of *M. caesalpiniaefolia* under different treatments. Shoot dry mass (**A**), root dry mass (**B**), plant height (**C**), root length (**D**), stem diameter (**E**), and leaf number (**F**). The values represent the mean of five replicates ± standard error. Uppercase letters indicate significant differences among Si levels within the same seaweed extract treatment (i.e., −*S. filiformis* or +*S. filiformis*). Uppercase letters placed above brackets, when present, indicate significant differences among Si levels, regardless of seaweed extract application. Lowercase letters and asterisks indicate significant differences between plants with and without seaweed extract (i.e., −*S. filiformis* or +*S. filiformis*) within the same Si level, according to the Scott–Knott test ($p \leq 0.05$). *, **, ns: *F*-test significance levels at $p \leq 0.05$, $p \leq 0.01$, and not significant, respectively.

3.2. Abundance of AMF Spores in the Soil and Mycorrhizal Colonization

The abundance of AMF spores in the soil significantly decreased with increasing Si levels, particularly at 300 mg kg^{-1} of Si, and with the application of *S. filiformis* seaweed extract (Figure 3A). The highest percentages of mycorrhizal colonization were observed at 150 mg kg^{-1} of Si, regardless of *S. filiformis* seaweed extract application, and in the presence of *S. filiformis* seaweed extract, regardless of Si levels (Figure 3B).

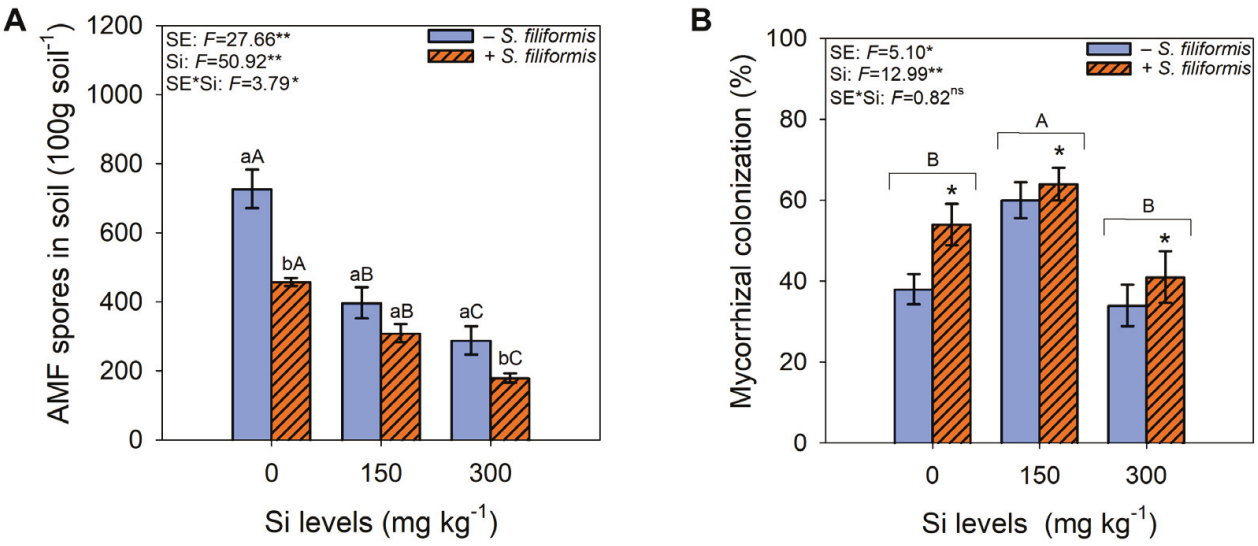

Figure 3. Abundance of AMF spores in the soil (**A**) and total mycorrhizal colonization (**B**) in *M. caesalpiniaefolia* plants subjected to different treatments. The values in the figure represent the mean of five replicates ± standard error. Uppercase letters indicate significant differences among Si levels within the same seaweed extract treatment (i.e., −*S. filiformis* or +*S. filiformis*). Uppercase letters placed above brackets, when present, indicate significant differences among Si levels, regardless of seaweed extract application. Lowercase letters and asterisks indicate significant differences between plants with and without seaweed extract (i.e., −*S. filiformis* or +*S. filiformis*) within the same Si level, according to the Scott–Knott test ($p \leq 0.05$). *, **, ns: *F*-test significance levels at $p \leq 0.05$, $p \leq 0.01$, and not significant, respectively.

The roots of *M. caesalpiniaefolia* colonized by AMF exhibited endogenous structures, including Arum-type arbuscules, vesicles, and intraradical and extraradical hyphae (Figure 4).

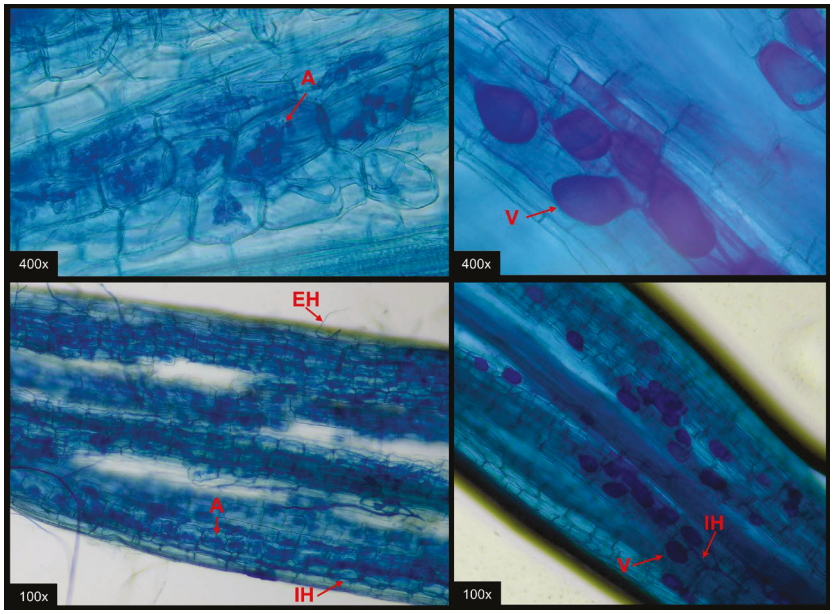

Figure 4. Optical microscope photograph of *M. caesalpinieafolia* roots after staining. V: vesicle; IH: intraradicular hypha; EH: extraradicular hypha; A: arbuscule.

3.3. Silicon in Shoots and Roots and Phosphorus, Sodium, and Potassium in Shoots

The highest Si concentrations in the shoot were observed at Si levels of 150 and 300 mg kg^{-1} in the soil, regardless of *S. filiformis* seaweed extract application, and in the presence of *S. filiformis* seaweed extract, regardless of the applied Si levels (Figure 5A). The

highest Si concentrations in the root were found at 300 mg kg^{-1} of Si applied to the soil (Figure 5B). The highest Na concentrations in the shoot were observed at 300 mg kg^{-1} of Si, in the absence of *S. filiformis* seaweed extract (Figure 5C). K concentrations were higher at 150 mg kg^{-1} of Si, regardless of *S. filiformis* seaweed extract application, and with the application of *S. filiformis* seaweed extract, regardless of the Si levels applied to the soil (Figure 5D). There was no significant effect on P concentrations in the shoot in response to the analyzed treatments (Figure 5E).

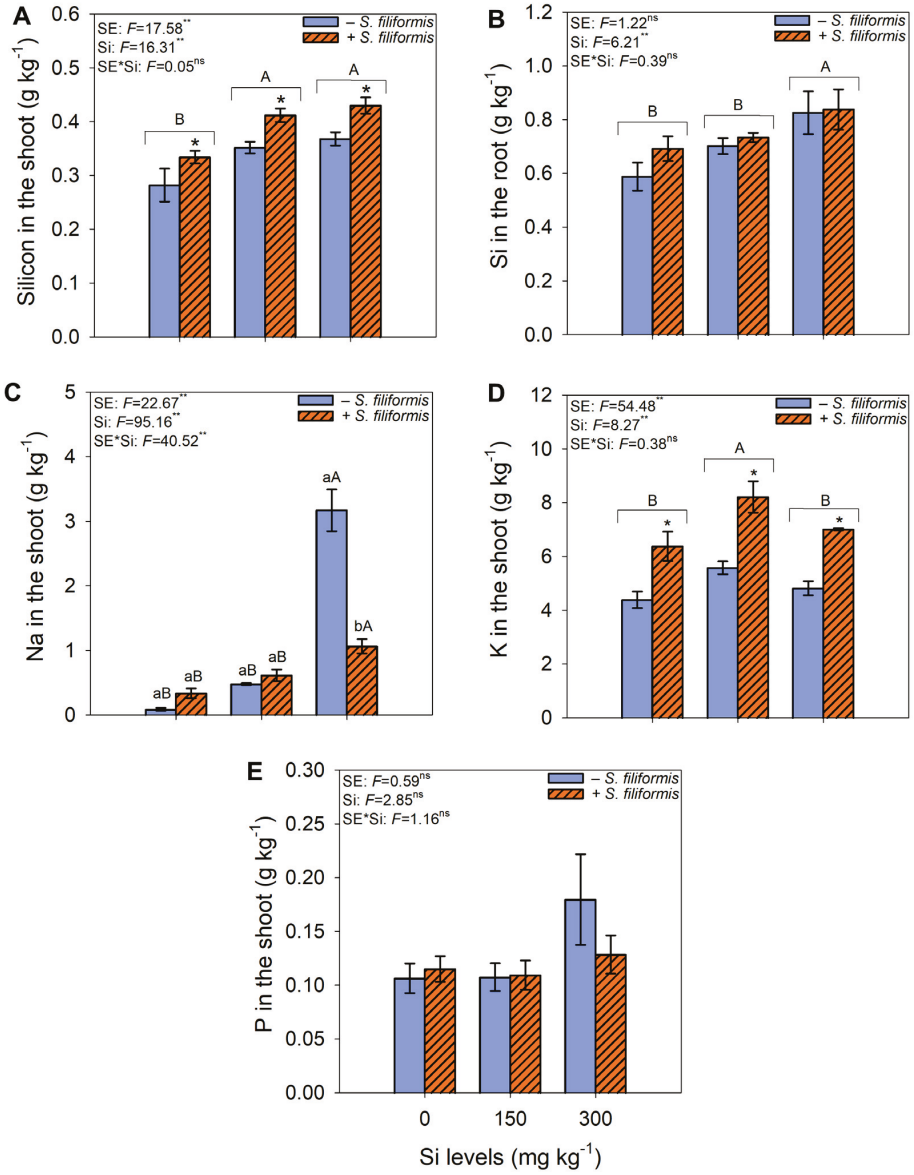

Figure 5. Silicon in shoots (**A**) and roots (**B**) and Na (**C**), K (**D**), and P (**E**) in shoots in *M. caesalpiniaefolia* plants subjected to different treatments. The values in the figure represent the mean of five replicates ± standard error. Uppercase letters indicate significant differences among Si levels within the same seaweed extract treatment (i.e., −*S. filiformis* or +*S. filiformis*). Uppercase letters placed above brackets, when present, indicate significant differences among Si levels, regardless of seaweed extract application. Lowercase letters and asterisks indicate significant differences between plants with and without seaweed extract (i.e., −*S. filiformis* or +*S. filiformis*) within the same Si level, according to the Scott–Knott test ($p \leq 0.05$). *, **, ns: *F*-test significance levels at $p \leq 0.05$, $p \leq 0.01$, and not significant, respectively.

3.4. Soil Chemical Analysis

The application of *S. filiformis* seaweed extract did not significantly affect the soil pH, EC, or Na content (Table 2). An increase in the soil solution pH was observed at the highest Si dose (300 mg kg^{-1}), while EC rose with both 150 and 300 mg kg^{-1} of Si (Table 2). The greatest availability of Si in the soil occurred at 300 mg kg^{-1} of Si, specifically in the absence of the seaweed extract (Table 2). Likewise, the highest Na content was recorded at this Si rate. K concentrations were elevated at 0 mg kg^{-1} of Si without the extract and at 150 mg kg^{-1} with the extract (Table 2). No significant differences were observed in P content across treatments, with the exception of the application of 300 mg kg^{-1} of Si in the presence of *S. filiformis* SE (Table 2).

Table 2. The pH, EC, and the contents of Si, Na, K, and P in the soil cultivated with *M. caesalpiniaefolia* under different treatments. Uppercase letters indicate significant differences among Si levels within the same seaweed extract treatment (i.e., *−S. filiformis* or *+S. filiformis*). Lowercase letters indicate significant differences between plants with and without seaweed extract (i.e., *−S. filiformis* or *+S. filiformis*) within the same Si level, according to the Scott–Knott test ($p \leq 0.05$). *, **, ns: *F*-test significance levels at $p \leq 0.05$, $p \leq 0.01$, and not significant, respectively.

Treatments		pH	EC	Si	Na	K	P
SE	**Si (mg kg^{-1})**	**(H_2O)**	**(μS cm^{-1})**	**(mg kg^{-1})**	**($cmol_c$ kg^{-1})**	**($cmol_c$ kg^{-1})**	**(mg kg^{-1})**
−S. filiformis	0	4.60 ± 0.12 C	204.60 ± 16.54 B	2.49 ± 0.08 aC	0.15 ± 0.003 C	0.04 ± 0.001 aA	20.95 ± 1.29 aA
	150	5.55 ± 0.07 B	227.92 ± 17.77 A	3.96 ± 0.19 aB	0.54 ± 0.008 B	0.03 ± 0.0009 bB	21.31 ± 1.12 aA
	300	6.21 ± 0.05 A	255.60 ± 7.89 A	7.87 ± 0.64 aA	0.87 ± 0.031 A	0.01 ± 0.001 bC	16.36 ± 0.79 bB
+S. filiformis	0	4.56 ± 0.02 C	210.56 ± 8.18 B	2.58 ± 0.17 aB	0.16 ± 0.003 C	0.03 ± 0.001 bA	20.95 ± 1.00 aA
	150	5.68 ± 0.07 B	263.00 ± 11.15 A	3.45 ± 0.13 aB	0.55 ± 0.005 B	0.04 ± 0.001 aA	22.67 ± 0.42 aA
	300	6.31 ± 0.08 A	240.20 ± 8.12 A	6.01 ± 0.17 bA	0.86 ± 0.011 A	0.03 ± 0.001 aB	21.48 ± 1.10 aA
F test							
SE		0.95 ns	0.72 ns	9.70 **	0.21 ns	20.04 **	7.00 *
Si		226.60 **	6.74 **	116.93 **	1213.11 **	63.10 **	4.86 *
SE*Si		0.65 ns	2.12 ns	5.56 *	0.45 ns	33.53 **	2.52 *

4. Discussion

The application of a seaweed extract (*S. filiformis*) and Si maximized the early growth of *Mimosa caesalpiniaefolia*, possibly due to the bioactive composition of the seaweed extract. This extract contains polysaccharides, phytohormones, lipids such as fatty acids and sterols, pigments like carotenoids, oxylipins, minerals, peptides, amino acids, and proteins, compounds that promote plant growth [5]. Furthermore, there is evidence that seaweed extracts stimulate AMF, which support plant development [8,9], an effect also observed in this study. However, it is worth noting that the seaweed extract used in our study was subjected to heating and filtration, processes that may have altered its initial composition. Some compounds may have been retained in the discarded residue; however, the gelled extract retains sulfated polysaccharides from the seaweed cell wall, capable of interacting with soil minerals and promoting their gradual release. This mechanism reduces leaching and improves nutrient availability for plants, favoring their development [6,42].

The gel formulation of the seaweed extract used in our study reduces dispersion by rain and leaching, prolonging root contact and improving nutrient absorption. This factor is particularly relevant for seedlings intended for reforestation, which need to develop autonomy in the final environment, where input availability is limited. The interaction between Si and seaweed extracts may provide better conditions for plant growth since both inputs enhance water and nutrient absorption while strengthening plant cell structure [43]. Si contributes to silica deposition in cell walls, increasing mechanical resistance and re-

ducing water stress, while bioactive seaweed compounds promote beneficial microbial activity and optimize plant metabolism [44]. The absence of Si resulted in greater dry mass production and root length. This effect may be related to the fact that, under certain conditions, Si reduces root growth without compromising the shoot [45]. Reduced root expansion may indicate greater efficiency in resource uptake since Si contributes to water use efficiency and structural resistance in the shoot [46].

The abundance of AMF spores in the soil decreased with the application of the seaweed extract and increasing levels of Si. This behavior may be related to the lower root density observed under these conditions and the signaling dynamics between plants and AMF in the rhizosphere. A study demonstrated that plants under greater environmental stress release root exudates, such as strigolactones and flavonoids, to stimulate the establishment of symbiosis with AMF [47]. These molecules function primarily as exo-signals that promote hyphal branching and facilitate root colonization. In our study, however, even with improved plant nutritional status and reduced stress due to SE and Si application, AMF colonization increased. This suggests that the mechanisms driving colonization in our experimental conditions may not be directly dependent on the elevated exudation of signaling compounds. On the other hand, a reduction in AMF spore abundance in the soil was observed. Since strigolactones and flavonoids are not directly involved in sporulation, this reduction may instead be related to changes in carbon allocation by the host plant, shifts in AMF life strategies, or even the suppression of sporulation under more favorable root-colonizing conditions. Similar findings were reported by [23], highlighting that increased colonization does not necessarily correlate with higher spore production.

Mycorrhizal colonization in *M. caesalpiniaefolia* increased in response to the application of the seaweed extract and Si. Although this treatment led to reduced AMF sporulation, it did not negatively affect the plant. On the contrary, greater mycorrhizal colonization resulted in significant benefits for *M. caesalpiniaefolia* growth, indicating that spore abundance and mycorrhizal colonization are not always directly correlated. Studies suggest that seaweed extract application stimulates mycorrhization compared to its absence [8]. This effect may be related to the increased expression of genes associated with mycorrhizal symbiosis establishment, such as those involved in infectivity and colonization efficiency, as observed in *Medicago truncatula* [9]. Additionally, Si may favor mycorrhizal colonization by modulating the availability of dissolved organic compounds in the soil, increasing the supply of carbon sources for AMF [21]. Furthermore, there is evidence that Si influences the metabolism of phenolic substances, including flavonoids, which play a crucial role in signaling and recruiting AMF to the host plant rhizosphere [48]. Thus, although Si deposition in root cell walls is traditionally associated with a potential barrier to fungal infection, the present study suggests that this element may, in fact, create a biochemically favorable environment for mycorrhizal colonization in *M. caesalpiniaefolia*. Therefore, our findings suggest that the interaction between the seaweed extract and Si fosters a more conducive environment for mycorrhizal symbiosis, promoting greater colonization regardless of reduced AMF sporulation in the soil.

It is important to acknowledge that, under natural soil conditions, AMF symbioses occur within complex networks formed by multiple fungal species interacting with diverse plant roots across the soil matrix. Such networks are essential for nutrient transfer, colonization dynamics, and spore production. However, our experimental design, based on pot conditions with a single plant species, does not replicate the full complexity of field scenarios. Consequently, although we quantified root colonization and spore abundance in the soil, we did not assess the development of the extraradical mycelial network nor identify the AMF species involved. This constitutes a limitation of the study, as the diversity and connectivity of AMF networks can influence both colonization and sporulation.

Therefore, future studies under more complex or field-based conditions are necessary to expand the understanding of AMF network functioning and its implications for symbiotic performance and ecosystem services.

The application of seaweed extract influenced Si uptake in *M. caesalpiniaefolia*, resulting in the higher accumulation of this element in the shoot, while the Si levels in the roots increased proportionally with higher Si application to the soil. These results indicate that despite the reduction in root growth observed at high Si doses, the absorption and storage of this element in the root remained active, corroborating the findings of [45]. This effect may be related to the intensification of mycorrhizal colonization since AMF can enhance Si uptake by expanding the soil exploration surface through their hyphal network, acting as an extension of the root system [8,49]. Moreover, the composition of the seaweed extract may have contributed to increased Si levels in the plant shoots. Studies indicate that green and red macroalgae have higher Si concentrations compared to brown macroalgae [50]. Although we applied a highly soluble silicon source, it is important to recognize that in natural soils, silicate-solubilizing bacteria can also enhance Si availability by transforming insoluble minerals into forms absorbable by plants. These bacteria act through acidification and organic acid production, contributing to nutrient cycling and potentially interacting with AMF to improve plant nutrition and stress tolerance [20].

Thus, the interaction between the bioactive compounds of *S. filiformis* seaweed extract and soil Si availability may have favored the absorption and transport of the element, leading to its greater accumulation in shoot tissues. However, it is important to acknowledge that the speciation of Si in the soil solution was not determined in this study. Since sodium silicate is a highly soluble source, high application rates may have exceeded the solubility threshold of monomeric silicic acid, potentially leading to polycondensation and reduced bioavailability. This represents a limitation for the precise interpretation of Si dynamics under our experimental conditions.

The high Si concentration influenced sodium uptake by the plant in our study, possibly due to the use of sodium silicate as a Si source, which contains Na^+ in its composition. Although Si is known to mitigate salt stress by regulating Na^+ transport in plant tissues [45,51,52], the presence of Na^+ in the fertilizer may have contributed to its accumulation in the shoot. However, the observed Na^+ levels did not indicate toxicity for *M. caesalpiniaefolia* [53]. The lower Na^+ translocation in the presence of the *S. filiformis* seaweed extract may be associated with its gelatinous matrix, rich in sulfated polysaccharides, which have negative charges capable of retaining cations in the soil.

The *S. filiformis* seaweed extract increased the K levels in the shoot of *M. caesalpiniaefolia*, likely due to the supply of this nutrient and plant hormones that stimulate growth, favoring its absorption [8,54]. Additionally, the symbiosis with AMF, enhanced by the seaweed extract and Si, expands the root absorption area, boosting K uptake [9]. Si application to the soil also contributes to K uptake by improving its availability and facilitating transport within the plant, potentially reducing K fixation in soil particles and increasing its mobility in solution [55]. Si further strengthens the cell structure, reducing K losses through exudation and regulating its redistribution in plant tissues [56]. Studies indicate that under K deficiency, Si can stimulate compensatory mechanisms, promoting plant growth and nutrient homeostasis [51]. In our study, there were no significant differences in the P content in the shoot of *M. caesalpiniaefolia* among the treatments. This result may be related to the experimental period, which was possibly insufficient for the *S. filiformis* extract to significantly release P into the soil, thus limiting its availability to plants. As reported by [57], the mineralization of organic P can vary with the incubation time, influencing the nutrient's availability to plants.

The soil application of Si directly influenced the pH of the soil solution and electrical conductivity (EC). The increase in the pH, especially observed in the treatment with the highest level of Si, is likely due to the alkalinizing effect of sodium silicate. This effect occurs because silicate anions act as weak bases, neutralizing H^+ ions in the soil solution. Additionally, Na^+ can compete with H^+ for exchange sites on soil colloids, displacing H^+ into the solution and promoting its neutralization [51,58]. On the other hand, the increase in the EC can be attributed to the dissociation of Na_2SiO_3 in the soil, which releases Na^+ ions and silicate anions (SiO_4^{4-}), increasing the concentration of dissolved ions in the soil solution and, consequently, the EC [52].

Soil Si availability increased with the application of increasing doses of this element, as expected. In contrast, the application of the *S. filiformis* seaweed extract resulted in a reduction in soil Si availability. This decrease may be related to the higher accumulation of Si in the shoot of *M. caesalpiniaefolia* under this treatment, indicating greater uptake of the element. This effect may be associated with the intensification of mycorrhizal colonization, as observed in our study, since arbuscular mycorrhizal fungi (AMF) are also known to enhance Si uptake by plants [49].

The increase in the soil sodium content with higher Si levels can be attributed to the chemical composition of common Si sources, which often include soluble salts like sodium or potassium silicate. Si application may also alter the soil's colloidal structure and ion exchange processes, facilitating the release of Na^+ into the soil solution [59]. SEs, however, may moderate this effect through ionic complexation by sulfated polysaccharides or by enhancing microbial activity that influences cation dynamics [60].

The soil K levels decreased with the application of Si, likely due to the increased uptake of this nutrient by plants under higher Si treatments, resulting in reduced K availability in the soil. Potassium availability is influenced by competition with other cations and by plant uptake during periods of rapid growth. Moreover, the *S. filiformis* SE can enhance K release from soil minerals through the action of organic compounds such as humic, fulvic, and phenolic acids, which aid in nutrient solubilization [60]. The SE may also stimulate the activity of rhizospheric microorganisms and AMF, which play key roles in the mobilization of K and P. Notably, the effects on P availability in the soil were more pronounced in the presence of the SE and under the highest Si application level. Phosphorus dynamics are particularly complex due to its high reactivity, but SEs can reduce P fixation by promoting the release of chelating substances and enhancing microbial activity.

5. Conclusions

The co-application of *S. filiformis* SE and Si promotes the early growth of *M. caesalpiniaefolia*, particularly at Si levels of 150 and 300 mg kg^{-1}, enhancing its development. Si, in the form of Na_2SiO_3, and the *S. filiformis* SE reduce AMF spore abundance in the soil cultivated with *M. caesalpiniaefolia*, possibly due to lower root density and reduced exudate release. The application of *S. filiformis* SE and Si increased mycorrhizal colonization in *M. caesalpiniaefolia*, benefiting plant growth despite the reduction in AMF sporulation, suggesting that symbiosis can be stimulated independently of spore abundance. The co-application of *S. filiformis* SE and Si shows potential for promoting the growth of *M. caesalpiniaefolia* and modulating its interaction with AMF, partially confirming the hypothesis of this study. However, further field studies are needed, considering different soil types, plant species, and a longer experimental period to assess AMF sporulation dynamics, mycorrhizal colonization, and nutrient availability in the soil solution over time.

Author Contributions: Conceptualization, K.G.V.G.; methodology, I.A.d.S., K.G.V.G., M.d.S.A., J.L.S.d.A., M.L.H.A. and F.L.A.B.; validation, K.G.V.G. and M.d.S.A.; formal analysis, I.A.d.S., K.G.V.G., M.d.S.A., J.L.S.d.A. and F.L.A.B.; investigation, K.G.V.G.; resources, K.G.V.G.; data curation, K.G.V.G.; writing—original draft, K.G.V.G., I.A.d.S., M.d.S.A., A.S.F.A. and A.P.d.A.P.; writing—review and editing, K.G.V.G., M.d.S.A., F.L.A.B., A.S.F.A. and A.P.d.A.P.; visualization, K.G.V.G., I.A.d.S., F.L.A.B., M.L.H.A., A.S.F.A., A.J.d.S. and A.P.d.A.P.; supervision, K.G.V.G. and A.P.d.A.P.; funding acquisition, A.P.d.A.P. All authors have read and agreed to the published version of the manuscript.

Funding: This research received no external funding.

Institutional Review Board Statement: Not applicable.

Informed Consent Statement: Not applicable.

Data Availability Statement: The original contributions presented in this study are included in the article. Further inquiries can be directed to the corresponding author.

Conflicts of Interest: The authors declare no conflicts of interest.

References

1. Engel, D.C.H.; Feltrim, D.; Rodrigues, M.; Baptistella, J.L.C.; Mazzafera, P. Algae extract increases seed production of soybean plants and alters nitrogen metabolism. *Agriculture* **2023**, *13*, 1296. [CrossRef]
2. Ramos, G.; Russi, P.M.; da Nóbrega Souza, G.; Alves, V.M.; Boas, B.G.V.; Derner, R.B.; Owatari, M.S. Effects of crude extract from the macroalgae *Kappaphycus alvarezii* on the common bean (*Phaseolus vulgaris*) crops. *Braz. J. Anim. Environ. Res.* **2025**, *8*, e76538. [CrossRef]
3. Jmaili, K.; Asbai, Z.; Waddi, K.; Bahlaouan, B.; Silkina, A.; Boutaleb, N. Non-Microbial Biostimulants for Plant Growth and Abiotic Stress Mitigation: A Review of Recent Scientific Innovations. *Int. J. Environ. Stud.* **2025**, *74*, 401–431. [CrossRef]
4. Oliveira, A.C.V. *Efeitos da Aplicação do Extrato Bruto da Alga Vermelha Gracilaria birdiae em Cultura de Alface (Lactuca sativa)*; Trabalho de Conclusão de Curso, Universidade Federal do Ceará: Fortaleza, Brazil, 2017; p. 80.
5. Ali, O.; Ramsubhag, A.; Jayaraman, J. Biostimulant properties of seaweed extracts in plants: Implications towards sustainable crop production. *Plants* **2021**, *10*, 531. [CrossRef]
6. Castro, G.M.C.D.; Benevides, N.M.B.; Cabral, M.C.; Miranda, R.D.S.; Gomes Filho, E.; Rocha, M.V.P.; Araújo, M.L.H. Optimized acid hydrolysis of the polysaccharides from the seaweed *Solieria filiformis* (Kützing) PW Gabrielson for bioethanol production. *Acta Sci. Biol. Sci.* **2017**, *39*, 423. [CrossRef]
7. Ribeiro, E.E.; Nobre, I.G.; Silva, D.R.; da Silva, W.M.; Sousa, S.K.; Holanda, T.B.; Matos, W.O. Profile of Inorganic Elements of Seaweed from the Brazilian Northeast Coast. *Mar. Pollut. Bull.* **2024**, *202*, 116413. [CrossRef]
8. Rasouli, F.; Nasiri, Y.; Hassanpouraghdam, M.B.; Asadi, M.; Qaderi, T.; Trifa, A.; Szczepanek, M. Seaweed extract and arbuscular mycorrhiza co-application affect the growth responses and essential oil composition of *Foeniculum vulgare* L. *Sci. Rep.* **2023**, *13*, 11902. [CrossRef]
9. Hines, S.; van der Zwan, T.; Shiell, K.; Shotton, K.; Prithiviraj, B. Alkaline extract of the seaweed *Ascophyllum nodosum* stimulates arbuscular mycorrhizal fungi and their endomycorrhization of plant roots. *Sci. Rep.* **2021**, *11*, 13491. [CrossRef]
10. Wang, M.; Wang, Z.; Guo, M.; Qu, L.; Biere, A. Effects of Arbuscular Mycorrhizal Fungi on Plant Growth and Herbivore Infestation Depend on Availability of Soil Water and Nutrients. *Front. Plant Sci.* **2023**, *14*, 1101932. [CrossRef]
11. Garcia, K.G.V.; Mendes Filho, P.F.; Pinheiro, J.I.; do Carmo, J.F.; de Araújo Pereira, A.P.; Martins, C.M.; de Abreu, M.G.P.; de Souza Oliveira Filho, J. Attenuation of Manganese-Induced Toxicity in *Leucaena leucocephala* Colonized by Arbuscular Mycorrhizae. *Water Air Soil. Pollut.* **2020**, *231*, 22. [CrossRef]
12. Begum, N.; Qin, C.; Ahanger, M.A.; Raza, S.; Khan, M.I.; Ashraf, M.; Ahmed, N.; Zhang, L. Role of Arbuscular Mycorrhizal Fungi in Plant Growth Regulation: Implications in Abiotic Stress Tolerance. *Front. Plant Sci.* **2019**, *10*, 1068. [CrossRef]
13. Dowarah, B.; Gill, S.S.; Agarwala, N. Arbuscular Mycorrhizal Fungi in Conferring Tolerance to Biotic Stresses in Plants. *J. Plant Growth Regul.* **2022**, *41*, 1429–1444. [CrossRef]
14. Boyno, G.; Rezaee Danesh, Y.; Demir, S.; Teniz, N.; Mulet, J.M.; Porcel, R. The Complex Interplay Between Arbuscular Mycorrhizal Fungi and Strigolactone: Mechanisms, Synergies, Applications and Future Directions. *Int. J. Mol. Sci.* **2023**, *24*, 16774. [CrossRef]
15. Schaller, J.; Puppe, D.; Kaczorek, D.; Ellerbrock, R.; Sommer, M. Silicon Cycling in Soils Revisited. *Plants* **2021**, *10*, 295. [CrossRef]
16. Tayade, R.; Ghimire, A.; Khan, W.; Lay, L.; Attipoe, J.Q.; Kim, Y. Silicon as a Smart Fertilizer for Sustainability and Crop Improvement. *Biomolecules* **2022**, *12*, 1027. [CrossRef]

17. Zargar, S.M.; Mahajan, R.; Bhat, J.A.; Nazir, M.; Deshmukh, R. Role of Silicon in Plant Stress Tolerance: Opportunities to Achieve a Sustainable Cropping System. *3 Biotech* **2019**, *9*, 73. [CrossRef]
18. Ahmed, M.; Ullah, H.; Attia, A.; Tisarum, R.; Cha-um, S.; Datta, A. Interactive Effects of *Ascophyllum nodosum* Seaweed Extract and Silicon on Growth, Fruit Yield and Quality, and Water Productivity of Tomato under Water Stress. *Silicon* **2023**, *15*, 2263–2278. [CrossRef]
19. Wang, M.; Wang, R.; Mur, L.A.J.; Ruan, J.; Shen, Q.; Guo, S. Functions of Silicon in Plant Drought Stress Responses. *Hortic. Res.* **2021**, *8*, 254. [CrossRef]
20. Etesami, H.; Schaller, J. Improving Phosphorus Availability to Rice through Silicon Management in Paddy Soils: A Review of the Role of Silicate-Solubilizing Bacteria. *Rhizosphere* **2023**, *27*, 100749. [CrossRef]
21. Bhardwaj, S.; Sharma, D.; Singh, S.; Ramamurthy, P.C.; Verma, T.; Pujari, M.; Prasad, R. Physiological and Molecular Insights into the Role of Silicon in Improving Plant Performance under Abiotic Stresses. *Plant Soil* **2023**, *486*, 25–43. [CrossRef]
22. Moradtalab, N.; Hajiboland, R.; Aliasgharzad, N.; Hartmann, T.E.; Neumann, G. Silicon and the Association with an Arbuscular-Mycorrhizal Fungus (*Rhizophagus clarus*) Mitigate the Adverse Effects of Drought Stress on Strawberry. *Agronomy* **2019**, *9*, 41. [CrossRef]
23. Carmo, J.F.; Garcia, K.G.V.; Mendes Filho, P.F.; de Araújo Pereira, A.P.; Pinheiro, J.I. Silicon Application and Mycorrhiza Inoculation Promoted *Leucaena leucocephala* Growth in a Soil Highly Contaminated by Manganese. *Nativa* **2022**, *10*, 410–416. [CrossRef]
24. Garcia, K.G.V.; Gomes, V.F.F.; Mendes Filho, P.F.; Martins, C.M.; da Silva Júnior, J.M.T.; Cunha, C.S.M.; Pinheiro, J.I. Arbuscular Mycorrhizal Fungi in the Phytostabilization of Soil Degraded by Manganese Mining. *J. Agric. Sci.* **2018**, *10*, 192–202. [CrossRef]
25. Maia, E.P.V.; Garcia, K.G.V.; de Souza Oliveira Filho, J.; Pinheiro, J.I.; Mendes Filho, P.F. Co-Inoculation of Rhizobium and Arbuscular Mycorrhiza Increases *Mimosa caesalpiniaefolia* Growth in Soil Degraded by Manganese Mining. *Water Air Soil Pollut.* **2023**, *234*, 289. [CrossRef]
26. Silva Borges, M.P.; Silva, D.V.; de Freitas Souza, M.; Silva, T.S.; da Silva Teófilo, T.M.; da Silva, C.C.; Dos Santos, J.B. Glyphosate Effects on Tree Species Natives from Cerrado and Caatinga Brazilian Biome: Assessing Sensitivity to Two Ways of Contamination. *Sci. Total Environ.* **2021**, *769*, 144113. [CrossRef]
27. Paiva, L.L.D.; Azevedo, T.K.B.D.; Pimenta, A.S.; Canto, J.L.D.; Souza, M.J.C.D.; Ucella Filho, J.G.M. Effect of thinning on volumes of biomass and bark tannins content of *Mimosa caesalpiniifolia* Benth. trees. *Rev. Árvore* **2023**, *47*, e4728. [CrossRef]
28. Pinheiro, E.S.; Alves, A.R.; Holanda, A.C.D.; Silveira, G.V.D.S.; Loiola, Â.T.; Silva, P.C.D.; Silva, K.E.D. Effects of planting density on characteristics of sabiá wood. *Rev. Caatinga* **2024**, *37*, e11927. [CrossRef]
29. Alvares, C.A.; Stape, J.L.; Sentelhas, P.C.; Gonçalves, J.L.M.; Sparovek, G. Köppen's Climate Classification Map for Brazil. *Meteorol. Z.* **2013**, *22*, 711–728. [CrossRef]
30. Silva, F.C.; Dasilva, F.C. *Manual de Métodos de Análise de Solo*, 3rd ed.; Embrapa: Brasília, Brazil, 2009; 573p.
31. Liang, Y.; Wong, J.W.C.; Wei, L. Silicon-Mediated Enhancement of Cadmium Tolerance in Maize (*Zea mays* L.) Grown in Cadmium Contaminated Soil. *Chemosphere* **2005**, *58*, 475–483. [CrossRef]
32. Jupri, A.; Fanani, R.A.; Syafitri, S.M.; Mayshara, S.; Nurijawati.; Pebriani, S.A.; Sunarpi, H. Growth and Yield of Rice Plants Sprayed with *Sargassum polycystum* Extracted with Different of Concentration. *AIP Conf. Proc.* **2019**, *2199*, 70009. [CrossRef]
33. Mughunth, R.J.; Velmurugan, S.; Mohanalakshmi, M.; Vanitha, K. A Review of Seaweed Extract's Potential as a Biostimulant to Enhance Growth and Mitigate Stress in Horticulture Crops. *Sci. Hortic.* **2024**, *334*, 113312. [CrossRef]
34. Hungria, M.; Araujo, R.S. *Manual de Métodos Empregados em Estudos de Microbiologia Agrícola*, 1st ed.; Embrapa: Brasilia, Brazil, 1994.
35. Allen, R.G.; Pereira, L.S.; Raes, D.; Smith, M. *Crop Evapotranspiration: Guidelines for Computing Crop Water Requirements*, 1st ed.; FAO: Rome, Italy, 1998.
36. Phillips, J.M.; Hayman, D.S. Improved procedures for clearing roots and staining parasitic and vesicular-arbuscular mycorrhizal fungi for rapid assessment of infection. *Trans. Br. Mycol. Soc.* **1970**, *55*, 158–161. [CrossRef]
37. Vierheilig, H.; Coughlan, A.P.; Wyss, U.; Piché, Y. Ink and Vinegar, a Simple Staining Technique for Arbuscular-Mycorrhizal Fungi. *Appl. Environ. Microbiol.* **1998**, *64*, 5004–5007. [CrossRef]
38. McGonigle, T.P.; Miller, M.H.; Evans, D.G.; Fairchild, G.L.; Swan, J.A. A New Method Which Gives an Objective Measure of Colonization of Roots by Vesicular—Arbuscular Mycorrhizal Fungi. *New Phytol.* **1990**, *115*, 495–501. [CrossRef]
39. Gerdemann, J.W.; Nicolson, T.H. Spores of Mycorrhizal Endogone Species Extracted from Soil by Wet Sieving and Decanting. *Trans. Br. Mycol. Soc.* **1963**, *46*, 235–244. [CrossRef]
40. Elliott, C.L.; Snyder, G.H. Autoclave-Induced Digestion for the Colorimetric Determination of Silicon in Rice Straw. *J. Agric. Food Chem.* **1991**, *39*, 1118–1119. [CrossRef]
41. Korndörfer, G.H.; Pereira, H.; Nolla, A. *Análise de Silício: Solo, Planta e Fertilizante*; Embrapa Soja (CNPSo): Londrina, Brazil, 2004; No. 2; p. 34.

42. Silva, I.B.; Fujii, M.T.; Scaff, M.F. *Diversidade de Algas Marinhas: Programa de Pós-Graduação em Biodiversidade Vegetal e Meio Ambiente, Programa de Capacitação de Monitores e Educadores*; Instituto de Botânica—Jardim Botânico de São Paulo: São Paulo, Brazil, 2010; Available online: https://smastr16.blob.core.windows.net/pgibt/sites/242/2023/10/diversidade-algas-marinhas-ingrid-balesteros.pdf (accessed on 24 February 2025).
43. González-Moscoso, M.; Juárez-Maldonado, A.; Cadenas-Pliego, G.; Meza-Figueroa, D.; SenGupta, B.; Martínez-Villegas, N. Silicon Nanoparticles Decrease Arsenic Translocation and Mitigate Phytotoxicity in Tomato Plants. *Environ. Sci. Pollut. Res.* **2022**, *29*, 34147–34163. [CrossRef]
44. Wang, D.; Hou, L.; Zhang, L.; Liu, P. The Mechanisms of Silicon on Maintaining Water Balance under Water Deficit Stress. *Physiol. Plant* **2021**, *173*, 1253–1262. [CrossRef]
45. Ribeiro, R.V.; Silva, L.D.; Ramos, R.A.; Andrade, C.A.D.; Zambrosi, F.C.B.; Pereira, S.P. High Soil Silicon Concentrations Inhibit Coffee Root Growth without Affecting Leaf Gas Exchange. *Rev. Bras. Ciênc. Solo* **2011**, *35*, 939–948. [CrossRef]
46. Cassel, J.L.; Gysi, T.; Rother, G.M.; Pimenta, B.D.; Ludwig, R.L.; dos Santos, D.B. Benefícios da Aplicação de Silício em Plantas. *Braz. J. Anim. Environ. Res.* **2021**, *4*, 6601–6615. [CrossRef]
47. Pires, G.C.; de Lima, M.E.; Zanchi, C.S.; de Freitas, C.M.; de Souza, J.M.A.; de Camargo, T.A.; de Souza, E.D. Arbuscular Mycorrhizal Fungi in the Rhizosphere of Soybean in Integrated Crop Livestock Systems with Intercropping in the Pasture Phase. *Rhizosphere* **2021**, *17*, 100270. [CrossRef]
48. Hajiboland, R.; Cheraghvareh, L.; Poschenrieder, C. Improvement of Drought Tolerance in Tobacco (*Nicotiana rustica* L.) Plants by Silicon. *J. Plant Nutr.* **2017**, *40*, 1661–1676. [CrossRef]
49. Etesami, H.; Li, Z.; Maathuis, F.J.; Cooke, J. The Combined Use of Silicon and Arbuscular Mycorrhizas to Mitigate Salinity and Drought Stress in Rice. *Environ. Exp. Bot.* **2022**, *201*, 104955. [CrossRef]
50. Fu, F.F.; Akagi, T.; Yabuki, S.; Iwaki, M.; Ogura, N. Distribution of Rare Earth Elements in Seaweed: Implication of Two Different Sources of Rare Earth Elements and Silicon in Seaweed. *J. Phycol.* **2000**, *36*, 62–70. [CrossRef]
51. Etesami, H.; Jeong, B.R. Silicon (Si): Review and Future Prospects on the Action Mechanisms in Alleviating Biotic and Abiotic Stresses in Plants. *Ecotoxicol. Environ. Saf.* **2018**, *147*, 881–896. [CrossRef]
52. Sobral, L.F.; Barreto, M.D.V.; Da Silva, A.J.; Dos Anjos, J.L.; Barretto, M.C.D.V.; Airon, J.D.S.; Joezio, L.D.A. *Guia Prático para Interpretação de Resultados de Análises de Solo*; Embrapa Tabuleiros Costeiros (Cpatc): Aracaju, Brazil, 2015; 13p, Available online: https://ainfo.cnptia.embrapa.br/digital/bitstream/item/142260/1/Doc-206.pdf (accessed on 4 March 2025).
53. Inocencio, M.F.; Carvalho, J.G.D.; Furtini Neto, A.E. Potássio, sódio e crescimento inicial de espécies florestais sob substituição de potássio por sódio. *Rev. Árvore* **2014**, *38*, 113–123. [CrossRef]
54. Tejasree, A.; Mirza, A. Synergistic effects of silicon and seaweed extract on growth and leaf nutrient content of papaya cv Red Lady. *J. Appl. Nat. Sci.* **2024**, *16*, 1250–1255. [CrossRef]
55. Pavlovic, J.; Kostic, L.; Bosnic, P.; Kirkby, E.A.; Nikolic, M. Interactions of silicon with essential and beneficial elements in plants. *Front. Plant Sci.* **2021**, *12*, 697592. [CrossRef]
56. Ali, A.M.; Bijay-Singh. Silicon: A Crucial Element for Enhancing Plant Resilience in Challenging Environments. *J. Plant Nutr.* **2025**, *48*, 486–521. [CrossRef]
57. Santos, H.C.; Oliveira, F.H.T.; Souza, A.P.; Salcedo, I.H.; Silva, V.D.M. Phosphorus Availability as a Function of Its Time of Contact with Different Soils. *Rev. Bras. Eng. Agrícola Ambient.* **2016**, *20*, 996–1001. [CrossRef]
58. Tavakkoli, E.; Lyons, G.; English, P.; Guppy, C.N. Silicon Nutrition of Rice Is Affected by Soil PH, Weathering and Silicon Fertilisation. *J. Plant Nutr. Soil Sci.* **2011**, *174*, 437–446. [CrossRef]
59. Zhao, K.; Yang, Y.; Zhang, L.; Zhang, J.; Zhou, Y.; Huang, H.; Luo, S.; Luo, L. Silicon-based additive on heavy metal remediation in soils: Toxicological effects, remediation techniques, and perspectives. *Environ. Res.* **2022**, *205*, 112244. [CrossRef]
60. Kumar, A.; Hart, P.; Thakur, V.K. Seaweed Based Hydrogels: Extraction, Gelling Characteristics, and Applications in the Agriculture Sector. *ACS Sustain. Resour. Manag.* **2024**, *1*, 1876–1905. [CrossRef]

microorganisms

MDPI

Article

Nocardia mangyaensis NH1: A Biofertilizer Candidate with Tolerance to Pesticides, Heavy Metals and Antibiotics

Tatiana V. Shirshikova [1], Maria I. Markelova [2], Shanshan Zhou [3], Lydia M. Bogomolnaya [4], Margarita R. Sharipova [1] and Irina V. Khilyas [1,*]

[1] Institute of Fundamental Medicine and Biology, Kazan (Volga Region) Federal University, 420008 Kazan, Russia
[2] Laboratory of Multiomics Technologies of Living Systems, Institute Fundamental Medicine and Biology, Kazan (Volga Region) Federal University, 420008 Kazan, Russia
[3] State Key Laboratory of Microbial Diversity and Innovative Utilization, Institute of Microbiology, Chinese Academy of Sciences, Beijing 100101, China
[4] Department of Biomedical Sciences, Marshall University Joan C. Edwards School of Medicine, Huntington, WV 25755-0001, USA
* Correspondence: irina.khilyas@gmail.com

Abstract

The extensive use of agrochemicals, heavy metals, and antibiotics in agriculture poses significant challenges to environmental sustainability and soil health. Plant growth-promoting bacteria (PGPB) offer a promising solution for sustainable agriculture; however, their selection requires careful evaluation of factors such as genome stability, metal tolerance, antibiotic resistance, and pesticide degradation capacity. This study characterizes the endolithic *Nocardia mangyaensis* NH1, focusing on its physiological and genomic features that enhance its potential as a biofertilizer in contaminated soils. Genomic analysis revealed a low number of antibiotic resistance genes with susceptibility to broad-spectrum antibiotics, minimizing the risk of horizontal gene transfer. The genome of *N. mangyaensis* NH1 contains two non-pathogenic genomic islands and prophage regions, with a CRISPR–Cas9 system. These findings highlight *N. mangyaensis* NH1 as a promising candidate for biofertilizers, combining pesticide and metal tolerance with genomic stability, thereby supporting sustainable agricultural practices and reducing environmental risks associated with agrochemical use.

Keywords: *Nocardia*; heavy metals; pesticides; antimicrobial resistance; biofertilizer

1. Introduction

The extensive use of agrochemicals and pesticides, metal tolerance and antibiotic resistance represent significant challenges to modern agriculture and environmental sustainability [1]. The co-occurrence of heavy metals and pesticides in agricultural soils often leads to joint toxicity for plants and soil microorganisms, which can be either synergistic or antagonistic [2]. The agricultural application of metal-containing fertilizers and pesticides plays an important role in the maintenance and selection of antibiotic resistance among microorganisms, which in turn affects the formation of microbial communities and healthy plant rhizosphere [3].

One of the strategies employed in the practice of sustainable agriculture is the introduction of plant growth-promoting bacteria (PGPB), which serve to reduce reliance on chemical pesticides. However, the screening and selection of bacterial strains that are applicable for

microbial-based fertilizers represent a significant challenge. Among bacteria, *Nocardia*, a genus of actinobacteria, are ubiquitous in a variety of ecological niches due to their high metabolic activity and capacity for adaptation to a range of stressors. A high resistance to heavy metals, the ability to biodegrade pesticides and plastics, synthesis of metabolites with activity against pathogenic bacteria and fungi, production of phytohormones and formation of nodules in actinorhizal plants were demonstrated for different strains of *Nocardia* [4,5]. Furthermore, the genomes of *Nocardia* species contain a variety of biosynthetic gene clusters (BGCs) responsible for the biosynthesis of bioactive secondary metabolites with antibacterial, antifungal and antiviral activities [6]. This metabolic potential, combined with their resilience to environmental stressors, positions *Nocardia* as a promising candidate for agrobiotechnological applications.

The tolerance of bacteria to heavy metals depends on the metal transportome, which represents a network of transport proteins involved in the uptake, efflux and sequestration of metal ions [7]. The control of metal homeostasis and cycling by transport systems enables microorganisms to survive in metal-rich environments. In addition to the significance of the diversity and the richness of the bacterial metal transportome, the antibiotic resistome is a pivotal factor in the distribution of antibiotic resistance genes within microbial communities in agricultural soils [7]. The goal in identification of novel PGPB candidates is to ensure that they will minimize environmental reservoirs of resistance genes, thereby preventing their transfer to phytopathogens and protecting agricultural ecosystems. The mechanisms of antibiotic and metal resistance co-selection have been extensively studied in bacteria from agricultural and industrial environments [8]. Furthermore, agricultural ecosystems are exposed to a variety of pesticides, the uncontrolled use of which has resulted in the bioaccumulation of these chemicals in plants, soil, air and water [2]. This has also led to an imbalance in microbial communities, with a predominance of phytopathogenic microorganisms.

Apart from above mentioned biosafety concerns related to pesticides, metal tolerance and antibiotic resistance, the genetic plasticity and stability of PGPB in the biofertilizers are also very important [9]. Bacterial genome integrity and stability are vital for their adaptation to a changing environment [10]. It is also crucial to maintain a balance between genome stability and plasticity when selecting bacterial strains for integration into agricultural practice. It is therefore essential to select PGPB as a component of biofertilizers based on investigation of their genome stability, metal transportome, antibiotic resistance and pesticide tolerance in order to advance sustainable agriculture. The objective of the present study was to characterize the physiological properties and genomic features of the endolithic *Nocardia mangyaensis* NH1 that contribute to its resistance to pesticides, heavy metals and antibiotics, thereby enhancing its potential as a biofertilizer in agricultural practice in poor and contaminated soils.

2. Materials and Methods

2.1. Bacterial Strain

Experiments were carried out using the endolithic strain *N. mangyaensis* NH1 isolated from the hydromagnesite mineral [11]. *N. mangyaensis* NH1 was grown on Mueller–Hinton agar. A bacterial suspension was then prepared in sterile 0.9% saline and left undisturbed to allow large clumps to settle. The resulting suspension was diluted to an OD600 of 0.1 or 0.5 according to MacFarland standards [12]. *N. mangyaensis* NH1 was deposited in the Russian National Collection of Industrial Microorganisms under collection number of VKPM: Ac-2226. The whole-genome shotgun project of *N. mangyaensis* NH1 was deposited at DDBJ/ENA/GenBank under accession JAUMIP000000000.

2.2. Assessment of Pesticide Resistance

N. mangyaensis NH1 was tested for sensitivity/resistance against field application rates of single fungicides (difenoconazole, fludioxonil, chlorothalonil), mixture of fungicides (tebuconazole and propiconazole) and herbicide (glufosinate ammonium) obtained from their respective manufacturers (SI_Table S1). Pesticide sterility was evaluated before their use in the experiments. Diluted pesticide solutions were freshly prepared prior to each experiment. The resulting suspension of *N. mangyaensis* NH1 was inoculated in Mueller–Hinton broth with the addition of pesticides at concentrations ranging from 1.0 to 4000 mg/L. Pesticide-free medium was used as a positive control. The incubation was performed at 30 °C for 72 h. The assessment of bacterial survival in the presence of pesticides was conducted through the enumeration of colony-forming units (CFU/mL). All experiments were performed in duplicate.

2.3. Heavy Metal Resistance

The minimum inhibitory concentration (MIC) to heavy metals was determined using a serial spot assay. The stock solutions of metals ($NiSO_4 \cdot 7H_2O$, $CoCl_2 \cdot 6H_2O$, $K_2Cr_2O_7$, $CuSO_4 \cdot 5H_2O$, $ZnSO_4$, $FeCl_3 \cdot 6H_2O$, $AlCl_3$) were prepared in distilled water and filter-sterilized. The resulting suspensions and their appropriate serial dilutions were spotted onto agar plates supplemented with a gradient of metal concentrations (1.0–10.0 mM). Agar plates without metals served as a positive growth control. After incubation at 30 °C for 72 h a bacterial growth was assessed by enumerating CFU/mL. The MIC was defined as the lowest concentration of heavy metals that completely inhibited visible growth. All experiments were performed in triplicate.

The metal transportome of *N. mangyaensis* NH1 was predicted by using the TransportDB database 2.0 through the BLASTp v2.2.26 tool, with an E-value threshold of 1×10^{-100} [13]. The Antibacterial Biocide and Metal Resistance Genes Database (BacMet, experimentally confirmed database) v2.0 was used to search for resistance genes to biocides and metals through the BLASTp v2.2.26 tool, with an E-value threshold of 1×10^{-50} [14].

2.4. Antibiotic Susceptibility

The susceptibilities of *N. mangyaensis* NH1 were determined by E-test strip and disk diffusion assay on Mueller–Hinton agar (BD Difco) according to the Clinical and Laboratory Standards Institute (CLSI) guidelines (www.clsi.org). The resulting suspension of NH1 was streaked on the Mueller–Hinton agar using a sterile cotton-tipped applicator. E-test strips (Ezy MIC™, HIMEDIA, Kennett Square, PA, USA) and disks with antibiotics (MASTDISCS® AST and Bio-Rad® discs) were placed on the agar surface. The plates were incubated at 30 °C for 72 h, after which the inhibition zones surrounding the antimicrobial discs were measured. *N. mangyaensis* NH1 was categorized as sensitive or resistant according to previously published criteria [12,15,16]. Experiments were performed in triplicate. The Comprehensive Antibiotic Resistance Database ("CARD") was used for predicting antibiotic resistance genes in the genome [17].

2.5. Genome Plasticity of N. mangyaensis NH1

The identification of signature genes for CRISPR–Cas types and subtypes was performed by using the online platform CRISPRCasFinder [18]. The genome of *N. mangyaensis* NH1 was analyzed using the PHASTEST (PHAge Search Tool with Enhanced Sequence Translation) web server to predict prophage sequences [19]. The classification of protein sequences into families was performed using the InterPro resource (https://www.ebi.ac.uk/interpro, accessed on 20 March 2025). The prediction of genomic islands in the *N. mangyaensis* NH1 genome was carried out with the IslandViewer web-

server (http://www.pathogenomics.sfu.ca/islandviewer/, accessed on 20 March 2025) using the complete reference genome of *Nocardia asteroides* strain FDAARGOS 1485 [20].

2.6. Statistical Analysis of Data

The statistical analysis of the data was conducted using GraphPad Prism v. 8.0.1 (GraphPad Software, San Diego, CA, USA). The *p*-value was considered to be statistically significant if it was less than 0.05, and this was determined by the Kruskal–Wallis test.

3. Results

3.1. The Survival of N. mangyaensis NH1 in the Presence of Pesticides

The present study examined the viability of *N. mangyaensis* NH1 in pesticide solutions at field application rates over a 72 h period at 30 °C (Figure 1). The NH1 strain remained viable in a medium with glufosinate-ammonium, difenoconazole, fludioxonil and chlorothalonil with no significant reduction in cell count from the initial inoculation rate. However, statistically significant reduced bacterial growth of the NH1 strain was observed when exposed to glufosinate-ammonium in comparison with the untreated control. The fungicide mixture of tebuconazole and propiconazole (100 and 150 mg/L, respectively) was a notable exception, causing a statistically significant decrease in bacterial survival (Figure 1). The results revealed a positive correlation between the decrease in pesticide concentration and the increase in growth demonstrated by *N. mangyaensis* NH1 (SI_Figure S1).

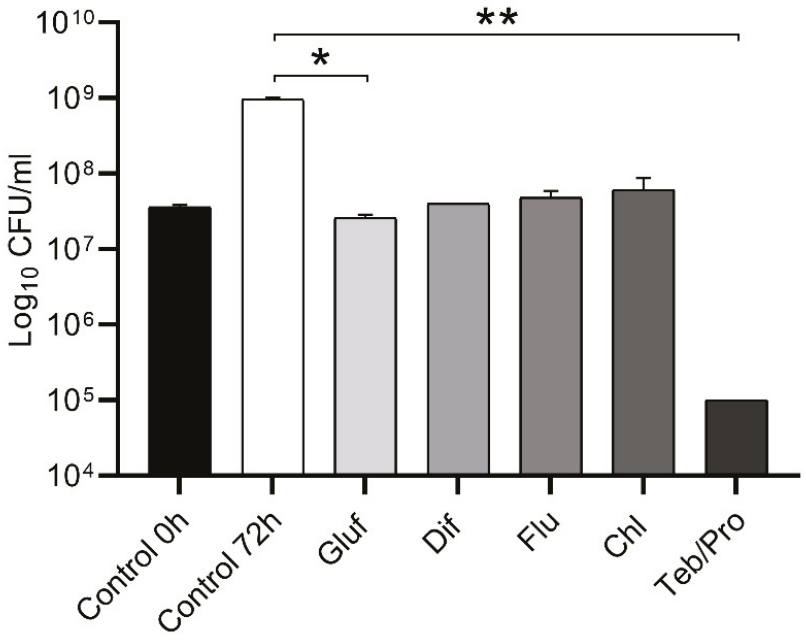

Figure 1. The survival of *N. mangyaensis* NH1 at field application rates of pesticides (Gluf, glufosinate-ammonium (2500 mg/L), Dif, difenoconazole (100 mg/L), Flu, fludioxonil (1500 mg/L), Chl, chlorothalonil (4000 mg/L) and Teb/Pro, tebuconazole and propiconazole (100/150 mg/L)) after 72 h growth at 30 °C in Mueller–Hinton medium. Values are means ± standard deviations. *—*p*-value < 0.05 and **—*p*-value < 0.01 are used to indicate significant differences between the control and experimental groups. All experiments were performed in duplicate.

3.2. Heavy Metal Resistance and Metal Transportome of N. mangyaensis NH1

N. mangyaensis NH1 demonstrated multiple resistance to heavy metals, with MIC values varying across a range of concentrations (Table 1, SI_Figure S2). The order of metal resistance, based on the MIC values, was as follows: $Al^{3+} > Zn^{2+}/Fe^{3+}/Ni^{2+} > Co^{2+} > Cu^{2+}/Cr_2O_7^{2-}$.

Table 1. The minimum inhibitory concentration (MIC) of heavy metals for *N. mangyaensis* NH1.

Resistance Level	Metal Ions	MIC (mM)
Highest	Al^{3+}	10
High	Zn^{2+}, Fe^{3+}, Ni^{2+}	7
Medium	Co^{2+}	5
Lowest	Cu^{2+}, $Cr_2O_7^{2-}$	4

In order to determine the basic composition of the metal transportome involved in the metal resistance of *N. mangyaensis* NH1, the TransportDB 2.0 database was used, aiming to identify and assign putative function to all transport proteins. The following metal transporter groups were identified: ATP-dependent (ABC superfamily, P-type ATPase superfamily), ion channels (MIT, VIC), secondary transporters (ACR3, CaCA, CDF, CPA3, DASS, DMT, MFS, MOP, RND) and unclassified (MgtE) (Table 2).

Table 2. The metal transportome of *Nocardia mangyaensis* NH1.

Metal Transporter Type/Family	Number of Transporters
I ATP-Dependent	**116**
P-type ATPase (P-ATPase) Superfamily	5
ATP-binding cassette (ABC) Superfamily	111
II Ion Channels	**2**
CorA/Mrs2 Metal Ion Transporter (MIT) Family	1
Voltage-gated Ion Channel (VIC) Superfamily	1
III Secondary Transporters	**50**
Arsenical Resistance-3 (ACR3) Family	1
Ca^{2+}: Cation Antiporter (CaCA) Family	1
Cation Diffusion Facilitator (CDF) Family	1
Monovalent Cation (K^+ or Na^+): Proton Antiporter-3 (CPA3) Family	2
Divalent Anion:Na^+ Symporter (DASS) Family	1
Drug/Metabolite Transporter (DMT) Superfamily	1
Major Facilitator Superfamily (MFS)	26
Multidrug/Oligosaccharidyl-lipid/Polysaccharide (MOP) Flippase Superfamily	3
Resistance-Nodulation-Cell Division (RND) Superfamily	14
IV Unclassified	**2**
Mg^{2+} Transporter-E (MgtE) Family	2
Total	**170**

Screening for heavy metal resistance genes in the genome of *N. mangyaensis* NH1 was conducted using the Antibacterial Biocide and Metal Resistance Genes (BacMet) database (Table 3). Seven genes encoding proteins that participate in cobalt, nickel, copper, iron, cadmium and lead resistance were identified, as well as one gene (*ideR*) that is involved in peroxide and naphthoquinone stress response. The results revealed that in the genome of *N. mangyaensis* NH1, two genes, *ctpD* and *kmtR*, are likely associated with resistance to cobalt (Co) and nickel (Ni). It was also suggested that three genes (*ideR*, *furA* and *acn*) might be involved in regulating of iron homeostasis (Table 3).

Table 3. Prediction of antibacterial biocide and metal resistance genes in the genome of *Nocardia mangyaensis* NH1.

Gene	ID	Species	Metal	Query	% Identity	N Identity	Length	E Value
ctpD	A0R3A7	*Mycobacterium smegmatis*	Cobalt (Co), Nickel (Ni)	WP_302872979.1	63.1	395	626	0
mctB	P64883	*Mycobacterium tuberculosis*	Copper (Cu)	WP_302872657.1	46.8	146	312	3.67×10^{-80}
furA	P0A582	*Mycobacterium tuberculosis*	Iron (Fe)	WP_071931421.1	72.1	101	140	6.78×10^{-72}
ideR	P0A672	*Mycobacterium tuberculosis*	Iron (Fe), Hydrogen Peroxide (H_2O_2) [class: Peroxides], Plumbagin [class: Naphthoquinone]	WP_071929125.1	73.9	170	230	1.65×10^{-199}
nmtR	O69711	*Mycobacterium tuberculosis*	Nickel (Ni), Cadmium (Cd), Lead (Pb)	WP_302872707.1	75.63	90	119	1.99×10^{-63}
kmtR	O53838	*Mycobacterium tuberculosis*	Nickel (Ni), Cobalt (Co)	WP_302871740.1	77.876	88	113	3.60×10^{-59}
acn	O53166	*Mycobacterium tuberculosis* H37Rv	Iron (Fe)	WP_302870970.1	79.38	743	936	0

3.3. Antibiotic Resistance Profile of N. mangyaensis NH1

Genomic analysis using the Comprehensive Antibiotic Resistance Database (CARD) identified a limited resistance gene repertoire of *N. mangyaensis* NH1, which correlates with the observed phenotypic profile (Table 4). The antibiotic resistome of *N. mangyaensis* NH1 includes two genes, *vanY* and *vanW,* that encode proteins responsible for glycopeptide antibiotic resistance. Additionally the presence of one gene encoding rifampin monooxygenase, which participates in the inactivation of rifamycin, and the *aac(3)-I* gene, which encodes aminoglycoside 3-N-acetyltransferase and confers resistance to gentamicin and tobramycin were predicted. It is important to note that the results of the genomic analysis of *N. mangyaensis* NH1 are in good agreement with the phenotypic results of antibiotic susceptibility to glycopeptide antibiotics and aminoglycosides.

Table 4. The CARD-based antibiotic resistome prediction of *Nocardia mangyaensis* NH1.

RGI Critera	ARO Term	Detection Criteria	AMR Gene Family	Drug Class	Resistance Mechanism	% Identity of Matching Region	% Length of Reference Sequence	Predicted phenotype (ResFinder)
Strict	*vanY* gene in *vanB* cluster	protein homolog model	*vanY*, glycopeptide resistance gene cluster	glycopeptide antibiotic	antibiotic target alteration	32.17	64.18	-
Strict	*vanY*	protein homolog model	*vanW*, glycopeptide resistance gene cluster	glycopeptide antibiotic	antibiotic target alteration	28.91	166.22	-
Strict	*Nocardia farcinica rox*	protein homolog model	rifampin monooxygenase	rifamycin antibiotic	antibiotic inactivation	71.61	100.21	-
Strict	*aac(3)-IVa*	protein homolog model	AAC(3)	aminoglycoside antibiotic	antibiotic inactivation	98.84	103.49	Gentamicin, Tobramycin

Antibiotic Resistance Ontology (ARO), Resistance Gene Identifier (RGI). *aac(3)-IVa* is a plasmid-encoded aminoglycoside acetyltransferase in *E. coli*, *C. jejuni* and *P. stutzeri. Nocardia farcinica rox* is a rifampin monooxygenase that inactivates rifampin.

The present study also characterized the antibiotic resistance profile of *N. mangyaensis* NH1. The NH1 strain showed resistance to several antibiotics, including select aminoglycosides (kanamycin, tobramycin, streptomycin), cephalosporins (cefazolin), nitrofurans (nitrofurantoin), tetracyclines (tetracycline, doxycycline), and the glycopeptide vancomycin (SI_Table S2). Intermediate sensitivity was observed for gentamicin, erythromycin, and ciprofloxacin. The E-test determination of the minimum inhibitory concentration (MIC) confirmed susceptibility to these antibiotics at low concentrations (0.75, 1.5, and 1.0 μg/mL, respectively). The NH1 strain also demonstrated susceptibility to the aminoglycoside antibiotics neomycin and amikacin.

3.4. Genome Plasticity of N. mangyaensis NH1

To assess genome plasticity, a number of accessory genes beneficial under environmental conditions were explored. Five genomic islands (GIs) consisting of diverse insertion sequences (IS), integrases and transposases, were found in the genome of *N. mangyaensis* NH1 (SI_Table S3). The results showed the absence of pathogen-associated genes, curated virulence factors and resistance genes. One GI contains the Cas cluster. The Cas cluster, with an evidence level of 1 belonging to CAS-Type II-U, was detected in the contig NZ_JAUMIP010000046.1 (Figure 2). The contig contains five genes encoding Cas9 hypothetical protein, aminoglycoside N-acetyltransferase AAC(3)-IVa, IS6 family transposase, type II CRISPR RNA-guided endonuclease Cas9 and CII family transcriptional regulator. The Cas9 protein of *N. mangyaensis* NH1 was annotated by using InterPro, and the following domains were identified: HNH nuclease, CRISPR-associated endonuclease Cas9 with REC lobe and bridge helix, Cas9-type HNH domain and Ribonuclease H superfamily (Table 5). Additionally, our findings revealed that the genome of *N. mangyaensis* NH1 contains nine CRISPR arrays with direct repeats and spacers with an evidence level of 1, while one has an evidence level of 2 (SI_Table S4).

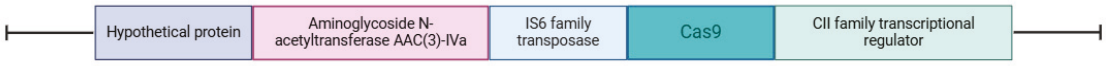

Figure 2. The genomic island in the genome of *N. mangyaensis* NH1 containing the type II CRISPR RNA-guided endonuclease Cas9.

Table 5. InterPro annotation for the type II CRISPR RNA-guided endonuclease Cas9 (WP_302876581.1) of *N. mangyaensis* NH1.

Accession	Short Name	Accession
IPR003615	HNH_nuc	HNH nuclease
IPR028629	Cas9	CRISPR-associated endonuclease Cas9
IPR033114	HNH_CAS9	Cas9-type HNH domain
IPR032240	Cas9_REC	CRISPR-associated endonuclease Cas9, REC lobe
IPR032239	Cas9-BH	CRISPR-associated endonuclease Cas9, bridge helix
IPR036397	RNaseH_sf	Ribonuclease H superfamily

In this work, the composition of prophage genes and regions within the *N. mangyaensis* NH1 was studied using bioinformatic tools. The identification and annotation of prophage genes and regions within the *N. mangyaensis* NH1 genome revealed two regions containing incomplete and intact prophages, respectively, with total scores of 70 and 100 (SI_Figure S3, SI_Table S5). The average length of intact prophage sequences was found to be ~12.5 kb. The GC content of the sequences analyzed was approximately 64% (SI_Table S5). Both prophage regions are located in the contig NZ_JAUMIP010000013.1 and are in close proximity to each other. The region 1 consists of nine proteins, including a regulated protein homologous to AraC family transcriptional regulator (PHAGE_Bordet_vB_BbrM_PHB04_NC_047861), a hypothetical protein, a phage-like protein

homologous to gp132 (PHAGE_Mycoba_Cali_NC_011271), and six tail proteins homologous to minor tail proteins of different phages. The region 2 consists of 14 proteins, including two head proteins homologous to head-to-tail connector complex proteins (PHAGE_Strept_Rowa_NC_047906 and PHAGE_Rhodoc_Sleepyhead_NC_048782); four phage-like proteins homologous to pentapeptide repeat family proteins (PHAGE_Microc_MaMV_DC_NC_029002, PHAGE_Microc_MaMV_DC_NC_029002); a putative major virion structural protein (PHAGE_Brevib_Jenst_NC_028805) and a putative lysin (PHAGE_Gordon_GMA4_NC_030939); one lysis protein homologous to lysin B (PHAGE_Gordon_Attis_NC_041883); one repressor homologous to immunity repressor (PHAGE_Rhodoc_Jace_NC_047974); and four tail proteins homologous to minor tail proteins of different phages. In the *N. mangyaensis* NH1 genome, thirteen insertion elements (IS) belonging to eight IS families (IS5/IS1182, IS1380, IS630, IS3, ISAs1, IS6, IS21, IS30 and IS110 family transposases) were identified on the basis of the GenBank annotation (GCA_030519415.1). It was observed that, among all insertion sequences detected, those belonging to the IS5/IS1182 family transposase were found to be more prevalent.

4. Discussion

The agricultural sector is a major consumer of fertilizers, pesticides and soil supplements that contain heavy metals as impurities. The primary source of heavy metals (particularly Cd, Cu, Zn, Pb, Ni, As and Cr) are phosphorus fertilizers, which are extensively utilized in agricultural practices across numerous countries [21]. The application of pesticides, intended to treat plants against bacterial, fungal or insect diseases, is typically carried out through foliar spraying. However, this practice results in the wash-off of pesticides from treated plants and subsequent sorption of the pesticides onto soil particles [22]. The application of fertilizers and pesticides in greenhouse farming over an extended period has resulted in their accumulation, including heavy metals, and leading to a negative impact on soil fertility and crop productivity [23].

Over the last decade, there has been a global trend in agricultural practices towards the use of microbial inoculants, formulations or biofertilizers to enhance crop productivity and practice sustainable agriculture [24]. Plant growth-promoting bacteria (PGPB) are a core component of biofertilizers due to their beneficial properties such as secretion of extracellular lytic enzymes, production of phytohormones and increase in nutrient bioavailability [5]. Among PGPB, actinomycetes are beneficial microorganisms for agricultural application as biofertilizers due to their bioactive properties. The effectiveness of biofertilizer application depends on many factors, including biotic and abiotic factors present in the environment. Moreover, given the invasive nature of microbial inoculants toward indigenous microbial communities within agricultural systems, there is a growing concern regarding the assessment of unexpected consequences arising from their application [25]. Therefore, it is important to select microbial candidates for biofertilizers with consideration for their resistance to pesticides, heavy metals and antibiotics, as well as for their genome stability. This will increase their efficiency and minimize the distribution of resistant genes within the microbial communities in agricultural soils.

Members of the genus *Nocardia* are known for their biotechnological potential, multiple heavy metal resistance and ability to biodegrade organic compounds [26,27]. Recently, the genomic and metabolomic features of the endolithic strain *N. mangyaensis* NH1 were investigated, with the aim of determining their potential application beneficial in agricultural and environmental biotechnology [11]. A critical practical consideration is that microbial biofertilizers are typically applied as tank mixtures in combination with various pesticides. This study therefore presents an extensive analysis of the survival of *N. mangyaensis* NH1 at the field application rates of both single and mixture pesticides. It was established that *N. mangyaensis* NH1 maintained viability without a reduction in the initial CFU count

throughout the extended incubation period with glufosinate-ammonium, difenoconazole, fludioxonil and chlorothalonil. This sustained survival during prolonged contact time with pesticides is critical when extending the time between tank mixing and field application is necessary.

The impact of fungicides on *Nocardia* species has been poorly explored in literature. In a recent study, it was demonstrated that one of the potential candidates for the bioremediation of environments contaminated with difenoconazole, which is categorized within the triazole group of chemicals, is strain *Pseudomonas putida* A-3, which possesses unique metabolic pathways for enzymatic biodegradation [28]. Several fungal strains, including *Fusarium oxysporum*, *Lentinula edodes*, *Penicillium brevicompactum* and *Lecanicillium sakseniae*, have been shown to biodegrade pesticides, including difenoconazole [29]. Biodegradation of the fungicide chlorothalonil, a tetrachlorinated benzonitrile, has been demonstrated for various bacterial genera (*Ochrobactrum*, *Shinella*, *Caulobacter*, *Rhizobium*, *Bordetella*, *Pseudoxanthomonas*, *Pseudomonas* and *Lysobacter*) [30]. Conversely, the effect of chlorothalonil on *Nocardia* strains remains to be elucidated. The biodegradation of fludioxonil, a fluorinated fungicide, was observed among numerous bacterial genera, including *Pseudomonas*, *Ochrobactrum* and *Comamonas* within agricultural soils [31].

Glufosinate-ammonium is an organophosphorus herbicide that was initially discovered as a tripeptide named bialaphos from actinomycetes belonging to the genus *Streptomyces* [32]. In order to control the growth of weeds that compete with the soybean plant, two bacterial genes (*hpat* and *mat*) encoding phosphinothricin and methionine sulfone acetyltransferases from bialaphos-resistant bacteria *Streptomyces* sp. strain AB3534 and *Nocardia* sp. strain AB2253 were selected to generate transgenic plants with confirmed resistance to glufosinate (PPT, phosphinothricin) [33,34]. Genome mining of *N. mangyaensis* NH1 revealed a sequence identity of 67% for GCN5-related N-acetyltransferases family (GNAT) with methionine sulfone acetyltransferase of *Nocardia* sp. strain AB2253. Although MTC of *N. mangyaensis* NH1 for glufosinate-ammonium remains below field application doses *in vitro*, the presence of the GNAT acetyltransferase (WP_302876268.1) implies potential for enzymatic detoxification of the herbicide under field conditions.

Agricultural management practice commonly involves simultaneous application of several pesticides. The present study evaluated the influence of a propiconazole and tebuconazole mixture on the viability of *N. mangyaensis* NH1. The results demonstrated a significant reduction in the initial CFU, indicating that separate application of the pesticides is necessary. For instance, the synergistic effect of a propiconazole and tebuconazole mixture in combination with the biocontrol strain *Bacillus subtilis* Czk1 was demonstrated against the fungus *Pyrrhoderma noxium*, which causes brown root rot of rubber trees [35]. The mechanism of the synergistic effect is thought to be the alteration of the metabolomic profile of the Czk1 strain, which leads to the synthesis of a diverse spectrum of metabolites, thereby increasing anti-phytopathogenic activity. Despite extensive use of tebuconazole and propiconazole in agricultural practice, their accumulation in soil has been demonstrated to induce shifts in microbial diversity and to promote the dissemination of a multidrug-resistant plasmid, as evidenced by the case of tebuconazole [36,37].

Along with pesticides, the issue of metal accumulation in agricultural ecosystems is a matter of concern. The heavy metal resistance profile of *N. mangyaensis* NH1 demonstrated distinct advantages over previously reported *Nocardia* strains. Although *Nocardia* MORSY2014 showed the effective removal of Ni^{2+}, Cr^{6+} and Zn^{2+} ions [38] and Nigerian *Nocardia* isolates exhibited broad heavy metal tolerance [39], the NH1 strain shows a high tolerance to aluminium, zinc, nickel and ferric iron. In comparison with the pesticide-degrading strain of *N. harenae* JJB5 [40], which has been demonstrated to have a lower metal

tolerance threshold, the NH1 strain exhibited balanced resilience to both heavy metals and pesticides.

An investigation of the metal transporter systems is crucial for the selection of PGPB for biofertilizers, since they directly impact the efficient regulation, uptake and detoxification of metals, as well as enhancing nutrient availability for plants. Genomic analyses indicate that *N. mangyaensis* NH1 encodes a large and diverse repertoire of potential metal transporters. A high number of transporters in the genome NH1 relate to the ABC superfamily. This family is known to participate in the uptake and efflux transport of a wide variety of molecules including nutrients, antibiotics, iron–siderophore complexes, virulence factors and envelope components [41,42]. Although transporters of the P-type ATPase superfamily are present in limited amount in the genome of *N. mangyaensis* NH1, they contain copper/mercury/heavy metal binding domains and catalyze the uptake and/or efflux of such cations as Mg^{2+}, Cu^{2+}, Ag^{+}, Zn^{2+}, Co^{2+}, Pb^{2+}, Ni^{2+} and Cd^{2+}.

Among secondary transporters, the genome of *N. mangyaensis* NH1 is dominated by members of the MFS superfamily. The MFS transporters participate in the uptake and efflux of small molecules such as simple sugars, oligosaccharides, amino acids, Krebs cycle intermediates, antibiotics and nucleotides [43]. Some of the most represented members of the of metal transporters in the genome *N. mangyaensis* NH1 are proteins related to the RND superfamily, which are involved in the efflux of a range of substrates, including heavy metals, multiple drugs, antibiotics, lipooligosaccharides, lipids and pigments.

Three transport proteins relating to the Multidrug/Oligosaccharidyl-lipid/Polysaccharide (MOP) Superfamily were also identified in the genome of *N. mangyaensis* NH1 in limited amounts. They catalyze the efflux of primary and secondary metabolites such as terpenoids, phenols, flavonoids, nicotine, alkaloids, phytohormones, proanthocyanidin and anthocyanins. The MIT family (CorA/Mrs2) and VIC superfamily were both found in a single variant in the genome of *N. mangyaensis* NH1. These ion channels are identified as responsible for the import of Mg^{2+}, Co^{2+}, Ni^{2+}, Zn^{2+} cations and are encoded by an ion-selective channel protein that facilitates the transport of K^{+}, Na^{+} or Ca^{2+} [44].

The horizontal transfer of antibiotic resistance genes is known to be possible through co-occurrence with biocide/metal resistance genes found in bacterial chromosomes [45]. Consequently, the presence of metals in fertilizers or pesticide-contaminated soils could promote the spread of antibiotic resistance in the PGPB of biofertilizers and microbial communities of agricultural soils.

An investigation into the antibiotic susceptibility profile of potential PGPB biofertilizers is helpful for selecting bacteria lacking transferable antibiotic resistance genes, thereby reducing the risk of horizontal gene transfer. This is of particular relevance when considering the widespread use of livestock and poultry manure, which contributes to the dissemination of heavy metal and antibiotic resistance genes in agricultural soils [46]. The genomic analysis of *N. mangyaensis* NH1 revealed a limited repertoire of antibiotic resistance genes, identifying only two putative determinants: one conferring resistance to aminoglycosides and another to rifamycin. This finding provides a genotypic context for the observed phenotypic resistance profile of NH1 strain.

The antibiotic susceptibility profiles of numerous clinical isolates of the *Nocardia* species are well characterized [15,47–50]. However, the interpretation of the antibiotic susceptibility of *Nocardia* species remains a topic of debate, even according to widely accessible guidelines the European Committee on Antimicrobial Susceptibility Testing (EUCAST), unlike the actual restricted accessibility of the CLSI standards developed for clinical isolates [51]. Furthermore, the susceptibility criteria might vary significantly between clinical and environmental strains, as well as between different species and geographical origins, making direct comparisons challenging [15,52].

The phenotypic analysis showed that the NH1 strain is resistant to select aminoglycosides (kanamycin, tobramycin, streptomycin) but sensitive to neomycin and amikacin. This finding supports a recent study reporting that 91% of clinical *Nocardia* species are sensitive to amikacin [53]. It was confirmed that high-level aminoglycoside resistance in a clinical isolate of *N. farcinica* IFM 10580 is attributed to homozygous mutations in the 16S rRNA genes [54]. The resistance profile of NH1 showed a high degree of agreement with patterns observed in clinical isolates for other antibiotics. The resistance of *N. mangyaensis* NH1 to ceftazidime aligns with the resistance in 98% of the clinical isolates of *Nocardia* [55]. Similarly, *N. mangyaensis* NH1 resistance to nitrofurantoin and vancomycin is consistent with nocardial species-specific resistance reported in previous studies [56,57]. Furthermore, the high rates of intermediate resistance of *Nocardia* strains to the tetracycline class of antibiotic partially confirmed the resistance of *N. mangyaensis* NH1 to doxycycline [53].

The genomic analysis of *N. mangyaensis* NH1 revealed the presence of genomic islands. Nevertheless, no pathogen-associated genes, curated virulence factors or resistance genes were identified, which is an advantage for the application of *N. mangyaensis* NH1 in agriculture. Moreover, one genomic island in the genome of *N. mangyaensis* NH1 harbors genes encoding type II CRISPR (clustered regularly interspaced short palindromic repeats) RNA-guided endonuclease Cas9. It is well established that *cas*9 is the signature gene of type II CRISPR–Cas systems protecting bacterial genome against exogenous mobile genetic elements [58]. The absence of other genes such as *cas*1 and *cas*2 in the same locus or elsewhere in the genome suggests that the type II CRISPR–Cas system of *N. mangyaensis* NH1 is not complete. However, recent discoveries have revealed significant progress in the classification of CRISPR–Cas systems (now 7 types and 46 subtypes), with many rare variants, such as those in NH1, being identified from diverse environmental niches [59].

Insertion elements, which represent mobile DNA repeats, have been shown to be capable of copying and moving to different locations within the bacterial genome via a transposition mechanism. This capacity contributes to the plasticity of the bacterial genome and the regulation of genes [60]. As demonstrated in previous studies, there is significant variation in the abundance of insertion sequences (IS) among *Nocardia* genomes. This variation is indicative of divergent genomic capacities for acquiring exogenous DNA and tolerance to these mobile genetic elements [61]. The genome of *N. mangyaensis* NH1 was found to contain 13 ISs, whereas the genome of its closest species *N. mangyaensis* Y48 (GCA_001886715.1) contains 25 ISs belonging to six different families, with three common families (IS30, IS110, IS630). These differences in IS composition highlight the genomic diversity within closely related *Nocardia* strains and suggest varied capacities for genome plasticity and adaptation, which may influence their environmental fitness and functional potential.

Given the fact that prophages might induce genomic variability under stressful conditions or impose an influence on bacterial virulence, the analysis of prophage genes is a subject of growing interest. It is noteworthy that only two prophage regions, containing a total of 23 genes, were identified in *N. mangyaensis* NH1. This finding indicates that the *N. mangyaensis* NH1 genome faced limited horizontal gene transfer (HGT) over the course of evolution. For instance, a study of the genome of another strain of *Nocardia soli* Y48, isolated from soils contaminated with crude oil in the Qinghai-Tibetan Plateau, predicted 17 GIs consisting of 173 genes, suggesting frequent HGT events [62]. Moreover, the genome of *N. mangyaensis* NH1 could be characterized as a relatively stable due to the presence of a limited number of prophages lacking phage attachment sites (*attL*/*attR*) and integrases, as well as a potentially active CRISPR–Cas system. However, further studies are necessary to fully elucidate the dynamics of these genetic elements in this species.

5. Conclusions

This study provides a comprehensive analysis of the physiological and genetic characteristics of the endolithic bacterium *N. mangyaensis* NH1 as a promising biofertilizer candidate. The NH1 strain demonstrates remarkable multi-stress resistance to pesticides and heavy metals, supported by a diverse metal transportome. The genomic safety of *N. mangyaensis* NH1 was confirmed by a minimal set of chromosomal antibiotic resistance genes and stable genomic islands lacking pathogenicity factors. The compatibility of *N. mangyaensis* NH1 with key pesticides, including glufosinate-ammonium, difenoconazole, chlorothalonil and fludioxonil, further supports its practical application.

Supplementary Materials: The following supporting information can be downloaded at: https://www.mdpi.com/article/10.3390/microorganisms13122806/s1, Table S1: Agrochemicals used in the present study; Figure S1: The pesticide resistance of *N. mangyaensis* NH1; Figure S2: The heavy metal resistance of *N. mangyaensis* NH1; Table S2: *Nocardia mangyaensis* NH1 antibiotic susceptibility; Table S3: Predicted genomic islands and virulence/resistance genes in the genome of *N. mangyaensis* NH1. The prediction was performed by integrating three different methods (IslandPath-DIMOB, SIGI-HMM, and IslandPick) using the IslandViewer webserver; Table S4: Summary of information on CRISPR arrays and cas gene clusters in the genome of *N. mangyaensis* NH1; Figure S3: Genome map (A) and linear genome sequence (B) of *N. mangyaensis* NH1; predicted phage genes and regions positioned relative to each other across the entire genome; Table S5: Prediction of prophage sequences in the genome of *N. mangyaensis* NH1 was performed by using the PHASTEST web server.

Author Contributions: Conceptualization, methodology, validation, formal analysis, investigation, data curation, visualization, T.V.S., M.I.M. and I.V.K.; writing—original draft preparation, I.V.K., S.Z., M.R.S. and L.M.B.; resources, supervision, project administration, I.V.K. and M.R.S.; writing—review and editing, I.V.K. and L.M.B.; funding acquisition, I.V.K. All authors have read and agreed to the published version of the manuscript.

Funding: This work was funded by the Russian Science Foundation project №24-24-00473.

Institutional Review Board Statement: Not applicable.

Informed Consent Statement: Not applicable.

Data Availability Statement: The original contributions presented in this study are included in the article/Supplementary Materials. Further inquiries can be directed to the corresponding author.

Conflicts of Interest: The authors declare no conflicts of interest.

References

1. Singer, A.C.; Shaw, H.; Rhodes, V.; Hart, A. Review of antimicrobial resistance in the environment and its relevance to environmental regulators. *Front. Microbiol.* **2016**, *7*, 1728. [CrossRef]
2. Alengebawy, A.; Abdelkhalek, S.T.; Qureshi, S.R.; Wang, M.Q. Heavy metals and pesticides toxicity in agricultural soil and plants: Ecological risks and human health implications. *Toxics* **2021**, *9*, 42. [CrossRef] [PubMed]
3. Gimeno-García, E.; Andreu, V.; Boluda, R. Heavy metals incidence in the application of inorganic fertilizers and pesticides to rice farming soils. *Environ. Pollut.* **1996**, *92*, 19–25. [CrossRef] [PubMed]
4. Ghodhbane-Gtari, F.; Nouioui, I.; Hezbri, K.; Lundstedt, E.; D'Angelo, T.; McNutt, Z.; Laplaze, L.; Gherbi, H.; Vaissayre, V.; Svistoonoff, S.; et al. The plant-growth-promoting actinobacteria of the genus *Nocardia* induces root nodule formation in *Casuarina glauca*. *Antonie van Leeuwenhoek* **2019**, *112*, 75–90. [CrossRef] [PubMed]
5. Silva, G.d.C.; Kitano, I.T.; Ribeiro, I.A.d.F.; Lacava, P.T. The potential use of *Actinomycetes* as microbial inoculants and biopesticides in agriculture. *Front. Soil Sci.* **2022**, *2*, 833181. [CrossRef]
6. Nonthakaew, N.; Sharkey, L.K.R.; Pidot, S.J. The genus *Nocardia* as a source of new antimicrobials. *NPJ Antimicrob. Resist.* **2025**, *3*, 5. [CrossRef]
7. Nies, D.H. The biological chemistry of the transition metal "transportome" of *Cupriavidus metallidurans*. *Met. Integr. Biometal Sci.* **2016**, *8*, 481–507. [CrossRef]

8. Gillieatt, B.F.; Coleman, N.V. Unravelling the mechanisms of antibiotic and heavy metal resistance co-selection in environmental bacteria. *FEMS Microbiol. Rev.* **2024**, *48*, fuae017. [CrossRef]
9. Khan, A.; Singh, A.V.; Gautam, S.S.; Agarwal, A.; Punetha, A.; Upadhayay, V.K.; Kukreti, B.; Bundela, V.; Jugran, A.K.; Goel, R. Microbial bioformulation: A microbial assisted biostimulating fertilization technique for sustainable agriculture. *Front. Plant Sci.* **2023**, *14*, 1270039. [CrossRef]
10. Patel, S. Drivers of bacterial genomes plasticity and roles they play in pathogen virulence, persistence and drug resistance. *Infect. Genet. Evol.* **2016**, *45*, 151–164. [CrossRef]
11. Khilyas, I.V.; Markelova, M.I.; Valeeva, L.R.; Ivoilova, T.M.; Shagimardanova, E.; Laikov, A.V.; Elistratova, A.A.; Berkutova, E.S.; Lochnit, G.; Sharipova, M.R. Genomic insights and anti-phytopathogenic potential of siderophore metabolome of endolithic *Nocardia mangyaensis* NH1. *Sci. Rep.* **2024**, *14*, 5676. [CrossRef] [PubMed]
12. Woods, G.L.; Brown-Elliott, B.A.; Conville, P.S.; Desmond, E.P.; Hall, G.S.; Lin, G.; Pfyffer, G.E.; Ridderhof, J.C.; Siddiqi, S.H.; Wallace, R.J., Jr.; et al. Susceptibility testing of *Mycobacteria, Nocardiae*, and other aerobic *Actinomycetes*. In *CLSI Standards: Guidelines for Health Care Excellence*; Clinical and Laboratory Standards Institute: Wayne, PA, USA, 2011.
13. Saier, M.H.; Reddy, V.S.; Moreno-Hagelsieb, G.; Hendargo, K.J.; Zhang, Y.; Iddamsetty, V.; Lam, K.J.K.; Tian, N.; Russum, S.; Wang, J.; et al. The transporter classification database (TCDB): 2021 update. *Nucleic Acids Res.* **2021**, *49*, D461–D467. [CrossRef] [PubMed]
14. Pal, C.; Bengtsson-Palme, J.; Rensing, C.; Kristiansson, E.; Larsson, D.G. BacMet: Antibacterial biocide and metal resistance genes database. *Nucleic Acids Res.* **2014**, *42*, D737–D743. [CrossRef] [PubMed]
15. Lebeaux, D.; Bergeron, E.; Berthet, J.; Djadi-Prat, J.; Mouniée, D.; Boiron, P.; Lortholary, O.; Rodriguez-Nava, V. Antibiotic susceptibility testing and species identification of *Nocardia* isolates: A retrospective analysis of data from a French expert laboratory, 2010–2015. *Clin. Microbiol. Infect* **2019**, *25*, 489–495. [CrossRef]
16. Xu, H.; Xu, R.; Wang, X.; Liang, Q.; Zhang, L.; Liu, J.; Wei, J.; Lu, Y.; Yu, D. Co-infections of *Aeromonas veronii* and *Nocardia seriolae* in largemouth bass (*Micropterus salmoides*). *Microb. Pathog.* **2022**, *173*, 105815. [CrossRef]
17. Raphenya, A.R.; Robertson, J.; Jamin, C.; de Oliveira Martins, L.; Maguire, F.; McArthur, A.G.; Hays, J.P. Datasets for benchmarking antimicrobial resistance genes in bacterial metagenomic and whole genome sequencing. *Sci. Data* **2022**, *9*, 341. [CrossRef]
18. Couvin, D.; Bernheim, A.; Toffano-Nioche, C.; Touchon, M.; Michalik, J.; Néron, B.; Rocha, E.P.C.; Vergnaud, G.; Gautheret, D.; Pourcel, C. CRISPRCasFinder, an update of CRISRFinder, includes a portable version, enhanced performance and integrates search for Cas proteins. *Nucleic Acids Res.* **2018**, *46*, W246–W251. [CrossRef]
19. Wishart, D.S.; Han, S.; Saha, S.; Oler, E.; Peters, H.; Grant, J.R.; Stothard, P.; Gautam, V. PHASTEST: Faster than PHASTER, better than PHAST. *Nucleic Acids Res.* **2023**, *51*, W443–W450. [CrossRef]
20. Bertelli, C.; Laird, M.R.; Williams, K.P.; Simon Fraser University Research Computing Group; Lau, B.Y.; Hoad, G.; Winsor, G.L.; Brinkman, F.S. IslandViewer 4: Expanded prediction of genomic islands for larger-scale datasets. *Nucleic Acids Res.* **2017**, *45*, W30–W35. [CrossRef]
21. Nziguheba, G.; Smolders, E. Inputs of trace elements in agricultural soils via phosphate fertilizers in European countries. *Sci. Total Environ.* **2008**, *390*, 53–57. [CrossRef]
22. Arias-Estévez, M.; López-Periago, E.; Martínez-Carballo, E.; Simal-Gándara, J.; Mejuto, J.-C.; García-Río, L. The mobility and degradation of pesticides in soils and the pollution of groundwater resources. *Agric. Ecosyst. Environ.* **2008**, *123*, 247–260. [CrossRef]
23. Abdu, N.; Abdullahi, A.A.; Abdulkadir, A. Heavy metals and soil microbes. *Environ. Chem. Lett.* **2017**, *15*, 65–84. [CrossRef]
24. Shahwar, D.; Mushtaq, Z.; Mushtaq, H.; Alqarawi, A.A.; Park, Y.; Alshahrani, T.S.; Faizan, S. Role of microbial inoculants as bio fertilizers for improving crop productivity: A review. *Heliyon* **2023**, *9*, e16134. [CrossRef] [PubMed]
25. Jack, C.N.; Petipas, R.H.; Cheeke, T.E.; Rowland, J.L.; Friesen, M.L. Microbial inoculants: Silver bullet or microbial Jurassic park? *Trends microbiol.* **2021**, *29*, 299–308. [CrossRef]
26. Alvarez, A.; Saez, J.M.; Davila Costa, J.S.; Colin, V.L.; Fuentes, M.S.; Cuozzo, S.A.; Benimeli, C.S.; Polti, M.A.; Amoroso, M.J. *Actinobacteria*: Current research and perspectives for bioremediation of pesticides and heavy metals. *Chemosphere* **2017**, *166*, 41–62. [CrossRef]
27. Nouioui, I.; Pötter, G.; Jando, M.; Goodfellow, M. *Nocardia noduli* sp. nov., a novel actinobacterium with biotechnological potential. *Arch. Microbiol.* **2022**, *204*, 260. [CrossRef]
28. Zhou, Y.; Wang, L.; Sui, J.; Chen, F.; Wang, T.; Yang, J.; Chen, S.-H.; Cui, X.; Yang, Y.; Zhang, W. Pathway elucidation and key enzymatic processes in the biodegradation of difenoconazole by *Pseudomonas putida* A-3. *J. Agric. Food Chem.* **2025**, *73*, 4770–4786. [CrossRef]
29. Álvarez, S.P.; Tapia, M.A.M.; Duarte, B.N.D.; Vega, M.E.G. Fungal bioremediation as a tool for polluted agricultural soils. In *Mycoremediation and Environmental Sustainability*; Prasad, R., Ed.; Springer International Publishing: Cham, Switzerland, 2017; Volume 1, pp. 1–15.

30. Liang, B.; Wang, G.; Zhao, Y.; Chen, K.; Li, S.; Jiang, J. Facilitation of bacterial adaptation to chlorothalonil-contaminated sites by horizontal transfer of the chlorothalonil hydrolytic dehalogenase gene. *Appl. Environ. Microbiol.* **2011**, *77*, 4268–4272. [CrossRef]
31. Alexandrino, D.A.M.; Mucha, A.P.; Almeida, C.M.R.; Carvalho, M.F. Microbial degradation of two highly persistent fluorinated fungicides—Epoxiconazole and fludioxonil. *J. Hazard. Mater.* **2020**, *394*, 122545. [CrossRef]
32. Takano, H.K.; Dayan, F.E. Glufosinate-ammonium: A review of the current state of knowledge. *Pest Manag. Sci.* **2020**, *76*, 3911–3925. [CrossRef]
33. Kita, Y.; Hanafy, M.; Deguchi, M.; Hasegawa, H.; Terakawa, T.; Kitamura, K.; Ishimoto, M. Generation and characterization of herbicide-resistant soybean plants expressing novel phosphinothricin N-acetyltransferase genes. *Breed. Sci.* **2009**, *59*, 245–251. [CrossRef]
34. Yun, C.S.; Hasegawa, H.; Nanamiya, H.; Terakawa, T.; Tozawa, Y. Novel bacterial N-acetyltransferase gene for herbicide detoxification in land plants and selection maker in plant transformation. *Biosci. Biotechnol. Biochem.* **2009**, *73*, 1000–1006. [CrossRef] [PubMed]
35. Gu, Z.-W.; Yin, J.-H.; Wu, H.; Liang, Y.-Q.; Wu, W.-H.; Lu, Y.; Li, R.; Tan, S.-B.; He, C.-P.; Yi, K.-X. Synergistic mechanism of *Bacillus subtilis* Czk1 combined with propiconazole and tebuconazole mixtures against *Pyrrhoderma noxium*. *Chem. Biol. Technol. Agric.* **2023**, *10*, 113. [CrossRef]
36. Baćmaga, M.; Wyszkowska, J.; Kucharski, J. Bacterial diversity and enzymatic activity in a soil recently treated with tebuconazole. *Ecol. Indic.* **2021**, *123*, 107373. [CrossRef]
37. Wang, Y.; Zheng, C.; Qiu, M.; Zhang, L.; Fang, H.; Yu, Y. Tebuconazole promotes spread of a multidrug-resistant plasmid into soil bacteria to form new resistant bacterial strains. *Sci. Total Environ.* **2024**, *928*, 172444. [CrossRef]
38. El-Gendy, M.M.A.A.; El-Bondkly, A.M.A. Evaluation and enhancement of heavy metals bioremediation in aqueous solutions by *Nocardiopsis* sp. MORSY1948, and *Nocardia* sp. MORSY2014. *Braz. J. Microbiol.* **2016**, *47*, 571–586. [CrossRef]
39. Oyetibo, G.O.; Ilori, M.O.; Adebusoye, S.A.; Obayori, O.S.; Amund, O.O. Bacteria with dual resistance to elevated concentrations of heavy metals and antibiotics in Nigerian contaminated systems. *Environ. Monit. Assess.* **2010**, *168*, 305–314. [CrossRef]
40. El-Sayed, M.H.; Abdellatif, M.M.; Mostafa, H.M.; Elsehemy, I.A.; Kobisi, A.E.A. Biodegradation and antimicrobial capability-induced heavy metal resistance of the marine-derived actinomycetes *Nocardia harenae* JJB5 and *Amycolatopsis marina* JJB11. *World J. Microbiol. Biotechnol.* **2024**, *40*, 202. [CrossRef]
41. Delepelaire, P. Bacterial ABC transporters of iron containing compounds. *Res. Microbiol.* **2019**, *170*, 345–357. [CrossRef]
42. Licht, A.; Schneider, E. ATP binding cassette systems: Structures, mechanisms, and functions. *Cent. Eur. J. Biol.* **2011**, *6*, 785–801. [CrossRef]
43. Kumar, S.; Lekshmi, M.; Parvathi, A.; Ojha, M.; Wenzel, N.; Varela, M.F. Functional and structural roles of the Major Facilitator Superfamily bacterial multidrug efflux pumps. *Microorganisms* **2020**, *8*, 266. [CrossRef] [PubMed]
44. Papp, K.M.; Maguire, M.E. The CorA Mg^{2+} transporter does not transport Fe^{2+}. *J. Bacteriol.* **2004**, *186*, 7653–7658. [CrossRef] [PubMed]
45. Pal, C.; Bengtsson-Palme, J.; Kristiansson, E.; Larsson, D.G.J. Co-occurrence of resistance genes to antibiotics, biocides and metals reveals novel insights into their co-selection potential. *BMC Genom.* **2015**, *16*, 964. [CrossRef] [PubMed]
46. Zhao, X.; Wang, J.; Zhu, L.; Wang, J. Field-based evidence for enrichment of antibiotic resistance genes and mobile genetic elements in manure-amended vegetable soils. *Sci. Total Environ.* **2019**, *654*, 906–913. [CrossRef]
47. Lao, C.K.; Tseng, M.-C.; Chiu, C.-H.; Chen, N.-Y.; Chen, C.-H.; Chung, W.-H.; Liu, T.-P.; Lu, J.-J.; Lai, H.-C.; Yang, L.-Y.; et al. Clinical manifestations and antimicrobial susceptibility of *Nocardia* species at a tertiary hospital in Taiwan, 2011–2020. *J. Formos. Med. Assoc.* **2022**, *121*, 2109–2122. [CrossRef]
48. Toyokawa, M.; Ohana, N.; Ueda, A.; Imai, M.; Tanno, D.; Honda, M.; Takano, Y.; Ohashi, K.; Saito, K.; Shimura, H. Identification and antimicrobial susceptibility profiles of *Nocardia* species clinically isolated in Japan. *Sci. Rep.* **2021**, *11*, 16742. [CrossRef]
49. Traxler, R.M.; Bell, M.E.; Lasker, B.; Headd, B.; Shieh, W.J.; McQuiston, J.R. Updated review on *Nocardia* species: 2006–2021. *Clin. Microbiol. Rev.* **2022**, *35*, e0002721. [CrossRef]
50. Zhao, P.; Zhang, X.; Du, P.; Li, G.; Li, L.; Li, Z. Susceptibility profiles of *Nocardia* spp. to antimicrobial and antituberculotic agents detected by a microplate Alamar Blue assay. *Sci. Rep.* **2017**, *7*, 43660. [CrossRef]
51. Caso Coelho, V.; Pereira Neves, S.D.A.; Cintra Giudice, M.; Benard, G.; Lopes, M.H.; Sato, P.K. Evaluation of antimicrobial susceptibility testing of *Nocardia* spp. isolates by broth microdilution with resazurin and spectrophotometry. *BMC Microbiol.* **2021**, *21*, 331. [CrossRef]
52. Prudhomme, C.; Joannard, B.; Lina, G.; De Launay, E.; Dumitrescu, O.; Hodille, E. Drug susceptibility testing of Nocardia spp. using the disk diffusion method. *Ann. Clin. Microbiol.* **2024**, *23*, 105. [CrossRef]
53. Hershko, Y.; Levytskyi, K.; Rannon, E.; Assous, M.V.; Ken-Dror, S.; Amit, S.; Ben-Zvi, H.; Sagi, O.; Schwartz, O.; Sorek, N.; et al. Phenotypic and genotypic analysis of antimicrobial resistance in *Nocardia* species. *J. Antimicrob. Chemother.* **2023**, *78*, 2306–2314. [CrossRef]

54. Kogure, T.; Shimada, R.; Ishikawa, J.; Yazawa, K.; Brown, J.M.; Mikami, Y.; Gonoi, T. Homozygous triplicate mutations in three 16S rRNA genes responsible for high-level aminoglycoside resistance in *Nocardia farcinica* clinical isolates from a canada-wide bovine mastitis epizootic. *Antimicrob. Agents Chemother.* **2010**, *54*, 2385–2390. [CrossRef] [PubMed]
55. Gnanam, H.; Rajapandian, S.G.K.; Gunasekaran, R.; Roshni Prithiviraj, S.; Ravindran, R.S.; Sen, S.; Prajna, L. Molecular identification of *Nocardia* species causing endophthalmitis using multilocus sequence analysis (MLSA): A 10-year perspective. *J. Med. Microbiol.* **2020**, *69*, 728–738. [CrossRef] [PubMed]
56. Hashemi-Shahraki, A.; Heidarieh, P.; Bostanabad, S.Z.; Hashemzadeh, M.; Feizabadi, M.M.; Schraufnagel, D.; Mirsaeidi, M. Genetic diversity and antimicrobial susceptibility of *Nocardia* species among patients with nocardiosis. *Sci. Rep.* **2015**, *5*, 17862. [CrossRef]
57. Tanzil, H.O.; Lintong, M. Differentiation of various nocardial species by susceptibility to nitrofurantoin. *Am. Rev. Respir. Dis.* **1971**, *104*, 438–439. [CrossRef] [PubMed]
58. Chylinski, K.; Makarova, K.S.; Charpentier, E.; Koonin, E.V. Classification and evolution of type II CRISPR-Cas systems. *Nucleic Acids Res.* **2014**, *42*, 6091–6105. [CrossRef]
59. Makarova, K.S.; Shmakov, S.A.; Wolf, Y.I.; Mutz, P.; Altae-Tran, H.; Beisel, C.L.; Brouns, S.J.J.; Charpentier, E.; Cheng, D.; Doudna, J.; et al. An updated evolutionary classification of CRISPR–Cas systems including rare variants. *Nat. Microbiol.* **2025**, *10*, 3346–3361. [CrossRef]
60. Tempel, S.; Bedo, J.; Talla, E. From a large-scale genomic analysis of insertion sequences to insights into their regulatory roles in prokaryotes. *BMC Genom.* **2022**, *23*, 451. [CrossRef]
61. Zoropogui, A.; Pujic, P.; Normand, P.; Barbe, V.; Belli, P.; Graindorge, A.; Roche, D.; Vallenet, D.; Mangenot, S.; Boiron, P.; et al. The *Nocardia cyriacigeorgica* GUH-2 genome shows ongoing adaptation of an environmental *Actinobacteria* to a pathogen's lifestyle. *BMC Genom.* **2013**, *14*, 286. [CrossRef]
62. Yang, R.; Liu, G.; Chen, T.; Li, S.; An, L.; Zhang, G.; Li, G.; Chang, S.; Zhang, W.; Chen, X.; et al. Characterization of the genome of a *Nocardia* strain isolated from soils in the Qinghai-Tibetan Plateau that specifically degrades crude oil and of this biodegradation. *Genomics* **2019**, *111*, 356–366. [CrossRef]

microorganisms

MDPI

Article

Construction and Functional Validation of a Cross-Niche Multifunctional Microbial Consortium for Straw-Returning Agricultural Systems

Shu Jia [1], Hang Qu [1], Bo Li [1], Jin Chu [2], Yinghua Juan [1], Yuehua Xing [1], Yan Liu [1], Hongjing Bao [1] and Wentao Sun [1,*]

[1] Institute of Plant Nutrition and Environmental Resources, Liaoning Academy of Agricultural Sciences, Shenyang 110161, China; jiashuin1987@126.com (S.J.); quhang8377@163.com (H.Q.); libocaas@163.com (B.L.); juanyong_001@sohu.com (Y.J.); lnzhsxyh@126.com (Y.X.); liuyan1980@163.com (Y.L.); baohjln@163.com (H.B.)
[2] Institute of Plant Protection, Liaoning Academy of Agricultural Sciences, Shenyang 110161, China; anthor0601@163.com
* Correspondence: wentaosw@163.com; Tel.: +86-18809808788

Abstract

Straw returning, a core practice in conservation tillage, promotes sustainable intensification; however, it faces challenges such as inefficient decomposition, nutrient competition, and pathogen accumulation. To address these limitations, this study aimed to develop a multifunctional microbial consortium specifically designed for straw-incorporating cropping systems. The consortium comprises four *Bacillus* strains with complementary enzymatic systems, isolated from diverse ecological niches. It exhibited robust lignocellulolytic enzyme production, with manganese peroxidase (7709.33 U/L), laccase (450.65 U/L), endo-β-1,4-glucanase (154.67 U/mL), and filter paper activity (309.18 U/L). The consortium significantly enhanced rice straw degradation by 37.18% and increased nitrogen (N) release by 16.13% compared to the control. Moreover, the consortium exhibited a 67.56% inhibition rate against *Magnaporthe oryzae* and reduced both the incidence rate and disease index of leaf blast and panicle blast. Field trials revealed increases in the rice grain yield of 9.63% and 6.94% when applied alone and 6.75% and 5.18% when co-applied with straw residues. These findings highlight the multifunctional agricultural potential of the consortium and provide a sustainable strategy to overcome the limitations of straw-incorporating farming systems.

Keywords: multifunctional microbial consortium; lignocellulose decomposition; enhanced nitrogen release; biocontrol; yield enhancement

1. Introduction

Crop straw is a highly valuable renewable resource, with global production reaching approximately 3.5 billion metric tons annually. It serves as an important source of organic fertilizer in agricultural ecosystems [1]. Straw return, a core measure in conservation tillage, mitigates the environmental pollution caused by open burning or improper disposal and reduces dependence on synthetic fertilizers, supporting sustainable agricultural intensification [2]. Previous studies have demonstrated that incorporating straw into soil enhances soil organic carbon sequestration, improves aggregate stability, and optimizes C–N cycling, thereby sustaining long-term soil fertility and productivity [3]. However, straw incorporation poses several technical challenges.

During straw decomposition, microbes compete with crops for nitrogen, leading to temporary nitrogen immobilization in the soil. Furthermore, the high carbon-to-nitrogen (C/N) ratio of straw reduces decomposition rates and nutrient release, resulting in a temporal mismatch between nutrient availability and crop demand [4]. This asynchrony causes transient nitrogen deficiency, which adversely affects crop growth and yield. Additionally, untreated crop straw may harbor pathogenic microorganisms and pest eggs. Straw return creates a favorable environment for certain plant pathogenic fungi by providing abundant nutrient substrates, promoting their proliferation [5]. For instance, a previous study reported that straw retention for three years significantly increased the abundance of *Magnaporthe oryzae* and *Ustilaginoidea virens* [6]. Similarly, long-term (10-year) crop residue retention significantly increased populations of *Fusarium graminearum* and *Fusarium moniliforme*, thereby increasing the risk of disease outbreaks [7].

The use of microbial inoculants can effectively alleviate these challenges. The combined application of crop straw and microbial decomposer inoculants enhances straw decomposition efficiency, facilitates nutrient release, and improves soil nutrient availability, thereby reducing microbial immobilization of soil nitrogen (N) [8]. Furthermore, the co-application of straw with biocontrol agents suppresses the relative abundance of phytopathogenic fungi and reduces seedling damage caused by pathogenic fungi [9]. Additionally, plant growth-promoting rhizobacteria (PGPR) enhance nutrient cycling through biological nitrogen fixation (e.g., *Rhizobium* spp. and *Azotobacter* spp.) and phosphate solubilization (e.g., *Pseudomonas* spp. and *Bacillus* spp.), thereby improving crop yields [10]. By systematically integrating these complementary functional traits, microbial consortia can be rationally engineered to effectively overcome the key limitations of straw-incorporating agricultural systems.

The development of multifunctional microbial consortia necessitates a prioritized examination of the functional compatibility among artificially combined strains. Furthermore, introduced strains are often subject to environmental stressors and competition from native microbiota, leading to target gene suppression and reduced functional performance. Based on the principles of multisource synergistic compensation (i.e., combining strains from different sources to enhance overall function) and enzymatic functional complementarity (i.e., using enzymes with non-overlapping activities for sequential substrate degradation), this study aimed to construct a novel multifunctional microbial consortium by integrating functional microorganisms from three distinct ecosystems (soil, insect gut, and animal biogas slurry). The performance of the consortium in lignocellulose decomposition, pathogen suppression, and yield enhancement was systematically evaluated. This study provides a sustainable strategy for the safe and efficient utilization of agricultural waste, contributing to the circular bioeconomy of agroecosystems.

2. Materials and Methods

2.1. Strains, Variety, and Experimental Site Description

M. oryzae, *Rhizoctonia solani*, *U. virens*, and *Fusarium fujikuroi* were provided by the Rice Disease Research Laboratory, Institute of Plant Protection, Liaoning Academy of Agricultural Sciences. The rice (*Oryza sativa* L.) cultivar utilized was Liaojing 327, and the rice seedlings were provided by the Liaoning Rice Research Institute, Liaoning Academy of Agricultural Sciences.

The study was conducted in Shimiaozhi Village (123°34′58″ E, 41°47′24″ N), Wangjia Township, Hunnan District, Shenyang City, Liaoning Province, China. This region has a temperate monsoon climate, with an average annual precipitation of 650 mm, a mean annual temperature of 6.2–9.7 °C, and a frost-free period of 155–180 d. The test soil was classified as hydragric anthrosol, with the following physicochemical properties in the

https://doi.org/10.3390/microorganisms14010135

surface layer (0–20 cm): pH, 5.81; soil organic carbon (SOC), 14.81 g/kg; total nitrogen (TN), 1.09 g/kg; total phosphorus (TP), 0.51 g/kg; total potassium (TK), 17.43 g/kg; alkali-hydrolyzable nitrogen (AN), 20.33 mg/kg; available phosphorus (AP), 7.40 mg/kg; and available potassium (AK), 71.10 mg/kg.

2.2. Screening of Straw Degradation Strains

Screening medium: Monoclonal strains from pure cultures were inoculated into Congo red cellulose medium and aniline blue medium [11] and cultured at 20 °C for 7 d. The colony diameter and the diameter of the surrounding transparent circle were measured, and the experiment was repeated three times.

The lignocellulolytic enzyme activity of a 1% inoculum of the candidate strain fermentation broth (10^7 CFU/mL) was transferred into 100 mL of a lysogeny broth (LB) and potato dextrose agar (PDA) liquid medium. Cultures were incubated at 20 °C with shaking at 150 rpm for 3 d. A 5 mL sample of the solution was aseptically collected from each flask and centrifuged at 4 °C and 12,000× *g* for 20 min. The supernatant was collected for further analysis. The activities of manganese peroxidase (MnP, Kit catalog numbers: MNP-W96S-N), laccase (Kit catalog numbers: LAC-W48S-N), endo-β-1,4-glucanase (Kit catalog numbers: CL-W48S-N), and filter paperase (FPA, Kit catalog numbers: FPA-W48S-N) were measured according to the manufacturer's instructions (Mlbio (Shanghai) Co., Ltd., Shanghai, China). As a comprehensive indicator of cellulose-degrading capability, FPA effectively reflects the strain's overall cellulolytic potential. And MnP serves as the primary enzymatic system for lignin depolymerization, while laccase contributes to lignin decomposition, ultimately forming complex humic substances during straw decomposition processes [12]. Cellulase activity typically represents a synergistic multi-enzyme complex. In this study, we measured endo-β-1,4-glucanase activity, a key component of the native cellulase complex, using a commercial assay kit with carboxymethyl cellulose (CMC) as the substrate. One unit of enzyme activity (U) is defined as the amount of enzyme required to catalyze the production of 1 μg of glucose per minute per milliliter of culture filtrate. FPA reflects the synergistic action of multiple cellulase components, including endoglucanase, exoglucanase, and β-glucosidase. Enzymatic activity is defined as the amount of enzyme required to release 1 mg of glucose per minute from filter paper per milliliter of culture filtrate under the conditions of 50 °C and pH 4.6.

Straw decomposition rate: The weight-loss method was used to determine the degradation rate of rice straw by the candidate strains [13]. Rice straw was rinsed thoroughly with clean water and dried at 80 °C until a constant weight was achieved. A total of 10 g of dried straw was placed in a sterilized Erlenmeyer flask, followed by the addition of 10 mL of the candidate strain fermentation broth (10^7 CFU/mL) and 100 mL of sterile water. The mixture was incubated at 20 °C for 15 d. The straw degradation rate was calculated as follows:

$$\text{Straw decomposition rate } (\%) = \frac{Mo - Mt}{Mo} \times 100\%$$

where *Mo* is the dry weight of the added straw, and *Mt* is the dry weight of the straw at decomposition time *t*.

2.3. Screening of Antagonistic Strains Against Rice Pathogens

The plate confrontation method [14] was used to determine the antagonistic activity of the candidate strains against rice pathogens. Approximately 5 mm pathogen disks were placed at the center of a 90 mm diameter PDA plate, and bacteria were inoculated 25 mm from the center. In the controls, 5 mm pathogen disks were placed at the center of a 90 mm diameter PDA plate. Plates were cultured at 28 °C until the fungus in the control plate

https://doi.org/10.3390/microorganisms14010135

covered the entire plate. Antagonistic activity was evaluated using the inhibition rate (*IR*), calculated using the following formula:

$$\text{IR}\ (\%) = \frac{(D-5)-(d-5)}{D-5} \times 100\%$$

where D is the diameter of the pathogen disks in the control treatment, d is the diameter of the pathogen disks with antagonistic bacteria, and 5 is the diameter (mm) of the disks inoculated with the pathogens.

2.4. Inter-Strain Antagonism Assessment

Candidate strains demonstrating strong antagonistic activity, high lignocellulolytic enzyme production, and high straw decomposition efficiency were selected for compatibility assessment. Bacterial interactions were analyzed using LB agar cross-streak assays, and fungal compatibility was assessed using a PDA dual culture. Bacterial–fungal interactions were examined through PDA co-cultivation, with inhibition zones as phenotypic indicators.

2.5. Construction of the Multifunctional Microbial Consortium

Seed cultures of the selected strains at 10^7 CFU/mL were inoculated into LB liquid medium at a 1:1 ratio and incubated at 20 °C with shaking at 150 rpm for 3 d. Lignocellulolytic enzyme activities and straw degradation rates of the resulting microbial consortia were measured. The toxic medium method [15] was used to determine the antibacterial activity of the multifunctional consortium against pathogenic fungi.

2.6. Identification of Strains

Strains were identified based on morphological observations and molecular identification. Selected strains were inoculated onto LB plates using the continuous streaking method and incubated at 20 °C for 1 d. Colony growth and morphological characteristics were also recorded. The strains were identified using 16S rDNA and *gyrB* gene sequences. Genomic DNA was extracted using a bacterial genomic DNA FastPrep extraction kit (Sangon Biotech, Shanghai, China). DNA was quantified using a NanoDrop ND100 spectrophotometer (Thermo Fisher Scientific, Waltham, MA, USA) and stored at −20 °C. The primer sequences, polymerase chain reaction (PCR) mixtures, and conditions used are provided in Supplementary Table S1. The amplified products were sequenced by Sangon Biotech (Shanghai, China). The 16S rDNA and *gyrB* genes were sequenced using the Sanger method on an ABI 3730XL DNA analyzer (Foster City, CA, USA). The sequencing results were subjected to BLAST (https://www.ncbi.nlm.nih.gov/, accessed on 8 October 2025) analysis against nucleotide sequences from the GenBank database, using *Escherichia coli* as the external reference. Multiple sequence alignment with closely related *Bacillus* strains and similarity calculations were performed using CLUSTAL X [16]. Phylogenetic trees were constructed using MEGA 6.0 [17] using the neighbor-joining method with 1000 bootstrap replicates [18].

2.7. Pathogen Inhibition Test of the Microbial Consortium

Pot experiments were conducted in early April to assess the effectiveness of the microbial consortium in controlling *M. oryzae*, the causative agent of rice blast. The experimental treatments included (1) RS + *M. oryzae*: rice straw + *M. oryzae*, and (2) RS + *M. oryzae* + CG: rice straw + *M. oryzae* + microbial consortium. The pots used had dimensions of 40 cm (length) × 60 cm (width) × 28 cm (height). The rice straw application rate was set at 9000 kg·ha^{-1}, which corresponded to 0.21 kg of straw per pot based on the pot area. The straw was finely chopped and inoculated with the pathogen at a concentration of 1×10^5 CFU/mL, with an inoculation volume of 100 mL. Subsequently, the microbial

https://doi.org/10.3390/microorganisms14010135

consortium fermentation broth was inoculated at a concentration of 1×10^6 CFU/mL, with an inoculation volume of 210 mL. The inoculated straw was thoroughly mixed with 40 kg of soil and placed into the pots.

Rice seedlings were transplanted on May 28, with two rows per pot, four hills per row, and three seedlings per hill. Soil samples from the three pots were collected at 10, 20, 30, 50, 70, 100, and 170 d post-inoculation for quantitative real-time PCR (qRT-PCR) analysis to determine the abundance of *M. oryzae*. The primer sequences, PCR systems, and conditions are listed in Supplementary Table S1. The incidence, disease index, and control efficacy of leaf blast and panicle blast were evaluated at the late tillering (70 d) and maturity (170 d) stages. The grading criteria for leaf blast and neck blast were adopted from Tan et al. [19]. The disease incidence rate (*DIR*), disease index (*DI*), and control efficacy (*CE*) were calculated as follows:

$$DIR = \frac{n}{N} \times 100;\ DI = \frac{[\Sigma(Ni \times i)]}{N \times 4} \times 100;\ CE\ (\%) = \frac{DI_{CK} - DI_T}{DI_{CK}} \times 100$$

where n is the number of infected plants, N is the total number of investigated plants, Ni is the number of infected plants at a given severity level, i is the severity level, DI_{CK} is the disease index of the control, and DI_T is the disease index of the treatment.

2.8. Functional Evaluation of the Microbial Consortium for Straw Degradation and Yield Enhancement

A field microplot experiment was conducted from April 22 to October 11. Four treatments were established: (1) CK, blank control; (2) RS, rice straw only; (3) CG, microbial consortium only; and (4) RS + CG, rice straw + microbial consortium. Each plot measured 5×6 m (30 m^2), with three replicates per treatment. The rice straw application rate was set at 9000 kg·ha^{-1}, with 27 kg of straw applied per plot. The rice straw was chopped into 3–5 cm segments and evenly spread on the surface of the paddy field. A composite microbial consortium was applied at a dosage of 1.25 L, followed by uniform application of 90 g of urea. Straw was incorporated into the soil through rotary tillage, and the field was subsequently flooded. Water was managed using alternating wet and dry irrigation practices. Transplantation was conducted on May 28 at a spacing of 30 cm × 18 cm. Next, 10 g of rice straw was placed in mesh bags and buried in the soil of treatment groups 2 and 4. At 10, 20, 30, 50, 70, 100, and 170 d, three treatments were randomly sampled to calculate the decomposition rates of rice straw [13] as well as the release rates of nitrogen (N), phosphorus (P), and potassium (K) [20,21]. During the tillering stage, plant height and tiller number were measured for ten fixed rice hills in each plot using a fixed-point sampling method. Harvesting was conducted on October 11. A 1 m^2 area was randomly selected from each plot to determine rice yield. Additionally, three hills of rice plants were sampled to assess yield components, including plant height, effective panicle number, 1000-grain weight, grain number per panicle, and percentage of unfilled grains.

3. Results

3.1. Screening of Multifunctional Strains

Primary screening of 1295 bacterial and 32 fungal isolates on selective media identified 135 bacteria and 10 fungi that produced hydrolytic zones. Based on quantitative clearance zone measurements (Figure 1A,B; Supplementary Tables S2 and S3), strains exhibiting a decolorization halo diameter exceeding 40 mm on CMC-Na medium and 10 fungal strains were selected for secondary screening, and non-hydrolytic isolates were excluded from further characterization.

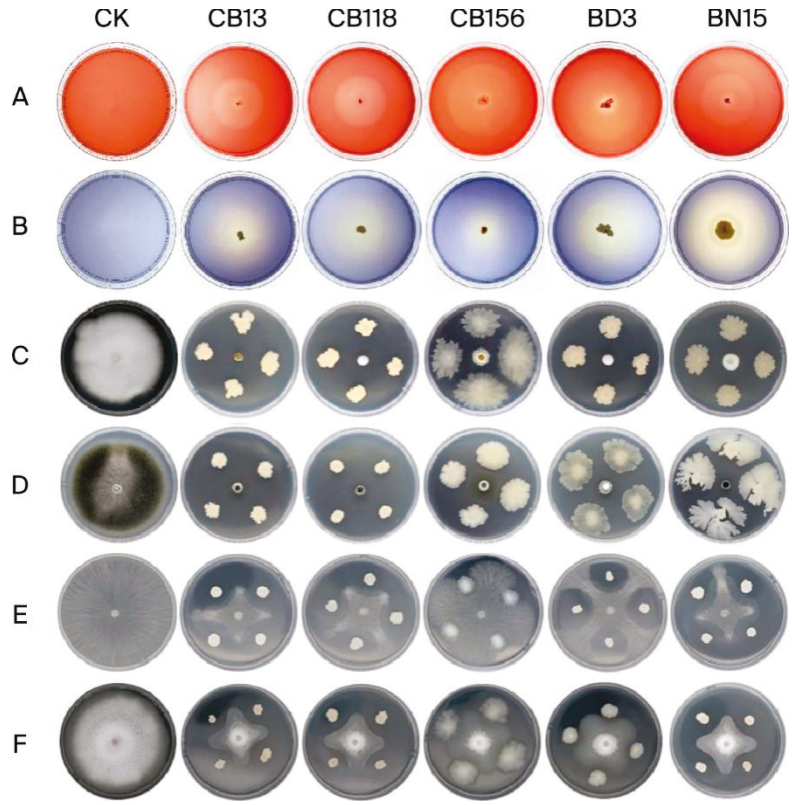

Figure 1. Colony and degradation cycles of some strains screened on cellulose Congo red medium (**A**) and aniline blue medium (**B**), and the antifungal effects of the partial strains against different rice pathogens. CK: blank control; (**C**) *Ustilaginoidea virens*; (**D**) *Magnaporthe oryzae*; (**E**) *Rhizoctonia solani*; (**F**) *Fusarium fujikuroi*.

Secondary screening identified BD3 as the most potent cellulolytic strain (Table 1), showing peak filter paper activity (FPA: 306.80 U/L) and straw degradation efficiency (24.7%) in a 15 d continuous reaction, reflecting a 41.4% improvement over the control (17.47%). Strain BN15 exhibited exceptional ligninolytic specialization, showing maximal MnP (4405.33 U/L) and laccase (438.31 U/L) activities, whereas CB118 displayed superior endo-β-1,4-glucanase production (157.53 U/mL). The fungal isolates demonstrated comparatively reduced cellulolytic performance, which was consistent with their enzymatic activity profiles.

Table 1. Enzyme activities and straw degradation rates of partial strains.

Isolates	MnP (U/L)	Laccase (U/L)	endo-β-1,4-glucanase (U/mL)	FPA (U/L)	Straw Degradation Rate (%)
CB118	275.33 ± 0.00	222.24 ± 21.38	157.53 ± 11.96	120.88 ± 16.57	21.50 ± 0.44
BD3	1101.33 ± 275.22	246.93 ± 37.55	81.28 ± 2.81	306.80 ± 41.09	24.70 ± 0.35
BN15	4405.33 ± 430.08	438.31 ± 12.35	81.38 ± 4.14	181.47 ± 21.85	22.90 ± 0.38
CB156	1376.67 ± 275.22	327.19 ± 34.37	69.02 ± 12.78	236.71 ± 30.62	23.60 ± 0.67
CB13	0.00	141.99 ± 6.17	139.81 ± 2.12	116.13 ± 26.48	19.00 ± 0.85

MnP: manganese peroxidase; FPA: filter paperase.

The bacterial strains CB13, CB118, CB156, BD3, and BN15 exhibited broad-spectrum inhibitory effects against major rice pathogens (Supplementary Table S4; Figure 1C–F). Strain CB13 exhibited the strongest antagonistic activity against rice pathogenic fungi, with suppression rates of 96.49% against *U. virens*, 92.68% against *M. oryzae*, 66.33% against *R.*

solani, and 69.62% against *F. fujikuroi*. Notably, the fungal isolates showed no measurable antagonistic effects against the tested pathogens.

3.2. Inter-Strain Antagonism Assessment

Based on a comprehensive evaluation of cellulolytic activity, rice straw decomposition efficiency, and antifungal activity against major rice pathogens, BD3, BN15, CB156 and CB118 showed superior lignocellulolytic enzyme activity and straw degradation efficiency. Strains CB13 and PY1 exhibited strong antagonistic activity against rice pathogenic fungi. For fungal strains, FH2, FH5, FF2, and FF3 showed superior lignocellulolytic enzyme activity and straw degradation efficiency.

Therefore, six bacterial strains and four fungal strains were subjected to inter-strain antagonism assays (Supplementary Table S5). Widespread antagonistic interactions were observed between candidate bacterial and fungal strains. The results revealed that strain PY1 exhibited antagonistic activity against nine other candidate strains. Bidirectional antagonistic interactions between CB118 and CB13 were also observed. Based on these results, strains CB156, BD3, and BN15 were selected to establish a core microbial consortium that demonstrated complementary enzymatic profiles. Notably, despite their mutual antagonism, strains CB13 and CB118 were retained as candidate strains for optimized composite formulations because of their individual endo-β-1,4-glucanase and antifungal activities.

3.3. Construction of a Multifunctional Microbial Consortium

Strain consortium screening revealed that the CB156 + BD3 + BN15 consortium exhibited superior lignocellulolytic enzyme production, achieving 24.88% straw degradation (Figure 2). Subsequent supplementation with CB13 further enhanced the consortium's enzymatic profile, yielding 7709.33 U/L (MnP), 450.65 U/L (laccase), 154.67 U/mL (endo-β-1,4-glucanase), and 309.18 U/L (FPA). This optimized consortium (CB156 + BD3 + BN15 + CB13) demonstrated a 24.90% straw degradation efficiency within 15 d, a 53.7% increase compared to the controls (16.20%). Notably, CB118 supplementation significantly impaired endo-β-1,4-glucanase activity ($p < 0.05$), FPA, and decomposition rates. Finally, CB156 + BD3 + BN15 + CB13 was identified as the optimal composition for the multifunctional microbial consortium. The sterile filtrates of the consortium showed broad-spectrum antifungal activity, suppressing pathogens by 73.95% (*M. oryzae*), 54.65% (*F. fujikuroi*), 39.56% (*U. virens*), and 29.98% (*R. solani*).

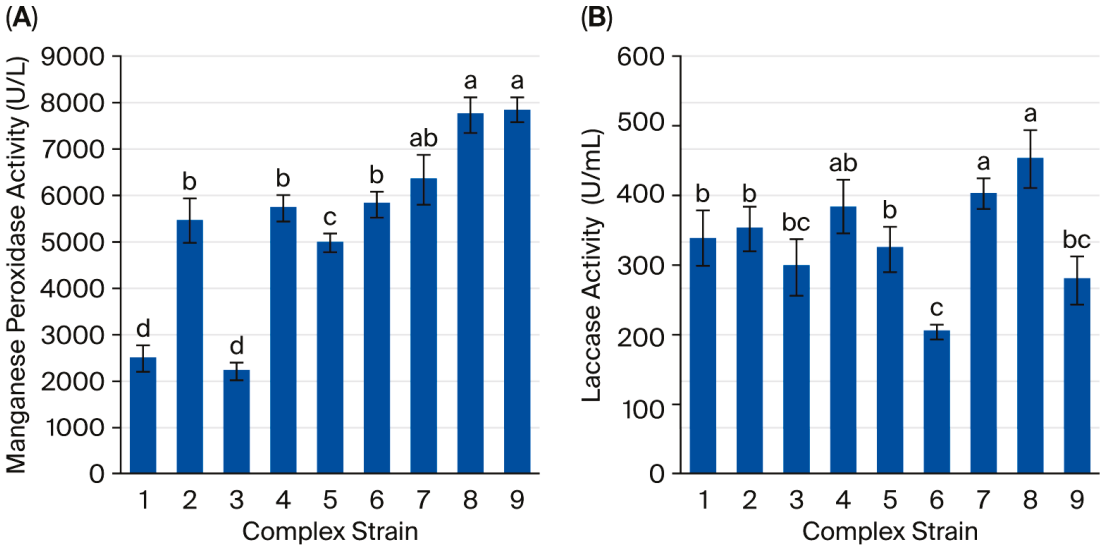

Figure 2. *Cont.*

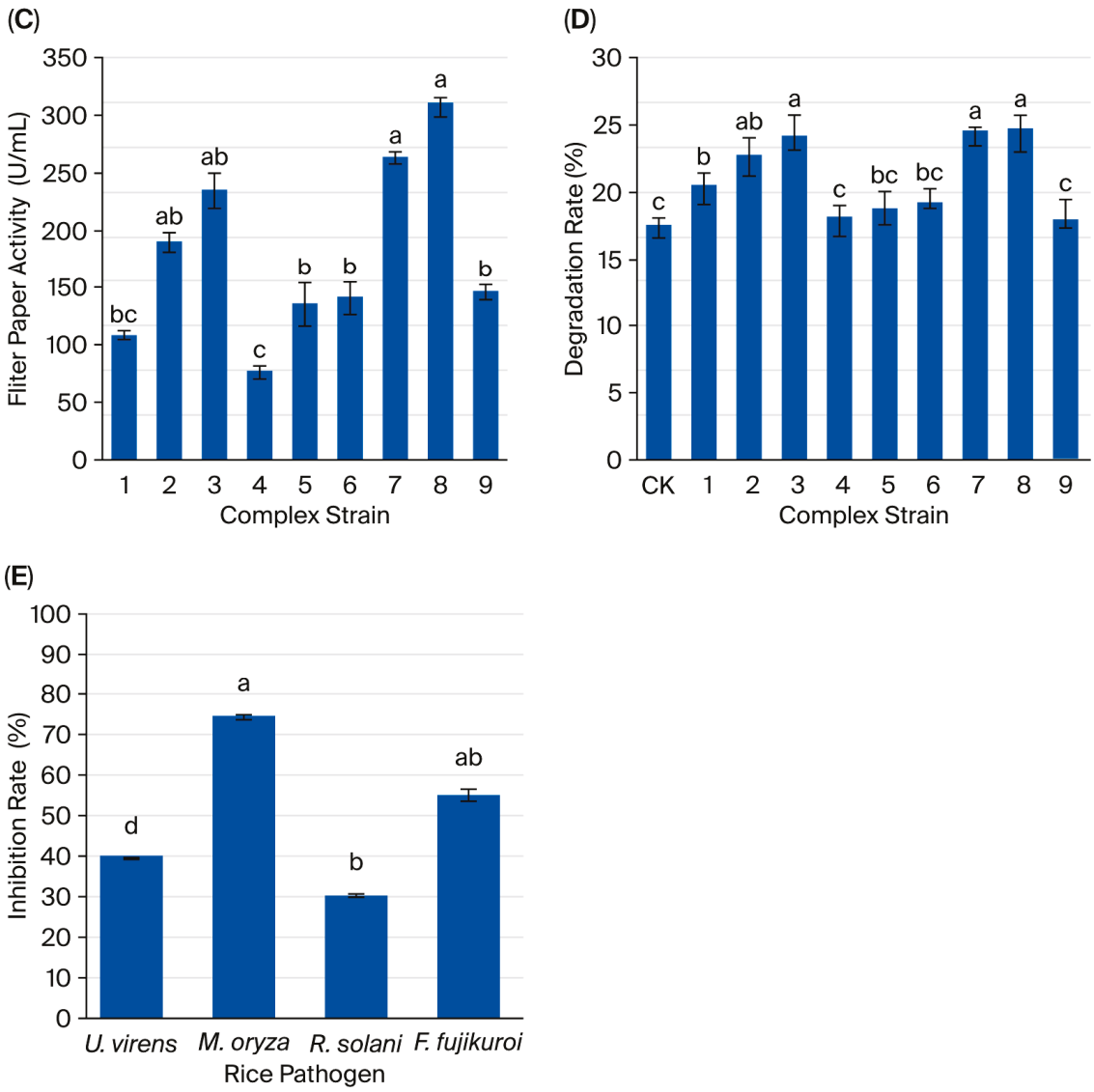

Figure 2. The enzymatic activities (**A**–**C**) and rice straw degradation rates (**D**) of different microbial consortia, and the inhibitory rates of the optimal microbial consortium against rice pathogenic fungi (**E**). (1) CB156; (2) BN15; (3) BD3; (4) BN15 + CB156; (5) BN15 + BD3; (6) CB156 + BD3; (7) BN15 + CB156 + BD3; (8) BN15 + CB156 + BD3 + CB13; and (9) BN15 + CB156 + BD3 + CB118. *U. virens*: *Ustilaginoidea virens*; *M. oryzae*: *Magnaporthe oryzae*; *R. solani*: *Rhizoctonia solani*; *F. fujikuroi*: *Fusarium fujikuroi*. Each value represents the mean ± standard error of values from three replicates per treatment. The different letters above the error bars indicate significant differences according to Duncan's test ($p < 0.05$).

3.4. Identification of Strains

Based on the culture characteristics, colony morphology on LB medium (Table 2), and neighbor-joining phylogenetic tree based on 16S rRNA gene and *gyrB* (Figure 3). The phylogenetic analysis based on the NCBI BLAST alignment revealed that strain BD3 clustered with *B. velezensis*, strain CB156 with *Bacillus amyloliquefaciens*, and strain BN15 with *Bacillus halotolerans*. Accordingly, the strains were taxonomically designated *B. velezensis* BD3, *B. amyloliquefaciens* CB156, and *B. halotolerans* BN15. Strain CB13 has been previously identified as *Bacillus velezensis* based on prior characterization [22]. The gene sequences of strains CB156, BD3, and BN15 were deposited in GenBank (accession numbers listed in Table 2).

Table 2. Colony morphology and identification results.

Strain Number	Colony Characteristics	Colony Morphology	The NCBI Registration Number	Strain Identified
CB13	Oval Milky-white Opaque Wrinkled surface Smooth edges		16S rRNA: OP430814 *gyr B*: OP889277	*Bacillus velezensis*
CB156	Oval Milky-white Opaque Smooth edges	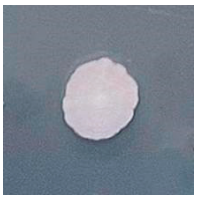	16S rRNA: PP809059 *gyr B*: PX767074	*Bacillus amyloliquefaciens*
BD3	Oval White Opaque Wrinkled surface Smooth edges		16S rRNA: PP033752 *gyr B*: PX767075	*Bacillus velezensis*
BN15	White Opaque Wrinkled surface Irregular edges		16S rRNA: PP809060 *gyr B*: PX767076	*Bacillus halotolerans*

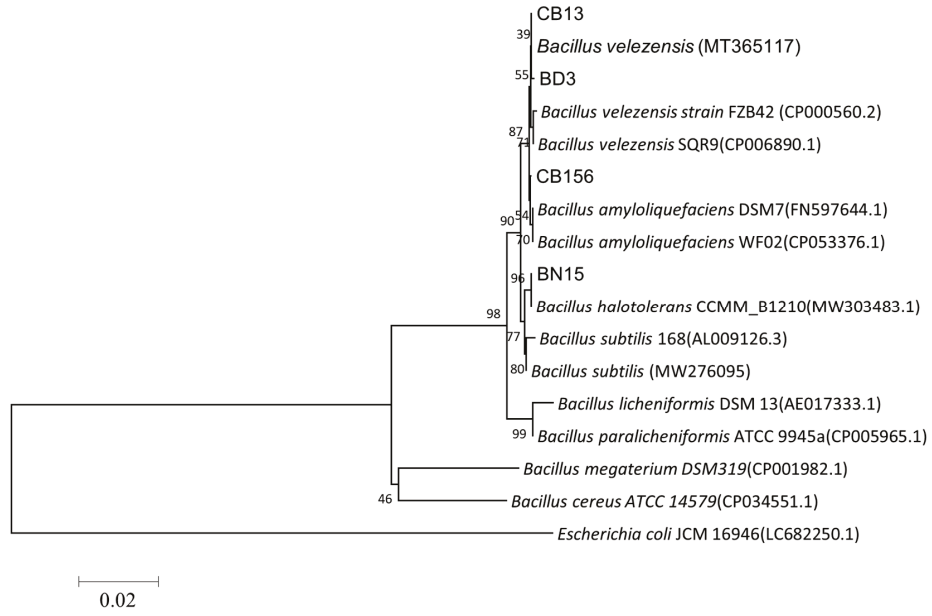

Figure 3. The phylogenetic tree based on 16S rRNA gene and *gyrB* gene sequence of the strains. The phylogenetic trees were constructed with the neighbor-joining method using the software package Mega, version 6.0, after multiple sequence alignments using Clustal X. GenBank accession numbers of bacterial strains are shown in parentheses. The number at each branch is the percentage of times the group of strains in that branch occurred, based on 1000 cycles, via bootstrap analysis.

3.5. Pathogen Inhibition by the Microbial Consortium Against M. oryzae

During the initial 10–30 d of straw incorporation, no significant difference in *M. oryzae* genomic copy number was observed between the two treatments ($p > 0.05$; Figure 4A). However, from 50 to 170 d of straw incorporation, the RS + *M. oryzae* + CG treatment resulted in a significantly lower *M. oryzae* genomic copy number than the RS + *M. oryzae* treatment ($p < 0.05$), demonstrating strong suppression of *M. oryzae* in the straw by the microbial consortium. By day 170, the inhibition rate had reached 67.57%.

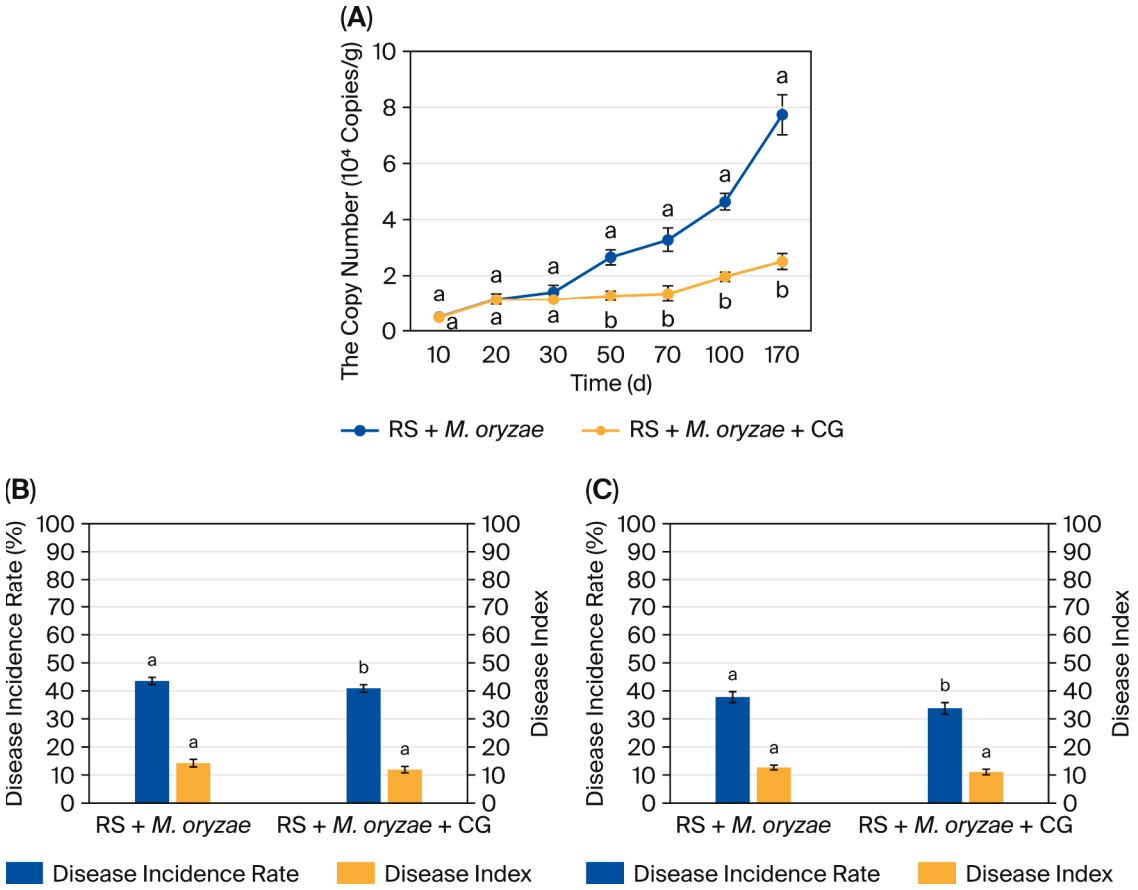

Figure 4. The inhibition rate of the microbial consortium against *Magnaporthe oryzae* (**A**) and the control efficacy against leaf blast (**B**) and panicle blast (**C**). Each value represents the mean ± standard error of values from three replicates per treatment. The different letters above the error bars indicate significant differences according to Duncan's test ($p < 0.05$). RS+ *M. oryzae*: rice straw + *M. oryzae*; RS+ *M. oryzae* + CG: rice straw + *M. oryzae* + microbial consortium.

The microbial consortium treatment also reduced the incidence rate and disease index of leaf blast and panicle blast (Figure 4B,C). At the late tillering stage, the incidence rate and disease index of leaf blast were 43.23% and 14.28% in the RS + *M. oryzae* treatment, whereas the RS + *M. oryzae* + CG treatment showed lower values (40.63% and 11.66). At the maturity stage, the incidence rate and disease index of panicle blast were 37.58% and 16.63% in the RS + *M. oryzae* treatment, compared with 33.54% and 10.88% in the RS + *M. oryzae* + CG treatment.

3.6. Straw Decomposition by the Microbial Consortium

During the tillering and heading stages (30–100 d), straw degradation in the RS + CG treatment was significantly higher than that in the control (RS) ($p < 0.05$; Figure 5A,B). At peak decomposition (day 70), the RS + CG treatment achieved a 54.87% degradation rate, an increase of 14.87 percentage points over RS (a 37.18% improvement over the

control). By maturity (day 170), decomposition rates reached statistically equivalent levels (RS + CG: 62.77% vs. RS: 59.80%, $p > 0.05$). During the initial decomposition phase (10 days post incorporation), no significant treatment-related differences in degradation efficiency were observed ($p > 0.05$). However, the RS + CG treatment exhibited significantly enhanced degradation efficiency compared with RS during the active decomposition phase (20–70 d) ($p < 0.05$). This period corresponds to accelerated microbial activity and cellulose breakdown. In the later stabilization phase (100–170 d), degradation rates progressively declined, with no significant inter-treatment differences observed ($p > 0.05$), suggesting the convergence of decomposition processes as labile fractions were depleted.

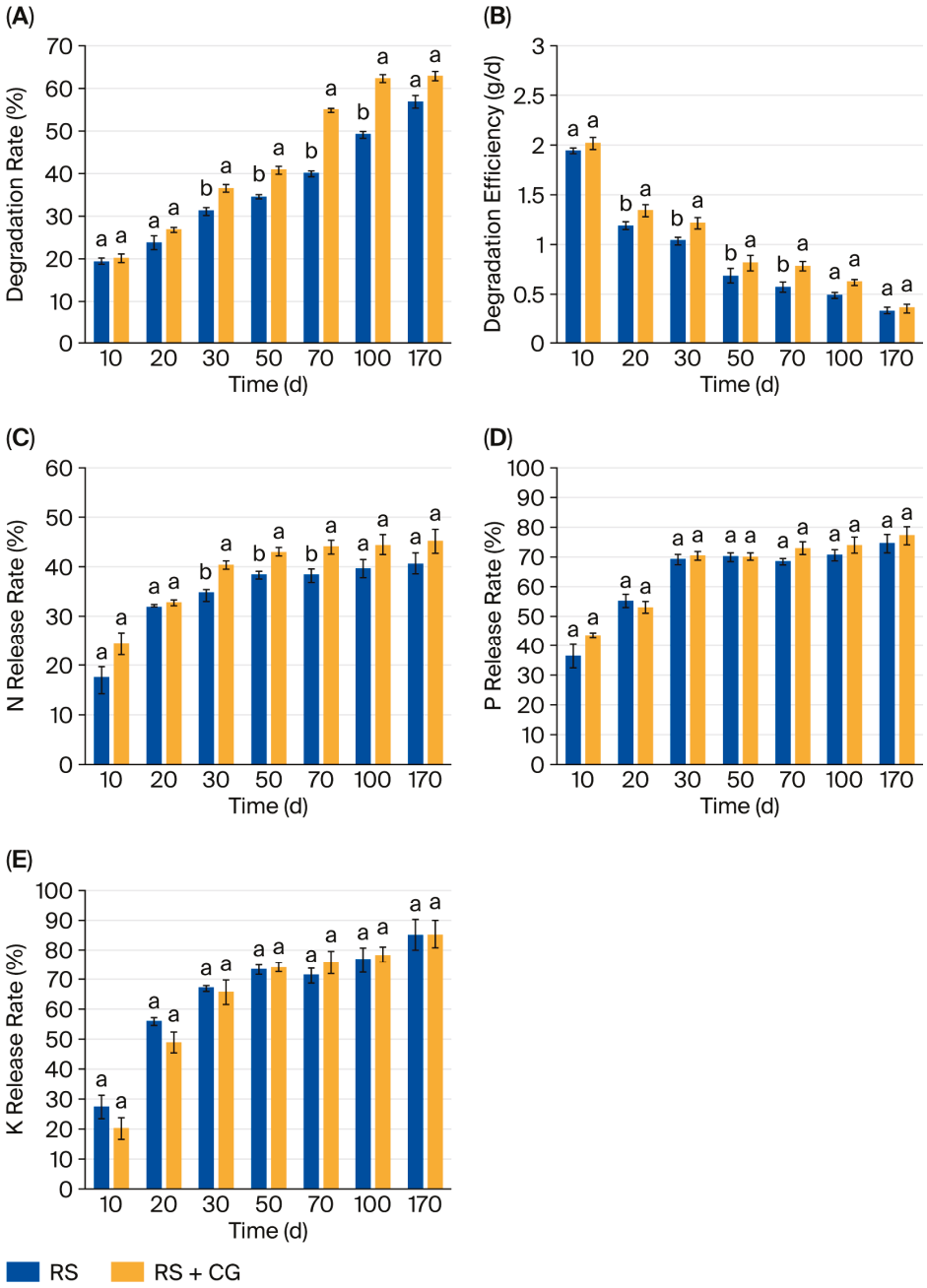

Figure 5. Degradation rates (**A**) and efficiency (**B**) of straw components by the composite microbial consortium, and the release rate of N (**C**), P (**D**), and K (**E**) from straw degradation. Each value represents the mean ± standard error of values from three replicates per treatment. The different letters above the error bars indicate significant differences according to Duncan's test ($p < 0.05$). RS: rice straw only; RS + CG: rice straw + microbial consortium.

Straw nutrient analysis demonstrated that the RS + CG treatment significantly increased the nitrogen (N) release rate compared to the RS treatment ($p < 0.05$; Figure 5C–E), whereas no statistically significant effects were observed on the release rates of phosphorus (P) or potassium (K) ($p > 0.05$). The microbial consortium accelerated N release, achieving a cumulative release rate of 40.42% by day 30, accounting for 89.38% of the total N release. During days 30–70, the N release rate in the RS + CG treatment was significantly higher than in the control, exceeding it by 4.66–5.75 percentage points (a 12.16–16.13% increase). This early-phase nutrient availability facilitates N supply during critical growth stages (tillering and heading) in rice. By day 170, the final N release rate had reached 45.22% in the RS + CG treatment, compared to 40.51% in the control.

3.7. Crop Yield Promotion by the Microbial Consortium

Rice growth parameters were monitored during the tillering stage (Figure 6). Although no significant differences in plant height were observed across the treatments ($p > 0.05$), the CG treatment significantly increased tiller production compared to the control ($p < 0.05$). In 2024, at the late tillering stage, the CG plants developed 25.9 tillers per hill versus 22.0 in the CK plants, representing a 17.7% increase. Although both RS and RS + CG treatments produced numerically more tillers than CK, these differences were not statistically significant ($p > 0.05$). In 2025, no significant differences in tiller number were detected across treatments ($p > 0.05$).

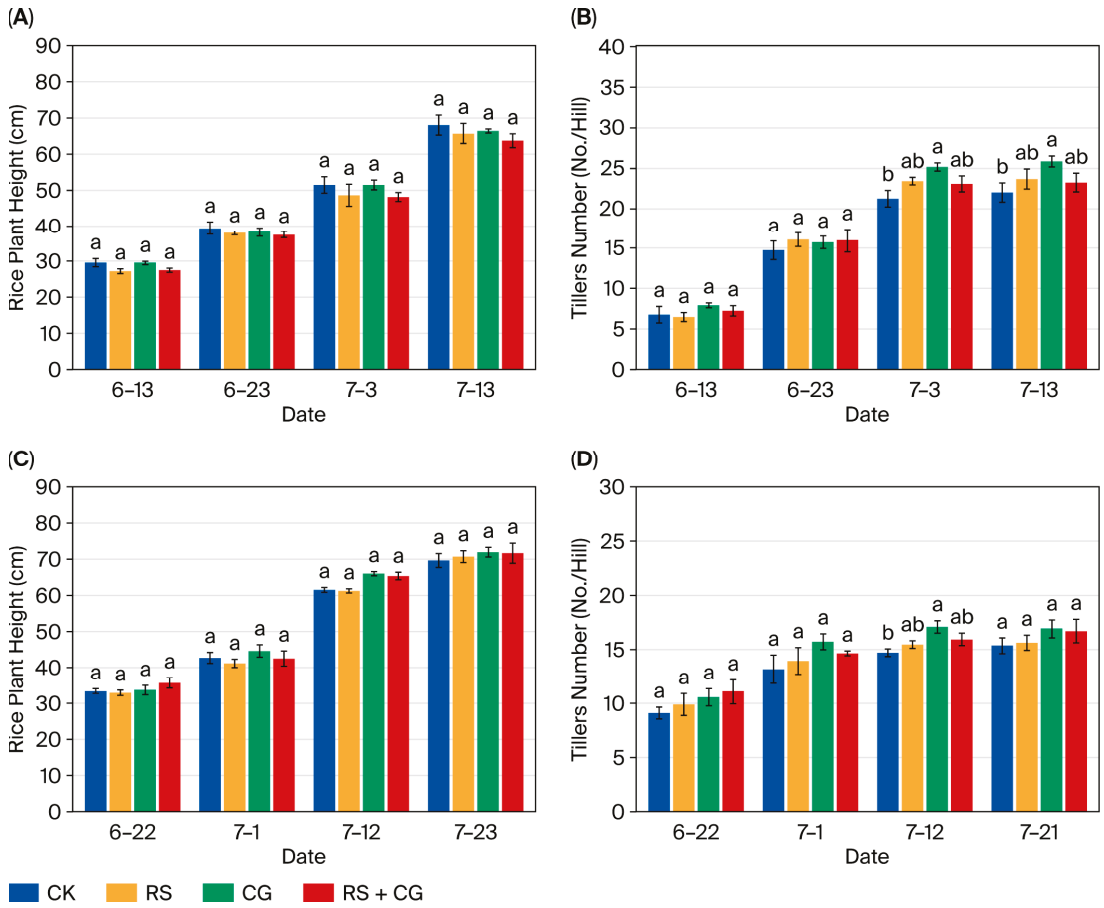

Figure 6. Dynamic changes in rice plant height (**A**,**C**) and tiller numbers (**B**,**D**) under different treatments. Each value represents the mean ± standard error of values from three replicates per treatment. The different letters above the error bars indicate significant differences according to Duncan's test ($p < 0.05$). CK: blank control; RS: rice straw only; CG: microbial consortium only; RS + CG: rice straw + microbial consortium.

The yield performance analysis (Tables 3 and 4) revealed that the CG treatment achieved the highest agronomic productivity, demonstrating 9.63% and 6.94% higher grain yields and effective panicle numbers, respectively, than CK. These results confirm the growth-promoting and yield-enhancing potential of the microbial consortium. By contrast, straw incorporation without microbial amendment (RS) resulted in the lowest productivity metrics. This reduction was attributed to the temporal overlap between straw decomposition and critical rice growth stages (tillering and heading), which induced microbial–crop competition for nitrogen, leading to nitrogen limitation during panicle initiation. However, later-stage nutrient release from straw decomposition improved grain-filling parameters (grains per panicle and 1000-grain weight). These compensatory effects partially offset the early growth penalty, resulting in a 2.08% and 5.68% yield reduction relative to CK. Importantly, microbial inoculation (RS + CG) effectively mitigated these adverse effects, increasing effective panicle numbers and providing a 6.75% and 5.18% yield improvement over the straw-only treatment through optimized nutrient cycling.

Table 3. Effects of different treatments on rice yields and yield components (2024).

Treatment	Effective Panicles ($\times 10^4$/hm^2)	Grains per Panicle (No.)	1000-Grain Weight (g)	Seed Setting Rate (%)	Yield (kg/hm^2)	Percentage Yield Increase (%)
CK	442.77 ± 4.82 a	105.11 ± 10.72 a	21.65 ± 0.27 a	93.44 ± 0.64 a	9201.18 ± 280.23 b	-
RS	402.39 ± 10.87 b	115.02 ± 6.38 a	22.26 ± 0.70 a	92.82 ± 0.98 a	9009.93 ± 272.30 b	−2.08
CG	448.95 ± 11.53 a	109.42 ± 4.62 a	21.61 ± 0.58 a	93.38 ± 0.69 a	10,086.87 ± 113.33 a	9.63
RS + CG	429.20 ± 13.42 ab	118.88 ± 7.27 a	21.77 ± 0.18 a	92.44 ± 1.21 a	9822.52 ± 116.13 a	6.75

CK: blank control; RS: rice straw only; CG: microbial consortium only; and RS + CG: rice straw + microbial consortium. Means followed by a different letter in the columns indicate significant differences according to one-way analysis of variance ($p < 0.05$).

Table 4. Effects of different treatments on rice yields and yield components (2025).

Treatment	Effective Panicles ($\times 10^4$/hm^2)	Grains per Panicle (No.)	1000-Grain Weight (g)	Seed Setting Rate (%)	Yield (kg/hm^2)	Percentage Yield Increase (%)
CK	413.63 ± 13.34 ab	108.24 ± 9.34 a	22.03 ± 0.89 a	94.37 ± 1.39 a	9028.82 ± 188.89 a	-
RS	386.72 ± 8.03 b	116.93 ± 10.43 a	22.67 ± 0.65 a	93.78 ± 1.89 a	8462.15 ± 229.33 b	−5.68
CG	420.03 ± 11.03 a	109.89 ± 7.78 a	21.98 ± 0.98 a	94.56 ± 1.47 a	9721.40 ± 176.30 a	6.94
RS + CG	397.78 ± 9.37 b	120.13 ± 8.37 a	22.86 ± 0.29 a	93.58 ± 0.96 a	9545.11 ± 142.53 a	5.18

CK: blank control; RS: rice straw only; CG: microbial consortium only; and RS + CG: rice straw + microbial consortium. Means followed by a different letter in the columns indicate significant differences according to one-way analysis of variance ($p < 0.05$).

4. Discussion

4.1. Construction of a Multifunctional Microbial Consortium

Screening multifunctional microbial strains is a pivotal step in the formulation of multifunctional composite microbial consortia. Three *Bacillus* spp. strains with high-efficiency cellulose/lignin degradation and broad-spectrum antagonism against phytopathogenic fungi were isolated from long-term straw-return soils using selective enrichment and dual-culture confrontation assays [23]. The exogenous degradative bacterium ZJW-6 enhanced cellulose degradation and promoted positive bacterial–fungal interactions and enriched key microbial taxa associated with straw degradation, ultimately improving the degradation rate and promoting rice growth and development [24]. In the present study, we used a functional screening strategy targeting lignocellulose decomposition and pathogen inhibition to obtain highly efficient multifunctional microbial strains.

Strains CB156, BD3, BN15, and CB13 were isolated from three distinct ecological niches: long-term straw-amended agricultural soil, pig biogas slurry, and the intestinal tracts of *Antheraea pernyi*. These environments, characterized by unique physicochemical properties, facilitate microbial enrichment and functional specialization, making them

highly enriched reservoirs of diverse functional microbiota. In soil ecosystems, straw return promotes significant enrichment of cellulose-degrading microorganisms, establishing soil as a natural reservoir for lignocellulolytic bacteria, such as *Trichoderma* and *Bacillus* species, which have been widely studied for their ability to effectively degrade straw [25]. Strains BD3 and CB156 were isolated from paddy field soil with a multi-year history of straw incorporation and demonstrated superior FPA activity. Biogas slurry, a primary byproduct of the anaerobic digestion of livestock manure, is widely used as a bio-organic fertilizer because it is rich in essential nutrients, including minerals, vitamins, hormones, and amino acids [26]. Additionally, it contains diverse antimicrobial compounds that exhibit inhibitory effects against over 50 phytopathogenic species and demonstrate field efficacy in terms of controlling various plant diseases [27]. The CB13 strain, isolated from swine biogas slurry, has been confirmed to exhibit significant antagonistic activity against multiple phytopathogens [22]. Numerous plant-feeding insects (e.g., grubs, mealworms, termites, and grasshoppers) are enriched with specialized lignocellulolytic bacterial communities in their gut [28–31]. *Bacillus* species isolated from white grub (*Holotrichia parallela*) and grasshopper guts have demonstrated significant potential for agricultural residue degradation [32,33]. Similarly, termite gut isolates, including *Bacillus* sp. BMP01 [34], and the fungal strains *Aspergillus nomius* (MN700028) and *Trichoderma harzianum* (MN700029), exhibit superior lignocellulose degradation capabilities [35]. The BN15 strain isolated from the gut of *A. pernyi* exhibited significant MnP and laccase activities, indicating its potential as a key microbial candidate for lignin biodegradation.

Bacteria, fungi, and actinomycetes all possess the ability to synthesize lignocellulolytic enzymes [25,36]. However, bacterial strains predominate in straw degradation systems because of their shorter generation times, faster enzyme production kinetics during fermentation, and the superior properties of bacterial cellulases, including broader substrate versatility and enhanced operational stability [37]. In the present study, all strains used to construct the microbial consortium belonged to *Bacillus* spp.

Bacillus species exhibit exceptional environmental adaptability, enabling their survival across diverse ecological niches [38]. Furthermore, genomic analyses indicate that approximately 5% of *Bacillus* genomes are dedicated to biosynthetic gene clusters (BGCs) responsible for bioactive compound production [39]. *Bacillus*-derived antimicrobial peptides show potent antimicrobial activity against various pathogenic bacteria and fungi [40]. *Bacillus velezensis* CH1 exhibits plant growth-promoting traits, including indole-3-acetic acid (IAA) production, biofilm formation, nitrogen fixation, and siderophore synthesis [41]. These findings highlight the significant potential of *Bacillus* spp. as multi-role agents for both biological control and biofertilization.

The synthetic microbial consortium constructed by combining bacterial strains from distinct ecological niches exhibited significantly enhanced metabolic activity and functional performance compared to the single-strain consortium. Similarly, a microbial consortium constructed from strains isolated from animal feces, soil, and straw samples achieved a rice straw degradation rate of 73.2% within 8 d, demonstrating significantly higher efficiency compared to individual strains [42].

4.2. Functional Validation of a Multifunctional Microbial Consortium

Conventional microbial consortia typically have functional limitations. Biocontrol agents demonstrate strong antimicrobial activity but poor straw degradation, whereas specialized lignocellulose-degrading consortia show only modest antimicrobial activity and suboptimal field performance [13]. Notably, the direct combined application of different functional consortia is frequently hindered by inter-strain antagonism. The development of multifunctional microbes offers effective solutions to these problems. Zhao et al. [37]

created HY-1, a composite microbial consortium that exhibited synergistic nitrogen fixation, lignocellulose degradation, and plant growth promotion. Based on the straw-degrading and phosphorus-solubilizing capabilities of its strains, the constructed microbial consortium achieved a straw degradation rate of 48.3% within 7 d (a 7% increase compared to monocultures) and solubilized 117.54 $mg \cdot L^{-1}$ of insoluble phosphorus (a 29.81% increase in phosphorus-solubilizing efficiency) [8]. The microbial consortium developed in this study demonstrated three key benefits: (1) it enhanced straw decomposition by 14.87% (37.18% increase over control); (2) it exhibited a 67.56% inhibition rate against *M. oryzae*; and (3) it led to significant improvements in rice grain yield (9.63% and 6.94% yield enhancement when applied alone, and 6.75% and 5.18% increases when co-applied with straw residues). These findings demonstrate the multifunctional potential of this consortium for sustainable agriculture.

5. Conclusions

We developed a novel multifunctional microbial consortium for a straw-incorporating agricultural system through the strategic integration of complementary microorganisms from three ecological niches, effectively overcoming inefficient straw decomposition, pathogen accumulation, and yield instability. This study provides a sustainable strategy for safe and efficient utilization of agricultural waste. However, the mechanisms underlying multifunctional coupling and the ecological strategies that maintain functional stability under environmental stress remain to be elucidated.

Supplementary Materials: The following supporting information can be downloaded at: https://www.mdpi.com/article/10.3390/microorganisms14010135/s1, Table S1: Sequences of primers and PCR conditions used in this study; Table S2: The strains selected for secondary screening formed decolorization circles on Congo red-cellulose; Table S3: The strains selected for secondary screening formed decolorization circles on aniline blue media; Table S4: Inhibition rates of partial strains against rice pathogens. Table S5: Antagonistic test among candidate strains.

Author Contributions: Conceptualization, S.J., H.Q. and W.S.; methodology, S.J., J.C., H.Q. and B.L.; software, J.C., B.L. and Y.X.; validation, S.J., W.S. and Y.L.; formal analysis, S.J., J.C., H.Q., B.L. and H.Q.; investigation, B.L., Y.L. and H.B.; resources, W.S.; data curation, Y.X.; writing—original draft preparation, S.J.; writing—review and editing, S.J., B.L., J.C. and W.S.; visualization, W.S.; supervision, Y.J. and W.S.; project administration, W.S.; funding acquisition, W.S. All authors have read and agreed to the published version of the manuscript.

Funding: This work was supported by the Shenyang Science and Technology Plan Project Black Land Special [grant nos. 23-409-2-05 and 22-317-2-09] and the National Key Research and Development Program of China [grant no.: 2024YFD1500703].

Institutional Review Board Statement: Not applicable.

Informed Consent Statement: Not applicable.

Data Availability Statement: The original contributions presented in this study are included in the article/Supplementary Materials. Further inquiries can be directed to the corresponding author.

Conflicts of Interest: The authors declare no conflicts of interest.

References

1. Huang, W.; Wu, J.F.; Pan, X.H.; Tan, X.M.; Zeng, Y.J.; Shi, Q.H.; Liu, T.J.; Zeng, Y.H. Effects of long-term straw return on soil organic carbon fractions and enzyme activities in a double-cropped rice paddy in South China. *J. Integr. Agric.* **2021**, *20*, 236–247. [CrossRef]

2. Liu, D.T.; Song, C.; Xin, Z.H.; Fang, C.; Liu, Z.H.; Xu, Y.P. Agricultural management strategies for balancing yield increase, carbon sequestration, and emission reduction after straw return for three major grain crops in China: A meta-analysis. *J. Environ. Manag.* **2023**, *340*, 117965. [CrossRef]
3. Zhou, G.P.; Fan, K.K.; Gao, S.J.; Chang, D.; Li, G.L.; Liang, T.; Liang, H.; Li, S.; Che, Z. Green manuring relocates microbiomes in driving the soil functionality of nitrogen cycling to obtain preferable grain yields in thirty years. *Sci. China Life Sci.* **2024**, *67*, 596–610. [CrossRef]
4. Li, C.L.; Wang, Q.; Shao, S.Z.; Chen, Z.M.; Nie, J.; Liu, Z.; Rogers, K.M.; Yuan, Y.W. Stable isotope effects of biogas slurry applied as an organic fertilizer to rice, straw, and soil. *J. Agric. Food Chem.* **2021**, *69*, 8090–8097. [CrossRef] [PubMed]
5. Kerdraon, L.; Laval, V.; Suffert, F. Microbiomes and Pathogen Survival in Crop Residues, an Ecotone Between Plant and Soil. *Phytobiomes J.* **2019**, *3*, 246–255. [CrossRef]
6. Jia, S.; Li, Y.D.; Qu, H.; Li, B.; Juan, Y.H.; Xing, Y.H.; Liu, Y.; Bao, H.J.; Sun, W.T. Straw retention drives microbial community succession to improve soil C/N cycling: Insights from a multi-year rice-based System. *Front. Microbiol.* **2025**, *16*, 1590788. [CrossRef] [PubMed]
7. Wang, H.H.; Li, X.; Li, X.; Wang, J.; Li, X.Y.; Guo, Q.C.; Yu, Z.X.; Yang, T.T.; Zhang, H.W. Long-term no-tillage and different residue amounts alter soil microbial community composition and increase the risk of maize root rot in northeast China. *Soil Till. Res.* **2020**, *196*, 104452. [CrossRef]
8. Che, S.H.; Xu, Y.F.; Qin, X.T.; Tian, S.Q.; Wang, J.N.; Zhou, X.Y.; Cao, Z.N.; Wang, D.C.; Wu, M.K.; Wu, Z.H.; et al. Building microbial consortia to enhance straw degradation, phosphorus solubilization, and soil fertility for rice growth. *Microb. Cell Fact.* **2024**, *23*, 232. [CrossRef]
9. Liu, H.L.; Qi, Y.Q.; Wang, J.H.; Jiang, Y.; Geng, M.X. Synergistic effects of crop residue and microbial inoculant on soil properties and soil disease resistance in a Chinese Mollisol. *Sci. Rep.* **2021**, *11*, 24225. [CrossRef]
10. Hossain, M.; Rion, M.; Das, P.; Rahman, A.; Quadir, Q. Plant Growth Promoting Rhizobacteria (PGPR) Increases Yield and Mineral Contents of Rice by Mobilizing Nutrients in the Rhizosphere. *Res. Agric. Livest. Fish.* **2023**, *10*, 73–81. [CrossRef]
11. Gong, R.G.; Ye, X.Y.; Wang, S.H.; Ren, Z.J. Isolation, identification, and biological characteristics of *Clostridium sartagoforme* from rabbit. *PLoS ONE* **2021**, *16*, e0259715. [CrossRef]
12. Atiwesh, G.; Parrish, C.C.; Banoub, J.; Le, T.A.T. Lignin degradation bymicroorganisms: A review. *Biotechnol. Prog.* **2022**, *38*, e3226. [CrossRef]
13. Gao, X.Y.; Liu, W.Z.; Li, X.Q.; Zhang, W.Z.; Bu, S.L.; Wang, A.J. A novel fungal agent for straw returning to enhance straw decomposition and nutrients release. *Environ. Technol. Innov.* **2023**, *30*, 103064. [CrossRef]
14. Zou, O.; Zhang, Y.M.; Niu, X.X.; Yang, H.M.; Chu, M.; Wang, N.; Bao, H.F.; Zhan, F.Q.; Yang, R.; Lou, K.; et al. Antifungal Activity of Rhizosphere Bacillus Isolated from *Ziziphus jujuba* Against *Alternaria alternata*. *Microorganisms* **2024**, *12*, 2189. [CrossRef] [PubMed]
15. Yun, T.Y.; Zang, X.P.; Amjad, M.; Vafadar, F.; Zahoor Li, X.J.; He, Y.D.; Eissa MADing, Z.L.; Jing, T.; Ma, W.H.; Xie, J.H. Antifungal activity of *Streptomyces lydicus* 6G-OA-10 against Colletotrichum gloeosporioides: Implications for avocado anthracnose control. *Hortic. Plant J.* 2025, *in press*. [CrossRef]
16. Thompson, J.D.; Gibson, T.J.; Plewniak, F.; Jeanmougin, F.; Higgins, D.G. The CLUSTAL_X windows interface: Flflexible strategies for multiple sequence alignment aided by quality analysis tools. *Nucleic Acids Res.* **1997**, *25*, 4876–4882. [CrossRef] [PubMed]
17. Kim, J.; Rohlf, F.J.; Sokal, R.R. The accuracy of phylogenetic estimation using the neighbor-joining method. *Evolution* **1993**, *47*, 471–486. [CrossRef] [PubMed]
18. Felsenstein, J. Confidence limits on phylogenies an approach using the bootstrap. *Evolution* **1985**, *39*, 783–791. [CrossRef]
19. Tan, Y.P.; Deng, S.Q.; Qin, Y.H.; Xu, X.; Yu, Y.; Cui, L.; Wang, C.T.; Jiang, C.J.; Liu, X.Q. Evaluation of medicinal plant extracts for rice blast disease Control. *Rice Sci.* **2023**, *1*, 6–10. [CrossRef]
20. Li, R.; Mian, Y.M.; Hou, X.Q.; Li, P.F.; Wang, X.N. Effects of nitrogen application on decomposition and nutrient release of returning straw, soil fertility, and maize yield. *Acta Agron. Sin.* **2023**, *49*, 2012–2022.
21. Wang, Q.; Song, Q.L.; Feng, Y.J.; Sun, Y.; Zeng, X.N.; Lai, Y.C. Effect of nitrogen fertilizer application on decomposition of rice traw. *Jiangsu Agric. Sci.* **2017**, *45*, 197–201.
22. Jia, S.; Song, C.; Dong, H.; Yang, X.J.; Li, X.H.; Ji, M.S.; Chu, J. Evaluation of efficacy and mechanism of *Bacillus velezensis* CB13 for controlling peanut stem rot caused by *Sclerotium rolfsii*. *Front. Microbiol.* **2023**, *14*, 1111965. [CrossRef]
23. Zhang, X.J.; Zhou, X.R.; Sun, H.Y.; Meng, Y.N.; Zeng, F.L. Screening and identification of cellulose/lignin-degrading strains against plant pathogenic fungi. *Microbiol. China* **2023**, *50*, 251–261. [CrossRef]
24. Wei, X.; Li, W.C.; Song, Z.; Wang, S.W.; Geng, S.J.; Jiang, H.; Wang, Z.H.; Tian, P.; Wu, Z.H.; Yang, M.Y. Straw Incorporation with Exogenous Degrading Bacteria (ZJW-6): An Integrated Greener Approach to Enhance Straw Degradation and Improve Rice Growth. *Int. J. Mol. Sci.* **2024**, *25*, 7835. [CrossRef] [PubMed]
25. Chen, K.J.; Tang, J.C.; Xu, B.H.; Lan, S.L.; Cao, Y. Degradation enhancement of rice straw by co-culture of phanerochaete chrysosporium and trichoderma viride. *Sci. Rep.* **2019**, *9*, 19708. [CrossRef] [PubMed]

26. Li, Z.W.; Tong, D.; Nie, X.D.; Xiao, H.B.; Jiao, P.P.; Jiang, J.Y.; Li, Q.; Liao, W.F. New insight into soil carbon fixation rate: The intensive co-occurrence network of autotrophic bacteria increases the carbon fixation rate in depositional sites. *Agric. Ecosyst. Environ.* **2021**, *320*, 107579. [CrossRef]
27. Chu, J.; Yan, H.; Han, T.; Xu, H.; Yang, H.; Miu, J.K.; Bai, Y.J.; Dong, H.; Li, Z.Q. Control Effect of Biogas Slurry on Rice Blast and Screening, Identification of Endophytic Antagonistic Bacteria. *Chin. J. Biol. Control* **2022**, *38*, 1516–1525. [CrossRef]
28. Ling, Y.; Li, W.J.; Li, F.F.; Xue, X.B.; Gao, Y.Y.; Wang, L.; Liang, K.; Li, X.J. Microbial gut diversity in four grasshopper species and its correlation with cellulose digestibility. *Front. Microbiol.* **2022**, *13*, 1002532. [CrossRef]
29. Wang, Y.C.; Yang, X.D.; Lin, Y.P.; Cao, Y.; Chi, D.F. Studies on the degradation effect of corn straw by Asian corn borer larva (*Ostrinia furnacalis*) digestive enzymes combined with white rot fungus (*Phanerochaetc chrysosporium*). *3 Biotech* **2023**, *13*, 298. [CrossRef]
30. Mao, X.; Li, J.; Meng, E.; Jin, W.; Han, W. Responses of physiological, microbiome and lipid metabolism to lignocellulose wastes in gut of yellow mealworm (*Tenebrio molitor*). *Bioresour. Technol.* **2024**, *401*, 130731. [CrossRef]
31. Wang, X.F.; Tian, X.R.; Liu, Z.; Liu, Z.H.; Shang, S.Y.; Li, H.F.; Qu, J.H.; Chen, P.X. Rearing of Black Soldier Fly Larvae with Corn Straw and the Assistance of Gut Microorganisms in Digesting Corn Straw. *Insects* **2024**, *15*, 734. [CrossRef] [PubMed]
32. Li, W.J.; Li, F.F.; Bai, J.; Liang, K.; Li, K.; Qin, G.Q.; Zhang, Y.L.; Li, X.J. Isolation and characterization of intestinal bacteria associated with cellulose degradation in grasshoppers (Orthoptera). *J. Insect Sci.* **2023**, *23*, 7. [CrossRef]
33. Vyasa, G.V.; Narasingappa, R.B.; Prakash, K.V.; Bhavani, P.; Gagandeep, K.R. Prospecting cellulolytic bacteria from white grubs (*Holotrichia serrata* (F.) and *Leucopholis coneophora* Burmeister) native to Karnataka region. *BMC Microbiol.* **2025**, *25*, 121. [CrossRef]
34. Tsegaye, B.; Balomajumder, C.; Roy, P. Biodelignification and hydrolysis of rice straw by novel bacteria isolated from wood feeding termite. *3 Biotech* **2018**, *8*, 447. [CrossRef]
35. Sijinamanoj, V.; Muthukumar, T.; Muthuraja, R.; Rayappan, K.; Karmegam, N.; Saminathan, K.; Govarthanan, M.; Kathireswari, P. Ligninolytic valorization of agricultural residues by *Aspergillus nomius* and *Trichoderma harzianum* isolated from gut and comb of Odontotermes obesus (Termitidae). *Chemosphere* **2021**, *284*, 131384. [CrossRef]
36. Ma, Y.Q.; Shen, Y.Q.; Liu, Y. State of the art of straw treatment technology: Challenges and solutions forward. *Bioresour. Technol.* **2020**, *313*, 123656. [CrossRef] [PubMed]
37. Zhao, S.C.; Wang, H.R.; Wang, J.H. Synthesis and application of a compound microbial inoculant for effective soil remediation. *Environ. Sci. Pollut. Res.* **2023**, *30*, 120915–120929. [CrossRef]
38. Deng, A.H.; Wang, T.T.; Wang, J.Y.; Li, L.; Wang, X.L.; Liu, L.; Wen, T.Y. Adaptive mechanisms of Bacillus to near space extreme environments. *Sci. Total Environ.* **2023**, *886*, 163952. [CrossRef] [PubMed]
39. Iqbal, S.; Begum, F.; Rabaan, A.A.; Aljeldah, M.; Shammari, B.R.A.; Alawfi, A.; Alshengeti, A.; Sulaiman, T.; Khan, A. Classification and Multifaceted Potential of Secondary Metabolites Produced by *Bacillus subtilis* Group: A Comprehensive Review. *Molecules* **2023**, *28*, 927. [CrossRef]
40. Zhang, J.Q.; Yang, X.M.; Qiu, J.J.; Zhang, W.; Yang, J.; Han, J.Z.; Ni, L. The Characterization, Biological Activities, and Potential Applications of the Antimicrobial Peptides Derived from *Bacillus* spp.: A Comprehensive Review. *Probiotics Antimicrob. Proteins* **2025**, *17*, 1624–1647. [CrossRef]
41. Cheng, C.; Su, S.F.; Bo, S.L.; Zheng, C.Z.; Liu, C.F.; Zhang, L.C.; Xu, S.H.; Wang, X.Y.; Gao, P.F.; Fan, K.X.; et al. A Bacillus velezensis strain isolated from oats with disease-preventing and growth-promoting properties. *Sci. Rep.* **2024**, *14*, 12950. [CrossRef] [PubMed]
42. Cui, H.L.; Liu, C.L.; Li, C.Y.; Song, Z.F.; Yang, Y.J.; Wang, Y.W. Analysis on the mechanism of synergistic improvement of rice straw transformation by microbial flora. *Acta Microbiol. Sin.* **2021**, *61*, 2791–2805. [CrossRef]

MDPI AG
Grosspeteranlage 5
4052 Basel
Switzerland
Tel.: +41 61 683 77 34

Microorganisms Editorial Office
E-mail: microorganisms@mdpi.com
www.mdpi.com/journal/microorganisms

Academic Open
Access Publishing

mdpi.com

ISBN 978-3-7258-8126-0